Summer 8-20-2021

Asymmetric Synthesis of Phosphate Mimics: From Chemistry to Biotechnology

Ahmed Numan
University of Maine, ahmed.numan@maine.edu

ASYMMETRIC SYNTHESIS OF PHOSPHATE MIMICS: FROM CHEMISTRY TO BIOTECHNOLOGY

By

Ahmed Numan

B.S. Al-Nahrain University, 2007

M.S. Al-Nahrain University, 2009

A DISSERTATION

Submitted in Partial Fulfillment of the

Requirements for the Degree of

Doctor of Philosophy

(in Chemistry)

The Graduate School

The University of Maine

August 2021

Advisory Committee:

Matthew Brichacek, Assistant Professor of Chemistry, Advisor

Alice E Bruce, Professor of Chemistry

Mitchell R. Bruce, Professor of Chemistry

William M Gramlich, Associate Professor of Chemistry

Michael Kienzler, Assistant Professor of Chemistry

ASYMMETRIC SYNTHESIS OF PHOSPHATE MIMICS: FROM CHEMISTRY TO BIOTECHNOLOGY

By Ahmed Numan

Dissertation Advisor: Dr. Matthew Brichacek

An Abstract of the Dissertation Presented
in Partial Fulfillment of the Requirements for the
Degree of Doctor of Philosophy
(in Chemistry)
August 2021

Oligonucleotide based therapeutics have been pursued in the clinic for the treatment of many disease indications. However, unmodified oligonucleotides are polyanionic macromolecules with poor drug-like properties. Modifications of the phosphodiester backbone provide resistance to nucleases in vivo, making them more efficacious than unmodified nucleotides. However, these backbone modifications have added the structural complexity of a stereogenic phosphorus center. Stereochemically pure isomers exhibit differential efficiency dependent on its enantiopurity. The catalytic, stereocontrolled synthesis of a phosphorus-stereogenic center is challenging, and traditionally, depends on a resolution or use of stochiometric auxiliaries. Herein, asymmetric nucleophilic catalysis has been investigated to provide enantio-enriched phosphonates using phosphoramidite or *H*-phosphonate approaches. Both investigations utilized commercially available chiral catalysts with the enantioselectivity determined by HPLC on a chiral stationary phase. The requisite starting materials, phosphoramidite and *H*-phosphonates, have been prepared in racemic form with a variety of alcohol substituents. Chiral phosphonate products were synthesized in acceptable yield (33%-92%) and modest enantioselectivity (up to 62% *ee*) after identification of an appropriate chiral catalyst and optimization of the solvent, base, temperature, and stoichiometric additives. The potential applications of these approaches will be discussed in the context of catalysis and biotechnology. Following our interest in phosphorus nuclear magnetic resonance spectroscopy (^{31}P NMR), quantitative analysis of phosphorus abundance in environmental samples was

conducted. To prepare samples for NMR analysis pre- and post-treatment, extraction, dissolution, and pH adjustment were performed. Quantitatively accurate ^{31}P NMR were acquired by optimizing delay time, proton decoupling parameters, and acquisition time.

DEDICATION

I dedicate this body of work to my beloved father who encouraged and supported me always and showed me what an ideal father should be like. I also dedicate this to my mother and my family who have stood beside me always. I could not have finished without their love. I also dedicate this to Claudia, who has shown me the meaning of true love.

ACKNOWLEDGEMENTS

I would like to express my gratitude to my advisor and mentor, Dr. Matthew Brichacek, for his unwavering support, guidance, advice, patience, and encouragement throughout my PhD program. I appreciate the time we have had together.

I would like to thank my advisory committee: Dr. Alice Bruce, Dr. Mitchell Bruce, Dr. William Gramlich, and Dr. Michael Kienzler for their guidance, advice, and suggestions throughout my PhD work. This work could not have been completed without the help of David LaBrecque with the instruments. I am grateful to all the current and previous members of Brichacek group, specifically Billy, Sudeera, Elain, Saad, and Robin.

I would like to thank Dr. Aria Amirbahman and his student, Bailey, for collaborating with me on my fourth chapter. I could not have finished my research without their hard work collecting and preparing samples from Highland Lake in Maine.

I extend my thanks to my family, my parents, my brothers and sisters, who have believed in me and supported me throughout my entire journey. I also thank Claudia for her constant support and encouragement. I love all of you.

I am grateful for my sponsor, Higher Committee for Education Development in Iraq (HECD), who has allowed me this opportunity and has supported my scholarship.

TABLE OF CONTENTS

LIST OF TABLES

LIST OF SCHEMES

LIST OF FIGURES

CHAPTER 1

INTRODUCTION

1.1 RNA-Based Therapeutics

1.1.1 Drug discovery

After the primary sequence of the human genome was completed in 2001, the number of protein-coding regions in the human genome was identified to be 20,000-25,000. Of all the proteins in the human genome only around 3,000 were predicted to be suitable drug targets.[1] Most currently marketed medications have a non-covalent interaction with a particular proteins. Consequently, these drugs can have off-target interactions and produce side effects through unexpected pathways.[2] Therefore, ongoing research in academia and pharmaceutical industry is developing therapeutic drugs with improved selectivity and efficacy.

Proteins have multiple roles which include functioning as hormones, enzymes, ion-channels, cell membranes, and cell receptors.[1] Proteins are synthesized in a two-step process within the cell. Firstly, the transcription step takes place when the genetic information of DNA is converted into a single strand of messenger ribonucleic acid (mRNA) in the nucleus. After the mRNA translocates to the cytoplasm, then translation can occur. The codons contained in mRNA dictate the structure and sequence of the protein produced by the ribosome. Therefore, the primary function of mRNA is to transfer information from DNA into the proteins of given cells.[3] Although not as common as directly targeting proteins, blocking protein production by targeting RNA is a viable therapeutic strategy as seen in Figure 1.1.[4] For example, cytotoxic therapeutic agents interact directly with DNA and aminoglycosides binds to bacterial ribosomal RNAs.[5]

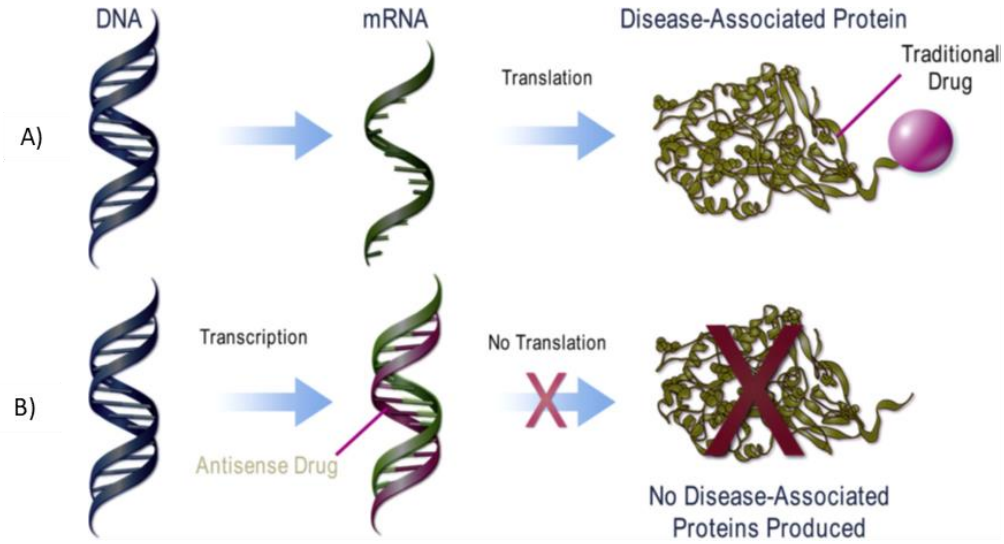

Figure 1.1 Mechanism of protein inhibition. A) Traditional approach to drug discovery where a small molecule directly binds to the protein of interest. B) An antisense oligonucleotide approach to drug discovery where translation is blocked by a therapeutic oligonucleotide. Reprinted from ref.3 with permission from Elsevier.

1.1.2 RNA based approaches

RNAs possess diverse roles in cellular processes that range from disrupting DNA and protein interaction, suppressing genetic functions, silencing other RNA, and aiding in cellular metabolism.[6] RNA-based therapies are widely utilized in the pharmaceutical industry.[6] Most of these therapies are categorized into three approaches: nucleic acid-targeting through either DNA or RNA, protein targeting, and protein-encoding.

Oligonucleotide binds to their RNA target by Watson-Crick base pairing with high selectivity and affinity. Oligonucleotide therapies seek to mimic enzymatic mechanisms.[7] This includes antisense oligonucleotides (ASO), short interference RNA (siRNA), microRNA (miRNA), ribozymes, and aptamers. These therapeutics can either exploit degradation pathways or modulate RNA splicing by blocking ribosomal machinery as seen in Figure 1.2. [5,6,8–11]

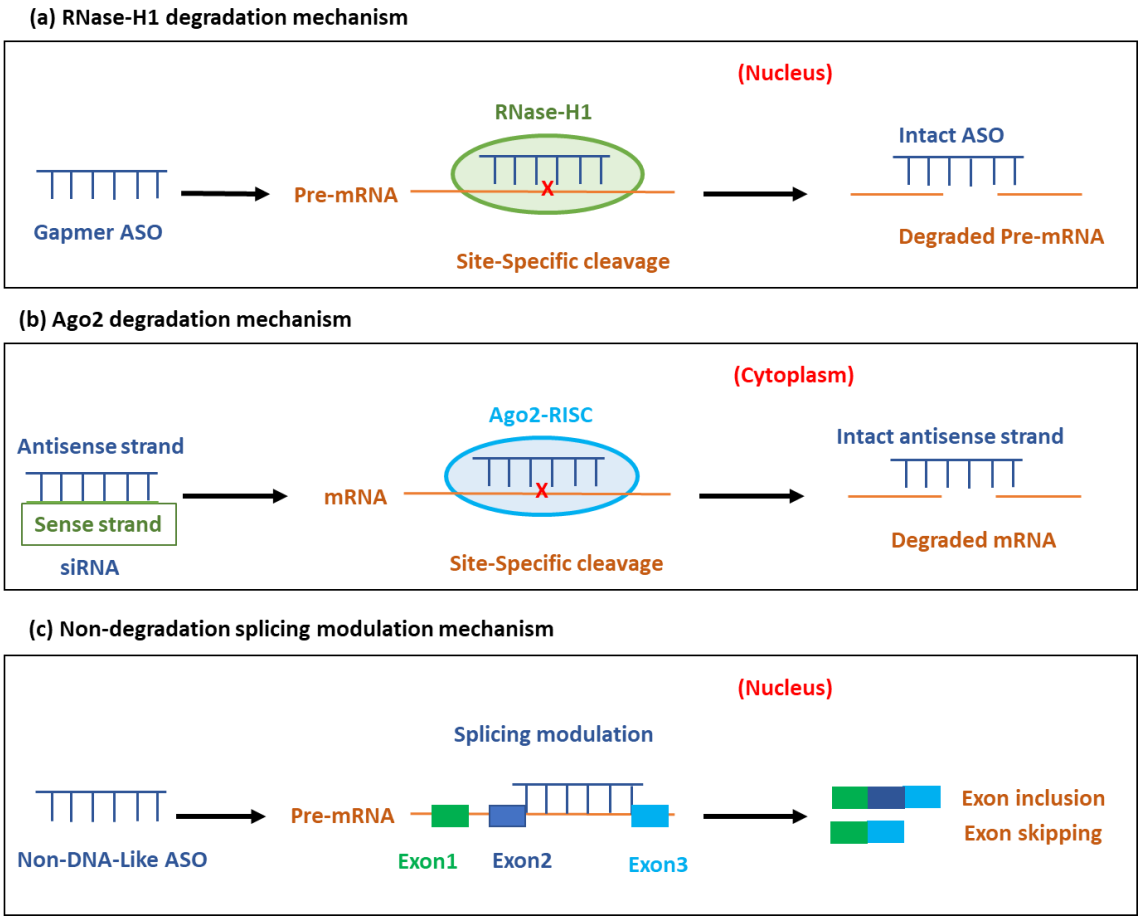

Figure 1.2 Three different oligonucleotide mechanisms depicted for approved antisense oligonucleotides (ASOs) and siRNA (a) Gamper ASO, ASO with a central gap of DNA, interacts with target mRNA in the nucleus. Then, RNase-H1 recognizes the DNA-RNA heteroduplex complex and cleaves the complementary RNA strand and leaves the ASO strand intact to bind to another target. (b) A duplex siRNA interacts with other proteins to form the RISC complex which contains the antisense strand and the protein Ago2. The Ago2-RISC complex helps the antisense strand to bind to the target mRNA and selectively degrades the target RNA while leaving the antisense strand intact. (c) A modified ASO sterically blocks and alters the mRNA splicing process in the nucleus. ASO, antisense oligonucleotide; mRNA, messenger RNA; siRNA, short interference RNA; Ago2, argonaute-2; RISC, RNA-induced silencing complex.[12]

The most direct strategy of targeting RNA is to bind to RNA with single stranded antisense oligonucleotides (ASOs).[13] ASOs are short (12-24) synthetic nucleotides in length that bind to complementary mRNA through Watson-Crick base pairing, and modulate the function of the targeted mRNA. The ASOs can act on a precursor mRNA (pre-mRNA) in the nucleus and modulate its function by promoting endogenous RNase-H1 degradation as seen in Figure 1.2a. RNase-H1 is utilized to degrade RNA-DNA heteroduplexes that are formed followed by the synthetic ASO being released to target additional pre-mRNA.[12] ASOs do not include oligonucleotides that form triple helix structure with DNA, or oligonucleotides that bind to proteins.[14]

Utilizing short interference RNA (siRNA) is another method of targeting RNA that induces enzymatic degradation of the target RNA. In this process, Argonaute 2 (Ago2) is responsible for the cleavage of the target RNA by an RNase-H like mechanism as seen in Figure 1.2b.[12] First, a single stranded siRNA binds to the target RNA and subsequently to Ago2 and other unknown factors to form the RNA-induced silencing complex (RISC complex).[12,14] RISC facilitates cleavage of the RNA at a specific site followed by release of the intact siRNA to target additional RNA as seen in Figure 1.2b. [12,14]

A final method of action for oligonucleotide therapeutics works by blocking modification of the mRNA during the maturation process. This process can either be disrupting the interaction between the target RNA and essential ribosomal subunits or modulating the splicing process to arrest protein translation as seen in Figure 1.2c.[12] Before forming a mature mRNA, a pre-mRNA is enzymatically modified and spliced resulting in multiple isoforms.[8] Thus, modified ASOs are usually designed to avoid the enzymatic degradation by RNase-H or Ago2. For example, Eteplirsen™ is a morpholino modification that was approved by the FDA to treat Duchene muscular dystrophy (DMD) in 2016.[15] Eteplirsen™ disrupts the splicing of pre-mRNA that is necessary for DMD to occur, therefore decreasing the production of dystrophin lacking exon 51.[16]

1.1.3 Approved Oligonucleotide therapeutics

Oligonucleotide therapies represent a promising platform that has the ability to selectively target RNAs in the cell. In this strategy nucleic acids indirectly block protein production and therefore have the potential to produce many therapeutic.[14] For example, preliminary work has done by Zamecnik et al. in 1977 that shows the inhibition of Rous sarcoma virus by targeting 13 nucleotides of a viral RNA sequence.[17] Furthermore, over the last decade the FDA has approved multiple oligonucleotide therapeutics for the treatment of various diseases indication as seen in Table 1.1.[7,18]

Table 1.1 FDA approved oligonucleotide therapeutics[7]

Drug name	Indication	Company	Type	FDA Approval
Kynamro™ (mipomersen sodium)	Homozygous Familial Hypercholesterolemia	Kastle Therapeutics LLC	Antisense Oligonucleotide	2013
Defitelio™ (defibrotide sodium)	Hepatic Veno Occlusive Disease	Jazz Pharmaceuticals Plc	Oligonucleotide, natural product	2016
Exondys 51™ (eteplirsen)	Duchenne Muscular Dystrophy	Sarepta Therapeutics	Antisense Oligonucleotide	2016
Spinraza (nusinersen)	Spinal Muscular Atrophy	Biogen	Antisense Oligonucleotide	2016
Heplisav-B™ (hepatitis B vaccine, adjuvanted)	Hepatitis B	Dynavax Technologies	Cytidine phosphoguano-sine (CpG) oligonucleotide as adjuvant	2017
Tegsedi™ (inotersen sodium)	Familial Amyloid Neuropathies	Akcea Therapeutics	Antisense Oligonucleotide	2018
Onpattro (patisiran)	Familial Amyloid Neuropathies	Alnylam Pharmaceuticals	siRNA	2018
Givlaari™ (givosiran)	Acute Hepatic Porphyria	Alnylam Pharmaceuticals	siRNA	2019
Vyondys 53™ (golodirsen)	Duchenne Muscular Dystrophy	Sarepta Therapeutics	Antisense Oligonucleotide	2019

1.1.4 Medical Chemistry of Oligonucleotides

Natural oligonucleotide are phosphodiesters, which contain three major components: phosphate, sugar, and nucleobase as seen in Figure 1.3.[14] Unmodified nucleic acids are unstable molecules in biological systems. Specifically, they are rapidly degraded by nuclease enzymes which cleave their phosphodiester linkages before reaching their target preventing their use as therapeutic agents.

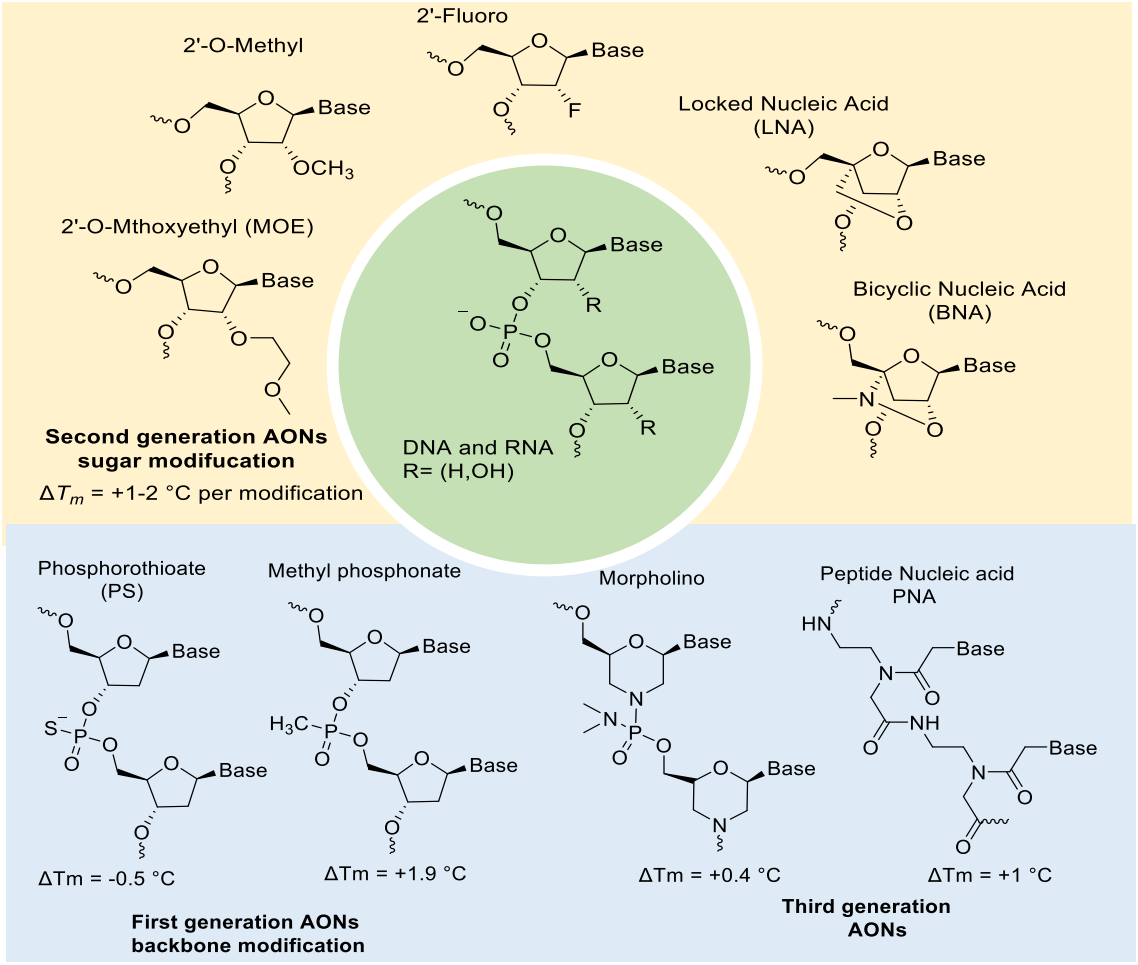

Figure 1.3 Evolution of antisense oligonucleotide therapeutics and their chemical modifications; melting temperature changing (ΔT_m) per modification compared with corresponding RNA/DNA pairing.[14]

In addition to enzymatic degradation, the inefficient pharmacokinetic properties of oligonucleotide therapeutics make them non-ideal drug candidates because they are weakly bound to plasma proteins

and thus rapidly filtered by the kidney and excreted.[6] Also, in order for the antisense oligonucleotides (ASOs) to be an efficacious drug, they must have a high affinity for their RNA/DNA targets.[6,19] Next, to overcome poor permeation across the cell membrane, the use of chemical modifications to the oligonucleotide structure have been utilized to enhance the drug-like properties. The desirable properties to achieve include improving nuclease resistance, cellular uptake, target affinity, pharmacokinetic, and base-pairing specificity.[19] Modifying each of the 25 different positions of a dinucleotide subunit results in additive effects. According to these modifications, the antisense oligonucleotides (ASOs) have been categorized into three generations as seen in Figure 1.3.[20,21]

The effect of modifying ASOs is usually done by measuring the duplex or triplex melting temperature (T_m) using UV thermal analysis. Melting temperature (T_m) is the temperature where exactly half of the oligonucleotide molecules are single-stranded and the other half remain double-stranded. Typically, the change of T_m per modification (ΔT_m/ mod) is calculated and compared with a native duplex reference. However, multiple sequences need to be examined to determine the binding affinity per modification for a specific sequence.[22]

Modifying the nucleobase is not common because it is responsible for binding with the complementary mRNA target with Watson-Crick base pairing.[19,20] Modification of the furanose sugar can enhance binding affinity, improve enzymatic stability, or increase plasma protein interactions thereby preventing renal secretion. For example, phosphorodiamidate morpholino oligomers (PMO) and peptide nucleic acids (PNA) are third generation ASOs with the most favorable properties in *vitro* and in *vivo*. Thermal stability increases for PMO-DNA complexes are 0.4 °C/modification while PNA-RNA duplexes are up to 1 °C/modification compared with their corresponding RNA/DNA pairing as shown in Figure 1.3.[20,23,24]

The phosphodiester backbone (Figure 1.3) can be chemically modified to substitute one of the non-bridging oxygen atoms for sulfur (phosphorothioate), methyl (methyl phosphonate), nitrogen (phosphoroamidate), or boron (boranophosphate). Backbone modifications increase stability toward

nucleases, improve solubility in water, and improve binding affinity to mRNA. Collectively, these modifications make them more efficacious in antisense technology and more stable during automated oligonucleotide synthesis.[19–21] In *vitro* studies showed that methyl substitutions increased the thermal stability in α-methyl phosphonate (MP)-DNA duplex by 1.9 °C per modification compared to the corresponding RNA-DNA complexes.[25] In contrast, the thermal stability decreased for all phosphorothioate (PS)-DNA duplexes by 0.5 °C per modification.[26]

In addition to therapeutic applications, phosphorothioate oligonucleotides have been successfully used in gene silencing and as a probe to discover the functions of internucleotide phosphates.[27] Many clinical candidates have the PS moiety. For example, Spinraza™ is a phosphorothioate (18-mer) that was recently approved by FDA for the treatment of a genetic condition, spinal muscular atrophy, that causes infant death (Figure 1.4).[28]

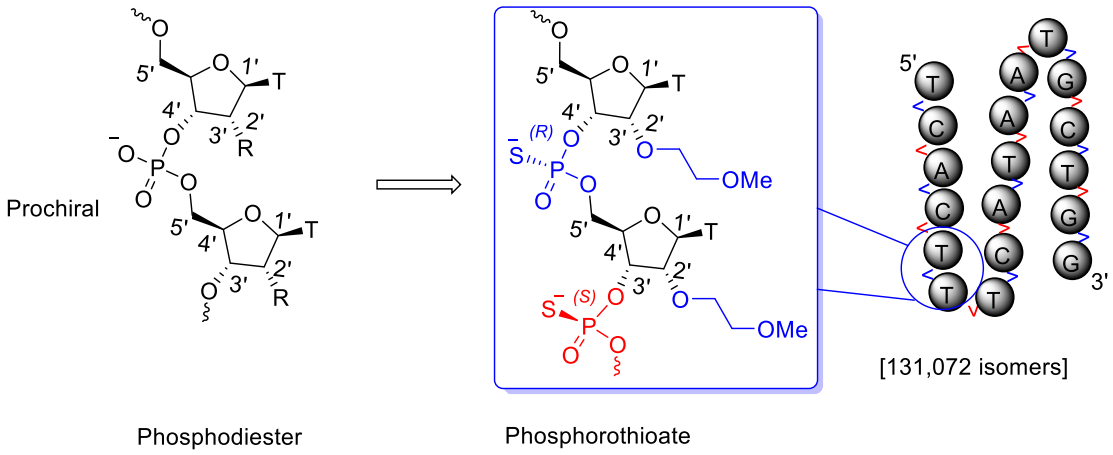

Figure 1.4 Spinraza™: FDA approved for the treatment of spinal muscular atrophy in 2016. The structure of a prochiral phosphodiester and the corresponding phosphorothioate moiety in Spinraza™ containing 131,072 individual isomers.

1.1.5 Chirality of Phosphodiester backbone

For biological activity of chiral drug is dependent on the spatial arrangement of atom in three dimensions. When these stereoisomers interact with biological systems, metabolization may occur at different rates or use different pathways. While one enantiomer shows activity the other enantiomer may be non-active, affect different targets, or even be toxic.[29] In order to optimize the therapeutic qualities of chiral drugs, while avoiding unwanted effects, new approaches are needed to selectively synthesize an enantiopure compound.

Although backbone modification of oligonucleotides improves pharmaceutical profiles, it converts an achiral phosphodiester linkage into a chiral phosphorus center with two different stereochemical configurations designated S_P (blue) and R_P (red) (Figure 1.4). Due to synthetic limitations, a mixture of both configurations at the P-center is present in current FDA-approved ASOs. Iwamoto et al. studied the duplex stability of stereochemically pure oligonucleotide components of Mipomersen™ and several of its stereodefined (Table 1.2).[30] Furthermore, many studies have confirmed that a stereodefined center in a single molecule can dramatically impact the pharmaceutical properties of the ASOs by affecting their thermal stability.[19,30–32]

Table 1.2 Mipomersen^{TM} and its stereocontrolled isomers

ASO	Sequence	Number of stereoisomers	T_m (°C)
Mipomersen^{TM}		524,288	80.2
WV-1		1	84.7
WV-2		1	74.7
WV-3		1	78.8
WV-4		1	80.0
WV-5		1	81.6
WV-6		1	78.3
WV-7	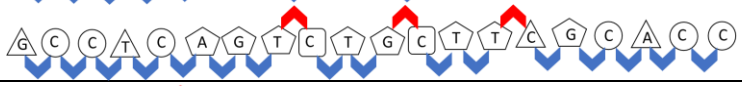	1	68.2

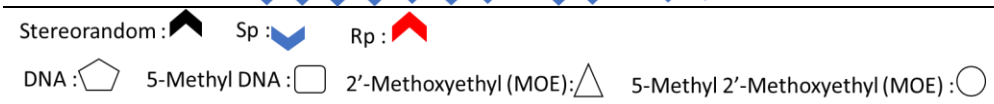

Mipomersen^{TM} is 20-mer oligonucleotide with phosphorothioate (PS) linkages, DNA core, and 2'-MOE modified end. Due to the incorporation of PS linkages a total of 524,288 isomers are possible with mixture having a melting temperature of 80.2 °C as in Table 1.2 (Entry 1). The T_m of the all-R_P (WV-1) was higher at 84.7 °C, whereas the T_m of the all-S_P (WV-2) was 74.7 °C (Table 1.2 Entries 2 and 3). The studies also investigated the duplex stability of nucleotides that have controlled incorporation of R_P or R_S linkages at specific locations. Although no absolute rule can be formed about backbone modification, the stability of the DNA complexes are sensitive to the stereochemical relationship at specific sites on the oligonucleotide (Table 1.2 WV-3 through WV-7).[30]

1.2 Asymmetric synthesis

1.2.1 Asymmetric Reaction pathways

Asymmetric synthesis is the reaction or reaction sequence that selectively forms one or more new stereogenic elements. In asymmetric synthesis, achiral molecules are enantioselectivity converted into chiral molecules. In other words, asymmetric synthesis is a method for producing enantiomerically pure compounds by favoring one stereoisomer over.[33] Stereoisomers are the molecules with the same connectivity, but with the different arrangement in three-dimensional space.[34] Asymmetric synthesis is challenging because it takes a racemic mixture and converts it preferentially into one stereoisomer over another (Figure 1.5**)**.[35]

Since the early 1980s, asymmetric synthesis has become a powerful tool to produce enantioenriched molecules for use in pharmaceutical applications. Generally, the formation of a new stereogenic center on a substrate is caused by induction of a chiral group. Several types of asymmetric induction are known.[36] First, internal asymmetric induction occurs when a reactive center is connected by a covalent bond to a stereogenic center and they remain together during the reaction. Alternatively, relayed asymmetric induction occurs when a stereogenic center is introduced temporarily and then removed in separate chemical reaction.

Enantiopure compounds can be synthesized by covalently attaching a chiral molecule to an achiral substrate and subsequently removing the functionality later. Chiral molecules utilized in this manner are called chiral auxiliaries (Figure 1.5**)**.[35,37] The stereochemistry of the chiral auxiliary controls the stereoselectivity of the asymmetric synthesis. Stoichiometric amounts of the chiral auxiliary are always required to achieve a single enantiomer, but this process can be cost-efficient if the chiral auxiliary can be recycled.[37]

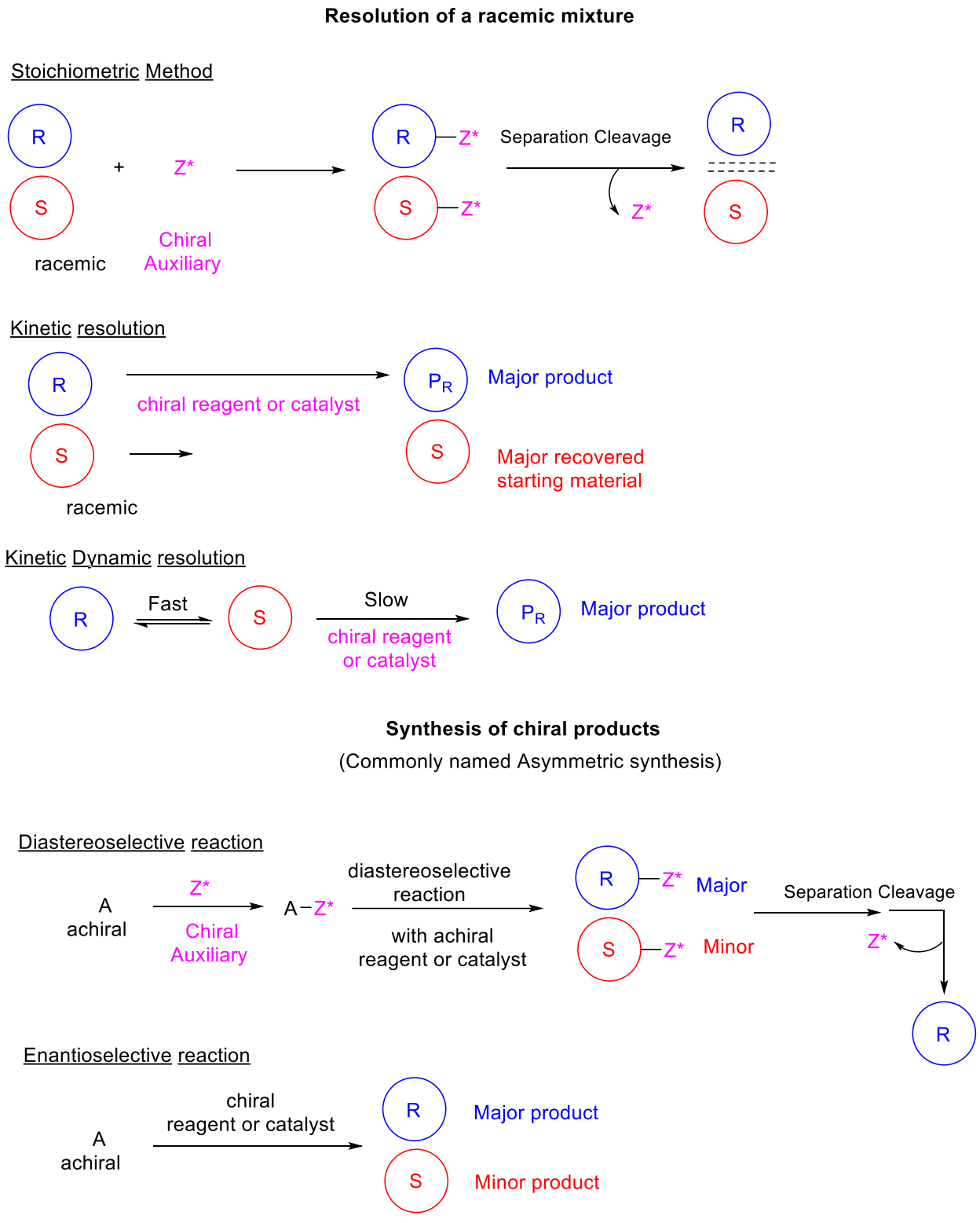

Figure 1.5 Approaches for the synthesis of enantioenriched compounds[35]

Using a chiral reagent is a widely used approach to obtaining enantioenriched substances.[38] Similar to chiral auxiliaries, the selectivity of the reaction is controlled by the chirality of the reagent. However, the chiral reagent is not covalently attached to the starting material or product of a reaction and thus does not have to be removed in a separate synthetic step. For example, the asymmetric hydration of an alkene utilizes a chiral borane reagent to hydroborate the alkene followed by oxidation and hydrolysis.[38] Despite the development of many chiral reagents, substrate scope and selectivity are often limited.

Another method of obtaining enantioenriched materials is to use a resolution. In a resolution, an equimolar mixture of enantiomers is separated using either physical or chemical approaches. The separation of the enantiomers is possible after they have been converted into diastereomers using a chiral reagent. Diastereomers are able to be separated due to their different physical or chemical properties. Once separated, the chiral reagent is removed providing pure enantiomers.

As an alternative to a classic resolution, a kinetic resolution (KR) occurs when there is a large difference between the reaction rates of the enantiomers. Typically, the unwanted enantiomer is converted into a different molecule using a chiral reagent leaving the desired enantiomer intact (Figure 1.5). For this strategy to be successful, a selective chiral reagent is needed and there is always 50% yield lost to the byproduct.[35,39–41] Enzymes have been extensively used as reagents in kinetic resolutions.

Unlike the kinetic resolution (KR), the dynamic kinetic resolution (DKR) is a powerful approach in asymmetric synthesis by efficiently combining the KR and racemization of the slower reacting enantiomer (Figure 1.5**)**.[35,40,42,43] Therefore, a racemic mixture can be converted into an enantiopure compound with a theoretical yield of 100%.

A potential energy diagram of a DKR is shown in Figure 1.6.[39,40] The (*R*) and (*S*) enantiomers of the starting material (SM) are in rapid equilibrium. $\Delta G_{rac}^{\ddagger}$ represents activation energy associated with the interconversion. Both enantiomers (SM_S and SM_R) have equal free energies and can associate with the chiral catalyst. The enantiomers react at different rates since the transition states are diastereomeric. One pathway has a higher transition state, in this schematic TS_S, and the other is a more kinetically accessible pathway that has a lower transition state, TS_R in Figure 1.6.[44] The reactivity difference of the two pathways is designated by $\Delta\Delta G^{\neq}$. The selectivity of the chiral catalyst to produce a single isomer can be correlated to its ability to increase $\Delta\Delta G^{\neq}$. As a result, controlling the reaction rates enable the stereoselective synthesis of a chiral product from racemic starting materials.[44]

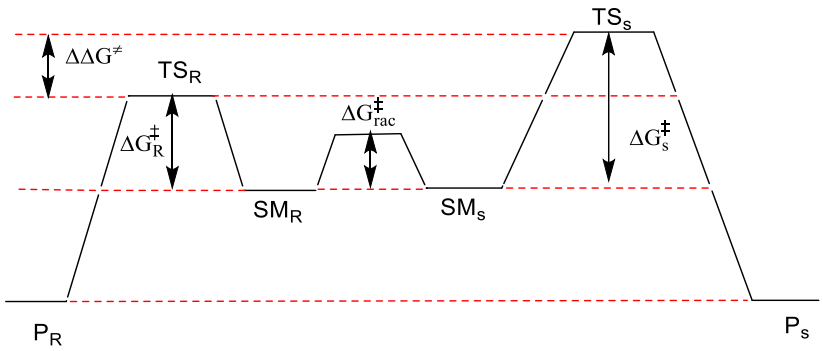

Figure 1.6 Energy diagram of dynamic kinetic resolution for (R and S) enantiomers, in which a catalyst can selectively lower a transition state (TS) for one isomer leading to favorable reaction outcome.[44]

When considering all methods of obtaining single enantiomers, the DKR can be considered the most effective approach to produce stereoselective products because DRKs utilize non-stochiometric amounts of a chiral reagent, can be catalyzed, and theoretically provide 100% yield. Numerous examples of DKRs are reported in the literature to provide pharmaceuticals and natural products.[39,40,44]

1.3 Asymmetric phosphate mimics

As previously mentioned, the chemical modification of the phosphodiester backbone in oligonucleotides enables efficacious oligonucleotide therapies.[28] Substitution of either of the two non-bridging oxygen atoms of the internucleotide phosphorus creates a chiral phosphoryl center, and the properties of these oligonucleotide analogs are affected by the chirality of the phosphorus atom. Therefore, the stereocontrolled synthesis of chiral phosphate oligonucleotides in literature have been pursued extensively.[45,46]

1.3.1 Diastereomeric separation by chromatography

The first approach to obtaining *p*-chiral oligonucleotide analogs was chromatographic separation of diastereomers. A racemic mixture of a dinucleotide can be separated using high-performance liquid chromatography (HPLC) to obtain single isomers of stereodefined phosphorus centers. The chiral stationary phase can be used in either normal- or reverse-phase modes to separate the diastereomers. The diastereopure product can be utilized for further chemical or biological studies. For example, diastereopure dinucleotide analogs can be converted into the corresponding 3'-phosphoramidite dinucleotide building blocks (**1-3**) which are used in the solid-phase syntheses of oligonucleotides as in Scheme 1.1.[47,48]

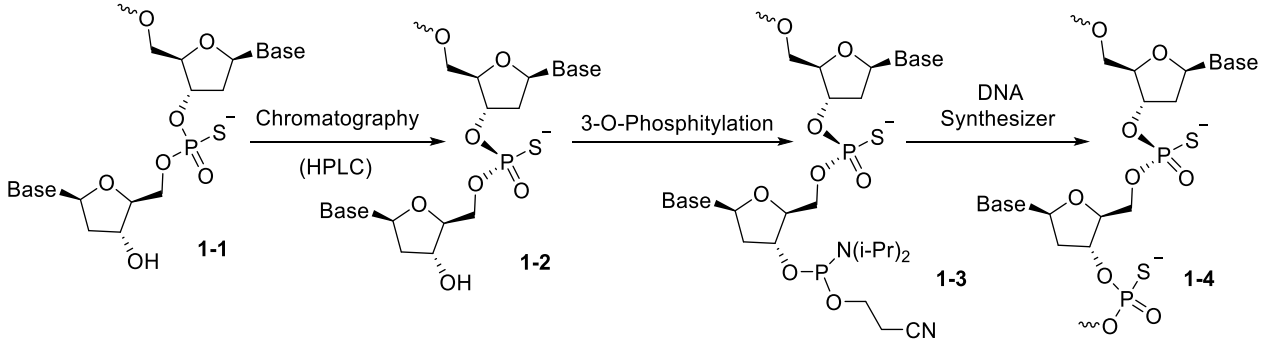

Scheme 1.1 Synthesis of diastereomerically pure dimer building blocks with a chiral P-center.[46]

Oligonucleotides with multiple stereogenic phosphorus centers can be synthesized in a non-stereocontrolled manner analogous to the synthesis of dinucleotides. However, the chromatographic separation is not guaranteed since the target structure contains many chiral phosphorus moieties. Furthermore, the reactivity of dimer building blocks is typically lower than monomers.[47,48]

1.3.2 Enzymatic enantioselective synthesis

Enzymatic synthesis of oligonucleotides can be achieved using ribo- or 2'deoxyribo-nucleoside 5'-triphosphates and various enzymes including DNA polymerase I and T7 RNA polymerase. Modifying the nucleoside 5'-triphosphate results in P-chiral oligonucleotides instead of a natural phosphodiester as shown in Scheme 1.2. For example, α-P-thiothymidine 5'-triphosphate (**1-5, X = S**) was used to synthesize fully modified phosphorothioate oligonucleosides. Unlike chromatographic-separation approaches, stereodefined products are always achieved here. Therefore, oligonucleotides longer than 10-20 mers can be synthesized that contain diastereomerically pure phosphorothioates, phosphoroselenoates, and methyl-phosphonates.[49–51] Mechanistic studies by Rayn et al. have shown that enzymes lower the barrier to phosphorus-oxygen bond formation through different scenarios including nucleophilic activation by base catalysis, leaving group activation by acid catalysis, and oxyanion hole-type stabilization of the transition state (Figure 1.7).[52,53]

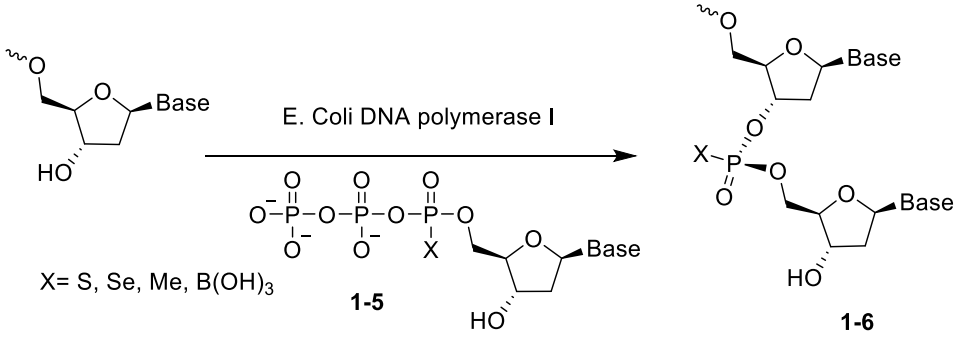

Scheme 1.2 Phosphorothioate, phosphoroselenoate, methylphosphonate and boranophosphate have been synthesized using α-P-modified nucleoside 5'triphosphates.

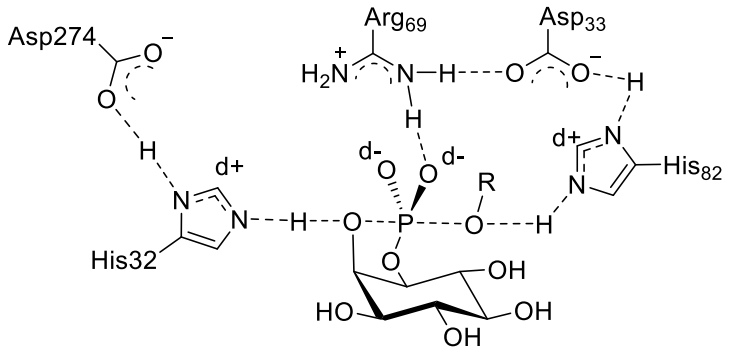

Figure 1.7 Phosphatidylinositol-specific phospholipase catalyzes the phosphorus-oxygen bond formation using leaving group activation, nucleophilic activation, and pentavalent transition state stabilization as proposed by Ryan et al.[52]

However, there are some limitations in enzymatic asymmetric synthesis. First, phosphate-forming enzymes are very substrate specific and may not process P-modified nucleotide triphosphates. Second, both enantiomers of the phosphate mimic are often not available due to enzyme specificity. For example, only (R_P)-phosphorothioate, S_P-boranophosphate, and S_P-methylphosphonate linkages have been enzymatically obtained using S_P-isomers of compound **1-5**. Next, large-scale production of oligonucleotides has not been achieved using enzymatic synthesis. Lastly, the oligonucleotide products have to be purified from byproducts before subsequent chemical treatments.[54]

1.3.3 Utilizing the chirality of ribose

The stereocontrolled chemical synthesis of chiral phosphorus oligonucleotide analogs has also been approached utilizing the chirality of ribose.[55,56] Traditional phosphoramidite synthesis of dinucleotide thiophosphates results in a mixture of R_P and S_P but isn't equal.[57] Therefore, the inherent chirality of ribose or deoxyribose has induced an asymmetric environment for the stereoselective synthesis of P-chiral internucleotide phosphate mimics. For example, Seio et al. have developed a 3'-phosphoramidite moiety possessing a covalent linker with the phosphorus atom (compound **1-7**).[58] This tethered phosphoramidite

has used as a building block to synthesize dithymidine phosphorothioate. The macrocycle provides steric hindrance around the phosphorus center, which favors one formation of one enantiomer. A high stereoselectivity of the R_P-diastereomer was obtained (R_P:S_P = 86:14) without using any other chiral source.[58]

Despite the asymmetric environment created using the chirality of ribose, it is still challenging to obtain higher stereoselectivity because of structural limitations. Moreover, only one of two phosphorus isomers are obtained within this approach as a result of the chirality of ribose.[54]

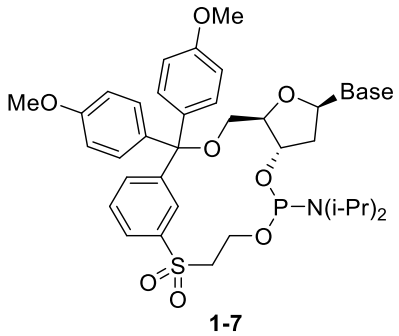

1-7

Figure 1.8 Cyclic phosphoramidite monomer used for the stereoselective synthesis of thiophosphate dinucleotide.

1.3.4 Utilizing chiral auxiliary

P-chiral phosphite triesters can be synthesized using P(III) or P(V)-chiral auxiliaries that are covalently bonded to the phosphorus center as seen in Scheme 1.3.[59] For example, Agrawal *et al.* have utilized a prolinol moiety to promote a condensation process that utilizes oxazaphospholidine analogues.[60] Specifically, P-chloro-oxazaphospholidine (**1-9**) was coupled with protected nucleoside **1-10** to give a single diastereomer of **1-11** in 90% yield. Notably, both D- and L-proline can be used to obtain either configuration of the oxazaphospholidine. The condensation of compound **1-11** with a polymer-bound nucleoside (**1**-**12**) was facilitate by 1*H*-tetrazole. After sulfurization and deprotection reactions,

oligonucleotide phosphorothioate **1-14** was obtained with high stereoselectivity (R_P : S_P = 10 : 90 to 14 : 86).[54,60]

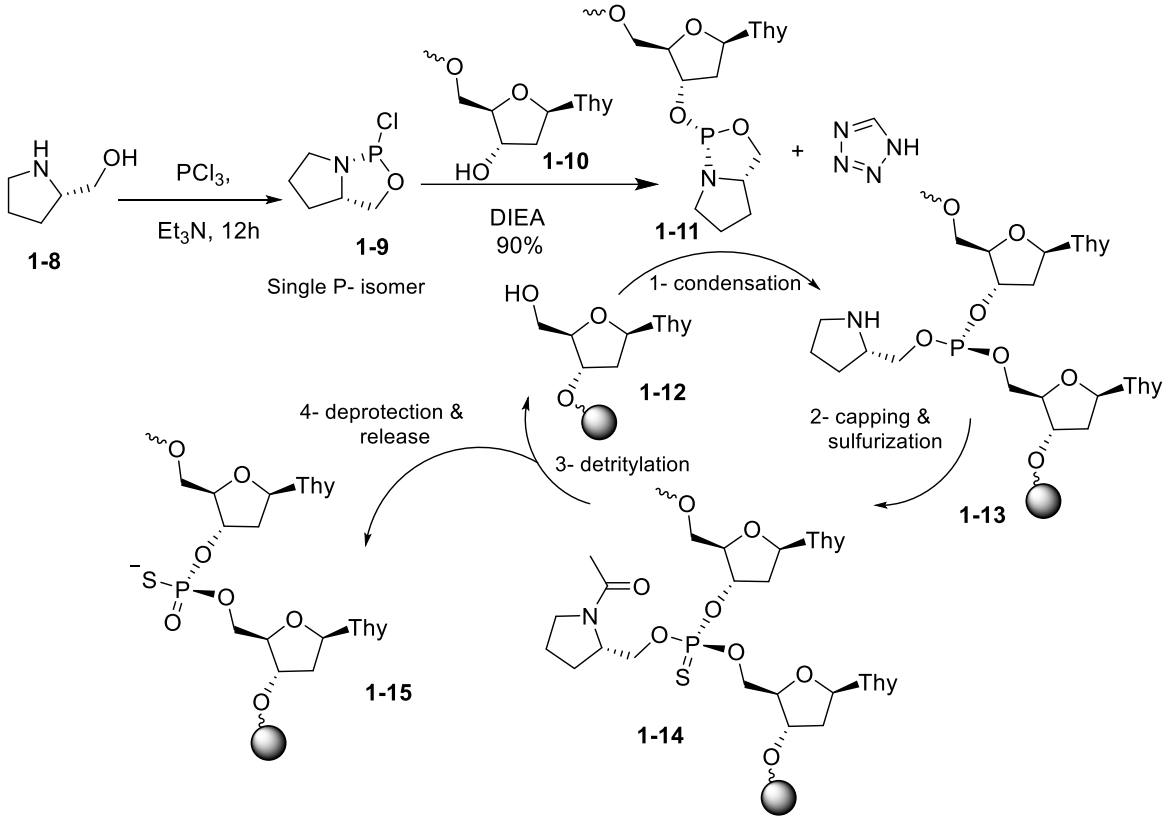

Scheme 1.3 Stereoselective synthesis of prolinol oxazaphospholidine derivative (**1-9**) as a precursor for stereospecific synthesis of compound (**1-15**).[60]

Other chiral auxiliaries have been developed for the synthesis of phosphorothioate oligonucleotides (Figure 1.9).[54] Chiral auxiliary approaches allow both R_P and S_P to be synthesized with excellent diastereoselective using solid-phase phosphorothioate synthesis me.[54] However, covalent attachment of the chiral auxiliary requires additional chemical reactions and purifications to isolate the desired dinucleotide products. Additionally, a stoichiometric amount of the chiral auxiliary is always required because the stereoselectivity is dependent on the structure of the chiral auxiliary.[54,61]

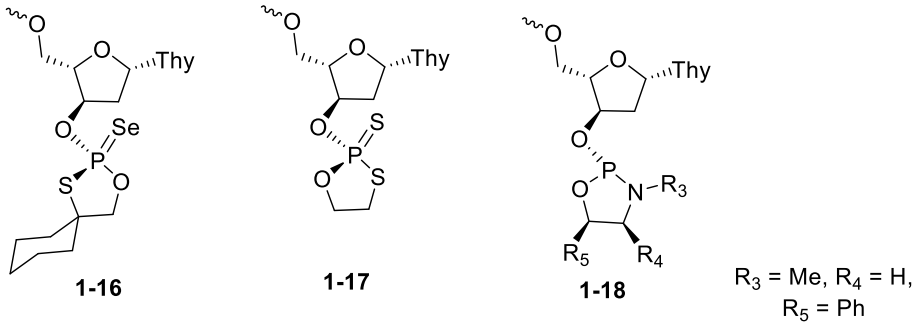

Figure 1.9 Nucleoside-3'-oxazaphospholidine monomers used as chiral auxiliaries for the stereocontrolled synthesis of oligonucleotide phosphorothioates or phosphoroselenoates.[54]

1.3.5 Utilizing a chiral activator

Despite the inherent advantages of utilizing a dynamic kinetic asymmetric transformation (DYKAT) to synthesize P-stereogenic compounds, very few reports are in the literature.[53] DYKATs employ a chiral activator to selectively transform a racemic mixture into a single stereoisomer. In most cases, a substoichiometric amount of a chiral substance can still achieve high levels of enantioselectivity whereas a stoichiometric amount was necessary for a chiral auxiliary or chiral reagent. DiRocco *et al.* has successfully assembled biologically active prodrugs via a catalytic stereoselective approach by coupling P-chiral phosphonamidates (**1-19)** to nucleotides as shown in Scheme 1.4.[53] Despite this success, asymmetric synthesis of P-stereogenic compounds suffers from low catalytic turnover, low stereoselectivity, and limited substrate scope. Therefore, no general protocol for the synthesis of chiral phosphorus compounds has been reported and developing a method is challenging since the P(V) bond formation mechanism is still not fully understood.[62–64]

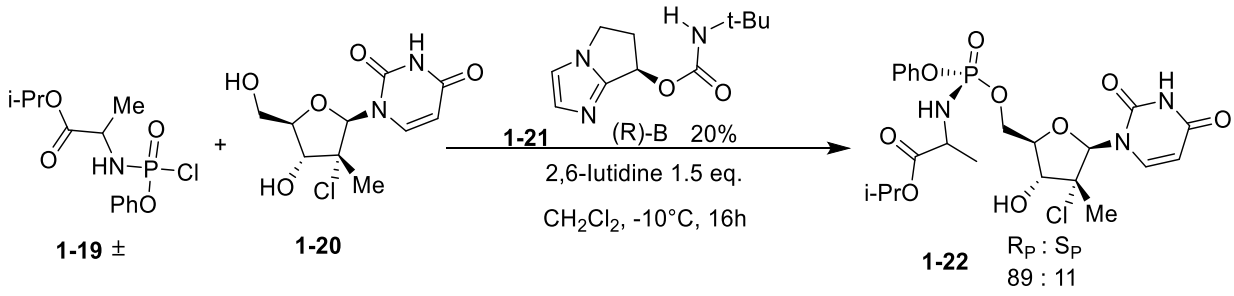

Scheme 1.4 Dynamic kinetic asymmetric transformation (DYKAT) towards the synthesis of ProTide™ nucleotides (**1-22**).[53]

1.4 Thesis Overview

Phosphate mimics have been developed to improve RNA therapeutic properties including stability to nuclease degradation, enhancement of binding affinity to complementary sequences, and improved cell membrane permeability. However, these modifications have added the structural complexity of a stereogenic phosphorus center. Stereochemically pure isomers exhibit differential activity in vitro and in vivo dependent on its enantiopurity.[30,65]

The main goal of this research is to synthesize P-stereogenic phosphate mimics in a stereocontrolled manner. Specifically, asymmetric nucleophilic catalysis has been investigated to provide enantio-enriched phosphonates using *H*-phosphonate (Chapter 2) and phosphoramidite approaches (Chapter 3) as shown in Scheme 1.5. Both approaches utilized commercially available chiral catalysts with the enantioselectivity determined by HPLC on a chiral stationary phase. The requisite starting materials, either phosphoramidites or *H*-phosphonates, have been prepared in racemic form and subsequently reacted with a variety of alcohols.

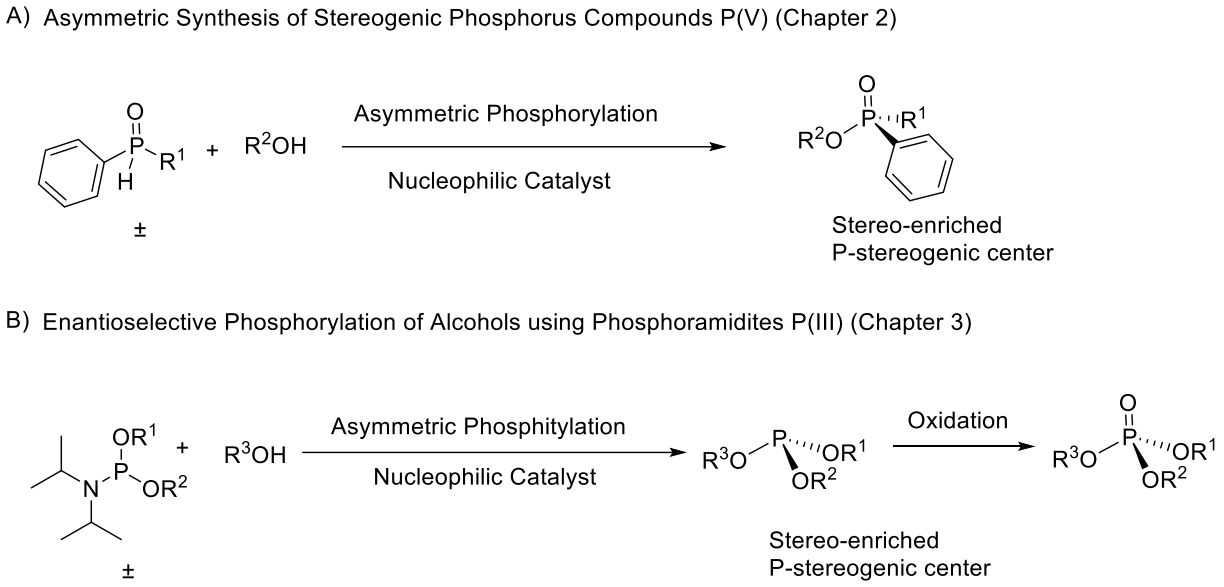

Scheme 1.5 Overview of the thesis

In chapter two, chiral phosphonate products were synthesized in excellent yield (up to 92%) and modest enantioselectivity (up to 62% *ee*) after identification of an appropriate chiral catalyst and optimization of the solvent, base, temperature, and stoichiometric additives. The potential applications of these approaches could be extended to P-chiral nucleotide analogs.

In chapter three, asymmetric phosphorylation using racemic phosphoramidites P(III) was carried out utilizing a chiral nucleophilic amine in catalytic amounts (10 mol %). Phenyl isocyanate was used during the reaction as an amine scavenger to increase the catalyst turnover. Many conditions were tested

involving the solvent, temperature, acid, and chiral nucleophilic catalyst. The catalyst (*S*)-5-(1-Boc-Pyrolidin-2-yl)1*H*-tetrazole (**3-16**) in CH_2Cl_2 at a reduced temperature was found to be the most selective conditions with enantioselectivities up to 23% and a modest phosphate yield (**3-15**) up to 49%. Based on the identification of a tetrazole as a requisite structure in the nucleophilic catalyst, the synthesis of a chiral cyclophane that contains a 1*H*-tetrazole moiety (**3-24**) was pursued to provide a novel catalyst structure. The target tetrazole **3-24** was synthesized in racemic form using a zinc bromide catalyzed [3+2] cycloaddition of a cyclophane nitrile with sodium azide albeit in poor yield (10%).

In chapter four, Phosphorus nuclear magnetic resonance (^{31}P NMR) spectroscopy was used for quantitative analysis of organic phosphorus in environmental samples. Preparation of samples for the ^{31}P NMR analysis, including pre- and post-treatment, extraction, and redissolving samples for the ^{31}P NMR experiment was conducted. To obtain quantitative data, the delay time, proton decoupling, and experiment length needed to be optimized. Sample pH was found to significantly affect the ^{31}P NMR resolution.

CHAPTER 2

2 ASYMMETRIC SYNTHESIS OF STEREOGENIC PHOSPHORUS P(V) CENTERS USING CHIRAL NUCLEOPHILIC CATALYSIS

2.1 Introduction

Organophosphorus compounds are common motifs in nucleotides,[30,49,66] pesticides,[67,68] herbicides[69,70] and flame retardants.[71] Commonly, phosphate mimics with tri, tetra, or pentacoordinate geometries, with unique substitutions, create a chirality center on the phosphorus atom as shown in Figure 2.1. These compounds normally have stable configurations, but their stabilities change corresponding to the coordination and the nature of the substitution around the phosphorus center.[72] Chiral phosphate mimics have been extensively utilized in transition metal catalysts,[73] as chiral reagents,[74–76] and in coordination chemistry.[77,78] Furthermore, compounds with stereogenic phosphate centers are of great interest in biological applications.[79] For example, using phosphorus-stereogenic analogues in antisense therapy improves potency, stability against enzymatic degradation, and bioavailability.[10] However, current nucleotide therapeutics are stereoisomeric mixtures. Previous studies have shown that nucleotide stereoisomers at phosphorus possess distinct therapeutic activities and physical properties.[30,80–82]

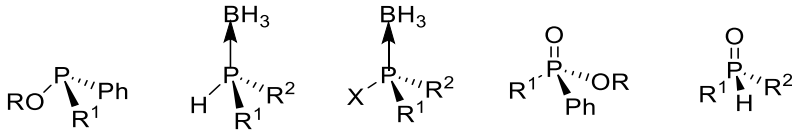

Figure 2.1 Structure of asymmetric phosphate mimics

Despite the importance of enantiopure P-stereogenic compounds, the chemical synthesis remains unsolved. Various strategies have been pursued using either P-O, P-N, or P-C bond formation to create a stereogenic center.[72] Traditionally, P-stereogenic centers have been synthesized using multi-step

approaches involving the transfer of achiral or prochiral phosphorus groups to chiral-pool amines and alcohols as seen in Scheme 2.1a. However, the desymmetrization of prochiral substrates is limited by substrate scope and modest stereoselectivity. [83]

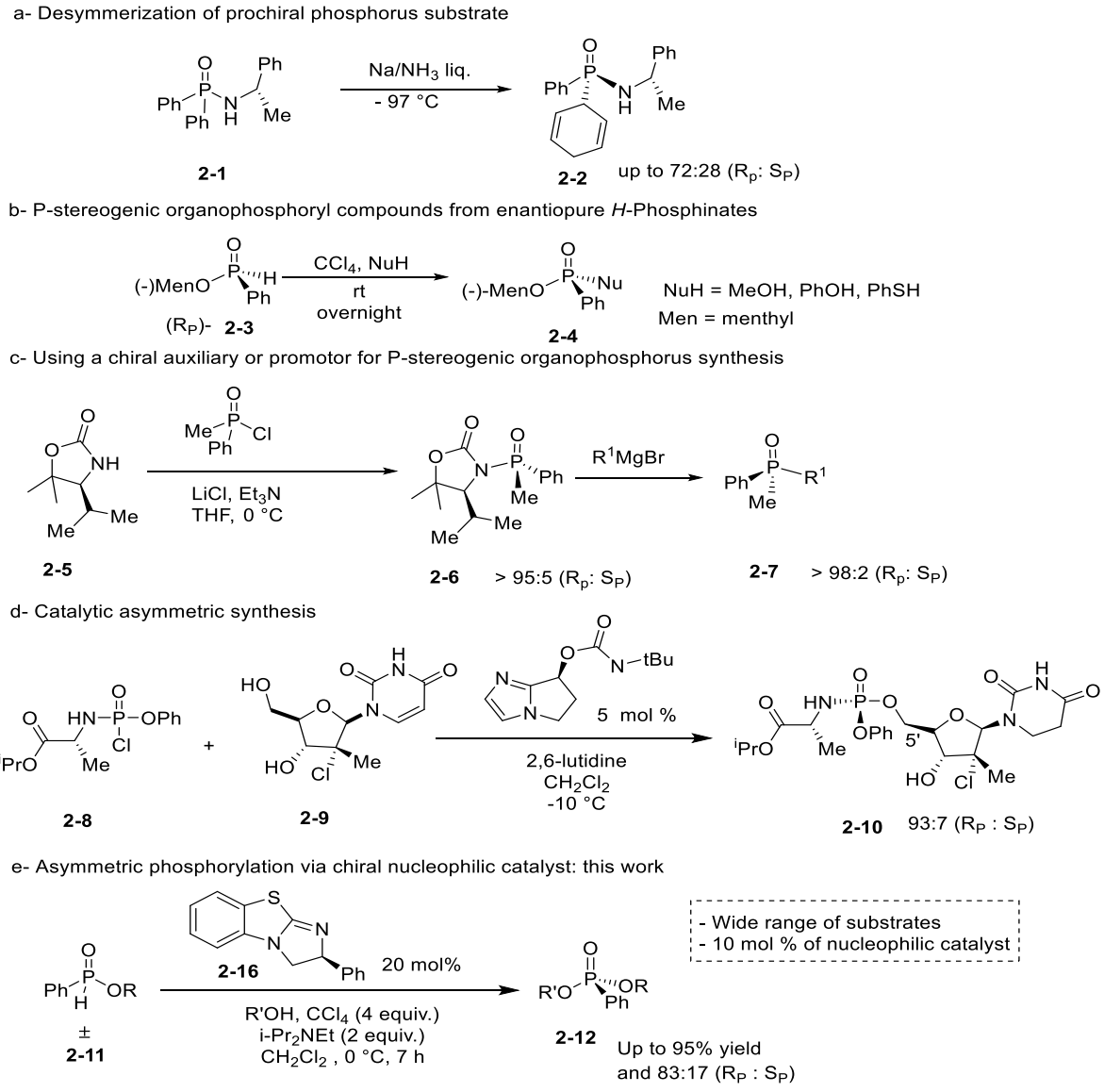

Scheme 2.1 Synthetic approaches towards P-stereogenic organophosphorus compounds. a) desymmerization of prochiral phosphorus substrate, b) P-stereogenic organophosphoryl compounds from enantiopure *H*-Phosphinates, c) Using a chiral auxiliary or promotor for P-stereogenic organophosphorus synthesis, d) Catalytic asymmetric synthesis, e) Asymmetric phosphorylation via chiral nucleophilic catalyst.

Another approach to chiral phosphorus centers involves the transformation of non-racemic *H*-phosphinates (**2-3**) to corresponding P-stereogenic compounds (**2-4**) through dehydrogenative coupling known as the Atherton-Todd reactions (Scheme 2.1b). Although *H*-Phosphonates cleanly transfer the stereochemistry to the product, construction of the enantiopure substrate often requires multiple synthetic steps.[84] Alternatively, a racemic phosphorus center can be coupled with a chiral auxiliary or promotor as shown Scheme 2.1c. However, the stoichiometric amount of chiral auxiliary is always required to achieve high stereoselectivity in the products. Moreover, a chiral auxiliary is covalently bonded to the product, necessitating subsequent chemical reactions and purifications to remove it from the desired product.[85]

In 2010, Jordan et al. synthesized a phosphate moiety through a highly-selective kinetic resolution using a chiral, peptide-based phosphorylation catalyst.[86] The chiral peptide was able to efficiently mimic enzymatic catalysts that phosphorylate nucleotides using nucleophilic activation, leaving group activation, and oxyanion-hole transition state stabilization.[87,88] However, this approach is limited in scope because each peptide is optimized for a single substrate. Based on this work, DiRoco et al. designed a general chiral nucleophilic catalyst for the synthesis of enantiopure prodrugs via a dynamic kinetic asymmetric transformation (DKAT) as seen in Scheme 2.1d.[53] The prodrug moiety contains an amino acid that makes hydrogen bonds to the nucleophilic catalyst to stabilize the transition state. Therefore, DiRoco's catalyst is limited to phosphates with amino acid substituents.[53] Other approaches to produce P-stereogenic compounds, that are not shown in scheme 2.1, include chiral-stationary phase separation and resolution using physical properties.[47,54,72,89,90]

To overcome the synthetic limitations found in the synthesis of P-stereogenic phosphate mimics, a DKAT utilizing a chiral nucleophilic catalyst was pursued (Scheme 2.1e). A racemic *H*-phosphinate moiety (**2-11**) can be coupled to nucleophilic alcohols under halogenation conditions to produce chiral

phosphonate products as shown in Scheme 2.1e. This general approach would utilize a catalytic amount of a chiral substance and a wide range of racemic phosphorus substrates could be used including nucleotides or prodrug structures.

2.2 Results and discussion

H-Phosphinates and phosphonate are useful precursors to a wide range of P-stereogenic compounds. [91–93] Therefore, racemic *H*-Phosphinate **2-13** was an ideal substrate to investigate the proposed DKAT using chiral nucleophilic catalysts. To obtain substrate **2-13**, esterification of phenyl phosphinic acid in neat isopropanol at an elevated temperature (138 °C) provides the product in 70% yield. Coupling of *H*-Phosphinate **2-13** with phenol (**2-14**) under halogenation conditions (CCl_4, 4 equiv.) provides the phosphonate product (**2-15**) in 76% yield. Stoichiometric amounts of *N,N*-diisopropylethyl amine are included to consume the HCl byproduct of the halogenation product.

Using the optimized conditions for the racemic formation of **2-15**, a wide a variety of chiral nucleophilic catalysts were screened to quantify the enantiomeric enrichment of the phosphorus center (Scheme 2.2). Using the catalyst developed by DiRoco et al. (**2-18** and **2-19**) minimal stereoselectivity (-9% *ee* and 8% *ee* respectively) was observed.[53] The suboptimal enantioselectivities are likely due to the remote chiral site being unable to effectively induce asymmetry in substrates that do not possess a H-bonding functionality. Planar-chiral catalyst **2-20**, known as Fu's catalyst, is a ferrocene analogue of 4-diethylaminopyridine (DMAP) with high nucleophilicity and low steric hindrance at the nucleophilic nitrogen atom.[94] The product **2-15** was obtained with an improved selectivity of 34% *ee* and a moderate yield of 45%. Alternative heterocyclic nucleophilic catalysts **2-21** and **2-22** provide similar enantioselectivities (-24% and 11% *ee*) and chemical yields (38% and 42%). Chiral thiourea **2-23**, which does not operate as a nucleophilic catalyst, does not induce significant levels of stereoselectivity (10% *ee*) while resulting in a dramatically diminished yield of 14%. Despite limited success with common

nucleophilic catalysts, the results demonstrate the enantiomeric enrichment was significantly impacted by catalyst structure.

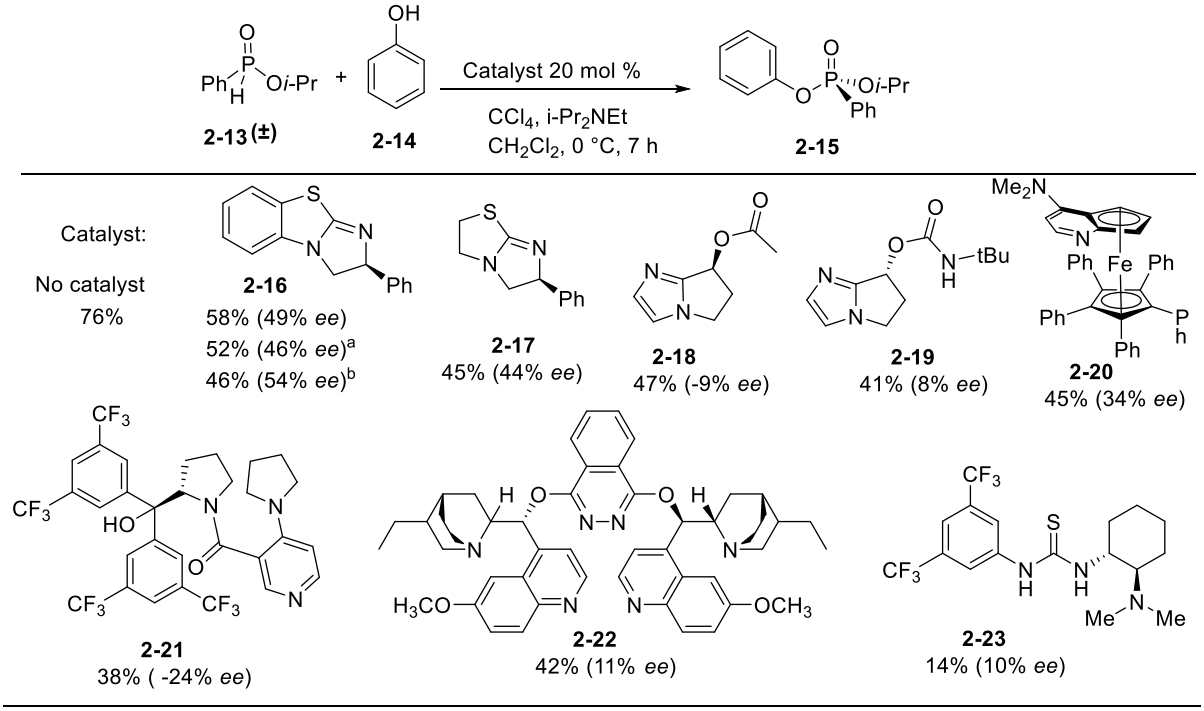

Conditions: **2-13** (1 equiv.), CCl_4 (4 equiv.), PhOH (0.5 equiv.) *i*-Pr_2NEt (2 equiv.), Cat. 20 mol %, CH_2Cl_2 (0.1 M solution), 7 h; Enantiomeric excess (*ee*) was determined by HPLC analysis; [a] catalyst 10 mol %; [b] catalyst 50 mol %.

Scheme 2.2 Nucleophilic catalysts investigated. Yield and enantiomeric excess of isolated products are given.

Benzotetramisole (BTM, **2-16**) was originally developed by Briman et al for the kinetic resolution of alcohols and is now commercially available.[95–97] BTM was tested in the standard *H*-Phosphinate coupling of **2-13** and **2-14** under halogenation conditions and was found to produce the highest levels of enantioselectivity. Specifically, 20 mol % of (*S*)-BTM produced phosphonate **2-15** in 58% yield and 49% *ee* (Scheme 2.2). Increasing the catalyst loading from 10 mol % to 20 mol % to 50 mol % resulted in small increases in enantioselectivity of 46%, 49%, and 54% *ee* respectively. Structurally similar Tetramisole (**2-**

17) is a capable catalyst providing **2-15** in 45% yield and 44% *ee*. Mechanistically, we envisioned the nucleophilic BTM catalyst becoming covalently bonded to the phosphoryl center while facilitating racemization to produce the observed enantioenrichment. Consequently, BTM was identified as the optimal catalyst for the DKAT of racemic *H*-phosphinates into chiral phosphonates.

In order to optimize the yield and enantioselectivity of **2-15**, the effect of the base was investigated and results are shown in Table 2.1. As established in the catalyst screen, *N,N*-diisopropylethylamine (DIPEA) has the highest enantioselectivity (49% *ee*) and a respectable yield of 58% (Table 2.1**,** Entry 7). Among the investigated bases, potassium tert-butoxide (KOtBu) provided the highest chemical yield of 63%, but with near-complete loss of enantioselectivity (7% *ee*). Non-nucleophilic amine bases, including DBU, ABCO and DABCO, provided **2-15** with diminished enantioselectivities of 20% *ee*, 30% *ee* and 33% *ee* respectively. The starting material was recovered and no product was observed when using hindered bases such as proton sponge (1,8-bis(dimethylamino)naphthalene) or di-*tert*-butyl pyridine (Table 2.1 Entries 5 and 6). All other reactions showed complete consumption of *H*-phosphine starting material and no ongoing product formation as judged by ^{31}P NMR.

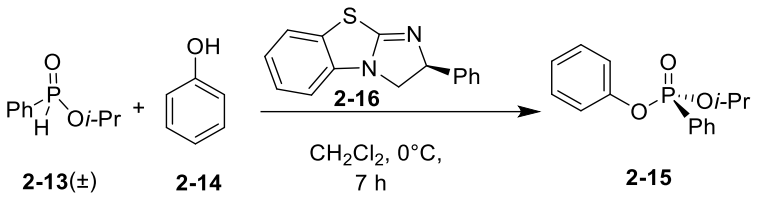

Table 2.1 Base effects on the reaction conditions.

Entry[a]	Base	pKa in DMSO*	Yield (%)[b]	*ee* (%)[c]
1	KOtBu	19.2[98]	60	7
2	DBU	12[98]	63	20
3	ABCO	9.8[99]	50	32
4	DABCO	2.97, 8.93[99,100]	15	33
5	Proton Sponge	7.50[100]	0	---
6	DTBP	0.81[101]	0	---
7	DIPEA	9[98]	58	49

[a]Conditions: **2-13** (1 equiv.), CCl_4 (4 equiv.), PhOH (1 equiv.), Base (2 equiv.), **2-16** (20 mol %), CH_2Cl_2 (0.1 M solution), 7 h; [b]Yields were determined by HPLC analysis; [c]*ee* values were determined by HPLC analysis. KOtBu, Potassium *tert*-butoxide; DBU, 1,8-Diazabicyclo [5.4.0] undec-7-ene; ABCO, Quinuclidine; DABCO, 1,4-diazabicyclo[2.2.2]octane; Proton Sponge, 1,8-Bis(dimethylamino)naphthalene; DTBP, Di-*tert*-butyl pyridine; DIPEA*, N,N*-diisopropylethylamine.* pKa was shown for conjugate acid.

After identifying *N,N*-diisopropylethylamine as the optimal base, the effect of solvent and temperature were evaluated and results are shown in Table 2.2. A nonpolar solvent, toluene, results in nearly identical enantioselectivity, when compared to the standard solvent methylene chloride, except with a dramatic decrease in yield to 17%. In contrast, acetonitrile reduced the enantioselectivity to 26 % *ee*, but formed the product in similar efficiency (47%) to methylene chloride. Interestingly, production of **2-15** is nearly eliminated when using tetrahydrofuran (THF) with respectable recovery of starting material.

After confirming dichloromethane as a suitable solvent for the DKAT, temperature effects on enantioselectivity were explored. Phosphorylation of **2-14** at -40 °C, 0 °C and 25 °C respectively resulted in enantioselectivities of 44%, 49%, and 45% *ee* respectively. Therefore, the optimal temperature was determined to be 0 °C, but a smaller than expected influence on enantioselectivity was observed. In addition, the product was obtained in the highest yield at 0 °C (58%), while increasing or decreasing the temperature results in a reduction in yield.

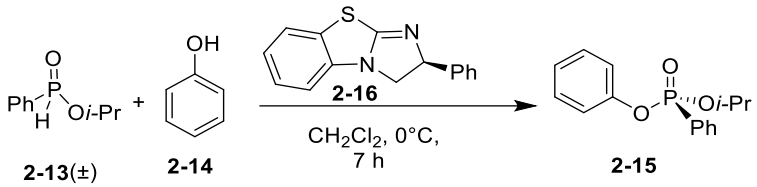

Table 2.2 Effect of solvent and temperature on the phosphorylation reaction

Entry[a]	Solvent	T (°C)	Yield (%)[b]	*ee* (%)[c]
1	THF	0	4	55
2	Toluene	0	17	51
3	CH_3CN	0	47	26
4	CH_2Cl_2	0	58	49
5	CH_2Cl_2	25	53[d]	45
6	CH_2Cl_2	-40	7[e]	44

[a]Conditions: **2-13** (1 equiv.), CCl_4 (4 equiv.), PhOH (1 equiv.), *i*-Pr_2NEt (2 equiv.), **2-16** (20 mol %), solvent (0.1 M solution)**,** 7 h; [b] Yields were determined by HPLC analysis; [c]*ee* values were determined by HPLC analysis; [d]2 hours; [e]16 hours.

To assess the *H*-phosphinate substrate scope, the alcohol and the aryl group were varied a coupled with phenol under the optimized reaction conditions (Table 2.3). Of note, the experiments in Table 2.3 were performed with an altered stoichiometry (0.5 equiv. of alcohol) to improve the enantioselectivity of the transformation at the expense of chemical yield. The products (**2-25** – **2-28**) of

ethyl substituted *H*-phosphinates are obtained in comparable enantioselectivities, but with typically higher yield due to the decreased steric environment around the phosphorus center (Table 2.3 Entry 3-6). As an aside, the HPLC elution order of methyl-substituted phosphonate (**2-24)** was reversed compared to other synthetic phosphonate analogues due to indeterminate interactions with the stationary phase (Figure C3 in appendix C). Modulation of the aromatic group on the *H*-Phosphinate was also investigated. When dramatically altering the steric environment around the phosphorus by replacing the phenyl group with an o-tolyl (Entries 3 and 4), the yield is unsurprisingly decreased from 95% to 67%. Similarly, the increased steric hindrance did not improve the enantioselectivity. Additionally, electronic effects were studied by substituting the phenyl group with a 4-methoxy- and a 4-fluoro-phenyl group, respectively. A decline in enantioselectivity to 22% *ee* was obtained with both the electron-withdrawing and donating substituents as shown in Table 2.3 Entries 5 and 6. The substrate scope for the *H*-phosphinate coupling was found to be very sensitive to the steric and electronic environment around the phosphorus center with improved yields and enantioselectivities observed than the model substrate (**2-13**), but with highly varied results even under the optimized conditions.

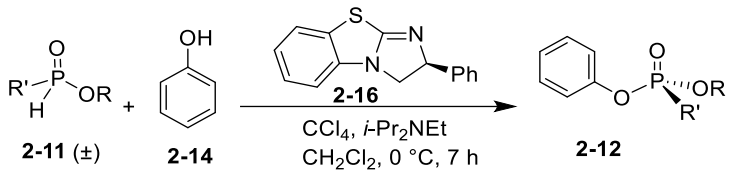

Table 2.3 Effect of electrophile on phosphorylation reaction

Entry[a]	R	R'	Product	Yield[b](%)	*ee*[c](%)
1	i-Pr	Ph	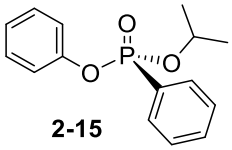 **2-15**	47 40[d]	55 -54[d]
2	Me	Ph	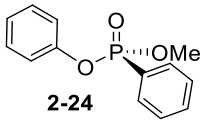 **2-24**	33	61
3	Et	Ph	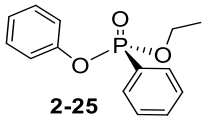 **2-25**	95	62
4	Et	2-MePh	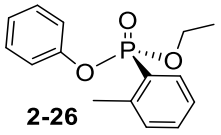 **2-26**	67	48
5	Et	4-OMePh	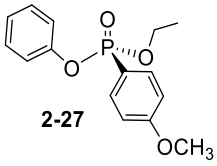 **2-27**	88	22
6	Et	4-F-Ph	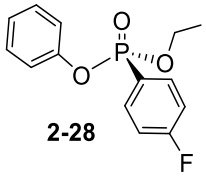 **2-28**	93	22

[a]Conditions: **2-11** (1 equiv.), CCl_4 (4 equiv.), PhOH (0.5 equiv.), *i*-Pr_2NEt (2 equiv.), **2-16**. 20 mol %, CH_2Cl_2 (0.1 M solution)**,** 7 h; [b]Isolated yield; [c]*ee* values were determined by HPLC analysis; [d](*R*)-(**2-16**) was used.

In the process of exploring the substrate scope in Table 2.3, known compounds **2-24** and **2-25** were prepared to correlate the observed enantioselectivity to an absolute configuration. High Performance Liquid Chromatography (HPLC) on a chiral stationary phase was used to measure all enantioselectivities reported. As seen in Figure 2.2, using a normal phase eluent of hexane and ethanol

with 0.1% trifluoroacetic acid (TFA) baseline resolves a racemic sample of **2-25** (red trace) formed when no chiral catalyst is used. The enantioenriched product from **Table 2.3** Entry 3 shows the correlating imbalance in peak areas (62% *ee*) when using (-)- or (*S*)-benzotetramisole (Figure 2.2, black trace). Correspondingly, the enantioenriched product from **Table 2.3** Entry 3 has a measured $[\alpha]_D^{20}$ of +21.7° (c 0.429, $CHCl_3$). Using the published data and sign for (*R*)-**2-25** ($[\alpha]_D^{20}$ +34.4° (c 2.16, $CHCl_3$), we observe that (*S*)-BTM produces the (*R*) enantiomer of **2-25** as the major product.[102] In addition, (*R*)-**2-24** was produced using (*S*)-BTM and agrees with reported values.[102] Finally, when the enantiomer of the catalyst ((*R*)-**2-16**) was used to synthesize **2-15**, a near-equal yield but opposite enantioselectivity (-54% *ee*) was observed, as expected.

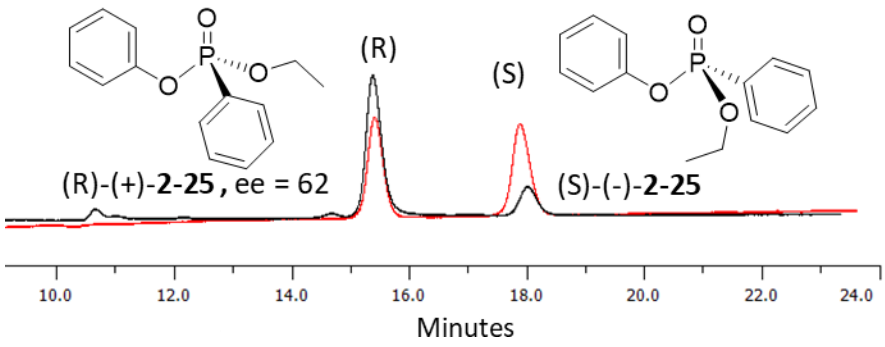

Figure 2.2 HPLC chromatogram of racemic (red) and chiral phosphonate analogues (black) of (**2-25)** using (*S*)-**2-16**. *Conditions.* Phenomenex Lux Amylose-2 chiral column (250 X 4.6 mm), eluent = hexane: ethanol (15 : 95 to 20 : 80) with 0.1% TFA, detection = 254 nm, flow rate = 0.5 ml/min, temperature = 25 °C.

Using catalyst (*S*)-**2-16**, a number of alcohols were tested as nucleophiles in the phosphorylation reaction to produce the corresponding phosphonates in Table 2.4. Our standard phosphorylation reaction utilized an aromatic alcohol (**2-14**) as a nucleophile so it was encouraging that BTM was an effective catalyst for alcohols like allyl, benzyl, methyl, or phenethyl alcohol. Under the optimized conditions, allyl alcohol, which differs greatly in structure from phenol, reacted with isopropyl-*H*-phosphinate in similar efficiency (49% yield and 43% *ee*). Small decreases in enantioselectivity (28% and 35% *ee*) were observed

when using phenethyl alcohol or benzyl alcohol as nucleophiles, but comparable yields were obtained. Under the optimized reaction conditions, *S*-BTM (**2-16**) provided the same stereochemical outcome of the (*R*)-phosphonate analogues in Table 2.4. However, due to Cahn-Ingold Prelog rules the priority of the substituents on phosphorus changed and resulted in the formation of (*S*)-**2-31** – (*S*)-**2-34**. Finally, even when using sterically unencumbered, methanol, the product (**2-34**) yield and enantioselectivity were not decreased (56 % yield and 51% *ee*). Similar to compound **2-24**, the HPLC elution order of the methyl phosphonate analogue (**2-34)** was reversed from the normal pattern (Appendix Figure C13). Moreover, (*S*)-**2-34** had a positive specific optical rotation of +0.1856° (c 0.5388, $CHCl_3$), which is consistent with analogous phosphonates.[103]

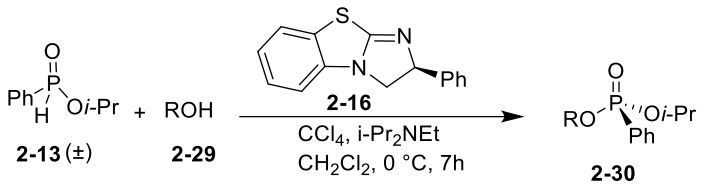

Table 2.4 Effect of the nucleophile on the phosphorylation reaction

Entry[a]	ROH	Product	Yield[b] (%)	*ee* (%)[c]
1	Phenol	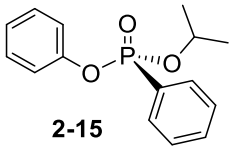 **2-15**	47	55
2	allyl alcohol	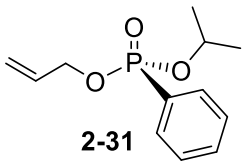 **2-31**	49	43
3	2-phenethyl alcohol	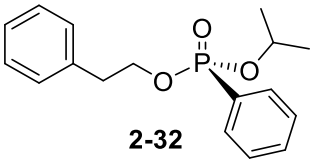 **2-32**	68	28
4	Benzyl alcohol	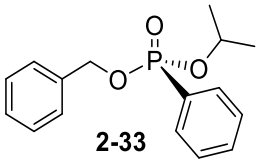 **2-33**	51	35
5	Methanol	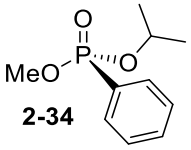 **2-34**	56	51

[a]Conditions: **2-13** (1 equiv.), CCl_4 (4 equiv.), alcohols (0.5 equiv.), *i*-Pr_2NEt (2 equiv.), **2-16** (20 mol %), CH_2Cl_2 (0.1 M solution)**,** 7h; [b]Isolated yield; [c]*ee* values were determined by HPLC analysis.

The (-)-bezotetramisole (**2-16**) has offered the highest yield and enantioselectivity among the nucleophilic catalysts tested. From a structural point of view, the chiral center is in close proximity to the nucleophilic nitrogen but is not too hindered to suppress nucleophilic catalysis (Figure 2.3). The adjacent sulfur and nitrogen atoms are a necessary component of the BTM catalyst by contributing greatly to the

nucleophilicity. In contrast, the aromatic ring is sparsely substituted and provides the ability to modulate the reactivity of the benzotetramisole structure for future catalyst development.

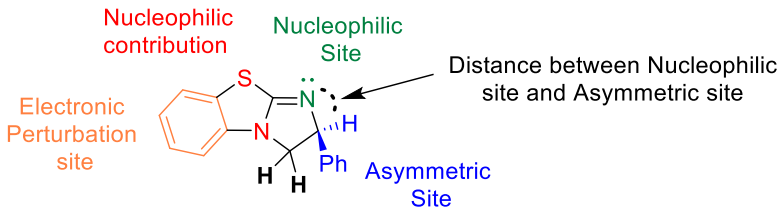

Figure 2.3 Structural analysis of asymmetric catalyst **2-16**

Based on the Atherton-Todd reaction, a mechanism is proposed that explains the formation of enantioenriched phosphonates (**2-25**) using the chiral nucleophilic catalyst **2-16**.[104] First, chlorination of the *H*-phosphine moiety (**2-35**) using tetrachloromethane, as the stoichiometric oxidant result in the formation of racemic phosphonochloridate **2-36** (Scheme 2.3). While monitoring the reaction using ^{31}P NMR, a species (29.3 ppm) consistent with a phosphonochloridate (**2-36**) was observed with concomitant consumption of the *H*-phosphinate.[105] Next, catalyst (*S*)-(**2-16**) attacks the phosphonochloridate and results in diastereomers **2-37** and **2-38** after substitution of the chlorine. Unfortunately, ^{31}P NMR did not allow unambiguous identification of an intermediate where the BTM catalyst was bonded to the phosphoryl center. Substitution reactions at the phosphorus atom typically involve either 1) a dissociative S_N1-type mechanism through the formation of stable metaphosphate (PO_3^-) or 2) an associative, two-step addition-elimination mechanism through the formation of a phosphorane intermediate.[36] In this case, the elementary steps of the substitution process are inconsequential to the product outcome.

Nucleophilic addition by phenol forms pentavalent intermediates **2-39** and **2-40**. Additional pentavalent intermediates are likely formed in the reaction but not shown in Scheme 2.3. Elimination of the BTM catalyst from the apical position of intermediate **2-39** provides the observed product **2-25** in the observed (*R*) configuration.[36] Elimination from pentavalent **2-39** is preferrable to elimination from **2-40**

because steric interactions between the phenyl groups on the phosphonate and the catalyst (*S*)-(**2-16**) are avoided. Alternatively, the stereoselectivity could be a result of π-π or π-cation interactions between the catalyst and phosphorus substrate analogous to previously published acylation studies with **2-16**.[95] It is known in the literature that trigonal bipyramidal phosphorus centers, such as **2-39** and **2-40**, readily undergo pseudorotation and provide an equilibration mechanism consistent with the dynamic kinetic transformation observed.[36] Alternatively, as mentioned above this could not be spectroscopically observed. Thus, enantiomeric enrichment is a result of the faster elimination ($k_1 > k_2$) of **2-39** and constitutes the stereodetermining step.

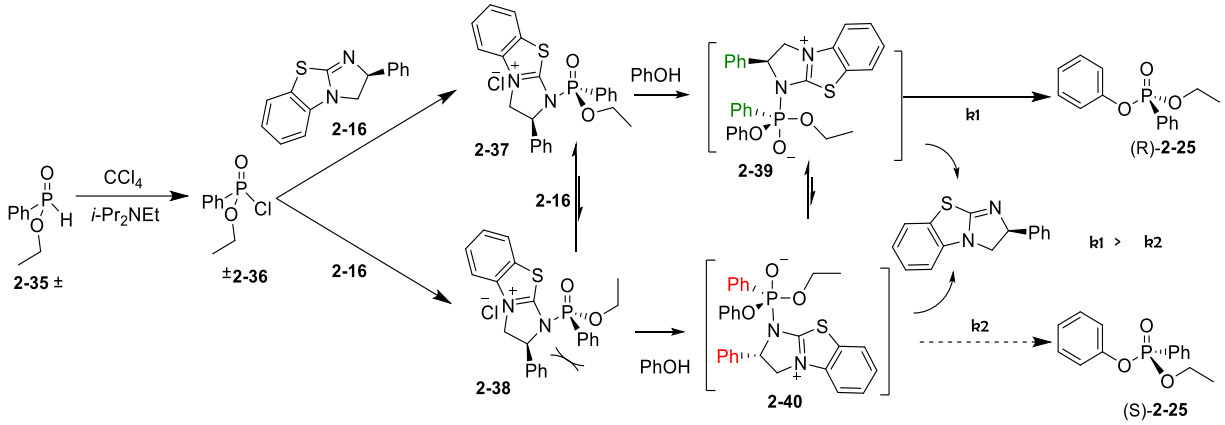

Scheme 2.3 Proposed asymmetric phosphorylation mechanism based on the dynamic kinetic asymmetric transformation of *H*-phosphinate **2-35** to phosphonate into (*R*)-**2-25** and (*S*)-**2-25** using chiral nucleophilic catalyst **2-16**.

Collectively, the reaction stereoselectivity was dependent on the solvent, catalyst structure & loading, and the nature of the base. The proposed mechanism explains the enantioselectivity dependence on the reaction conditions perturbing the relative rates of elimination (k_1, k_2). The similarity of these rates of elimination result in the modest stereoselectivity observed in this study. In contrast, the enantioselectivity was largely unaffected by reaction temperature indicating kinetic control was observed

as opposed to thermodynamic control. Finally, the proposed reaction mechanism in Scheme 2.3 shows the selective formation of the (*R*)-phosphonate using (*S*)-(-)-benzotetramisole catalyst (**2-16**) consistent optical rotations and absolute configurations.[102] Modifying the BTM catalyst, by increasing the steric hindrance of the phenyl group or electronically perturbing the fused benzo- system, may provide an opportunity to improve the stereoinduction.

2.3 Conclusion

A dynamic kinetic transformation that produces stereogenic-phosphorus centers using an asymmetric nucleophilic catalyst was developed. Alcohols, both aliphatic and aromatic, were coupled to racemic *H*-phosphinates under halogenation conditions. After optimization of the solvent, base temperature and catalyst loading, benzotetramisole was observed to provide asymmetric phosphonates in acceptable yield (33% - 95%) with moderate enantioselectivity (up to 62% *ee*). The reaction conditions were tolerant to a variety of alcohol and *H*-phosphinate substrates. Furthermore, a mechanism of selective phosphorylation was proposed that accounts for the stereoselectivity. Future development of the benzotetramisole catalyst could improve enantioselectivity and enable the synthesis of prodrugs for pharmaceutical or biological application.

2.4 Materials and Methods

2.4.1 General information

All reactions were carried out under a nitrogen atmosphere in oven-dried glassware. The products were purified by flash column chromatography using silica gel 60 (230-400 mesh Silicycle, Quebec, Canada). Solvent, reagents, and chemicals were received from a commercial vendor and further dried under activated 4 Å molecular sieves. Methylene chloride and THF were dried using the PURE SOLV MICRO purification system. Thin-layer chromatography (TLC) analysis was performed on Merck 0.25 mm silica gel

60 F254 plates. ^{1}H-NMR was recorded using an Oxford Varian Unity Instrument at 400 MHz and referenced using the residual solvent peak of $CDCl_3$ at 7.26 ppm. ^{13}P NMR spectra were acquired at 162 MHz and externally referenced to 85% H_3PO_4 at (0 ppm). The ^{13}C NMR were acquired at 101 MHz and referenced to 77.1 ppm for $CDCl_3$ solvent. The NMR data were processed with MestReNova11 NMR software. HPLC was performed using the Gilson GX-271 instrument at 254 nm with Trilution LC software V3. Analytical HPLC was carried out using a 5 μm 250 x 4.6 mm Phenomenex Lux chiral column (Amylose-2 or Cellulose-2). In analytical HPLC, the normal phase separation method used was: eluent hexane: ethanol (15 : 95 to 20 : 80) with 0.1% TFA, detection (254 nm), flow rate (0.5 ml/min), temperature (25 °C) and run time (20 minutes). Mass spectra were measured by University of Illinois Mass Spectrometry Laboratory using electrospray ionization technique (ESI). The optical rotations were measured for purified sample using digital polarimeter JASCO (model DIP-370). Specific rotation ($[\alpha]_D^{20}$) was reported for samples in solution at 20 °C in which the symbol D represents the sodium D line with wavelength of light is 589 nanometers and concentration in units of g/100ml.

2.4.2 Isopropyl phenyl-*H*- phosphinate (2-13)

A mixture of phosphinic acid (1.000 g, 7.04 mmol, 1 equiv.) and isopropanol (10 ml, 0.131 mol, 18.6 equiv.) was stirred in a well-sealed, 20 ml vial for 15 hours at 138 °C. Then, the solvent was evaporated under vacuum. The crude product was purified using silica gel column chromatography with 5% MeOH: 95% CH_2Cl_2 as an eluent to provide a colorless oil in 70% yield (0.90 g). The NMR data matched previously published results.[106] ^{1}H NMR (400 MHz, $CDCl_3$) δ 7.81 – 7.70 (m, 2H), 7.59 (d, J = 558.7 Hz, 1H, PH), 7.60-7.52 (m, 1H), 7.52 – 7.44 (m, 2H), 4.73 – 4.67 (m, 1H, OCH), 1.41 (d, J = 6.1 Hz, 3H, CH_3), 1.33 (d, J = 6.1 Hz, 3H, CH_3). ^{13}C NMR (101 MHz, $CDCl_3$) δ 133.1 (d, J = 2.9 Hz), 131.0 (d, J = 11.9 Hz), 130.6 (d, J = 133.0 Hz),

128.8 (d, J = 13.9 Hz), 71.5 (d, J = 5.5 Hz), 24.4 (d, J = 4.5 Hz), 24.0 (d, J = 4.2 Hz).[31]P NMR (162 MHz, $CDCl_3$) δ 22.5 (d, J = 21.5 Hz).

2.4.3 Ethyl Phenyl-*H*-phosphinate (2-35)

A mixture of phosphinic acid (1.00 g, 7.04 mmol, 1 equiv.) in ethanol (10 ml, 0.171 mol, 24.4 equiv.) was stirred in a well-sealed, 20 ml vial for 15 hours at 133 °C. Then, the solvent was evaporated under vacuum. The product was purified by flash silica gel column chromatography using 5% MeOH: 95% CH_2Cl_2 as an eluent to produce a colorless oil in 55% yield (0.65 g). The NMR data matched previously published results.[91] [1]H NMR (400 MHz, $CDCl_3$) δ 7.74 (m, 2H), 7.59–7.51 (m, 1H), 7.54 (d, J = 562.5 Hz, 1H, PH), 7.50 – 7.42 (m, 2H), 4.17 – 4.05 (m, 2H), 1.33 (t, J = 7.1 Hz, 3H).[13]C NMR (101 MHz, $CDCl_3$) δ 133.2 (d, J = 2.8 Hz), 131.0 (d, J = 11.9 Hz), 129.9 (d, J = 132.3 Hz), 128.9 (d, J = 13.9 Hz), 62.3 (d, J = 6.5 Hz), 16.5 (d, J = 6.5 Hz). [31]P NMR (162 MHz, $CDCl_3$) δ 24.96 (d, J = 19.3 Hz).

2.4.4 Methyl Phenyl-*H*-phosphinate (2-40)

A mixture of phosphinic acid (1 g, 7.04 mmol, 1 equiv.) in methanol (15 ml, 0.370 mol, 52.9 equiv.) was stirred in a well-sealed, 20 ml vial for 15 hours at 125 °C. Then, the solvent was evaporated under vacuum. The crude product was purified by flash silica gel column chromatography using 5% MeOH: 95% CH_2Cl_2 as an eluent to produce a colorless oil in 62% yield (0.68 g). The NMR data matched previously published results.[107] [1]H NMR (400 MHz, $CDCl_3$) δ 7.85 – 7.73 (m, 2H), 7.65–7.56 (m, 1H), 7.56 (d, J = 565.8 Hz, 1H, PH), 7.55 – 7.47 (m, 2H), 3.79 (d, J = 12.0 Hz, 3H).[13]C NMR (101 MHz, $CDCl_3$) δ 133.4 (d, J = 2.8 Hz), 131.2 (d, J = 11.9 Hz), 130.3 (d, J = 47.2 Hz), 129.0 (d, J = 13.8 Hz), 52.3 (d, J = 6.6 Hz).[31]P NMR (162 MHz, $CDCl_3$) δ 27.46 (d, J = 21.6 Hz).

2.4.5 Ethyl (2-methylphenyl)-*H*-phosphinate (2-41)

A solution of $P(OEt)_3$ (0.970 g, 5.84 mmol, 1 equiv.) in diethylether (0.71 ml) was added dropwise under N_2 to a solution of o-tolyl magnesium bromide (5.14 ml, 2 M, 10.28 mmol, 1.75 equiv.) in diethyl ether. After stirring the mixture at 34 °C for 5 hours, a solution of 1 M HCl is added at room temperature until the pH of the solution was 2. After stirring the mixture for another hour, the mixture was extracted with ethyl acetate (2 ml x 4). The combined organic layers were dried over $MgSO_4$. The solvent was removed under reduced pressure and purified by flash chromatography on silica gel using (5% MeOH: 95% CH_2Cl_2) to give an oily product in 63% yield (0.675 g). ^{1}H NMR (400 MHz, $CDCl_3$) δ 7.77 (m, 1H), 7.60 (d, J = 555.1 Hz, 1H, PH), 7.48 – 7.40 (m, 1H), 7.29 (m, 1H), 7.26–7.19 (m, 1H), 4.13 (m, J = 8.8, 7.1 Hz, 2H), 2.53 (s, 3H), 1.34 (t, J = 7.1 Hz, 6H). 13C NMR (101 MHz, $CDCl_3$) δ 141.2 (d, J = 10.8 Hz), 133.1 (d, J = 3.2 Hz), 132.1 (d, J = 7.2 Hz), 131.3 (d, J = 5.0 Hz), 128.2 (d, J = 131.1 Hz), 126.0 (d, J = 14.1 Hz), 62.2 (d, J = 6.0 Hz), 20.1 (d, J = 6.9 Hz), 16.5 (d, J = 3.1 Hz).^{31}P NMR (162 MHz, $CDCl_3$) δ 25.93 (d, J = 14.8 Hz).

2.4.6 Ethyl (4-methoxyphenyl)-*H*-phosphinate (2-42)

A solution of $P(OEt)_3$ (0.1 g, 0.602 mmol, 1 equiv.) in THF (1.2 ml) was added dropwise under N_2 to a solution of 4-methoxyphenylmegnesium-bromide (1.8 ml, 0.5 M, 0.900 mmol, 1.5 equiv.) in THF. After stirring the mixture at 66 °C for 5 hours, a solution of 1 M HCl is added at room temperature until the pH of the solution is 2. After stirring the mixture for another hour, the mixture was extracted with ethyl acetate (2 ml x 4). The combined organic layers were dried over $MgSO_4$. The solvent was removed under reduced pressure and purified by flash chromatography on silica gel using (5% MeOH: 95% CH_2Cl_2) to give an oily product in 87% yield (105 mg). The NMR data matched previously published results.[91] ^{1}H NMR (400 MHz, $CDCl_3$) δ 7.76 – 7.64 (m, 2H), 7.54 (d, J = 561.7 Hz, 1H, HP), 7.00 (m, 2H), 4.16 – 4.08 (m, 2H), 3.85 (s, 3H),1.36 (t, J = 7.1 Hz, 3H). ^{13}C NMR (101 MHz, $CDCl_3$) δ 163.5 (d, J = 3.2 Hz), 133.2 (d, J = 13.2 Hz), 121.3

(d, J = 138.8 Hz), 114.5 (d, J = 14.9 Hz), 61.9 (d, J = 6.4 Hz), 55.6 – 55.5 (m), 16.6 (d, J = 6.6 Hz) ^{31}P NMR (162 MHz, $CDCl_3$) δ 23.68 (d, J = 17.1 Hz).

2.4.7 Ethyl (4-fluorophenyl)-*H*-phosphinate (2-43)

A solution of $P(OEt)_3$ (0.5 g, 3.01 mmol, 1 equiv.) in THF (3.67 ml) was added dropwise under N_2 to solution of 4-fluoro magnesium bromide (4.5 ml, 0.8 M, 3.60 mmol, 1.2 equiv.) in THF. After stirring the mixture at 66 °C for 12 hours, a solution of 1 M HCl is added at room temperature until the pH of the solution is 2. After stirring the mixture for another hour, the mixture was extracted with ethyl acetate (2 ml x 4). The combined organic layers were dried over $MgSO_4$. The solvent was removed under reduced pressure and purified by flash chromatography on silica gel using (5% MeOH: 95% CH_2Cl_2) to give an oily product in 27% yield (153 mg). The NMR data matched previously published results.[91] ^{1}H NMR (400 MHz, $CDCl_3$) δ 7.81 – 7.73 (m, 2H,), 7.55 (d, J = 567.1 Hz, 1H, PH) 7.18 (m, 2H), 4.27 – 4.06 (m, 2H, OCH_2),1.36 (t, J = 7.1 Hz, 3H, CH_3). ^{13}C NMR (101 MHz, $CDCl_3$) δ 167.2 (d, J_{CP}= 3.2 Hz), 164.7 (d, JCF= 3.4 Hz), 133.8 (dd, JCP= 22.2 Hz JCF = 4.1 Hz), 127.6 (dd, JCP = 7.3 Hz, JCF= 7.9 Hz), 116.4 (dd, JCP= 36.7 Hz, JCF = 6.5 Hz), 62.4 (d, JCP = 6.2 Hz), 16.5 (d, JCP= 6.6 Hz)^{31}P NMR (162 MHz, $CDCl_3$) δ 23.48 (d, J = 18.0 Hz).

2.4.8 General procedure for Isopropyl (Alkyl)- phenyl-phosphonate

To a 7 mL reaction vial under an atmosphere of N_2 was added isopropyl phenyl-*H*-phosphinate (**2-13**) (0.1 g, 0.543 mmol, 1 equiv.) and carbon tetrachloride (0.210 mL, 2.17 mmol, 4 equiv.). Next, anhydrous CH_2Cl_2 (0.3 M solution) was added and the solution cooled to 0 °C. A solution of *N,N*-diisopropylethylamine (0.14 g, 1.08 mmol, 2 equiv.), benzotetramisole (**2-16**) (0.027g 0.11 mmol, 0.2 equiv.), and an alcohol (0.27 mmol, 0.5 equiv.) that was previously dried over 4 Å molecular sieves, in anhydrous CH_2Cl_2 (0.3 ml) was prepared. The alcohol solution was added dropwise to the original phosphinate solution and stirred for 9 hours at 0 °C. The mixture quenched with 1M HCl (1 ml) and extracted three times with ethyl acetate then

dried using $NaSO_4$. The product was purified by silica gel chromatography with ethyl acetate: hexane (30:70) as an eluent. The following products were synthesized.

2.4.8.1 (*R*)-Isopropyl (Phenyl)-phenyl-phosphonate (2-15)

Yield 35 mg (47%). The NMR data were matched for previously published results.[79] ^{1}H NMR (400 MHz, $CDCl_3$) δ 7.89 – 7.82 (m, 2H), 7.56 – 7.50 (m, 1H), 7.47 – 7.41 (m, 2H), 7.25 (t, J = 7.9 Hz, 1H), 7.16 – 7.12 (m, 2H), 7.12 – 7.06 (m, 3H), 4.91 – 4.81 (m, 1H), 1.35 (d, J = 6.2 Hz, 3H), 1.30 (d, J = 6.2 Hz, 3H). ^{13}C NMR (101 MHz, $CDCl_3$) δ 150.8 (d, J = 7.3 Hz), 132.7 (d, J = 7.9 Hz), 132.1 (d, J = 16.1 Hz), 129.7 (d, J = 7.7 Hz), 128.6 (d, J = 25.9 Hz), 128.6 (dd, J = 108.8, 82.8 Hz), 120.8 (d, J = 2.6 Hz), 72.3 (d, J = 5.9 Hz), 24.1 (d, J = 2.3 Hz), 24.0 (d, J = 5.6 Hz).^{31}P NMR (162 MHz, $CDCl_3$) δ 14.92. $[\alpha]_D^{20}$ +15.1° (c 0.26, $CHCl_3$, 55 % *ee*). The absolute configuration of compound **2-15** is designated the (*R*)-configuration based on the optical rotation of previously published analogue **2-25**.

2.4.8.2 (*S*)-Isopropyl (Allyl)-phenyl-phosphonate (2-31)

Yield 31.8 mg (49%). ^{1}H NMR (400 MHz, $CDCl_3$) δ 7.85 – 7.74 (m, 2H), 7.56 – 7.49 (m, 1H), 7.47 – 7.39 (m, 2H), 5.90 (m 2H), 5.30 (dq, J = 17.1, 1.6 Hz, 2H), 5.18 (dq, J = 10.4, 1.4 Hz, 1H), 4.73 (m, 1H), 4.58 – 4.41 (m, 1H), 1.30 (dd, J = 48.2, 6.2 Hz, 6H).^{13}C NMR (101 MHz, $CDCl_3$) δ 133.1 (d, J = 6.5 Hz), 132.5 (d, J = 2.2 Hz), 131.9 (d, J = 10.0 Hz), 130.0 (s), 128.6 (d, J = 15.2 Hz), 71.3 (d, J = 6.6 Hz), 66.4 (d, J = 4.7 Hz), 24.2 (d, J = 3.6 Hz), 24.0 (d, J = 4.9 Hz). ^{31}P NMR (162 MHz, $CDCl_3$) δ 18.53. HRMS (ES): m/z $[M+H]^+$: calcd for $C_{12}H_{18}O_3P$ 241.0994; found: 241.0983. $[\alpha]_D^{20}$ -1.30° (c 0.23, $CHCl_3$). The absolute configuration of compound **2-31** is designated to be the (*S*)-configuration based on the analogous reactivity of **2-25**.

2.4.8.3 (*S*)-Phenethyl (Isopropyl)-phenyl-phosphonate (2-32)

Yield 55.9 mg (68%). ^{1}H NMR (400 MHz, $CDCl_3$) δ 7.76 – 7.68 (m, 2H), 7.54 – 7.48 (m, 1H), 7.44 – 7.36 (m, 2H), 7.30 – 7.14 (m, 5H), 4.73 – 4.60 (m, 1H), 4.30 – 4.08 (m, 2H), 2.97 (t, J = 7.1 Hz, 2H), 1.27 (dd, J = 41.1, 6.2 Hz, 6H).^{13}C NMR (101 MHz, $CDCl_3$) δ 137.5 (s), 132.4 (d, J = 6.9 Hz), 131.9 (d, J = 8.0 Hz), 129.2 (d, J =

2.8 Hz), 129.0 (d, J = 188.6 Hz), 128.6 (d, J = 2.2 Hz), 128.5 (d, J = 9.6 Hz), 126.8 (d, J = 2.8 Hz), 71.2 (d, J = 14.7 Hz), 66.4 (d, J = 5.6 Hz), 37.1 (d, J = 6.7 Hz), 24.2 (d, J = 9.0 Hz), 24.0 (d, J = 9.9 Hz).^{31}P NMR (162 MHz, $CDCl_3$) δ 18.15.HRMS (ES)+: m/z $[M+H]^+$ calcd for $C_{17}H_{22}O_3P$: 305.1307; found: 305.1302. $[\alpha]_D^{20}$ -2.94° (c 0.68, $CHCl_3$). The absolute configuration of compound **2-32** is designated to be the (*S*)-configuration based on the analogous reactivity of **2-25**.

2.4.8.4 (*S*)-Benzyl (Isopropyl)-phenyl-phosphonate (2-33)

Yield 40 mg (51%). ^{1}H NMR (400 MHz, $CDCl_3$) δ 7.84 – 7.77 (m, 2H), 7.55 – 7.50 (m, 1H), 7.43 (m, 2H), 7.35 – 7.26 (m, 5H), 5.04 (m 2H), 4.73 (m, 1H), 1.29 (dd, J = 37.2, 6.2 Hz, 6H). ^{13}C NMR (101 MHz, $CDCl_3$) δ 136.5 (d, J = 7.2 Hz), 132.5 (d, J = 3.0 Hz), 131.9 (d, J = 9.9 Hz), 129.0 (d, J = 189.1 Hz), 128.6 (s), 128.5 (s), 128.4 (s), 127.9 (s), 71.4 (d, J = 4.0 Hz), 67.4 (d, J = 5.1 Hz), 24.2 (d, J = 4.1 Hz), 24.0 (d, J = 4.9 Hz).^{31}P NMR (162 MHz, $CDCl_3$) δ 19.25. HRMS (EI) m/z $[M+H]^+$ calcd for $C_{16}H_{19}O_3P$: 290.10719; found: 290.10667. $[\alpha]_D^{20}$ -6.309 (*c* 0.44, $CHCl_3$). The absolute configuration of compound **2-33** is designated to be the (*S*)-configuration based on the analogous reactivity of **2-25**.

2.4.8.5 (*S*)-Isopropyl (Methyl)-phenyl-phosphonate (2-34)

Yield 32.4 mg (56%). The NMR data were matched for previously publish results.[79] ^{1}H NMR (400 MHz, $CDCl_3$) δ 7.80 – 7.73 (m, 2H), 7.54 – 7.48 (m, 1H), 7.45 – 7.38 (m, 2H), 4.70 (m J = 2H), 3.68 (d, J = 11.2 Hz, 3H), 1.35 (d, J = 6.2 Hz, 3H), 1.22 (d, J = 6.2 Hz, 3H).^{13}C NMR (101 MHz, $CDCl_3$) δ 132.5 (d, J = 2.9 Hz), 131.9 (d, J = 9.8 Hz), 128.6 (d, J = 15.0 Hz), 128.6 (d, J = 188.7 Hz), 71.3 (d, J = 5.4 Hz), 52.5 (d, J = 2.8 Hz), 24.2 (d, J = 3.9 Hz), 24.0 (d, J = 4.9 Hz). ^{31}P NMR (162 MHz, $CDCl_3$) δ 19.12. $[\alpha]_D^{20}$ +0.1856° (c 0.5388, $CHCl_3$). The absolute configuration of compound **2-34** is designated to be the (*S*)-configuration based on the analogous structure (*S*)-Ethyl (Methyl)-phenyl-phosphonate.[103]

2.4.9 (*R*)-Methyl (Phenyl)-phenyl-phosphonate (2-24)

To a 7 mL reaction vial under an atmosphere of N_2 was added methyl phenyl-*H*- phosphinate (**2-40**) (0.1 g, 0.641 mmol, 1.0 equiv.) and carbon tetrachloride (0.234 mL, 2.422 mmol, 3.8 equiv.). Next, anhydrous CH_2Cl_2 (0.3 M solution) was added and the solution cooled to 0 °C. A solution of *N,N*-diisopropylethylamine (0.16 g, 1.211 mmol, 2 equiv.), benzotetramisole (*S*)-**2-16** (0.031 g, 0.121 mmol, 0.19 equiv.), and phenol (28.2 mg, 0.300 mmol, o.47 equiv.) that was previously dried over 4 Å molecular sieves, was prepared in anhydrous CH_2Cl_2 (0.3 ml). The alcohol solution was added dropwise to the phosphinate solution and stirred for 9 hours at 0 °C. The mixture was quenched with 1 M HCl (1 ml) and extracted three times with ethyl acetate then dried with Na_2SO_4. The product was purified by silica gel chromatography with ethyl acetate: hexane (50:50) as eluent. The NMR data matched previously published results.[79] Yield 24.6 mg, (33%). ^{1}H NMR (400 MHz, $CDCl_3$) δ 7.86 (m, 1H), 7.59 – 7.52 (m, 2H), 7.50 – 7.42 (m, 1H), 7.29 – 7.23 (m, 2H), 7.17 – 7.07 (m, 5H), 3.84 (d, J = 11.3 Hz, 1H).^{13}C NMR (101 MHz, $CDCl_3$) δ 150.7 (d, J = 7.2 Hz), 133.1 (d, J = 3.0 Hz), 132.2 (d, J = 10.1 Hz), 129.8 (s), 128.8 (d, J = 15.5 Hz), 127.1 (d, J = 191.0 Hz), 125.1 (s), 120.7 (d, J = 4.5 Hz), 53.31 (d, J = 3.5 Hz). ^{13}C NMR (101 MHz, $CDCl_3$) δ 150.7 (d, J = 7.2 Hz), 133.1 (d, J = 3.0 Hz), 132.2 (d, J = 10.1 Hz), 129.8 (s), 128.8 (d, J= 15.5 Hz), 127.4 (d, J = 115.1 Hz), 125.1 (s), 120.7 (d, J = 4.5 Hz), 53.3 (d, J = 3.5 Hz). ^{31}P NMR (162 MHz, $CDCl_3$) δ 17.39 (s). $[\alpha]_D^{20}$ +54.66° (c 0.2049, $CHCl_3$). The absolute configuration of compound **2-24** was determined to be (*R*)-configuration based on the previously published optical rotation of the **2-24** ($[\alpha]_D^{20}$ +38.1° (c 1.45, $CHCl_3$) which was defined using chiral shift reagents.[102]

2.4.10 General procedure for synthesis Ethyl (Aryl)-phenyl-phosphonate

To a 7 mL reaction vial under an atmosphere of N_2 was added ethyl aryl-*H*-phosphinate (**2-35**) (0.100 g, 0.588 mmol, 1 equiv.) and carbon tetrachloride (0.21 mL, 2.170 mmol, 3.7 equiv.). Next, anhydrous CH_2Cl_2 (0.3 ml solution) was added and the solution was cooled to 0 °C. A solution of *N,N*-diisopropylethylamine

(0.140 g, 1.100 mmol, 1.9 equiv.), benzotetramisole (*S*)-**2-16** (0.027 mg 0.110 mmol, 0.19 equiv.), and phenol (24 mg, 0.25 mmol, 0.43 equiv.) that was previously dried over 4 Å molecular sieves, was prepared in anhydrous CH_2Cl_2 (0.3 ml). The alcohol solution was added dropwise to the phosphinate solution and stirred for 9 hours at 0 °C. The mixture was quenched with 1 M HCl (1 ml) and extracted three times with ethyl acetate then dried with Na_2SO4. The product was purified by silica gel chromatography with ethyl acetate: hexane (30:70) as the eluent. The following products were synthesized.

2.4.10.1 (*R*)-Ethyl (Phenyl)- phenyl-phosphonate (2-25)

Yield 62.3 mg (95%). The NMR data were macheted with previously published results.[79] ^{1}H NMR (400 MHz, $CDCl_3$) δ 7.91 – 7.81 (m, 2H), 7.59 – 7.51 (m, 1H), 7.50 – 7.40 (m, 2H), 7.28 – 7.23 (m, 2H), 7.16 – 7.07 (m, 3H), 4.29 – 4.18 (m, 2H), 1.34 (t, J = 7.1 Hz, 3H). ^{13}C NMR (101 MHz, $CDCl_3$) δ 150.7 (d, J = 7.0 Hz), 132.9 (s), 132.19 (d, J = 10.1 Hz), 128.7 (d, J = 15.5 Hz), 127.4 (d, J = 485.6 Hz), 126.9 (s), 124.1 (s), 120.7 (d, J = 4.5 Hz), 63.0 (d, J = 5.6 Hz), 16.5 (d, J = 7.3 Hz).^{31}P NMR (162 MHz, $CDCl_3$) δ 14.43 (d, J = 12.7 Hz). $[\alpha]_D^{20}$ +21.7° (c 0.429, $CHCl_3$). The absolute configuration of compound **2-25** was determined to be the (*R*)-configuration based on the previously published optical rotation of **2-25** ($[\alpha]_D^{20}$ +34.4° (c 2.16, $CHCl_3$) which was defined using chiral shift reagents.[102]

2.4.10.2 (*R*)-Ethyl (2-methylphenyl)- phenyl-phosphonate (2-26)

Yield 46.3 mg (67%). ^{1}H NMR (400 MHz, $CDCl_3$) δ 7.91 – 7.82 (m, 2H), 7.29 – 7.23 (m, 2H), 7.17 – 7.07 (m, 5H), 4.29 – 4.18 (m, 2H), 1.33 (td, J = 7.1, 0.6 Hz, 3H).^{13}C NMR (101 MHz, CDCl3) δ 167.0 (d, J = 3.9 Hz), 164.4 (d, J = 3.8 Hz), 150.6 (d, J = 7.4 Hz), 134.8 (dd, J = 11.6, 9.0 Hz), 129.8 (s), 125.1 (s), 120.7 (d, J = 4.6 Hz), 116.1 (dd, J = 21.5, 16.8 Hz), 63.2 (d, J = 6.1 Hz), 16.5 (d, J = 6.5 Hz). ^{31}P NMR (162 MHz, $CDCl_3$) δ 14.78. HRMS (EI) m/z $[M+H]^+$ calcd for $C_{15}H_{17}O_3P$: 276.09154; found: 276.09189; $[\alpha]_D^{20}$ +17.35 (*c* 0.5525, $CHCl_3$). The absolute configuration of compound **2-26** is designated to be the (*R*)-configuration based on the analogous reactivity of **2-25**.

2.4.10.3 (*R*)-Ethyl (4-methoxyphenyl)-phenyl-phosphonate (2-27)

Yield 64.3 mg (88%). ^{1}H NMR (400 MHz, $CDCl_3$) δ 8.01 – 7.92 (m, 1H), 7.43 (m, 1H), 7.29 – 7.22 (m, 5H), 7.15 (m, 1H), 7.13 – 7.07 (m, 1H), 4.24 (m, 2H), 2.65 (d, J = 1.7 Hz, 3H), 1.33 (t, J = 7.1 Hz, 3H). ^{13}C NMR (101 MHz, $CDCl_3$) δ 155.1 (d, J = 6.9 Hz), 146.4 (d, J = 10.4 Hz), 138.6 (d, J = 10.6 Hz), 137.3 (s), 135.8 (d, J = 15.3 Hz), 134.1 (s), 130.0 (d, J = 15.4 Hz), 129.2 (s), 124.8 (d, J = 4.4 Hz), 67.7 (d, J = 6.0 Hz), 25.8 (d, J = 3.4 Hz), 20.7 (d, J = 6.4 Hz).^{31}P NMR (162 MHz, $CDCl_3$) δ 16.84. HRMS (EI) m/z $[M+H]^+$ calcd for $C_{15}H_{17}O_4P$: 292.08645; found: 292.08532. $[\alpha]_D^{20}$ +9.68 (*c* 0.6713, $CHCl_3$). The absolute configuration of compound **2-27** is designated to be the (*R*)-configuration based on the analogous reactivity of **2-25**.

2.4.10.4 (*R*)-Ethyl (4-fluorophenyl phenyl)- phenyl-phosphonate (2-28)

Yield 65.3 mg (93%). ^{1}H NMR (400 MHz, $CDCl_3$) δ 7.78 (m, 2H), 7.27 – 7.21 (m, 2H), 7.15 – 7.04 (m, 3H), 6.97 – 6.91 (m, 2H), 4.26 – 4.15 (m, 2H), 3.81 (s, 3H), 1.32 (t, J = 7.1 Hz, 3H). ^{13}C NMR (101 MHz, $CDCl_3$) δ 163.3 (d, J = 3.4 Hz), 150.9 (d, J = 7.0 Hz), 134.2 (d, J = 11.6 Hz), 129.8 (s), 124.9 (s), 120.8 (d, J = 4.4 Hz), 119.0 (d, J = 198.1 Hz), 114.3 (d, J = 16.6 Hz), 62.8 (d, J = 5.5 Hz), 55.5 (d, J = 2.3 Hz), 16.5 (d, J = 6.6 Hz). ^{31}P NMR (162 MHz, $CDCl_3$) δ 16.88. HRMS $(EI)^+$ m/z $[M+H]^+$: calcd for $C_{14}H_{14}O_3PF$: 280.06646; found: 280.06528. $[\alpha]_D^{20}$ +3.79 (*c* 0.5537, $CHCl_3$). The absolute configuration of compound **2-28** is designated to be the (*R*)-configuration based on the analogous reactivity of **2-25**.

CHAPTER THREE

3 ENANTIOSELECTIVE PHOSPHORYLATION OF ALCOHOLS USING PHOSPHORAMIDITES P(III)

3.1 Introduction

Organophosphorus compounds with chirality on phosphorus atoms are ubiquitous in agrochemicals,[108] pharmaceuticals, [109] as organocatalysts reagent,[110] and as ligands in metal-base complexes.[111] Among organophosphates, the trivalent phosphoramidite moiety is the most popular method for synthesizing oligonucleotides on a solid support.[112]

Large-scale synthesis of oligonucleotides for RNA therapeutic applications has increased interest in the phosphoramidite method of oligonucleotide synthesis.[13] Phosphoramidite protocol evolved from the phosphotriester method developed by Letsinger and Ogilvie.[113,114] The development of the method came from the replacement of the trivalent phosphorochloridite building blocks with more stable phosphoramidite substrates. After being activated with Brønsted acid, the protected nucleoside 3'-phosphoramidites (**3-1**) are coupled with the 5'-hydroxy of the solid-supported oligonucleotide as see in Scheme 3.1.[115]

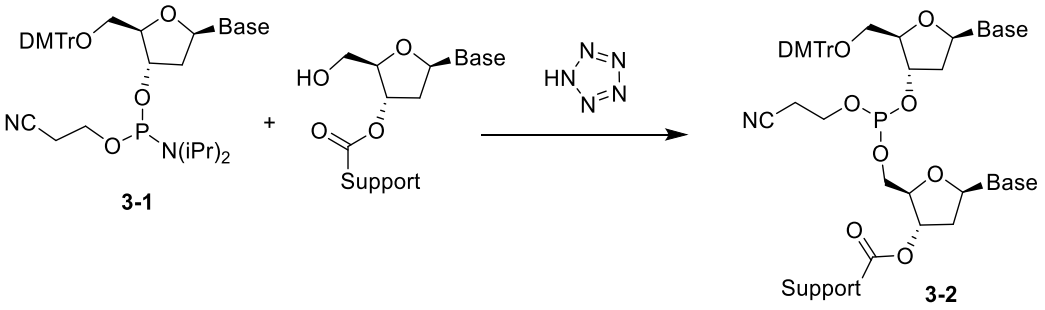

Scheme 3.1 Coupling step in phosphoramidite approach of oligonucleotide synthesis.

Phosphoramidites (**3-8**) are a variant of trivalent phosphorus acid (H_3PO_3) where one of the P-O bonds has been replaced with an amine as seen in Figure 3.1.[116] Based on the trivalent nature of phosphorus, three types of phosphorus amides can appear phosphoramidite (**3-8**), phosphordiamide (**3-9**), and phosphortriamide (**3-10**). Both the phosphorus and nitrogen atoms in phosphoramidite have unshared electron lone pairs which causes the phosphoramidite nitrogen to be basic and the resultant species is highly reactive. According to X-ray analysis studies of phosphoramidite compounds, the phosphorus atom has a pseudotetrahedral geometry while the nitrogen atom is trigonal planar.[117,118]

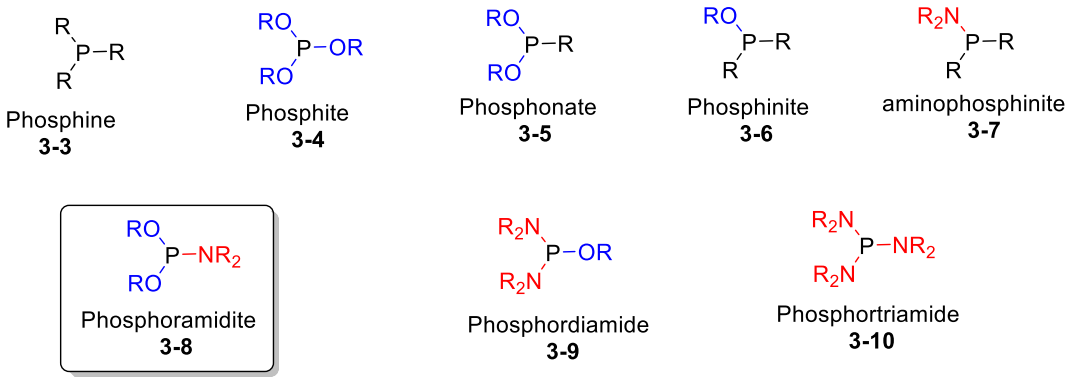

Figure 3.1 Trivalent phosphorus structures

Current synthetic approaches for trivalent stereogenic phosphorus moieties are depicted in Scheme 3.2. Enantiopure phosphine borane complex (**3-11**) has been widely used as precursors for diastereoselective nucleophilic substitution reactions. Thus, P-C or P-O bonds were selectively formed to reach up to 90 % *ee*. The boron moiety works as a protecting group for strongly Lewis basic phosphorus center, which can be removed with a basic amine as seen in Scheme 3.2a.[36,119,120] However, harsh conditions are required to prepare the borane complex resulting in limited substrate scope. Alternatively, stereogenic-P(III) centers can be synthesized through the transformation of a prochiral substrate to a chiral substance by the addition of a group as seen in Scheme 3.2b.[121] However, desymmetrization of prochiral substrates is limited by substrate scope and low enantioselective enrichment.

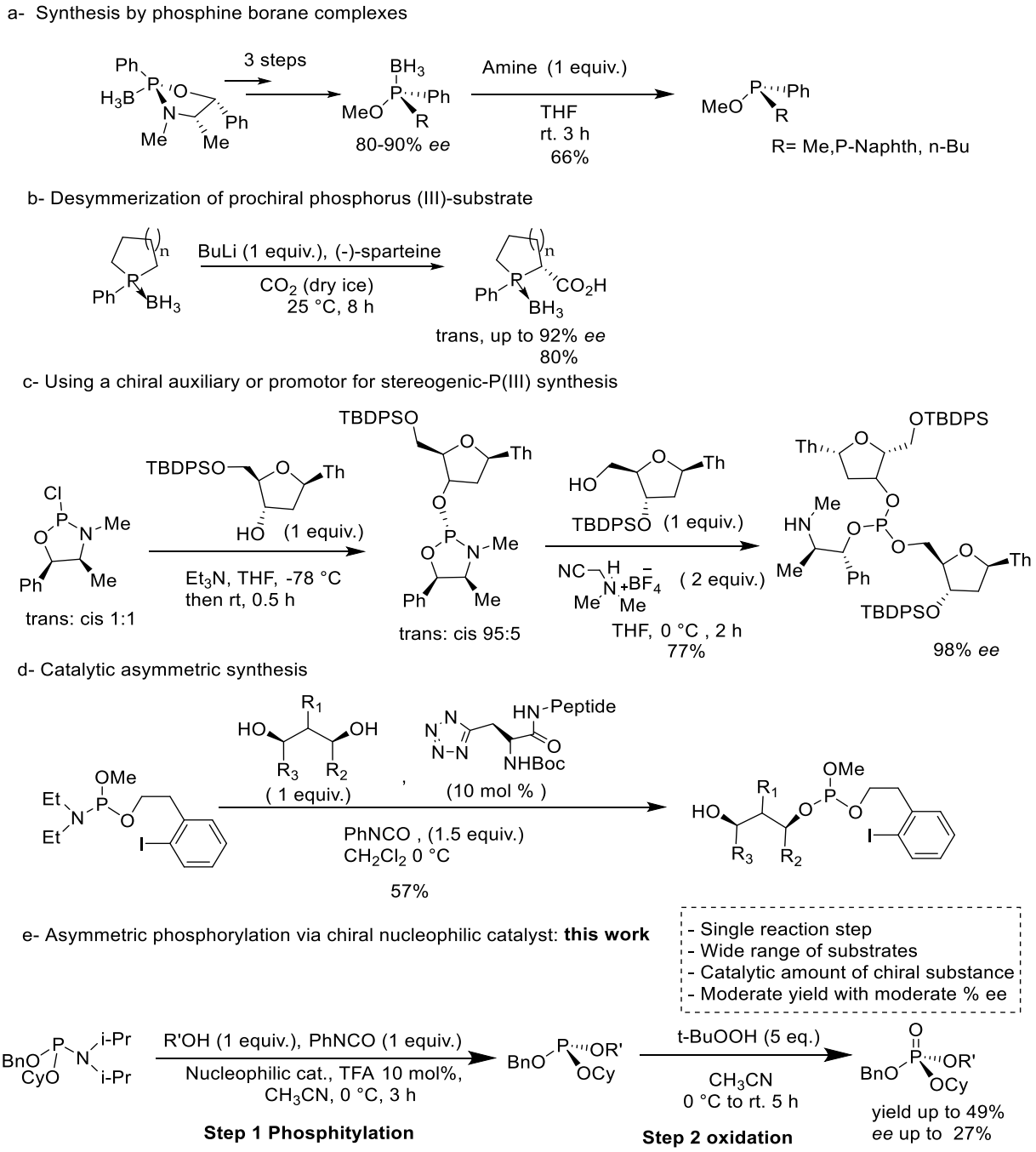

Scheme 3.2 Synthetic approaches to P(III)-stereogenic organophosphorus compounds: a) Synthesis by phosphine borane complex. b) Desymmerization of prochiral P(III)-substrate. c) Using a chiral auxiliary or promotor for P(III)-stereogenic synthesis. d) Catalytic asymmetric synthesis. e) Asymmetric phosphorylation via chiral nucleophilic catalyst: **this work**.

Another strategy, relays chiral information into the transition state using an enzyme, chiral auxiliary, chiral reagent, or catalyst as in Scheme 3.2c, d, e. For example, alcohols or amines have been widely utilized as chiral auxiliaries because they can be readily attached to trivalent phosphorus moieties as in Scheme 3.2c.[37] However, a stoichiometric amount of a chiral auxiliary is always required to achieve the desired stereoselectivity. Also due to a direct connection to a chiral auxiliary to the P(III) motif, additional chemical processes are required to remove the chiral auxiliary and isolate the desired product.[37] The use of natural products or enzymes have been used as external asymmetric inducers for the synthesis of trivalent phosphorus centers. Scott Miller et al. modified synthetic peptides, as an enzyme mimic, for alcohol phosphorylation as in Scheme 3.2d.[122] However, since the peptide catalyst interacts with the substrate using unique and unpredictable non-covalent interactions, this method fails to provide a general catalyst for the synthesis of stereogenic-P(III) molecules.

To avoid all these limitations, an enantioselective phosphitylation P(III) of alcohols has been investigated using a chiral nucleophilic catalyst and racemic trivalent phosphoramidite substrate as seen in Scheme 3.2e. This approach has several advantages. For example, a racemic substrate could be used to produce enantiomerically enriched phosphorus centers using substoichiometric amounts of a chiral catalyst. Also, the scope of phosphoramidite substrates could be expanded to include nucleotide chemistry.

3.2 Results and Discussion

Before developing an enantioselective phosphoramidite coupling, conversion of phosphoramidite **3-11** to racemic phosphate analog **3-15** was accomplished in a one-pot, two-step process. First, phosphitylation of chlorophenol with **3-11** occurred using a stoichiometric amount of 4,5-dicyanoimidazole promotor. Then, the phosphite product was oxidized by tertbutyl peroxide to provide the corresponding P(V) phosphate (**3-15**) as shown in Scheme 3.3.

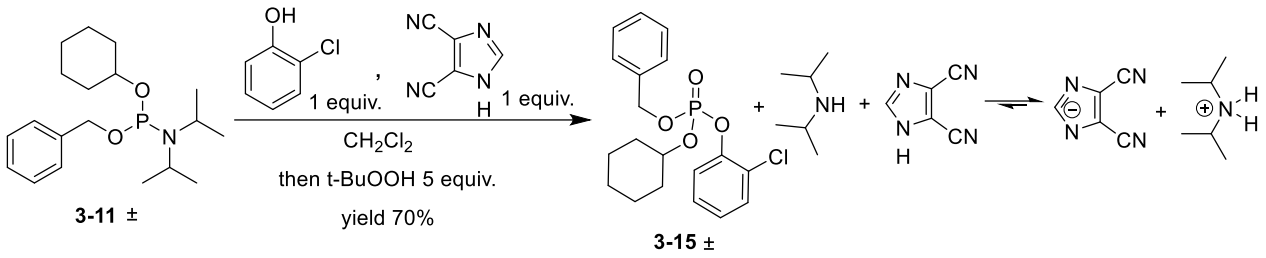

Scheme 3.3 Alcohol phosphitylation utilizing phosphoramidites followed by oxidation.

Phosphoramidites always require a stoichiometric amount of acid during an alcohol phosphitylation reaction progress because P-N bond breaking generates an equivalent of an alkylamine as a byproduct.[123–125] As the concentration of the amine increases, the concentration of the promoter decreases as seen in Scheme 3.3. Accordingly, Bradly et al. have demonstrated that isocyanates scavenge amines to enable catalyst turnover by converting the amine byproduct to urea which is no longer basic and it doesn't deactivate the catalyst.[125] Conversions up to 97% with 5 mol % of *H*-tetrazole catalyst were observed.[125] Therefore, scavenging the amine byproduct should alter the equilibrium allowing the promoter to function catalytically and overcome the conversion and catalyst deactivation limitations previously documented with asymmetric phosphoramidite couplings.

The phosphate analog product **3-15** was isolated with a 70% yield and characterized using ^{31}P and ^{1}H NMR. In addition, high performance liquid chromatography (HPLC) on a chiral stationary phase indicated the racemic material contains a 50:50 ratio of two enantiomers as seen in Figure 3.2.

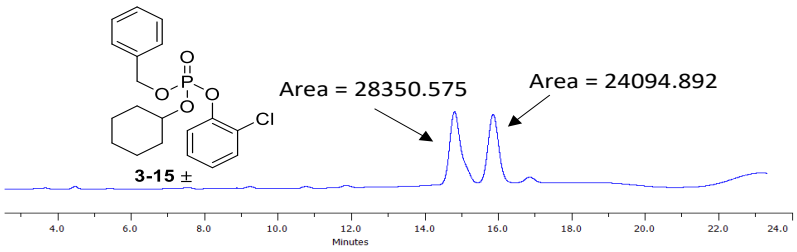

Figure 3.2 HPLC chromatogram of racemic **3-15**. *Conditions:* Phenomenex amylose-2 chiral column (250 X 4.6 mm), eluent acetonitrile : water (60 : 40 – 80 : 20), detection at 254 nm, flow rate 0.5 ml/min, temperature at 25 °C.

Under the optimized conditions for the racemic formation of **3-15,** addition of phenylisocyanate (1 equiv.), as amine scavenger, and a number of chiral nucleophilic catalysts were screened to investigate the enantiomeric enrichment of the phosphorus center (Scheme 3.4). Planar-chiral catalyst **3-18**, also known as Fu's catalyst, is a ferrocene analogue of 4-Diethylaminopyridine (DMAP) that is known to behave as a chiral nucleophilic catalyst. When using catalyst **3-18** along with 10 mol% of TFA, the product **3-15** was obtained 23% *ee* and 23% yield. TFA was included to protonate the pyridine of **3-18** and subsequently the phosphoramidite, to facilitate P-N bond cleavage and allow the alcohol to attack the phosphoramidite. Despite **3-18** being a proficient catalyst for the asymmetric substitution of acyl groups, it performs very poorly in the asymmetric substitution of phosphoryl groups.

Based on the success in the asymmetric synthesis of phosphonates (Chapter 2), heterocyclic nucleophilic catalyst **3-19** (BTM **2-16**) was tested in the synthesis of P(V) phosphates. Disappointingly, product **3-15** was obtained in only 21% *ee* and 15% yield. Similarly, imidazole **3-20** provides **3-15** in 16% *ee* and only 8% despite it being useful for the synthesis of ProTide^{TM} phosphates.

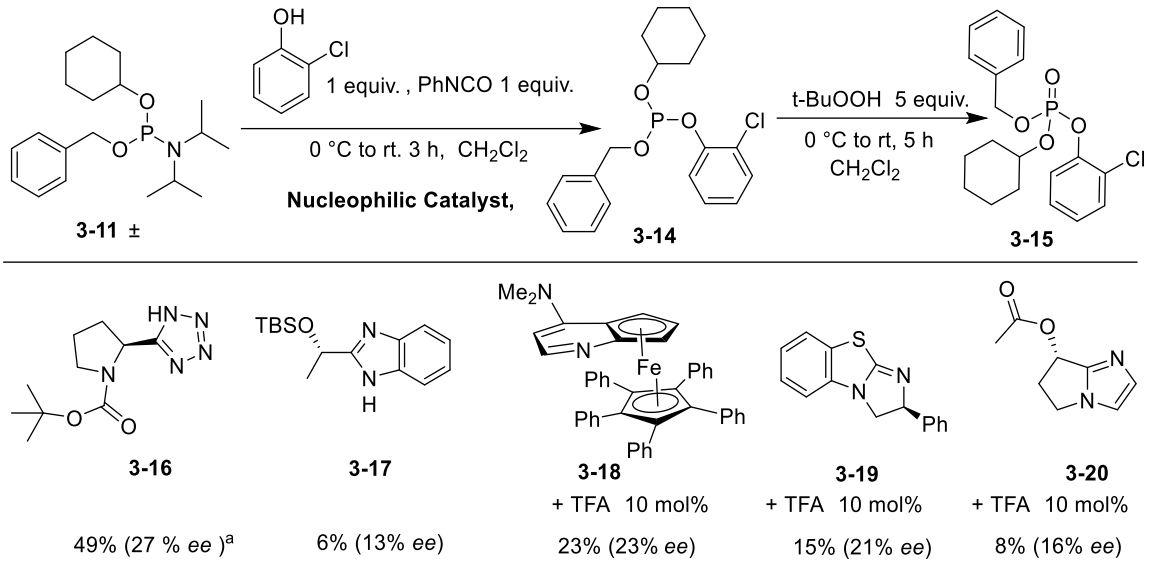

Conditions: **3-11** (1 equiv.), ClPhOH (1 equiv.), PhNCO (1 equiv.), Cat. (10 mol %), CH_2Cl_2 (0.1 M solution), 8 h; then t-BuOOH (5 equiv.). [a] *ee* values and yield were determined by HPLC analysis.

Scheme 3.4 A catalyst screening for asymmetric alcohol phosphitylation.

Catalysts **3-18**, **3-19**, and **3-20** all required addition of an exogenous acid to activate the phosphoramidite for substitution. However, traditional phosphoramidite coupling utilizes acid azoles, such as 1*H*-tetrazole, that have dual roles. First, the azole works as an acid to protonate the amine nitrogen as a leaving group. The other role is as a nucleophilic activator to displace the protonated diisopropylamine and form an activated intermediate. The intermediate then undergoes nucleophilic substitution with an alcohol to provide the phosphate product.[124]

Using chiral 1*H*-tetrazole analog **3-16** (10 mol %) the phosphate product (**3-15**) was obtained in 50% yield and 27% *ee*. Notably, the yield and enantioselectivity are highest observed results for **3-15** (Scheme 3.4). However, when compared with the desired enantioselectivity (>90% *ee*), the chiral site is likely flexible to induce asymmetric phosphitylation of the alcohol. Alternatively, a chiral 1*H*-benzimidazole analog **3-17,** which has not previously been reported as as nucleophilic catalyst, provides

3-15 in low enantioselectivity (13 % *ee*) and dramatically diminished yield (6 %). Thus, the asymmetric site of both chiral *H*-tetrazole **3-16** and 1*H*-benamidiazole **3-17** were not enough to favor one enantiomer over the other. However, the literature contains very few examples of using a substoichiometric amount of a chiral compound to induce enantioselectivity in phosphoramidite couplings making the results in Scheme 3.4 still noteworthy.

Prior to identifying **3-16**, which serves a dual catalytic role, trifluoroacetic acid (TFA) was used in combination with chiral nucleophilic bases to facilitate phosphoramidite coupling. In order to improve the modest enantioselectivities observed with TFA, the effect of acid and concentration were tested with catalyst **3-18** as seen in Table 3.1.

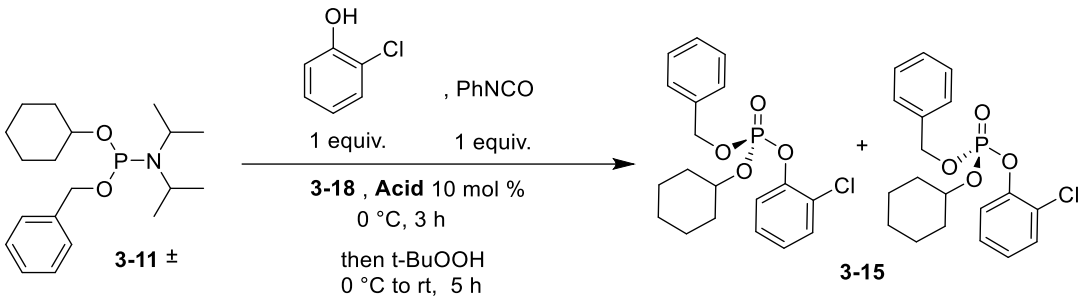

Table 3.1 Effect of acid on the catalytic phosphitylation

Entry	H^+	$[H^+]$	Yield (%)[a]	%*ee*[b]
1	HBF_4	10 mol%	10	23
2	TFA	10 mol %	30	23
3	TFA	5 mol %	12	18

Conditions: **3-11** (1 equiv.), ClPhOH (1 equiv.), PhNCO (1 equiv.), **3-18** (10 mol %), tetrafluoroboric acid (HBF_4), trifluoroacetic acid (TFA) , CH_2Cl_2 (0.1 M solution), 8 h, then t-BuOOH (5 equiv.). [a] Yields were determined by HPLC analysis. [b]*ee* values were determined by HPLC analysis.

In contrast to TFA, 10 mol % of tetrafluoroboric acid (HBF_4), a strong acid, was tested and the selectivity did not change (23% *ee*) but the yield dropped from 30% to 10% (Table 3.1 Entry 1 and 2). Possibly the phosphorus atom of the phosphoramidite can be protonated by HBF_4 resulting in a species that is less reactive towards nucleophilic attack.[123,126,127] Decreasing the acid concentration (TFA) to 5 mol %, decreased both the selectivity and yield of the product (**3-15**) to 18% *ee* and 12% respectively (Table 3.1 Entry 3). This result demonstrates the importance of the acid catalyst participation in the reaction.

The impact of solvent and temperature on the selectivity and yield of phosphate **3-15** was tested and the results shown in Table 3.2. Dichloromethane is a nonpolar, aprotic solvent that provided the product in 23% yield and 23% *ee*. Using a more solvent, acetonitrile, results in an equivalent or increased yield (22% and 58%), but a decrease in enantioselectivity (17% and 4% *ee*) as shown in Table 3.2 Entry 5.

In contrast, utilization of a nonpolar solvent, toluene, provided **3-15** in 30% yield and 22% *ee*. Future studies with nonpolar solvents may provide increases in enantioselectivity and yield in this type of transformation in the future. Finally, when tetrahydrofuran was used as a solvent, the reaction outcome was 17% yield and 15% *ee*.

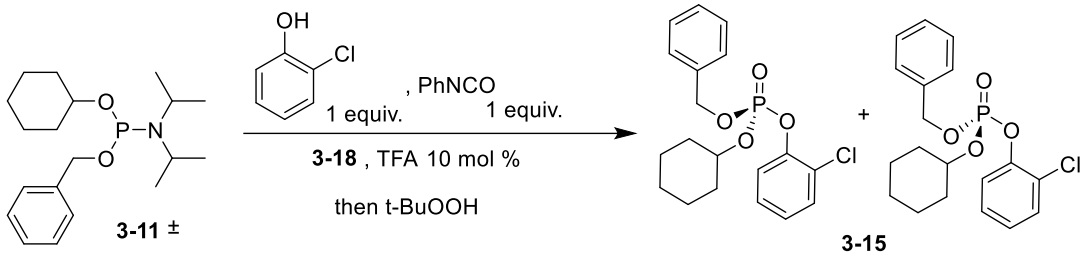

Table 3.2 Effect of the solvent and the temperature on the phosphoramidite phosphitylation

Entry	**Solvent**	**T (°C)**	**Yield (%)[a]**	**%*ee*[b]**
1	Toluene	0	30	22
2	THF	0	17	15
3	CH_2Cl_2	0	23	23
4	CH_3CN	0	22	17
5	CH_3CN	25	58	4

Conditions: **3-11** (1 equiv.), ClPhOH (1 equiv.), PhNCO (1 equiv.), **3-18** (10 mol %), trifluoroacetic acid (TFA) (10 mol %) , CH_2Cl_2 (0.1 M solution), 8 h, then t-BuOOH (5 equiv.). [a] Yields were determined by HPLC analysis. [b] *ee* values were determined by HPLC analysis.

Based on the above experimental data, a reasonable mechanism of enantioselective nucleophilic substitution at phosphorus (S_N2P) can be proposed (Scheme 3.5). A catalytic amount of chiral 1*H*-tetrazole analog **3-16** can react with racemic phosphoramidite (**3-11**) and form a diastereomeric mixture of tetrazole phosphoramidites (**3-12** and **3-13**).[124] In more detail, the chiral 1*H*-tetrazole analog **3-**

16 plays a dual role as a an acid to protonate the amine nitrogen and then as a nucleophilic catalyst to displace the protonated diisopropylamine.[124] Racemization of **3-12** and **3-13** by the chiral tetrazole causes a dynamic kinetic resolution of two diastereomer allowing for the asymmetric transformation to phosphite moiety (R_p)-**3-15** and (S_p)-**3-15**.[128] The thermodynamic stability of **3-12** and **3-13** are different and thus exist at different concentrations during the reaction. More importantly, the reactivity of these two diastereomeric intermediates is different, represented by k_1 and k_2 in Scheme 3.5. Thus, the effective resolution process is dependent on these reaction rates (ideally $k_1 << k_2$ or $k_1 >> k_2$). One equivalent of the phenyl isocyanate additive in the reaction helps to increase the catalyst turnover by scavenging the byproduct amine and converting it to a non-basic urea product whereby allowing the heterocycle to enter the catalytic cycle again.

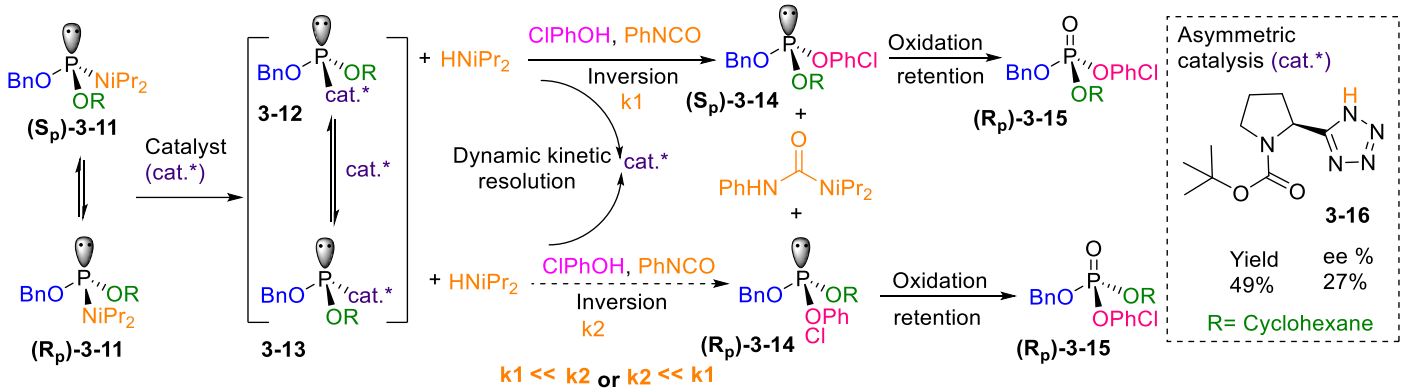

Scheme 3.5 Proposed mechanism of alcohol phosphitylation with phosphoramidites using substoichiometric amounts of chiral tetrazole analog **3-16** based on a dynamic kinetic resolution.

3.3 Catalyst Development

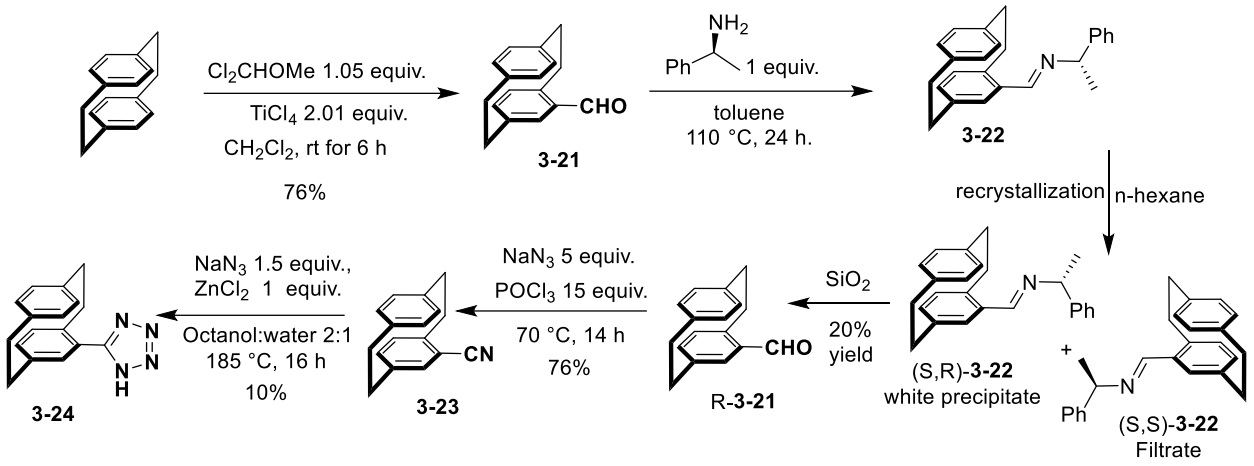

Scheme 3.6 Reaction sequence to produce 1*H*-tetrazole [2,2]paracyclophane (**3-24**)

Based on the effectiveness of chiral tetrazoles in the asymmetric synthesis of phosphates, synthetic studies to obtain a planar chiral cyclophane that contains a 1*H*-tetrazole moiety (**3-24**) was pursued. First, an aldehyde was installed on paracyclophane to get [2,2] paracyclophancarboxaldehyde (**3-21**). Aldehyde **3-21** is a key compound in the sequence because the enantiomers can be separated using a procedure by Quici.[129] To separate these enantiomers, aldehyde **3-21** was reacted with (*S*)-methylbenzylamine to produce diastereomeric imines **3-22** in quantitative yield. Next, the diastereomers are separated using recrystallization in n-hexane (Scheme 3.6). Cyclophane (*S,R*)-**3-22** hydrolyzes under the acidic environment of silica gel resulting in formation of cyclophane (*R*)-(**3-21**) in 96% ee and 22% yield (Figure 3.3). Isolation of (*R,R*)-**3-22** from the filtrate can be pursued to obtain cyclophane (*S*)-(**3-21**) but requires additional recrystallization to obtain the product in high enantioselectivity.

Subsequently, treatment of *R*-(**3-21**) with phosphoryl chloride in presence of sodium azide at 70 °C for 17 hours gave nitrile product **3-23** in 75% yield. After thorough optimization, enantiopure nitrile **3-23** was converted into tetrazole **3-24** using zinc bromide and sodium azide in 10 % yield. The low product yield in tetrazole formation is likely due to the sterically hindered environment of cyclophanes due to the

close proximity of the aromatic rings. During the tetrazole formation, the product **3-24** was found to have racemized under the high reaction temperature (180 °C). Since no milder methods could be found to convert the nitrile into the tetrazole without racemization, the tetrazole would need to be formed before resolution in order to obtain **3-24** in enantioenriched form.

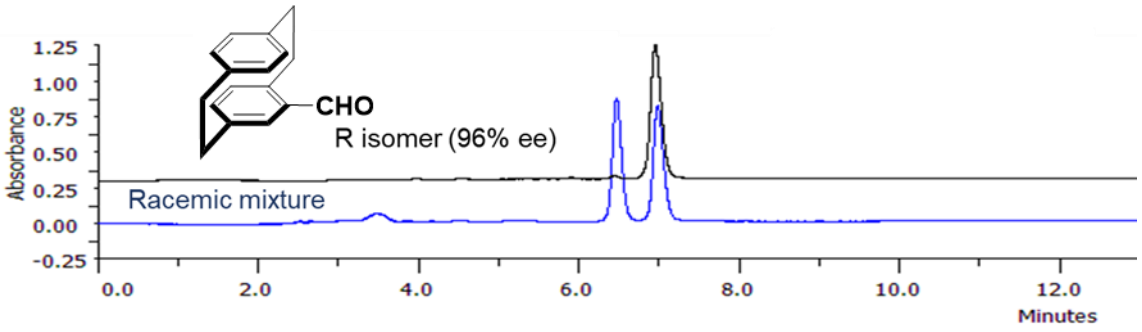

Figure 3.3 HPLC chromatogram of **3-21**. *Conditions:* Phenomenex amylose-2 chiral column (250 X 4.6 mm), eluent hexane: ethanol and 0.1% TFA (65:35), detection 254 nm. Flow rate 0.5 ml min^{-1}, temperature 25 °C.

Alternatively, catalyst development could be pursued to overcome the limitations of chiral 1*H*-tetrazole synthesis and enantiomer separation. For example, borylation of cyclophane and subsequent Suzuki coupling with a bromo-tetrazole could provide a chiral tetrazole-containing [2,2] cyclophane (**3-30**) as shown in scheme 3.7. This strategy would require a chiral auxiliary on tetrazole to facilitate diastereomer separation. Therefore, a [3+2] cycloaddition reaction of the sodium azide with (*R*)-methylbenzylamine was carried out to produce a chiral methyl tetrazole analog (**3-28**) in 75% yield. Then, tetrazole **3-28** was brominated to produce chiral bromo-tetrazole **3-29** in 90% yield. To facilitate a Suzuki coupling, borylation of cyclophane was carried out in two steps to produce unstable, cyclophane boronic acid **3-26** in 25% yield. The compound **3-26** was found to be unstable on silica gel column.

Finally, the Suzuki coupling product **3-30** needs to be hydrogenated to break the C-N bond and produce compound **3-24** as seen in scheme 3.7.

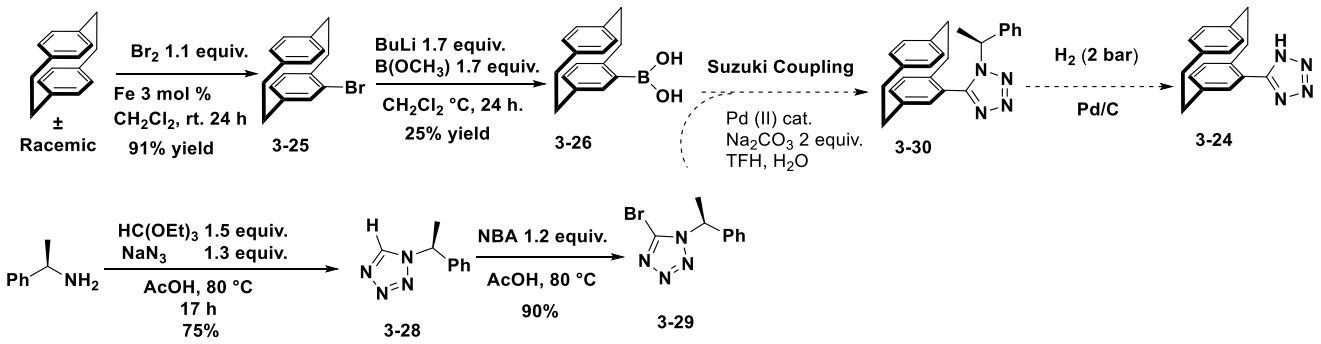

Scheme 3.7 Alternative reaction sequence to produce 1*H*-tetrazole [2,2]paracyclophane (**3-24**) by Suzuki coupling reaction.

3.4 Conclusion and future direction

Asymmetric phosphorylation using P(III) phosphoramidites was carried out with a variety of chiral nitrogen-containing heterocycles as catalysts. The reaction was performed in presence of phenyl isocyanate as an amine scavenger to increase the catalyst turnover. Various conditions were screened including solvent, temperature, acid, and chiral nucleophilic catalyst. (*S*)-5-(1-Boc-Pyrolidin-2-yl)-1*H*-tetrazole (**3-16**) in CH_2Cl_2 below room temperature was determined to be the best condition for phosphorylation with 23% *ee* and 49% yield. Despite the modest selectivity and yield, this approach has a number of advantages including utilizing a catalytic amount of a chiral amine. If a more capable catalyst were found, a wide range of enantioselective stereogenic phosphate mimics could be obtained using suitable oxidation conditions such as phosphorothioates by sulfurization, phosphoselenoates by selenation, or boranophosphates by boronation.

The synthesis of novel, chiral tetrazoles was pursued to identify a more selective catalyst. A chiral cyclophane was produced with a 1*H*-tetrazole moiety using a resolution by a chiral amine and subsequent conversion into the nitrile. However, the tetrazole-containing [2,2]-paracyclophane racemized during the

synthesis process making it inoperative as a chiral nucleophilic catalyst. An alternative synthetic route would need to be pursued to obtain the proposed tetrazole-containing [2,2]-paracyclophane.

3.5 Materials and Methods

3.5.1 General information

All reactions were carried out under a nitrogen atmosphere in oven-dried glassware. The products were purified by flash column chromatography using silica gel 60 (230-400 mesh Silicycle, Quebec, Canada). The solvent, reagents, and chemicals were received from a commercial vendor and further dried under activated 4 Å molecular sieves. Methylene chloride and THF were dried using a Pure Solv Micro purification system. Thin-layer chromatography (TLC) analysis was performed on Merck 0.25 mm silica gel 60 F_{254} plates. ^{1}H NMR was recorded using an Oxford Varian Unity Instrument at 400 MHz spectrometers. ^{1}H NMR data was referenced using the residual solvent peak of $CDCl_3$ at 7.26 ppm. ^{13}P NMR spectra were acquired at 162 MHz and externally referenced to 85% H_3PO_4 at (0 ppm). The ^{13}C NMR were acquired at 101 MHz and referenced to 77.1 ppm for the $CDCl_3$ solvent. The NMR data was processed with MestReNova11 NMR software. HPLC was performed using the Gilson GX-271 instrument with Trilution LC software (V3) and a 5µm 250 x 4.6 mm Phenomenex Lux Amylose chiral column. For analytical HPLC, the reverse phase separation method used was: eluent acetonitrile: water (60:40-80:20), detection (254 nm), flow rate (0.5 ml/min), temperature (25 °C), and run time (20 minutes).

3.5.2 Benzyloxy bis (*N,N*-diisopropyl)phosphordiamide (3-9)

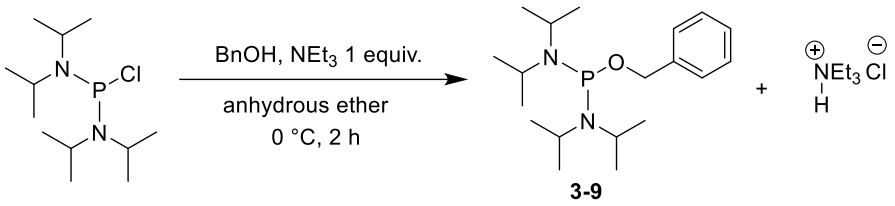

3-9

To a 7 mL reaction vial under an atmosphere of N_2 was added triethylamine (0.18 ml, 1.3 mmol, 1 equiv.). Next, anhydrous acetonitrile (0.3 mL) was added followed by benzyl alcohol (130 mg, 1.2 mmol, 1 equiv.) that was previously dried over 4 Å molecular sieves. A solution of bis(diisopropylamino)chloro-phosphine (300 mg, 1.12 mmol, 1 equiv.) in dry ether (2.5 ml) was prepared and cooled to 0 °C. The alcohol solution was added dropwise to the phosphine solution and stirred for 2 hours at 0 °C. After the reaction mixture was stirred for 2 hours at 0 °C, a white precipitate formed that was filtered off. The filtrate was concentrated dissolved in dry acetonitrile (3 ml). n-Hexane (2 x 1 mL) was added and the hexane layer was collected. The solvent was removed under reduced pressure to provide a colorless oil product **3-9** (341 mg, 90 % yield). The crude product was found to be unstable to purification by silica gel chromatography, so the product was used without further purification. ^{1}H NMR matched literature data.[130] ^{1}H NMR (400 MHz, $CDCl_3$) δ 7.35 – 7.13 (m, 5H), 4.60 (d, *J* = 7.3 Hz, 2H), 3.52 (4H, m), 1.13 (24H, m), ^{31}P NMR (162 MHz, $CDCl_3$) δ 124.70.

3.5.3 Benzyloxy Cyclohexanol N, N-diisopropylphosphoramidite (3-11)

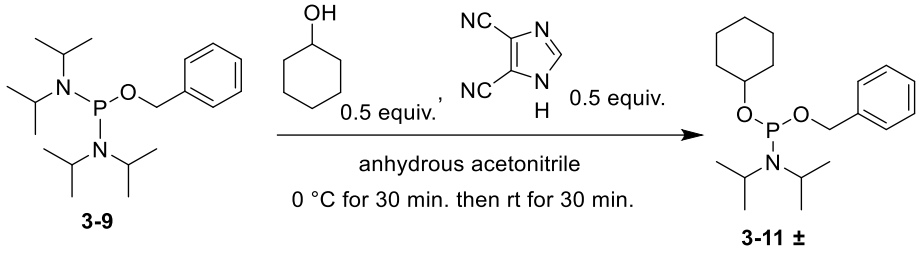

To a 7 mL reaction vial under an atmosphere of N_2 was added 4,5-dicyanoimidazole (11 mg, 0.094 mmol, 0.5 equiv.). Next, anhydrous acetonitrile (0.3 mL) was added followed by hexanol (9 mg, 0.094 mmol, 0.5 equiv.) that was previously dried over 4 Å molecular sieves. A solution Benzyloxybis-(diisopropylamino)phosphine (**3-9**) (63 mg, 0.187 mmol, 1 equiv.) in anhydrous in CH_3CN (0.2 mL) was prepared and cooled to 0 °C. The alcohol solution was added dropwise to the phosphine solution and stirred for 30 minutes. After removing the ice bath, the reaction mixture was left stirring for another 30 minutes. n-Hexane (2 x 1 mL) was added and the hexane layer was collected. The solvent was removed under reduced pressure to provide the product **3-11** (47 mg, 75% yield). The crude product was found to be unstable to purification by silica gel chromatography, so the product was used without further purification. After removing the solvent under reduced pressure, the product was isolated (47 mg, 75% yield). ^{1}H NMR (400 MHz, $CDCl_3$) δ 7.45 – 7.17 (m, 5H), 4.83 – 4.57 (2H, m), 3.66 (2H, m), 1.99 – 0.99 (22H, m), ^{31}P NMR (162 MHz, $CDCl_3$) δ 145.52.

3.5.4 General procedure for asymmetric phosphitylation

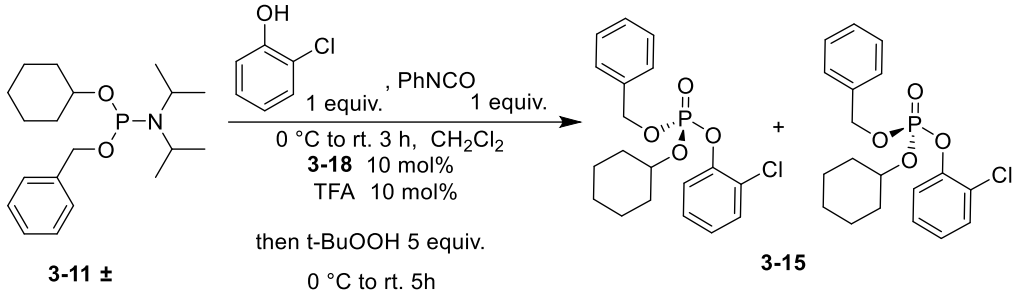

To a 7 mL reaction vial under an atmosphere of N_2 was added chiral nucleophilic catalyst (**3-18**) (4.89 mg, 0.0074 mmol, 10 mol%), and trifluoroacetic acid (TFA) (0.84 mg, 0.0074 mmol, 10 mol %). Next, anhydrous CH_2Cl_2 (0.2 mL) was added followed by chlorophenol (9.5 mg, 0.074 mmol, 1 equiv.) that was previously dried over 4 Å molecular sieves. A solution Benzyloxy Cyclohexanol *N,N*-diisopropylphosphoramidite (**3-11**) (25 mg, 0.074 mmol, 1 equiv.) in anhydrous in CH_2Cl_2 (0.35 mL) was prepared. The alcohol solution was added dropwise to the phosphoramidite solution. After 3 hours, the reaction was monitored with TLC and ^{31}P NMR to confirm phosphite production. The reaction mixture was cooled to 0 °C followed by addition of a solution of tert-butyl hydrogen peroxide (0.04 ml, of 5.5 M solution in decane, 0.37 mmol). The reaction was warmed to room temperature and left to stir for 5 hours. Then, the reaction was quenched with aqueous $NaHCO_3$, extracted three times with ethyl acetate, and dried with Na_2SO_4. The product was purified by silica gel chromatography with ethyl acetate: hexane (10:90) as eluent. ^1H NMR and ^{31}P NMR showed products with (9 mg, 54% yield). ^1H NMR (400 MHz, $CDCl_3$) δ 7.52 – 6.96 (m, 7H), 5.29 – 5.09 (m, 2H), 4.55 (qt, *J* = 8.9, 3.8 Hz, 2H), 2.01 – 1.01 (m, 10H), 1.00 – 0.65 (m, 1H), ^{31}P NMR (162 MHz, $CDCl_3$) δ -6.47.

3.5.5 Synthesis (*S*)-5-(1-Boc-Pyrolidin-2-yl)1*H*-tetrazole (3-16)

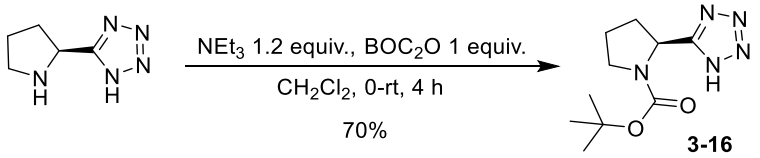

To solution of (*S*)-5-(1*H*-Pyrolidin-2-yl)1*H*-tetrazole (50 mg, 0.359 mmol, 1 equiv.), and triethylamine (44 mg, 0.431 mmol, 1.2 equiv.) in CH_2Cl_2 (0.6 ml), a solution of di-tert-butyl dicarbonate (Boc_2O) (78 mg, 0.359 mmol, 1 equiv.) in CH_2Cl_2 (0.6 ml) was added at 0 °C. After raising the temperature to room temperature, the mixture was stirred for 16 hours until the TLC showed the starting material had been consumed. Then, the crude product was purified by silica gel chromatography using MeOH: CH_2Cl_2 (10:90). The product Yield 59 mg (69% yield). The NMR data were matched for previously publish results.[131] ^{1}H NMR (400 MHz, $CDCl_3$) δ 5.09 (dd, *J* = 8.3, 2.6 Hz, 1H), 3.49 (s, 1H), 2.76 (ddd, *J* = 10.8, 5.4, 2.2 Hz, 1H), 2.41 – 1.89 (m, 1H), 1.45 (s, 10H), 1.31 – 1.20 (m, 5H).

3.5.6 1*H*-Benzimidazole, 2-[(1S)-1-[[(1,1-dimethylethyl) dimethylsilyl]oxy]ethyl] (3-17)

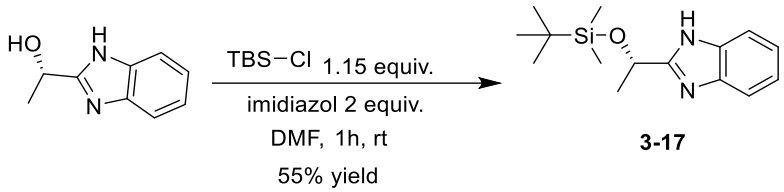

A solution of (*S*)-1-)1*H*-Benzimidazol-2-yl) ethanol (100 mg, 0.617 mmol, 1 equiv.), imidazole (74 mg, 1.23 mmol, 2 equiv.), and tert-butyldimethylsilyl chloride (107mg, 0.709 mmol, 1.15 eq.) in DMF (3.1ml) was stirred at room temperature for 50 minutes. After checking the TLC, the product was extracted with ethyl acetate, then purified with silica gel chromotography using EtOAC: Hexane (30:70). Yield 94 mg (55% yield). ^{1}H NMR (400 MHz, $CDCl_3$) δ 9.76 (s, 1H), 7.72 – 7.54 (m, 1H), 7.35 (d, *J* = 5.8 Hz, 1H), 7.15 (td, *J* =

7.2, 6.2, 2.0 Hz, 2H), 5.15 (dd, *J* = 6.5, 1.0 Hz, 1H), 1.53 (dd, *J* = 6.5, 1.0 Hz, 3H), 0.85 (d, *J* = 1.1 Hz, 8H), 0.03 (dd, *J* = 22.0, 1.0 Hz, 5H).

3.5.7 Synthesis 6,7-dihydro-5*H*-pyrrolo[1,2-a] imidazole-7-ol (3-30)

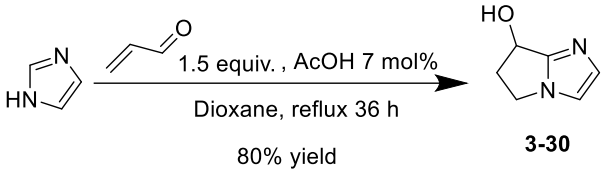

According to the procedure from previously published by Zhenfeg zhang et al.[130] A solution of imidazole (0.1 g, 1.47 mmol, 1 equiv.), acrolein (0.147 ml, 2.203 mmol, 1.5 eq.) and acetic acid (58 µl, 0.1 mmol, 7 mol %) in dioxane (2.1 ml) was refluxed for 36 h at 101 °C. After monitoring the reaction by TLC, the solvent was evaporated under reduced pressure. The crude product was purified by silica gel chromatography using MeOH: CH_2Cl_2 (10:90) to provide 0.146 g (80% yield). The NMR data were matched for previously publish results.[130] The ^{1}H NMR matched the published results. ^{1}H NMR (400 MHz, $CDCl_3$) δ 7.06 (dd, *J* = 4.4, 1.3 Hz, 1H), 6.83 (d, *J* = 1.3 Hz, 1H), 5.18 (ddd, *J* = 9.2, 7.3, 3.1 Hz, 1H), 4.29 – 3.79 (m, 2H), 2.99 – 2.38 (m, 2H).

3.5.8 Resolution of 6,7-dihydro-5*H*-pyrrolo[1,2-a] imidazole-7-ol (3-30)

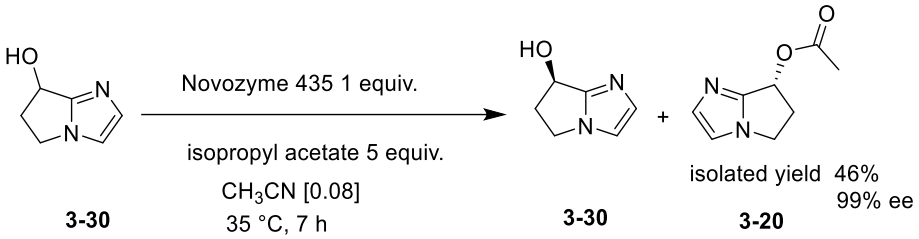

A racemic solution of 6,7-dihydro-5*H*-pyrrolo[1,2-a] imidazole-7-ol, (81.6 mg, 6.58 mmol, 1 equiv.), Nov. 435 enzyme (81.6 mg, 1 equiv.) and isopropenyl acetate (3.79 ml, 32.22 mmol, 5 equiv.) in acetonitrile (82.2 ml) was stirred for 7 h at 35 °C. After monitoring the reaction with TLC, the crude reaction was

purified with silica gel column chromatography using MeOH/CH_2Cl_2 (10:90) to isolate the unreacted starting material. Acetylated product **3-20** was obtained in 46% yield (52 mg). The NMR data were matched for previously publish results.[130] ^{1}H NMR (400 MHz, $CDCl_3$) δ 7.19 (q, *J* = 1.3 Hz, 1H), 7.00 – 6.88 (m, 1H), 5.98 (dt, *J* = 7.2, 2.7 Hz, 1H), 4.25 – 3.85 (m, 2H), 3.15 – 2.43 (m, 2H), 2.13 – 1.98 (m, 4H).

3.5.9 Enantiomeric excess evolution from resolution

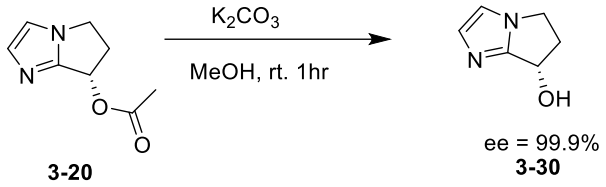

A solution of 6,7-dihydro-5*H*-pyrrolo[1,2-a] imidazole-7-acetate (**3-20**) (20 mg, 0.119 mmol, 1 equiv.) and K_2CO_3 (20 mg, 0.143 mmol, 1.2 equiv.) in CH_3OH (1.2 ml) was stirred for 1h at room temperature. After checking the TLC, the crude residue was analyzed with HPLC to determine the enantiomeric excess (% *ee*).

3.5.10 Synthesis rac-formyl [2,2]paracyclophane (3-21)

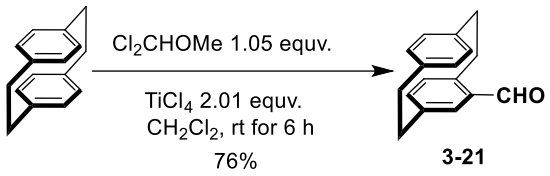

A solution [2,2] paracyclophane (300 mg, 1.4402 mmol, 1 equiv.) in CH_2Cl_2 (10 ml) was prepared and cooled to 0°C. Then, a solution of dichloromethyl methyl ether (173 mg, 1.05 mmol, 1.05 equiv.) and 1 M solution of titanium chloride (IV) (2.89 ml, 2.9 mmol, 2 equiv.) in CH_2Cl_2 (3 ml) was prepared. The dichloromethyl methyl ether solution was added to the paracyclophane solution at 0°C. The mixture was stirred for 6 hours at room temperature followed by water (10 ml) addition and stirred for 2 hours. After the two phases formed, the aqueous phase was extracted with CH_2Cl_2 (10 ml) three times. The combined

organic layers were dried over $MgSO_4$ and concentrated under reduced pressure. The crude product was purified by silica gel column chromatography using ethyl acetate: hexane (5:95) as eluent. Yield 26 mg (76% yield) . The NMR data were matched for previously publish results. [132] ^{1}H NMR (500 MHz, $CDCl_3$) δ = 9.95 (s, 1H), 7.02 (d, J = 1.9 Hz, 1H), 6.73 (dd, J = 7.8 Hz, 1.9 Hz, 1H), 6.59 (d, J = 7.8 Hz, 1H), 6.56 (dd, J = 7.9 Hz, 1.8 Hz, 1H), 6.50 (dd, J = 7.9 Hz, 1.8 Hz, 1H), 6.43 (dd, J = 7.9 Hz, 1.8 Hz, 1H), 6.37 (dd, J = 7.9 Hz, 1.8 Hz, 1H), 4.10 (ddd, J = 11.8 Hz, 9.6 Hz, 1.5 Hz, 1H), 3.27 (ddd, J = 12.5 Hz, 10.4 Hz, 2.0 Hz, 1H), 3.21 (dd, J = 11.7 Hz, 4.5 Hz, 1H), 3.18 (dd, J = 11.7 Hz, 4.5 Hz, 1H), 3.14-2.97 (m, 3H), 2.95 (ddd, J = 13.1 Hz, 10.1 Hz, 6.7 Hz, 1H). ^{13}C NMR (100 MHz, $CDCl_3$): δ = 191.1, 143.2, 140.6, 139.5, 139.4, 138.1, 136.6, 136.3, 136.1, 133.2, 132.9, 132.3, 132.1, 35.2, 35.1, 35.0, 33.6.

3.5.11 Resolution of (3-21)

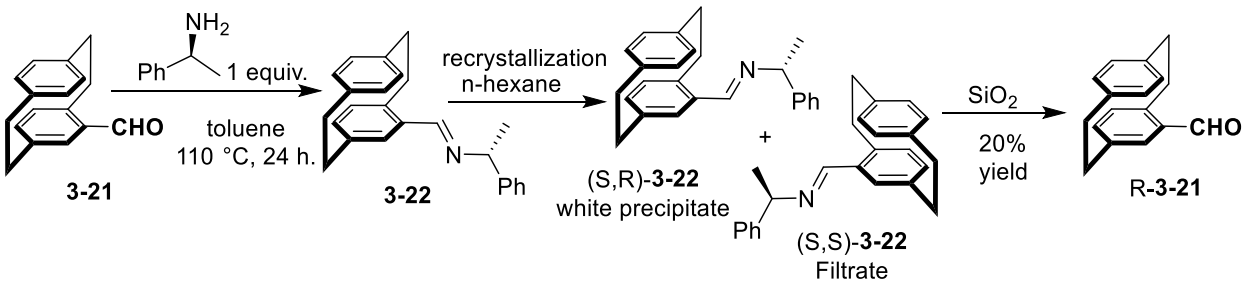

According to a previously published procedure,[132] a mixture of racemic formyl [2,2]paracyclophane **3-21**) (500 mg, 2.116 mmol, 1 equiv.) and (-)-S-(phenyl) ethylamine (256 mg, 2.116 mmol, 1 equiv.) in toluene (14.1 ml) was stirred for 24 hours at 110 °C. A diastereomeric mixture of imine moiety (**3-22**) was formed. After removing the toluene solvent by reducing pressure, the mixture was dissolved again in n-hexane (10.6 ml). The diastereomeric mixture (**3-22**) was put in the fridge for 1 hour until a white solid precipitate formed. Filtration and drying of the precipitate produced (S, R)-**3-22** 0.465 mg (22% yield) and 96% *ee*. Then, the compound (S, R)-(**3-22**) was dissolved in CH_2Cl_2 and filtered through a silica column to give the enantiopure aldehyde moiety due to acidic properties of silica gel. The enantiomeric enrichment of the aldehyde was confirmed by HPLC using chiral amylose-2 and an eluent of

hexane/2-propanol (65:35) and 0.1 % of TFA, 0.5 ml /min, at 25°C. (*S*)-**3-21** elutes at 6.5 minutes and (*R*)-**3-21** elutes at 7 minutes.

3.5.12 Synthesis nitrile-[2,2]paracyclophane (3-23)

To a 20 ml reaction vial was added formyl [2,2]paracyclophane (**3-21**) (171 mg, 0.724 mmol, 1 equiv.), sodium azide (235.5 mg, 3.622 mmol, 5 equiv.) and phosphorus oxychloride (1 ml, 10.87 mmol, 15 equiv.). The reaction mixture was stirred for 16 hours at 70 °C. Then, the reaction was quenched with water and extracted with ethyl acetate (2 ml). The combined organic layers were dried over $MgSO_4$ and concentrated under reduced pressure. The crude product was purified by silica gel column chromatography using ethyl acetate: hexane (10:90) as eluent to produce 128 mg (76% yield). ^{1}H NMR (400 MHz, $CDCl_3$) δ 6.91 (dd, *J* = 8.1, 1.4 Hz, 2H), 6.77 – 6.70 (m, 2H), 6.62 – 6.45 (m, 6H), 5.30 (s, 1H), 3.64 – 3.40 (m, 9H), 3.30 (dddd, *J* = 12.8, 10.2, 4.5, 0.6 Hz, 2H), 3.21 – 2.97 (m, 11H), 1.91 – 1.79 (m, 4H), 1.78 – 1.63 (m, 4H). ^{13}C NMR (101 MHz, $CDCl_3$) δ 148.9, 144.2, 140.9, 139.5, 139.1, 137.1, 136.7, 134.5, 133.5, 132.9, 132.7, 130.9, 77.3, 77.0, 76.7, 35.3, 35.1, 34.4, 34.2.

3.5.13 Synthesis 1*H*-tetrazle [2,2] paracyclophane (3-24)

To 20 ml, well-sealed vial was added the nitrile-[2,2]paracyclophane (**3-23**) (9.6 mg, 0.041 mmol, 1 equiv.), sodium azide (5.3 mg, 0.082 mmol, 2 equiv.), zinc bromide (18.4 mg, 0.0819 mmol, 2 equiv.), and solution of 2:1 octanol: water (0.1 ml). The reaction mixture was vigorously stirred for 36 hours at 185 °C. After HPLC showed a partial formation of the product, the mixture was quenched with 3 N HCl (0.3 ml) and extracted three times with ethyl acetate then dried with sodium sulfate. The product was purified by silica gel chromatography with ethyl acetate: hexane (30:70) as eluent. Yield 1 mg (10%). ^{1}H NMR (500 MHz, $CDCl_3$) δ 6.62 (dd, *J* = 7.8, 1.9 Hz, 1H), 6.56 – 6.50 (m, 3H), 6.43 (dd, *J* = 7.9, 1.5 Hz, 1H),

3.78 (ddd, *J* = 12.8, 10.2, 2.4 Hz, 1H), 3.32 – 2.80 (m, 8H). ^{13}C NMR (126 MHz, $CDCl_3$) δ 140.3, 140.0, 139.9, 139.3, 136.3, 135.7, 132.8, 132.7, 132.6, 132.2, 131.9, 35.5, 35.4, 35.3, 35.1.

3.5.14 (rac)-4-Bromo[2,2]paracyclophane (3-25)

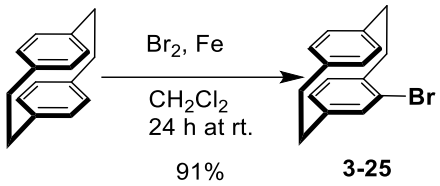

According to a previously published procedure[132], a solution of bromine (0.11 ml, 2.1123 mmol, 1.1 equiv.) was prepared in CH_2Cl_2 (1.5 ml). A solution of iron powder (3.4 mg, 0.0609 mmol, 3 mol %) and the bromine solution (0.3 ml) were mixed and stirred for 1 hour at room temperature. The reaction mixture was diluted with CH_2Cl_2 (7 ml) and [2,2]paracyclophane (400 mg, 1.9203 mmol, 1 equiv.) was added. The mixture was stirred for a further 20 min, followed by dropwise addition of the rest bromine solution (1.2 ml) over 3 h. The reaction mixture was stirred for 16 h at room temperature. After confirming the product by TLC, a saturated aqueous solution of $Na_2S_2O_3$ was added. The aqueous phase was extracted three time with CH_2Cl_2 (3 x 9 ml) and combined organic layers were dried over Na_2SO_4. The solvent was removed under reduced pressure to give a white product 501 mg (91% yield). The NMR data matched with a literature data.[132] ^{1}H NMR (500 MHz, $CDCl_3$) δ 7.17 (dd, *J* = 7.8, 2.0 Hz, 1H), 6.65 – 6.33 (m, 9H), 3.47 (ddd, *J* = 13.4, 10.2, 2.2 Hz, 1H), 3.30 – 2.70 (m, 10H).^{13}C NMR (126 MHz, $CDCl_3$) δ 141.6, 139.6, 139.3, 139.1, 137.3, 135.1, 133.3, 133.0 (d, *J* = 14.2 Hz), 132.3, 131.5, 128.7, 127.0, 35.9, 35.7, 35.5, 34.8, 33.5.

3.5.15 [2,2]paracyclophayl-4-boronic acid pinacol ester (3-26)

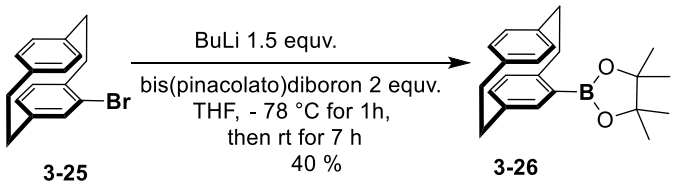

To a 20 mL reaction vial under an atmosphere of N_2 was prepared a solution of 4-bromo[2,2]paracyclophane (**3-25**) (0.5 g ,1.741 mmol, 1 equiv.) in THF (5.7 ml) . The solution was cooled to -78 °C followed by dropwise addition of n-butyllithium solution (1.04 ml, 2.5M in hexane, 2.6114 mmol, 1.5 equiv.) and stirred for 1 hour. A solution of bis(pinacolato)diboron (884 mg, 3.4818 mmol, 2 equiv.) in THF (3 ml) was prepared. The solution of bis(pinacolato)diboron was added to the reaction mixture and left to stir for 1 hour at the same temperature. After the reaction temperature was left at room temperature, the reaction was stirred for seven hours until the HPLC analysis confirmed the product **3-26**. The reaction was quenched with saturated ammonium chloride (9 ml) and extracted three times with ethyl acetate (3 x 10 ml). The combined organic layers were dried with $MgSO_4$ and concentrated under reduced pressure. The product **3-26** was purified with preparation HPLC using a C18 column as the stationary phase and acetonitrile: water (35:65-95:5) as the eluent. Yield 145 mg (40%). The NMR data was matched the literature.[133] ^{1}H NMR (500 MHz, $CDCl_3$) δ 7.04 (d, *J* = 1.9 Hz, 1H), 6.61 – 6.42 (m, 5H), 6.38 (dd, *J* = 7.7, 1.8 Hz, 1H), 3.96 (ddd, *J* = 12.6, 10.3, 2.1 Hz, 1H), 3.24 – 2.77 (m, 7H), 1.40 (d, *J* = 4.5 Hz, 12H). ^{13}C NMR (126 MHz, $CDCl_3$) δ 147.4, 140.3, 140.0, 139.6, 138.4, 135.3, 134.0, 133.2, 133.2, 132.6, 132.4, 83.2, 77.3, 77.0, 76.8, 35.9, 35.7, 35.6, 35.3, 25.1, 24.8.

3.5.16 [2,2]paracyclophayl-4-boronic acid (3-27)

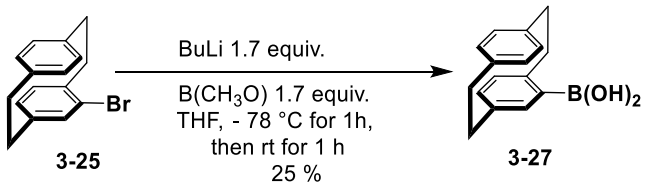

To a 20 mL reaction vial under an atmosphere of N_2 was prepared a solution of 4-bromo [2,2]paracyclophane (**3-25**) (50 mg ,0.174 mmol, 1 equiv.) in THF (1.7 ml) . The solution was cooled to -78 °C followed by dropwise addition of an n-butyl lithium solution (0.1155 ml, 2.5M in hexane, 0.296 mmol, 1.7 equiv.) and stirred for 1 hour. Then, trimethyl borate (0.033 ml, 0.296 mmol, 1.7 equiv.) was added to the reaction mixture and left to stir for 15 min. After the reaction temperature was at room temperature, the reaction was stirred for another 1 hour until the HPLC analysis confirmed the product **3-27**. The product **3-27** was purified with preparative HPLC using a C18 column as the stationary phase and acetonitrile: water (35:65-95:5) as the eluent. Yield 11 mg (25% yield). ^{1}H NMR (500 MHz, $CDCl_3$) δ 7.01 (dd, *J* = 7.8, 1.8 Hz, 1H), 6.65 – 6.12 (m, 5H), 5.54 (s, 1H), 4.45 (s, 1H), 3.47 – 3.24 (m, 1H), 3.18 – 2.81 (m, 7H), 2.66 (dt, *J* = 13.6, 8.9 Hz, 1H). ^{13}C NMR (126 MHz, $CDCl_3$) δ 153.8, 142.13, 139.8, 139.0, 135.6, 133.7, 132.9, 132.0, 128.1, 125.6, 125.2, 122.7, 77.4, 77.2, 76.9, 35.4, 35.0, 34.0, 31.2, 1.2.

3.5.17 (*S*)-Methylbenzyl-1*H*-tetrazole (3-28)

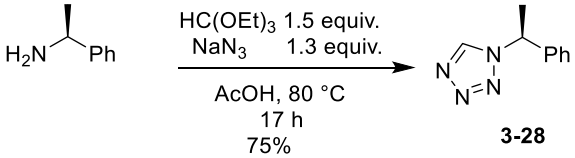

To 20 ml reaction vial was added (*S*)-Methylbenzylamine (0.5319 ml, 4.1261 mmol, 1 equiv.) and acetic acid (3 ml). Then, sodium azide (348 mg, 5.364 mmol, 1.3 equiv.) and triethylorthoformate (1 ml, 6.189 mmol, 1.5 equiv.) were added to the vial. The reaction mixture was stirred for 17 hours at 80 °C. After HPLC analysis confirmed the product, the solvent was removed by reducing the pressure. The

product was purified and isolated by preparative HPLC using a C18 column as the stationary phase and acetonitrile: water (10:90-100:0.0) as the eluent. Yield 75% yield (539 mg). ^{1}H NMR (500 MHz, $CDCl_3$) δ 8.43 (s, 1H), 7.52 – 7.36 (m, 3H), 7.36 – 7.16 (m, 4H), 5.83 (q, *J* = 7.1 Hz, 1H), 2.05 (d, *J* = 7.1 Hz, 3H). ^{13}C NMR (126 MHz, $CDCl_3$) δ 141.7, 138.3, 129.5, 129.4, 126.8, 59.5, 21.5.

3.5.18 (*S*)-Methylbenzyl-5-bromo-1*H*-tetrazole (3-29)

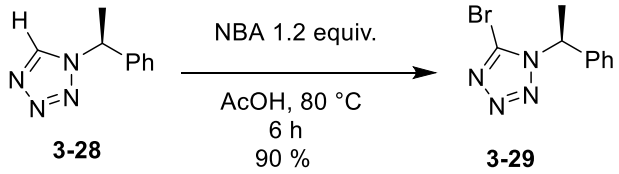

3-28 **3-29**

To 20 ml vial was added a (*S*)-Methylbenzyl-1*H*-tetrazole (3-28) (0.7188 g, 4.1261 mmol, 1 equiv.), n-bromosuccinimide (955 mg, 5.364 mmol, 1.3 equiv.), and acetic acid (4.13 ml). The solution was stirred for 6 hours at 80 °C until HPLC analysis confirmed the product (**3-29**). The reaction was cooled to room temperature and diluted with water (5 ml). The product was purified and by preparative HPLC using a C18 column as the stationary phase and acetonitrile: water (10:90-100:0.0) as the eluent. Yield 522 mg (50% yield). ^{1}H NMR (500 MHz, $CDCl_3$) δ 7.45 – 7.13 (m, 1H), 5.71 (q, J = 7.1 Hz, 0H), 2.07 (d, J = 7.1 Hz, 1H). ^{13}C NMR (126 MHz, $CDCl_3$) δ 138.0, 138.0, 132.7, 129.2, 129.0, 126.5, 59.7, 21.6.

CHAPTER FOUR

4 QUANTITATIVE ANALYSIS OF PHOSPHORUS IN ENIROMENTAL SAMPLES BY ^{31}P NUCLEAR MAGNETIC RESONANCE SPECTROSCOPY

4.1 Introduction

Phosphorus is an essential nutrient for all organisms in the marine system and can be part of necessary precursors for the biosynthesis of natural compounds.[134,135] However, high P concentrations can negatively affect the water quality by increasing the growth of nuisance algae, sedimentation, and hypoxia.[136,137] Therefore, controlling P concentration requires information about the various P chemical forms available, which in turn determines the bioavailability and environmental reactivity.[138,139]

Marine sediment is the main source of phosphorus in water samples which accumulates through biogeochemical processes.[140] Mineralization of P to the sediment is another possible mechanism in which P is released into the water.[141] Additionally, the sedimentary P is also released due to the decomposition of enzymes or bacterial that contain P in their cellular structure.[141,142]

The mechanism of inorganic P release into the sediment results from reductive dissolution of phosphate complexed with Fe(III) hydroxides which is catalyzed through iron-reductive bacteria (IRB) (Scheme 4.1).[140,143] When the reduced Fe(II) reaches the oxic zones, either in the water or sediment layer, it is re-oxidized to Fe(III) hydroxide and reabsorbed in the form of dissolved P onto the mineral surface. The P bioavailability increases in the sediment when hydrogen sulfide (HS^-) is present in the cycle due to consumption of the reduced Fe (II) and transformation into iron sulfide (FeS). The presence of aluminum hydroxides $Al(OH)_3$ can inhibit dissolved P through binding under reduced conditions.[143]

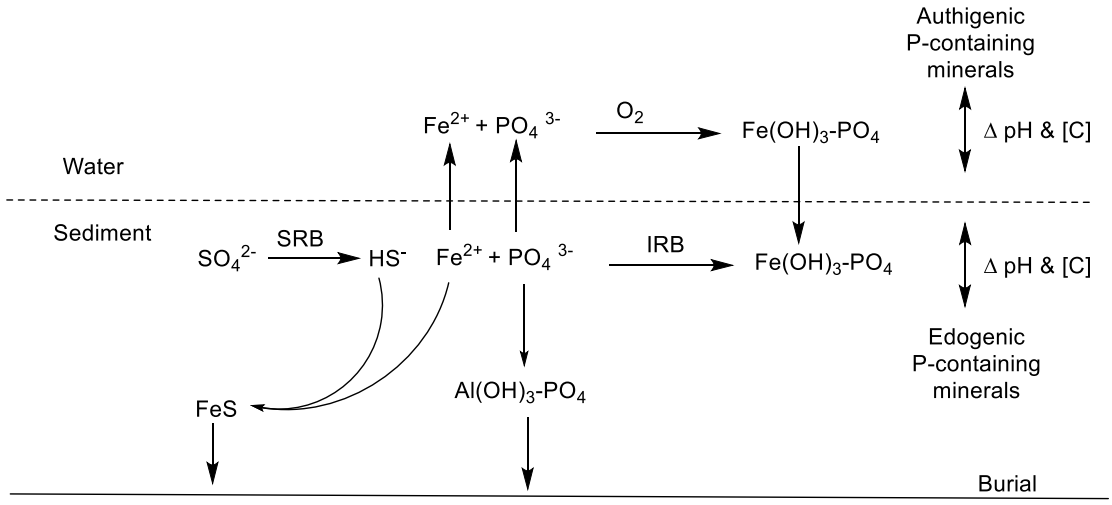

Scheme 4.1 Schematic diagram of inorganic phosphorus cycling in Maine lake sediment. Sulfate-reducing bacteria (SRB) and iron-reducing bacteria (IRB) catalyze sedimentary P release. $Fe(OH)_3$ and $Al(OH)_3$ represent the most abundant metal hydroxides.[143]

In a natural sample, phosphorus can be divided into inorganic P and organic P.[139,143] P is considered inorganic when it directly associates with metals in the form of orthophosphate, pyrophosphate, and polyphosphate. Organic P contains carbon-hydrogen bonds in its constituent structure such as orthophosphate monoesters, phosphate diesters, and organic polyphosphates. Orthophosphate monoesters have a general structure, $ROPO_3^{2-}$, in which R represents an organic motif per one phosphorus. For example, the sugar glucose 6-phosphate or the hexahydroxy cyclohexane in phytic acid, are orthophosphate monoesters as seen in Table 4.1 Entries 1 and 2.[139,144]

Orthophosphate diesters, with the general structure $R_1O(RO)PO_2^-$, have two R groups for each one phosphorus and include structures such as nucleic acids or phospholipids (Table 4.1 Entry 3). In polyphosphates, the structure contains multiple monoester or diester groups such as adenosine tripolyphosphate (ATP), as seen in Table 4.1 Entry 4. In phosphonates, phosphorus binds directly to carbon with the general structure $RP(O)(OH)_2$, as can be seen in 2-aminoethyl phosphonic acid (AEP) (Table 4.1 Entry 5).[144]

Table 4.1 Organic phosphorus classes in natural samples and their common structures [144]

Functional class	Example compound	Structure
Phosphate monoester	D-Glucose 6-phosphate	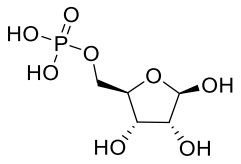
Phosphate monoester	Myo-Inositol Hexakisphosphate (phytic acid)	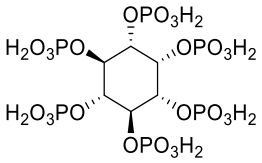
*Phosphate diester	L-α-Phosphatidyl choline (lecithin)	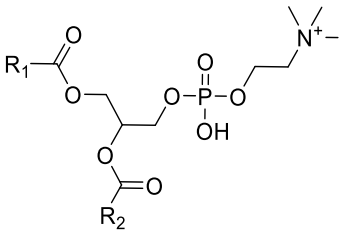
Organic polyphosphate	Adenosine 5'-triphosphate (ATP)	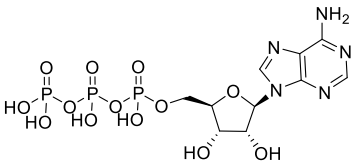
Phosphonate	2-Aminoethyl phosphonic acid (AEP)	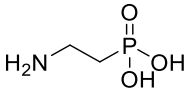

*R: non identical hydrophobic fatty acyl chains

Since most analytical techniques are compound dependent, a useful characterization method for determining sedimentary P level is a sequential fractionation method.[139,145] However, this method is laborious and time consuming, and depends on the solubility of the sample in various extractants. Also, it cannot identify the organic or inorganic P species.[139] NMR spectroscopy is well known as a powerful tool for identifying molecular structures as well as the measurement of various chemical and physical properties. The quantitative use of NMR has widely increased in the past decade [139,146–148].

Quantitative NMR has been used in environmental, agricultural, and pharmaceutical samples as a promising approach for organic molecule quantification.[138,149] Comparable to chromatographic

methods, quantitative ^{31}P NMR has high accuracy and precision with reliable results for pharmaceutical and food samples.[150] All P forms within environmental samples can be detected by NMR spectroscopy because ^{31}P is a ~100% naturally abundant isotope. Also, the area under the peak is proportional to the number of P nuclei when using inverse gated decoupling and an appropriate relaxation time. However, environmental samples need special treatment and extraction to avoid existing paramagnetic metals (Fe, and Al) before preparing to quantitate ^{31}P NMR. Generally, ^{31}P NMR environmental samples contain singlets between 25 and -25 ppm, as seen in Figure 4.1.[138]

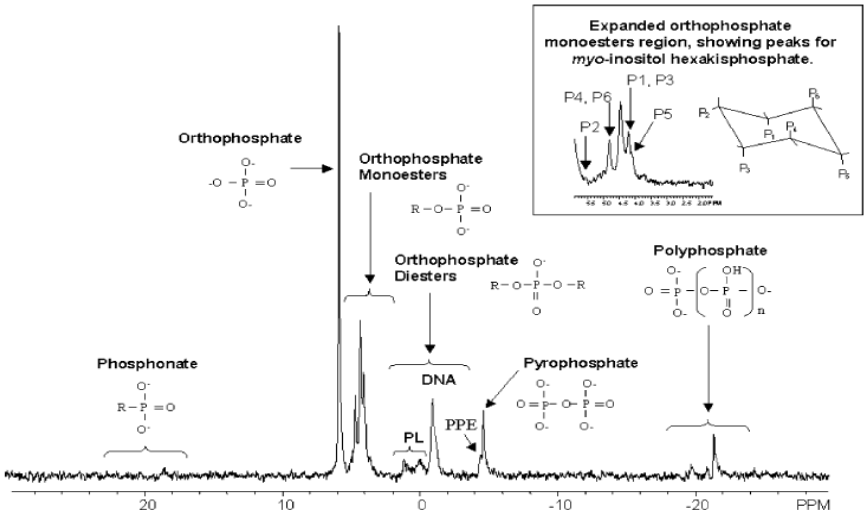

Figure 4.1 The ^{31}P NMR spectrum of forest floor sample after extraction with NaOH-EDTA shows diverse P species, including organic P and inorganic P. PPE indicates terminal P in the polyphosphate chain. Expanded orthophosphate monoesters region shows the peaks and structure of myo-inositol hexakisphosphate (phytic acid). Reprinted from ref.122 with permission from Elsevier.[138]

For example, phosphonates appear at 20 ppm, orthophosphate at 5-7 ppm, orthophosphate monoesters around 3-6 ppm, orthophosphate diesters at 2.5 to -1 ppm, pyrophosphate at -4 to -5 ppm and polyphosphate at -20 ppm, respectively (Figure 4.1).[138] Herein, ^{31}P NMR has been used for the quantitative analysis of organic phosphorus in samples from Highland Lake, Maine. The samples have

been subjected to several processes before running the ^{31}P NMR analysis, including pre- and post-treatment, extraction, and redissolving samples. Additionally, acquisition parameters have been optimized including delay time, proton decoupling, and experiment length in order to be as accurate as possible.

4.2 Materials and Methods

4.2.1 The sediment extraction procedure

The extraction procedure used for the ^{31}P NMR study has previously been reported and was conducted in collaboration with Aria Amirbahman.[140] This technique can distinguish between organic P (consisting of monoester and diester P), polyphosphates, and orthophosphate. Organic P and polyphosphates together constitute biogenic phosphorus. Sediment phosphorus was extracted by shaking approximately 10 g of wet sediment for 16 hr with 30 mL of 0.25 M NaOH/0.05 M EDTA. After centrifugation, the supernatant was neutralized with 6 N HCl to a pH of 7-8 to preserve polyphosphates during lyophilization.[151] The supernatants were frozen at -80°C and placed in a freeze dryer until completely dry. The dried samples were reconstituted in 3 mL of 1 M NaOH and centrifuged again. A 1 mL aliquot was removed for total P analysis using a Perkin Elmer 3300XL inductively coupled with optical emission spectrometer (ICP-OES) and another 1 mL aliquot transferred to an NMR tube. Deuterium oxide (100 µL) was added to provide a lock signal and 100 µL of 0.1 M bicarbonate/dithionite solution was added to reduce the remaining paramagnetic ions.

4.2.2 ^{31}P NMR Acquisition Parameters

The samples were acquired on a Bruker 500 MHz NMR spectrometer equipped with a broadband probe in 5 mm NMR tubes. The sample was locked and shimmed on the D_2O present in the sample. For quantitative NMR spectra, ^{31}P NMR was taken after optimizing the 90° pulse width (P1) for each sample

and using a delay time (d_1) of 5.489 s, which is five times the measured relaxation time (5 x t_1). The relaxation time was measured for phosphate species by an inversion recovery experiment (t_1= 1.0978 s). The samples were scanned for approximately 11 hours and 19 minutes (~7,000 transients) with a spectral window of 16,339.9 Hz, an acquisition time of 0.3 s, at 25 °C temperature, and a line-broadening of 10 Hz.

4.2.3 ^{31}P NMR Processing

The resulting free induction decay (FID) data were processed using MestreNova 11 software. An autophased and automated baseline correction for the FID data was carried out. Then, signal-to-noise ratios (SNR) were measured between (88.6 to 325.07) for phosphate species. All expected peaks were integrated and picked manually followed by calculation of the relative phosphorus abundances. The difference between the orthophosphate concentration and total phosphorus is the organic phosphorus concentration it was determined using ICP-OES.[152] The concentration for each species can be calculated by multiplying the relative abundance of the spectral peak by the total P concentration in the sample with the assumption being that all P compounds were within the designated spectral window.[140]

4.3 Result and discussion

^{31}P NMR analysis for an environmental sample is more complex than purified samples due to the low concentration of P species in environmental samples. Also, P species in nature are associated with paramagnetic ions including iron (Fe) and manganese (Mn). Therefore, a pretreatment and extraction with NaOH/EDTA lowers the concentration of paramagnetic ions and leads to accurate quantitative results.[153] The extraction process provides a high recovery of both organic and inorganic P.[139] Environmental samples were collected from Highland Lake in Maine at various depths between 19-34 cm in the middle of June to early July, 2019, due to the fact that the concentration of P increases in the lake waters during the summer.[140]

Quantitative ^{31}P NMR required accurate determination of the spin-lattice relaxation times (T_1) to ensure an appropriate delay time between pulses. If T_1 is insufficient, then the nuclei may not completely relax to equilibrium. Therefore, the relative intensity of the peaks reduced compared with those which are fully relaxed. Consequently, the integrated a peak area would not be comparable and would over- or under-represent specific P species. Therefore, an inversion-recovery experiment was carried out to measure T_1 for orthophosphate in an environmental sample, which was found to be 1.0978 s. For quantitative ^{31}P NMR, a delay time (d_1) five-times T_1 was used as seen in Figure 4.2.

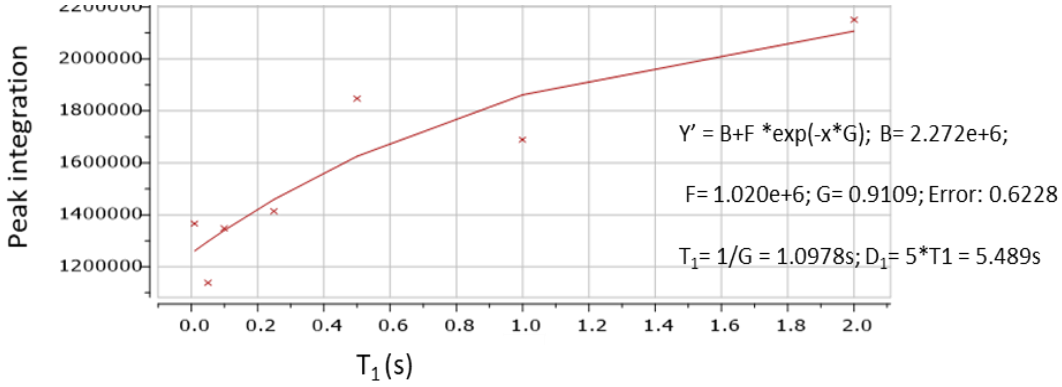

Figure 4.2 Diagram of measured **r**elaxation times (T_1).

The sediment depth has a strong influence on the P form because of the change in chemical and physical properties. The total P was determined to be between 10-20 ppm using an inductively coupled optical emission spectrometer (ICP-OES). The total P concentration is low on the surface and increases with the sediment depth, as shown in Table 4.2 Entries 1-3 and Entries 4-6.

The P speciation in the sediments was determined by ^{31}P NMR spectroscopy, as listed in Table 4.2 (spectra are shown in appendix F). The total organic P is a summation of phosphonate, orthophosphate monoester, phosphodiester, pyrophosphate, and polyphosphate. While the detected orthophosphate represents the inorganic phosphorus species, as seen in Table 4.2. The orthophosphate was determined

as the highest P concentration in the samples (up to 0.4357 μmol g^{-1}, 73%) due to the adsorption of orthophosphate to $Al(OH)_3$. The orthophosphate concentration was increased with sediment depth, as seen in Table 4.2 Entries 1-3. The orthophosphate monoester was the second-highest abundance P species found in the samples to reach up to 0.1387 μmol g^{-1} (25%) (Table 4.2 Entries 1).

Table 4.2 P analysis of the samples collected from Highland Lake, Maine.

From ^{31}P NMR Spectra

Entry	Sediment depth (cm)	Phosphonate (μmol g^{-1})	OrthoP (μmol g^{-1})	OrthoP Monoesters (μmol g^{-1})	Plipids (μmol g^{-1})	Pdiesters (μmol g^{-1})	PyroP (μmol g^{-1})	Total P (ppm) (ICP-OES Analysis)
*1-	33.7	0.0148	0.4357	0.1387	0.0007	0.0108	0.00142	18.7
2-	25.1	0.0012	0.2650	0.1020	0.0004	0.0232	0.00094	12.2
*3-	20.2	0.0046	0.2332	0.1186	0.00003	0.0104	0.00051	11.4
**4-	33.71	5E-05	0.4737	0.1478	0.00373	0.0106	5E-06	19.7
**5-	26.3	0.0002	0.2172	0.0873	0.0017	0.0161	0.0017	10.1
**6-	19	0.0008	0.2892	0.1269	0.0004	0.0143	0.00051	13.4

Phosphonate, Orthophosphate (Orthop), Phospho-lipids (Plipids), phosphodiester (Pdiesters), and pyrophosphate (pyroP) concentrations were determined using ^{31}P NMR at pH > 8 for solution. ^{31}P NMR were taken after optimization 90 pulse width (P1) and using a delay time (d1= 5.489 s) of $5xt_1$ where t_1 measured for phosphate species (t_1= 1.0978 s) by an inversion recovery array. The samples were scanned 7000 times (11h 19 m) until the signal to noise was > 88.69.*measured at pH > 13. ** samples were collected for the similar sediment's depth in middle of July 2019. ppm of P = $\frac{\text{mg of P}}{\text{kg of Total sample}}$ $\frac{\text{mmol of P}}{30.974\ \text{mg of P}} = \frac{\text{x mmol of P}}{\text{kg of Total Sample}} = \frac{\text{x μmol of P}}{\text{g of Total Sample}} = \frac{\mu\text{mol}}{\text{g}}$.

Phosphor diesters were detected up to 0.0108 μmol g^{-1} (1.8 %) and the majority of this species is due to microbial DNA. Phosphonate, Phospholipid and pyrophosphate species were determined to be the lowest P content in the samples (< 1%), as in Table 4.2. Samples were collected one month later in the middle of July at a similar sediment depth (19-34 cm) and analyzed by ^{31}P NMR as seen in Table 4.2 Entries 4-6. The total P concentration was similar for all samples compared to the samples taken in June (19-10 ppm), as seen in Table 4.2 entries 4-6. However, the P concentration at the middle depth (26.1 cm) was the lowest concentration when compared with the highest or lowest depth samples as seen in Table 4.2 Entries 4-6.

Due to the long experimental times, replicate ^{31}P NMR acquisitions were not obtained. However, to estimate the uncertainty associated with NMR processing, each acquisition was analyzed three times to calculate a relative error (Table 4.3).

Table 4.3 Measurement uncertainties associated with samples using ^{31}P NMR determined by replicate processing of each of spectrum.

Entry	P fraction	P contain range (μmol g^{-1})	Average Mean (μmol g^{-1})	Average Standard deviation	Average relative error (%)
1-	Phosphonate	0.00005 – 0.0148	0.027	0.006	21
2-	OrthoP	0.2172 – 0.4737	10.0	0.2	1
3-	OrthoP Monoesters	0.0873 – 0.1478	5.8	0.15	3
4-	Plipids	0.00003 – 0.0037	0.29	0.06	18
5-	Pdiesters	0.0104 – 0.0232	0.69	0.004	2
6-	PyroP	0.00005 – 0.0017	0.14	0.003	14

Relative error (%) = (SD/mean) X 100

Uncertainty for each P species is listed in more detail in Table F.1. Phosphorus concentration determinations contained uncertainties that ranged between 0.5% to 21% error (Table 4.3). The highest uncertainty was found for phosphonate and phospholipid species due to the lowest signal compared to other P species (up to 21% and 18.9 % respectively, as in Table 4.3 Entries 1 and 4). The uncertainty related to measuring orthophosphate and orthophosphate monoester decreased to 1.38% and 3.22% respectively due to the highest signal-to-noise ratio (Table 4.3 Entries 2 and 3). Finally, the uncertainty for measuring phosphodiester and pyrophosphate was acceptable at 0.57% and 2.40% respectively, as seen in Table 4.3 Entries 5 and 6.

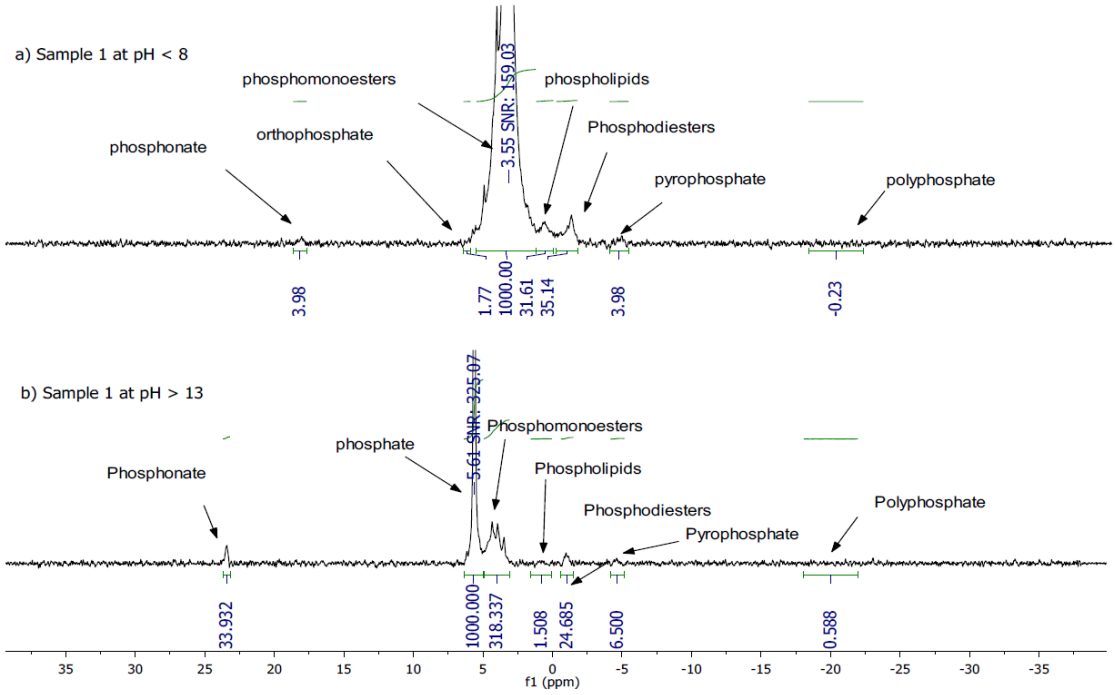

Figure 4.3 a) ^{31}P NMR spectrum of sample 1 at 33.7 cm sedmint depth of Highland Lake in Maine after NaOH/EDTA extracted at pH < 8. **b)** spectrum of the same sample at pH > 13. Spectra are ploted with 10-Hz line broadening.

An important requirement for all NMR experiments is to obtain the spectra with a good resolution and a high signal-to-noise ratio. In spectral resolution, the sharpness and separation of the peaks is affected, while the signal-to-noise ratio describe the height of the peak relative to baseline noise. pH samples can affect P speciation by influencing sample chemistry, organic matter decomposition, and the extractability of P compounds. Lower pH favors phosphonates, orthophosphates, and phosphomonoesters which are correlated to the pH of the solution.[138,139] Typically, ^{31}P NMR experiments are carried out at a pH < 8 to avoid P compound degradation. However, higher pH (pH > 13) is needed to increase the peak separation and resolution. Therefore, the pH of some solutions were increased to > 13

to obtain ^{31}P NMR spectrum with high resolution and increase the p species separation. For example, the spectrum resolution for sample 1 at 33.7 cm was increased with higher pH as seen in Figure 4.3.

4.4 Conclusion

Phosphorus nuclear magnetic resonance (^{31}P NMR) spectroscopy is used for the quantitative analysis of P forms in environmental samples. After pretreatment and extraction of the sediment in an alkaline solvent (NaOH/EDTA), the ^{31}P NMR was acquired. A spin-lattice relaxation time (T_1) for orthophosphate was calculated to be 1.078 s to ensure adequate delay time between pulses. To increase spectral resolution, the pH of the samples were adjusted to < 8 or > 13. The phophorus abundance was determined for sediments at different depths from Highland Lake, Maine during the summer. The highest abundance species were orthophosphate (up to 73%) and phosphomonoester (up to 25%). Other organic species detected were phospholipids and phosphodiesters (up to 5%) and originate predominately form microbial activity in the sediment. The remaining organic phosphorus species were detected in trace quantities. Quantitative ^{31}P NMR of dilute environmental samples was carried out to understand the origin and variation of phosphorus species over depth and time.

REFERNCES

(1) Dickenson J., Freeman F., Lloyd Mills C., Sivasubramaniam S., T. C. *Molecular Pharmacology from DNA to Drug Discovery*; John Wiley & Sons, Ltd.: NJ, USA, 2013.

(2) MacDonald, M.; Lamerdin, J.; Owens, S.; Keon, B.; Bilter, G.; Shang, Z.; Huang, Z.; Yu, H.; Dias, J.; Minami, T.; Identifying Off-Target Effects and Hidden Phenotypes of Drugs in Human Cells. *Nat. Chem. Biol.* **2006**, *2* (6), 329–337. https://doi.org/10.1038/nchembio790.

(3) Arenz, S.; Wilson, D. Bacterial Protein Synthesis as a Target for Antibiotic Inhibition. *Cold Spring Harb. Perspect. Med.* **2016**, *6* (9). https://doi.org/10.1101/cshperspect.a025361.

(4) Goldberg, A. Novel Therapies and New Targets of Treatment for Familial Hypercholesterolemia. *J. Clin. Lipidol.* **2010**, *4* (5), 350–356. https://doi.org/10.1016/j.jacl.2010.08.015.

(5) Lieberman, J. Tapping the RNA World for Therapeutics. *Nat. Struct. Mol. Biol.* **2018**, *25* (5), 357–364. https://doi.org/10.1038/s41594-018-0054-4.

(6) Bennett, C.; Swayze, E. RNA Targeting Therapeutics: Molecular Mechanisms of Antisense Oligonucleotides as a Therapeutic Platform. *Annu. Rev. Pharmacol. Toxicol.* **2010**, *50* (1), 259–293. https://doi.org/10.1146/annurev.pharmtox.010909.105654.

(7) Roberts, T.; Langer, R.; Wood, M. Advances in Oligonucleotide Drug Delivery. *Nat. Rev. Drug Discov.* **2020**, *19* (10), 673–694. https://doi.org/10.1038/s41573-020-0075-7.

(8) Watts, J.; Corey, D. Silencing Disease Genes in the Laboratory and the Clinic. *J. Pathol.* **2012**, *226* (2), 365–379. https://doi.org/10.1002/path.2993.

(9) Singh, J.; Kaur, H.; Kaushik, A.; Peer, S. A Review of Antisense Therapeutic Interventions for Molecular Biological Targets in Various Diseases. *International Journal of Pharmacology*. 2011, pp 294–315. https://doi.org/10.3923/ijp.2011.294.315.

(10) Gurav, B.; Srinivasan, G. Antisense Oligonucleotides as Therapeutics and Their Delivery. *Curr. Sci.* **2017**, *112* (3), 490–498. https://doi.org/10.18520/cs/v112/i03/490-498.

(11) Crooke, S. T. Molecular Mechanisms of Antisense Oligonucleotides. *Nucleic Acid Ther.* **2017**, *27* (2), 70–77. https://doi.org/10.1089/nat.2016.0656.

(12) Yin, W.; Rogge, M. Targeting RNA: A Transformative Therapeutic Strategy. *Clin. Transl. Sci.* **2019**, *12* (2), 98–112. https://doi.org/10.1111/cts.12624.

(13) Deweert, S. RNA Therapies Explained. *Nature* **2019**, *574*, S2–S3. https://doi.org/https://doi-org.wv-o-ursus-proxy02.ursus.maine.edu/10.1038/d41586-019-03068-4.

(14) Bennett, C.; Swayze, E. RNA Targeting Therapeutics: Molecular Mechanisms of Antisense Oligonucleotides as a Therapeutic Platform. *Annu. Rev. Pharmacol. Toxicol.* **2010**, *50*, 259–293. https://doi.org/10.1146/annurev.pharmtox.010909.105654.

(15) Railroading at the FDA. *Nature Biotechnology*. **2016**, p 1078. https://doi.org/10.1038/nbt.3733.

(16) Shen, X.; Corey, D. Chemistry, Mechanism and Clinical Status of Antisense Oligonucleotides and Duplex RNAs. *Nucleic Acids Res.* **2018**, *46* (4), 1584–1600. https://doi.org/10.1093/nar/gkx1239.

(17) Zamecnik, P. Inhibition of Rous Sarcoma Virus Replication and Cell Transformation by a Specific Oligodeoxynucleotide. *Proc. Natl Acad. Sci. USA.* **1977**, *75* (1), 280–284.

(18) U.S. Department of Health and Human Services. Drugs@FDA: FDA Approved Drug Products https://www.accessdata.fda.gov/scripts/cder/daf/ (accessed July 18, 2020).

(19) Brad Wan, W.; Seth, P. The Medicinal Chemistry of Therapeutic Oligonucleotides. *J. Med. Chem.* **2016**, *59* (21), 9645–9667. https://doi.org/10.1021/acs.jmedchem.6b00551.

(20) Sharma, V.; Rungta, P.; Prasad, A. Nucleic Acid Therapeutics: Basic Concepts and Recent Developments. *RSC Adv.* **2014**, *4* (32), 16618–16631. https://doi.org/10.1039/c3ra47841f.

(21) Sharma, V.; Sharma, R.; Singh, S. Antisense Oligonucleotides: Modifications and Clinical Trials. *Medchemcomm* **2014**, *5* (10), 1454–1471. https://doi.org/10.1039/c4md00184b.

(22) Micklefield, J. Backbone Modification of Nucleic Acids: Synthesis, Structure and Therapeutic Applications. *Curr. Med. Chem.* **2001**, *8* (10), 1157–1179. https://doi.org/10.2174/0929867013372391.

(23) Langner, H.; Jastrzebska, K.; Caruthers, M. Synthesis and Characterization of Thiophosphoramidate Morpholino Oligonucleotides and Chimeras. *J. Am. Chem. Soc.* **2020**, *142* (38), 16240–16253. https://doi.org/10.1021/jacs.0c04335.

(24) Takiya, T.; Seto, Y.; Yasuda, H.; Suzuki, T.; Kawai, K. An Empirical Approach for Thermal Stability (Tm) Prediction of PNA/DNA Duplexes. *Nucleic Acids Symp. Ser. (Oxf).* **2004**, No. 48, 131–132. https://doi.org/10.1093/nass/48.1.131.

(25) Laurent, A.; Naval, M.; Debart, F.; Vasseur, J.; Rayner, B. Chiral and Steric Effects in the Efficient Binding of α-Anomeric Deoxyoligonucleoside N-Alkylphosphoramidates to SsDNA and RNA. *Nucleic Acids Res.* **1999**, *27* (21), 4151–4159. https://doi.org/10.1093/nar/27.21.4151.

(26) Wan, W.; Migawa, M.; Vasquez, G.; Murray, H.; Nichols, J.; Gaus, H.; Berdeja, A.; Lee, S.; Hart, C.; Lima, W.; Synthesis, Biophysical Properties and Biological Activity of Second Generation Antisense Oligonucleotides Containing Chiral Phosphorothioate Linkages. *Nucleic Acids Res.* **2014**, *42* (22), 13456–13468. https://doi.org/10.1093/nar/gku1115.

(27) Verma, S.; Eckstein, F. MODIFIED OLIGONUCLEOTIDES: Synthesis and Strategy for Users. *Annu. Rev. Biochem.* **1998**, *67* (1), 99–134. https://doi.org/10.1146/annurev.biochem.67.1.99.

(28) Knouse, K.; deGruyter, J.; Schmidt, M.; Zheng, B.; Vantourout, J.; Kingston, C.; Mercer, S.; Mcdonald, I.; Olson, R.; Zhu, Y.; Unlocking P(V): Reagents for Chiral Phosphorothioate Synthesis. *Science.* **2018**, *361* (6408), 1234–1238. https://doi.org/10.1126/science.aau3369.

(29) Lin, G.; You, Q.; Cheng, J. *Chiral Drugs: Chemistry and Biological Action*; John Wiley & Sons, Incorporated: Somerset, United States, 2011. https://doi.org/10.1002/9781118075647.

(30) Iwamoto, N.; Butler, D.; Svrzikapa, N.; Mohapatra, S.; Zlatev, I.; Sah, D.; Standley, S.; Lu, G.; Apponi, L.; Frank-Kamenetsky, M. .; Zhang, J.;Vargeese, C.; Verdine, G. Control of Phosphorothioate Stereochemistry Substantially Increases the Efficacy of Antisense Oligonucleotides. *Nat. Biotechnol.* **2017**, *35* (9), 845–851. https://doi.org/10.1038/nbt.3948.

(31) Tomaszewska-Antczak, A.; Jastrzębska, K.; Maciaszek, A.; Mikołajczyk, B.; Guga, P. P-Stereodefined Phosphorothioate Analogs of Glycol Nucleic Acids—Synthesis and Structural Properties. *RSC Adv.* **2018**, *8* (44), 24942–24952. https://doi.org/10.1039/c8ra05568h.

(32) Laurent, a; Naval, M.; Debart, F.; Vasseur, J. J.; Rayner, B. Chiral and Steric Effects in the Efficient Binding of Alpha-Anomeric Deoxyoligonucleoside N-Alkylphosphoramidates to SsDNA and RNA. *Nucleic Acids Res.* **1999**, *27* (21), 4151–4159.

(33) Koskinen, A. *Asymmetric Synthesis of Natural Products*; John Wiley & Sons, Incorporated: New York, UNnited State, 2012. https://doi.org/10.1002/9781118347300.

(34) Ouellette, R.; Rawn, J. Organic Chemistry - Structure, Mechanism, and Synthesis. In *Organic Chemistry*; Elsevier: Saint Louis, United States, 2014; pp 315–342.

(35) Kagan, H.; Gopalaiah, K. Early History of Asymmetric Synthesis: Who Are the Scientists Who Set up the Basic Principles and the First Experiments? *New J. Chem.* **2011**, *35* (10), 1933–1937. https://doi.org/10.1039/c1nj20216b.

(36) Kolodiazhnyi, O.; Kolodiazhna, A. Nucleophilic Substitution at Phosphorus: Stereochemistry and Mechanisms. *Tetrahedron Asymmetry* **2017**, *28* (12), 1651–1674. https://doi.org/10.1016/j.tetasy.2017.10.022.

(37) Oka, N.; Wada, T.; Saigo, K. An Oxazaphospholidine Approach for the Stereocontrolled Synthesis of Oligonucleoside Phosphorothioates. *J. Am. Chem. Soc.* **2003**, *125* (27), 8307–8317. https://doi.org/10.1021/ja034502z.

(38) Pak, G.; Kim, J. A Novel Synthesis of (E)-2-Alkenylborane from Chiral Borane and Diazoalkene: Asymmetric Alkenylboration of Aldehydes. *Bull. Korean Chem. Soc.* **2019**, *40* (12), 1154–1155. https://doi.org/10.1002/bkcs.11909.

(39) Li, P.; Hu, X.; Dong, X.; Zhang, X. Recent Advances in Dynamic Kinetic Resolution by Chiral Bifunctional (Thio)Urea-and Squaramide-Based Organocatalysts. *Molecules* **2016**, *21* (10), 1–14. https://doi.org/10.3390/molecules21101327.

(40) Steinreiber, J.; Faber, K.; Griengl, H. De-Racemization of Enantiomers versus de-Epimerization of Diastereomers-Classification of Dynamic Kinetic Asymmetric Transformations (DYKAT). *Chem. A Eur. J.* **2008**, *14* (27), 8060–8072. https://doi.org/10.1002/chem.200701643.

(41) Wurz, R. Chiral Dialkylaminopyridine Catalysts in Asymmetric Synthesis. *Chem. Rev.* **2007**, *107* (12), 5570–5595. https://doi.org/10.1021/cr068370e.

(42) Bergin, E.; O'Connor, C.; Robinson, S.; McGarrigle, E.; O'Mahony, C.; Gilheany, D. Synthesis of P-Stereogenic Phosphorus Compounds. Asymmetric Oxidation of Phosphines under Appel Conditions. *J. Am. Chem. Soc.* **2007**, *129* (31), 9566–9567. https://doi.org/10.1021/ja072925l.

(43) Pellissier, H. Dynamic Kinetic Resolution. *Tetrahedron* **2003**, *59* (42), 8291–8327. https://doi.org/10.1016/S0040-4020(03)01022-6.

(44) Coldham, I.; Dufour, S.; Haxell, T.; Patel, J.; Sanchez-Jimenez, G. Dynamic Thermodynamic and Dynamic Kinetic Resolution of 2-Lithiopyrrolidines. *J. Am. Chem. Soc.* **2006**, *128* (33), 10943–10951. https://doi.org/10.1021/ja061963m.

(45) Chinchilla, R. Special Issue: Asymmetric Synthesis 2017. *Molecules*. 2017. https://doi.org/10.3390/molecules22091504.

(46) Oka, N.; Wada, T. Stereocontrolled Synthesis of Oligonucleotide Analogs Containing Chiral Internucleotidic Phosphorus Atoms. *Chem. Soc. Rev.* **2011**, *40* (12), 5829–5843. https://doi.org/10.1039/c1cs15102a.

(47) Miller, P.; Annan, N.; McFarland, K.; Pulford, S. . Oligothymidylate Analogues Having Stereoregular, Alternating Methylphosphonate/Phosphodiester Backbones as Primers for DNA Polymerase. *Biochemistry* **1982**, *21* (10), 2507–2512. https://doi.org/10.1021/bi00539a033.

(48) Cosstick, R.; Eckstein, F. Synthesis of d(GC) and d(CG) Octamers Containing Alternating Phosphorothioate Linkages: Effect of the Phosphorothioate Group on the B-Z Transition. *Biochemistry* **1985**, *24* (14), 3630–3638. https://doi.org/10.1021/bi00335a035.

(49) Carrasco, N.; Caton-Williams, J.; Brandt, G.; Wang, S.; Huang, Z. Efficient Enzymatic Synthesis of Phosphoroselenoate RNA by Using Adenosine 5'-(α-P-Seleno)Triphosphate. *Angew. Chem. Int. Ed.* **2005**, *45* (1), 94–97. https://doi.org/10.1002/anie.200502215.

(50) Eckstein, F.; Matzura H. Polyribonucleotide Containing Alternating → P = O and → P = S Linkages. *Eurropean J. Biochem.* **1968**, *3* (4), 448–452. https://doi.org/10.1111/j.1432-1033.1967.tb19551.x.

(51) Hall, A.; Wan, J.; Shaughnessy, E.; Shaw, B.; Alexander, K. RNA Interference Using Boranophosphate SiRNAs: Structure-Activity Relationships. *Nucleic Acids Res.* **2004**, *32* (20), 5991–6000. https://doi.org/10.1093/nar/gkh936.

(52) Ryan, M.; Liu T.;Dahlquist, F.; Griffith, O. A Catalytic Diad Involved in Substrate-Assisted Catalysis: NMR Study of Hydrogen Bonding and Dynamics at the Active Site of Phosphatidylinositol-Specific Phospholipase C. *Biochemistry* **2001**, No. 40, 9743–9750.

(53) Mathew,R.; Reibarkh, M.; Campeau, L.; Klapars, A.; Ruck, R.; Limanto, J.; Maligres, P.; Hyde, A. DiRocco, D.; Ji, Y.; Dropinski, J.; Davies, I.; Brunskill, A.; A Multifunctional Catalyst That Stereoselectively Assembles Prodrugs. *Science.* **2017**, *356* (6336), 426–430. https://doi.org/10.1126/science.aam7936.

(54) Oka, N.; Wada, T. Stereocontrolled Synthesis of Oligonucleotide Analogs Containing Chiral Internucleotidic Phosphorus Atoms. *Chem. Soc. Rev.* **2011**, *40* (12), 5829–5843. https://doi.org/10.1039/c1cs15102a.

(55) Wickstrom, A. The Chirality Problem in P-Substituted Oligonucleotides. *Perspect. Drug Discov. Des.* **1996**, *4* (Antisense Therapeutics), 17–40. https://doi.org/10.1007/BF02172106.

(56) Lesnikowski, Z. Stereocontrolled Synthesis of P-Chiral Analogues of Oligonucleotides. *Bioorganic Chemistry*. 1993, pp 127–155. https://doi.org/10.1006/bioo.1993.1014.

(57) Wilk, A.; Stec, W. Analysis of Oligo(Deoxynucleoside Phosphorothioate)s and Their Diastereomeric Composition. *Nucleic Acids Res.* **1995**, *23* (3), 530–534. https://doi.org/10.1093/nar/23.3.530.

(58) Seio, K.; Kumura, K.; Bologna, J.; Sekine, M. Enhanced Stereoselectivity in Internucleotidic Bond Formation by the Use of the Chiral Ribose Moiety of Thymidine. *J. Org. Chem.* **2003**, *68* (10), 3849–3859. https://doi.org/10.1021/jo020533l.

(59) Nawrot, B.; Rębowska, B.; Michalak, O.; Bulkowski, M.; Błeziak, D.; Guga, P.; Stec, W. 1,3,2-Oxathiaphospholane Approach to the Synthesis of P-Chiral Stereodefined Analogs of Oligonucleotides and Biologically Relevant Nucleoside Polyphosphates. *Pure Appl. Chem.* **2008**, *80* (8), 1859–1871. https://doi.org/10.1351/pac200880081859.

(60) Iyer, R.; Guo, M.; Yu, D.; Agrawal, S. Solid-Phase Stereoselective Synthesis of Oligonucleoside Phosphorothioates: The Nucleoside Bicyclic Oxazaphospholidines as Novel Synthons. *Tetrahedron Lett.* **1998**, *39* (17), 2491–2494. https://doi.org/10.1016/S0040-4039(98)00380-3.

(61) Iwamoto, N.; Oka, N.; Sato, T.; Wada, T. Stereocontrolled Solid-Phase Synthesis of Oligonucleoside *H*-Phosphonates by an Oxazaphospholidine Approach. *Angew. Chem. Int. Ed.* **2009**, *48* (3), 496–499. https://doi.org/10.1002/anie.200804408.

(62) Pertusati, F.; McGuigan, C. Diastereoselective Synthesis of P-Chirogenic Phosphoramidate Prodrugs of Nucleoside Analogues (ProTides) via Copper Catalysed Reaction. *Chem. Commun.* **2015**, *51* (38), 8070–8073. https://doi.org/10.1039/c5cc00448a.

(63) Liu, S.; Zhang, Z.; Xie, F.; Butt, N.; Sun, L.; Zhang, W. First Catalytic Enantioselective Synthesis of P-Stereogenic Phosphoramides via Kinetic Resolution Promoted by a Chiral Bicyclic Imidazole Nucleophilic Catalyst. *Tetrahedron Asymmetry* **2012**, *23* (5), 329–332. https://doi.org/10.1016/j.tetasy.2012.02.018.

(64) Brown, C.; Boudreau, J.; Hewitson, B.; Hudson, R. Alkaline Hydrolysis of Cyclic Phosphoramidates. *J. Chem. Soc. Chem. Commun.* **1975**, No. 13, 504–505. https://doi.org/10.1039/C39750000504.

(65) Sofia, M.; Bao, D.; Chang, W.; Du, J.; Nagarathnam, D.; Rachakonda, S.; Reddy, P.; Ross, B.; Wang, P.; Zhang, H.; Discovery of a Luoro-2'-β- C -Methyluridine Nucleotide Prodrug (PSI-7977) for the Treatment of Hepatitis C Virus. *J. Med. Chem.* **2010**, *53* (19), 7202–7218. https://doi.org/10.1021/jm100863x.

(66) Hara, I.; Saito, T.; Kogure, T.; Hamamura, Y.; Uchiyama, N.; Nukaga, Y.; Iwamoto, N. Wada, T. Stereocontrolled Synthesis of Boranophosphate DNA by an Oxazaphospholidine Approach and Evaluation of Its Properties. *J. Org. Chem.* **2019**, *84* (12), 7971–7983. https://doi.org/10.1021/acs.joc.9b00658.

(67) Gao, B.; Zhao, S.; Zhang, Z.; Li, L.; Hu, K.; Kaziem, A.; He, Z.; Hua, X.; Shi, H. Wang, M. A Potential Biomarker of Isofenphos-Methyl in Humans: A Chiral View. *Environ. Int.* **2019**, *127*, 694–703. https://doi.org/10.1016/j.envint.2019.04.018.

(68) Jia, M.; Wang, Y.; Teng, M.; Wang, D.; Yan, J.; Miao, J.; Zhou, Z.; Zhu, W. Toxicity and Metabolomics Study of Isocarbophos in Adult Zebrafish (Danio Rerio). *Ecotoxicol. Environ. Saf.* **2018**, *163* (January), 1–6. https://doi.org/10.1016/j.ecoenv.2018.07.027.

(69) Gill, J.; Sethi, N.; Mohan, A.; Datta, S.; Girdhar, M. Glyphosate Toxicity for Animals. *Environ. Chem. Lett.* **2018**, *16* (2), 401–426. https://doi.org/10.1007/s10311-017-0689-0.

(70) Zhang, L.; Miao, Y.; Lin, C. Enantiomeric Separation of Six Chiral Pesticides That Contain Chiral Sulfur/Phosphorus Atoms by Supercritical Fluid Chromatography. *J. Sep. Sci.* **2018**, *41* (6), 1460–1470. https://doi.org/10.1002/jssc.201701039.

(71) L Levchik, S. *Phosphorus-Based FRs. In Non-Halogenated Flame Retardant Handbook,* 1st ed.; Morgan, B.; Wilkie, A.; Scrivener Publishing: Beverly, MA, 2014.

(72) Dutartre, M.; Bayardon, J.; Jugé, S. Applications and Stereoselective Syntheses of P-Chirogenic Phosphorus Compounds. *Chem. Soc. Rev.* **2016**, *45* (20), 5771–5794. https://doi.org/10.1039/c6cs00031b.

(73) Li, W.; Zhang, X. *Chiral Phosphines and Diphosphines, In Phosphorus(III) Ligands in Homogeneous Catalysis: Design and Synthesis*, 1st Ed.; Kamer, P.; Van Leeuwen, P., Ed.; John Wiley & Sons, Ltd Publication: New York, 2012.

(74) Rémond, E.; Bayardon, J.; Ondel-Eymin, M.; Jugé, S. Stereoselective Synthesis of Unsaturated and Functionalized L-NHBoc Amino Acids, Using Wittig Reaction under Mild Phase-Transfer Conditions. *J. Org. Chem.* **2012**, *77* (17), 7579–7587. https://doi.org/10.1021/jo3013622.

(75) Kleineweischede, R.; Hackenberger, C. Chemoselective Peptide Cyclization by Traceless Staudinger Ligation. *Angew. Chem. Int. Ed.* **2008**, *47* (32), 5984–5988. https://doi.org/10.1002/anie.200801514.

(76) Lacour, J.; Linder, D. Hexacoordinated Phosphates: How to Teach Old Chiral Anions New Asymmetric Tricks. *Chem. Rec.* **2007**, *7* (5), 275–285. https://doi.org/10.1002/tcr.20124.

(77) Park, A.; Kim, S.; Park, J.; Joe, S.; Min, B.; Oh, J.; Song, J.; Park, S. .; Park, S.; Lee, H. Structural and Experimental Evidence for the Enantiomeric Recognition toward a Bulky Sec-Alcohol by Candida Antarctica Lipase B. *ACS Catal.* **2016**, *6* (11), 7458–7465. https://doi.org/10.1021/acscatal.6b02192.

(78) Xu, G.; Senanayake, C.; Tang, W. P-Chiral Phosphorus Ligands Based on a 2,3-Dihydrobenzo[d][1,3]Oxaphosphole Motif for Asymmetric Catalysis. *Acc. Chem. Res.* **2019**, *52* (4), 1101–1112. https://doi.org/10.1021/acs.accounts.9b00029.

(79) Huang, H.; Denne, J.; Yang, C. H.; Wang, H.; Kang, J. Y. Direct Aryloxylation/Alkyloxylation of Dialkyl Phosphonates for the Synthesis of Mixed Phosphonates. *Angew. Chem. Int. Ed.* **2018**, *57* (22), 6624–6628. https://doi.org/10.1002/anie.201802082.

(80) Li, J.; Eastgate, M. Current Complexity: A Tool for Assessing the Complexity of Organic Molecules. *Org. Biomol. Chem.* **2015**, *13* (26), 7164–7176. https://doi.org/10.1039/c5ob00709g.

(81) Wan, B.; Seth, P. The Medicinal Chemistry of Therapeutic Oligonucleotides. *J. Med. Chem.* **2016**, *59* (21), 9645–9667. https://doi.org/10.1021/acs.jmedchem.6b00551.

(82) Tomaszewska-Antczak, A. .; Jastrzębska, K.; Maciaszek, A.; Mikolajczyk, B.; Guga, P. P-Stereodefined Phosphorothioate Analogs of Glycol Nucleic Acids—Synthesis and Structural Properties. *RSC Adv.* **2018**, *8* (44), 24942–24952. https://doi.org/10.1039/c8ra05568h.

(83) Stankevič, M. Diastereoselective Desymmetrization of Diarylphosphinous Acid-Borane Amides under Birch Reduction. *Org. Biomol. Chem.* **2015**, *13* (21), 6082–6102. https://doi.org/10.1039/c4ob02440k.

(84) Chen, T.; Han, L. Optically Active *H*-Phosphinates and Their Stereospecific Transformations into Optically Active P-Stereogenic Organophosphoryl Compounds. *Synlett* **2015**, *26* (9), 1153–1163. https://doi.org/10.1055/s-0034-1379996.

(85) Adams, H.; Collins, R.; Jones, S.; Warner, C. Enantioselective Preparation of P-Chiral Phosphine Oxides. *Org. Lett.* **2011**, *13* (24), 6576–6579. https://doi.org/10.1021/ol202916j.

(86) Jordan, P.; Kayser-Bricker, K.; Miller, S. Asymmetric Phosphorylation through Catalytic P(III) Phosphoramidite Transfer: Enantioselective Synthesis of D-Myo-Inositol-6-Phosphate. *PNAS* **2010**, *107* (48), 20620–20624. https://doi.org/10.1073/pnas.1001111107.

(87) Ryan, M.; Liu, T.; Dahlquist, F.; Griffith, O. A Catalytic Diad Involved in Substrate-Assisted Catalysis: NMR Study of Hydrogen Bonding and Dynamics at the Active Site of Phosphatidylinositol-Specific Phospholipase C. *Biochemistry* **2001**, *40* (32), 9743–9750. https://doi.org/10.1021/bi010958m.

(88) Lee, L.; Lee, Y.; Leu, R.; Shaw, J. Functional Role of Catalytic Triad and Oxyanion Hole-Forming Residues on Enzyme Activity of Escherichia Coli Thioesterase I/Protease I/Phospholipase L 1. *Biochem. J.* **2006**, *397* (1), 69–76. https://doi.org/10.1042/BJ20051645.

(89) Koizumi, T.; Amitanti, H.; Yoshii, E. A New Method of Preparing Optically Active Alkyl Phenyl Phosphonates. *Tetrahedron Lett.* **1978**, *39*, 3741–3742.

(90) Wagner, P.; Leavitt, R. With LAH Stereospecific Alkylation of Menthyl Sir : Diastereomerically Enriched Menthyl Phosphinates. *J. Am. Chem. Soc.* **1970**, No. 15, 5808–5809.

(91) Volle, J.; Filippini, D.; Midrier, C.; Sobecki, M.; Drag, M.; Virieux, D.; Pirat, J. Revisited Synthesis of Aryl-*H*-Phosphinates. *Synthesis (Stuttg).* **2011**, No. 15, 2490–2494. https://doi.org/10.1055/s-0030-1260109.

(92) Volle, J.; Filippini, D.; Krawczy, B.; Kaloyanov, N.; Van Der Lee, A.; Maurice, T.; Pirat, J.; Virieux, D. Drug Discovery: Phosphinolactone, in Vivo Bioisostere of the Lactol Group. *Org. Biomol. Chem.* **2010**, *8* (6), 1438–1444. https://doi.org/10.1039/b919345f.

(93) Iwamoto, N.; Oka, N.; Sato, T.; Wada, T. Stereocontrolled Solid-Phase Synthesis of Oligonucleoside *H*-Phosphonates by an Oxazaphospholidine Approach. *Angew. Chem. Int. Ed.* **2009**, *48* (3), 496–499. https://doi.org/10.1002/anie.200804408.

(94) Evans, J.; Fierman, M.; Miller, S.; Ellman, J. Catalytic Enantioselective Synthesis of Sulfinate Esters through the Dynamic Resolution of Tert-Butanesulfinyl Chloride. *J. Am. Chem. Soc.* **2004**, *126* (26), 8134–8135. https://doi.org/10.1021/ja047845l.

(95) Birman, B.; Li, X. Benzotetramisole: A Remarkably Enantioselective Acyl Transfer Catalyst. *Org. Lett.* **2006**, *8* (7), 1351–1354. https://doi.org/10.1021/ol060065s.

(96) McLaughlin, C.; Smith, A. Generation and Reactivity of C(1)-Ammonium Enolates by Using Isothiourea Catalysis. *Chem. Eur. J.* **2021**, *27* (5), 1533–1555. https://doi.org/10.1002/chem.202002059.

(97) Wu, J.; Young, C.; Smith, A. Isothiourea-Catalysed Transfer Hydrogenation of a,b-Unsaturated Para- Nitrophenyl Esters. *Tetrahedron* **2021**, *78*, 131758. https://doi.org/doi.org/10.1016/j.tet.2020.131758.

(98) Henderson, R.; Hill, A.; Redman, A.; Sneddon, H. Development of GSK's Acid and Base Selection Guides. *Green Chem.* **2015**, *17* (2), 945–949. https://doi.org/10.1039/c4gc01481b.

(99) Benoit, R.; Lefebvre, D.; Frechette, M. Basicity of 1,8-Bis(Dimethylamino)Naphthalene and 1,4-Diazabicyclo[2.2.2]Octane in Water and Dimethyl Sulfoxide. *Can. J. Chem.* **1987**, *65*, 996–1001. https://doi.org/DOI:10.1139/v87-170.

(100) Kreevoy, M.; Wang, Y. Kinetic and Equilibrium Acid-Base Behavior of Tertiary Amines in Anhydrous and Moist Dimethyl Sulfoxide. *J. Phys. Chem.* **1977**, *81*, 1924–1928. https://doi.org/DOI:10.1021/j100535a008.

(101) Benoit, R.; Fréchette, M.; Lefebvre, D. 2,6-Di- Tert -Butylpyridine: An Unusually Weak Base in Dimethylsulfoxide . *Can. J. Chem.* **1988**, *66* (5), 1159–1162. https://doi.org/10.1139/v88-190.

(102) Otsuki, T.; Okamoto, Y.; Sakurai, H. . Convenient Procedure for the Preparation of Optically Active Phosphonates Using the Chirality of (*S*)-(-)Alfa-Methylbezylamine. *Synthesis (Stuttg).* **1981**, 811–813.

(103) Hall, N.; William, C. 1,3,2-Thiazaphospholidin-2-Ones Derived From Ephedrine. Preparation and Stereochemistry of Ring-Opening Reactions. *J. Chem. Soc., Perkin Trans. 1* **1981**, No. 0, 2746–2750. https://doi.org/10.1039/P19810002746.

(104) Mitova, V.; Koseva, N.; Troev, K. Study on the Atherton-Todd Reaction Mechanism. *RSC Adv.* **2014**, *4* (110), 64733–64736. https://doi.org/10.1039/c4ra10228b.

(105) Nemeth, G.; Greff, Z.; Sipos A., Varga, Z.; Szekely, R.; Sebestye´n, M.´ Jaszay, Z.; Beni, S.; Nemes, Z.; Pirat, J.; Volle, J.; Virieux, D.; Gyuris, A.; Kelemenics, K.; Áy, E.;Minarovits, J; Szathmary, S.; Keri, G. .;´ Laszlo´, O. Synthesis and Evaluation of Phosphorus Containing, Specific CDK9/ CycT1 Inhibitors. *J. Med. Chem.* **2014**, *57*, 3939–3965. https://doi.org/dx.doi.org/10.1021/jm401742r | J.

(106) Kiss, N.; Ludányi, K.; Drahos, L.; Keglevich, G. Novel Synthesis of Phosphinates by the Microwave-Assisted Esterification of Phosphinic Acids. *Synth. Commun.* **2009**, *39* (13), 2392–2404. https://doi.org/10.1080/00397910802654880.

(107) Szelke, H.; Kovács, J. .; Keglevich, G. . Synthesis of *H*-Phosphinates by the UV Light - Mediated Fragmentation- Related Phosphorylation Using Simple P-Heterocycles. *Synth. Commun.* **2005**, *35* (22), 2927–2934. https://doi.org/10.1080/00397910500297404.

(108) O Duke, S.; B Powles, S. Glyphosate: A Once-in-a-Century Herbicide. *Pest Manag. Sci.* **2008**, *63* (11), 1100–1106. https://doi.org/10.1002/ps.

(109) Horsman, G.; Zechel, D. Phosphonate Biochemistry. *Chem. Rev.* **2017**, *117* (8), 5704–5783. https://doi.org/10.1021/acs.chemrev.6b00536.

(110) Methot, J.; Roush, W. Nucleophilic Phosphine Organocatalysis. *Adv. Synth. Catal.* **2004**, *346* (910), 1035–1050. https://doi.org/10.1002/adsc.200404087.

(111) Moncarz, J.; Laritcheva, N.; Glueck, D. Palladium-Catalyzed Asymmetric Phosphination: Enantioselective Synthesis of a P-Chirogenic Phosphine. *J. Am. Chem. Soc.* **2002**, *124* (45), 13356–13357. https://doi.org/10.1021/ja0267324.

(112) Li, N.; Frederiksen J.; Piccirilli, J. Automated Solid-Phase Synthesis of RNA Oligonucleotides Containing a Non-Bridging Phosphorodithioate Linkage via Phosphorothioamidites. *J. Org. Chem.* **2012**, *77* (21), 9889–9892. https://doi.org/10.1021/jo301834p.Automated.

(113) Letsinger, R.; Ogilvie, K. Synthesis of Oligothymidylates via Phosphotriester Intermediates. *J. Am. Chem. Soc.* **1969**, *91* (12), 3350–3355. https://doi.org/10.1021/ja01040a042.

(114) Beaucage, S.; Caruthers, M. Deoxynucleoside Phosphoramidites-A New Class of Key Intermediates for Deoxypolynucleotide Synthesis. *Tetrahedron Lett.* **1981**, *22* (20), 1859–1862. https://doi.org/10.1016/S0040-4039(01)90461-7.

(115) Nurminen, E.; Lönnberg, H. Mechanisms of the Substitution Reactions of Phosphoramidites and Their Congeners. *J. Phys. Org. Chem.* **2004**, *17* (1), 1–17. https://doi.org/10.1002/poc.681.

(116) Teichert, J.; Feringa, B. Phosphoramidites: Privileged Ligands in Asymmetric Catalysis. *Angew. Chem. Int. Ed.* **2010**, *49* (14), 2486–2528. https://doi.org/10.1002/anie.200904948.

(117) Hölscher, M.; Franciò, G.; Leitner, W. Origin of Enantioselectivity in Asymmetric Hydrovinylations Catalyzed by Phosphoramidite Nickel Catalysts: An Experimentally Supported Density Functional Study. *Organometallics* **2004**, *23* (23), 5606–5617. https://doi.org/10.1021/om040107l.

(118) Liang, L.; Guo, R.; Zhou, Z. O,O,'-(*R*)-(1,1'-Dinaphthyl-2,2'-Diyl) N-Benzyl-N-(2-Pyridyl)Phosphoramidite. *Acta Crystallogr. Sect. E Struct. Reports Online* **2003**, *59* (5), 599–600. https://doi.org/10.1107/S1600536803006640.

(119) Grabulosa, A.; Müller, G.; Ordinas, J.; Mezzetti, A.; Maestro, M.; Font-Bardia, M.; Solans, X. Allylpalladium Complexes with P-Stereogenic Monodentate Phosphines. Application in the Asymmetric Hydrovinylation of Styrene. *Organometallics* **2005**, *24* (21), 4961–4973. https://doi.org/10.1021/om050421v.

(120) Moulin, D.; Bago, S.; Bauduin, C.; Darcel, C.; Jugé, S. Asymmetric Synthesis of P-Stereogenic o-Hydroxyaryl-Phosphine (Borane) and Phosphine-Phosphinite Ligands. *Tetrahedron Asymmetry* **2000**, *11* (19), 3939–3956. https://doi.org/10.1016/S0957-4166(00)00372-4.

(121) Wiktelius, D.; Johansson, M.; Luthman, K.; Kann, N. A Biocatalytic Route to P-Chirogenic Compounds by Lipase-Catalyzed Desymmetrization of a Prochiral Phosphine-Borane. *Org. Lett.* **2005**, *7* (22), 4991–4994. https://doi.org/10.1021/ol0519893.

(122) Jordan, P.; Miller, S. An Approach to the Site-Selective Deoxygenation of Hydroxy Groups Based on Catalytic Phosphoramidite Transfer. *Angew. Chem. Int. Ed.* **2012**, *51* (12), 2907–2911. https://doi.org/10.1002/anie.201109033.

(123) Nurminen, E.; Mattinen, J.; Lönnberg, H. Kinetics and Mechanism of Tetrazole-Catalyzed Phosphoramidite Alcoholysis. *J. Chem. Soc. Perkin Trans. 2* **1998**, No. 7, 1621–1628. https://doi.org/10.1039/a801250d.

(124) Russell, M.; Laws, A.; Atherton, J.; Page, M. The Mechanism of the Phosphoramidite Synthesis of Polynucleotides. *Org. Biomol. Chem.* **2008**, *6* (18), 3270–3275. https://doi.org/10.1039/b808999j.

(125) Brady, P.; Morris, E.; Fenton, O.; Sculimbrene, B. Efficient Catalyst Turnover in the Phosphitylation of Alcohols with Phosphoramidites. *Tetrahedron Lett.* **2009**, *50* (9), 975–978. https://doi.org/10.1016/j.tetlet.2008.12.065.

(126) Nifant'ev, E. Protonated Aminophosphines. *Phosphorus. Sulfur. Silicon Relat. Elem.* **1992**, *70* (1–2), 159–174.

(127) Gonbeau, D.; Pfister-Guillouzo, G.; Mazières, M.; Sanchez, M. La Liaison Phosphore-Azote. ~tude Quantochimique de Modeles Neutres et Ioniques H_3PNH, $H_3PNH_2^+$, $H_2PNH_3^+$, H_2PNH^- et $HPNH_2^-$. *Can. J. Chem.* **1985**, *63* (11), 3242–3248. https://doi.org/10.1139/v85-536.

(128) Hayakawa, Y.; Hyodo, M.; Kimura, K.; Kataoka, M. The First Asymmetric Synthesis of Trialkyl Phosphates on the Basis of Dynamic Kinetic Resolution in the Phosphite Method Using a Chiral Source in a Catalytic Manner. *Chem. Commun.* **2003**, *3* (14), 1704–1705. https://doi.org/10.1039/b304163h.

(129) Banfi, S.; Manfredi, A.; Montanari, F.; Pozzi, G.; Quici, S. Synthesis of Chiral Mn(III)-Meso-Tetrakis-[2.2]-p-Cyclophanyl-Porphyrin: A New Catalyst for Enantioselective Epoxidation. *J. Mol. Catal. A Chem.* **1996**, *113* (1–2), 77–86. https://doi.org/10.1016/S1381-1169(96)00048-9.

(130) Iwashita, M.; Makide, K.; Nonomura, T.; Misumi, Y.; Otani, Y.; Ishida, M.; Taguchi, R.; Tsujimoto, M.; Aoki, J.; Arai, H.; et al. Synthesis and Evaluation of Lysophosphatidylserine Analogues as Inducers of Mast Cell Degranulation. Potent Activities of Lysophosphatidylthreonine and Its 2-Deoxy Derivative. *J. Med. Chem.* **2009**, *52* (19), 5837–5863. https://doi.org/10.1021/jm900598m.

(131) Valentina, A.; 1,3-Dipolar Cycloaddition: Click Chemistry for the Synthesis of 5-Substituted Tetrazoles from Organoaluminum Azides and Nitriles. *Angew. Chem. Int. Ed.* **2007**, *46* (44), 8440–8444. https://doi.org/10.1002/anie.200701045.

(132) Friedmann, C.; Ay, S.; Bräse, S. Improved Synthesis of Enantiopure 4-Hydroxy[2.2]Paracyclophane. *J. Org. Chem.* **2010**, *75* (13), 4612–4614. https://doi.org/10.1021/jo100468s.

(133) Roche, A.; Canturk, B. An Exploration of Suzuki Aryl Cross Coupling Chemistry Involving [2.2]Paracyclophane Derivatives. *Org. Biomol. Chem.* **2005**, *3* (3), 515–519. https://doi.org/10.1039/b415764h.

(134) Carman, R.; Edlund, G.; Damberg, C. Distribution of Organic and Inorganic Phosphorus Compounds in Marine and Lacustrine Sediments: A ^{31}P NMR Study. *Chem. Geol.* **2000**, *163* (1–4), 101–114. https://doi.org/10.1016/S0009-2541(99)00098-4.

(135) Lenevich, S.; Distefano, M. Nuclear Magnetic Resonance-Based Quantification of Organic Diphosphates. *Anal. Biochem.* **2011**, *408* (2), 316–320. https://doi.org/10.1016/j.ab.2010.08.030.

(136) Jarvie, H.; Sharpley, A.; Withers, P.; Scott, J.; Haggard, B.; Neal, C. Phosphorus Mitigation to Control River Eutrophication: Murky Waters, Inconvenient Truths, and "Postnormal" Science. *J. Environ. Qual.* **2013**, *42* (2), 295–304. https://doi.org/10.2134/jeq2012.0085.

(137) Bennet, E.; Elser, J. A Broken Geochemical Cycle. *Nature* **2011**, *478*, 29–31.

(138) Cade-Menun, B. Characterizing Phosphorus in Environmental and Agricultural Samples by 31P Nuclear Magnetic Resonance Spectroscopy. *Talanta* **2005**, *66* (2), 359–371. https://doi.org/10.1016/j.talanta.2004.12.024.

(139) Cade-Menun, B.; Liu, C. Solution Phosphorus-31 Nuclear Magnetic Resonance Spectroscopy of Soils from 2005 to 2013: A Review of Sample Preparation and Experimental Parameters. *Soil Sci. Soc. Am. J.* **2014**, *78* (1), 19–37. https://doi.org/10.2136/sssaj2013.05.0187dgs.

(140) Amirbahman, A.; Lake, B.; Norton, S. Seasonal Phosphorus Dynamics in the Surficial Sediment of Two Shallow Temperate Lakes: A Solid-Phase and Pore-Water Study. *Hydrobiologia* **2013**, *701* (1), 65–77. https://doi.org/10.1007/s10750-012-1257-z.

(141) Gächter, R.; Meyer, J.; Mares, A. Contribution of Bacteria to Release and Fixation of Phosphorus in Lake Sediments. *Limnol. Oceanogr.* **1988**, *33* (6), 1542–1558. https://doi.org/10.4319/lo.1988.33.6part2.1542.

(142) Golterman, H.; Paing, J.; Serrano, L.; Gomez, E. Presence of and Phosphate Release from Polyphosphates or Phytate Phosphate in Lake Sediments. *Hydrobiologia* **1997**, *364* (1), 99–104. https://doi.org/10.1023/A:1003212908511.

(143) Lakes; Anders, B. Biogeochemical Phosphorus Cycling in the Sediments of Shallow Temperate Lakes, 2009 (Unpublished Doctoral Dissertation, University of Maine, Orono).

(144) Turner, B.; Cade-Menun, B.; Condron, L.; Newman, S. Extraction of Soil Organic Phosphorus. *Talanta* **2005**, *66* (2), 294–306. https://doi.org/10.1016/j.talanta.2004.11.012.

(145) Jan, J.; Borovec, J.; Kopáček, J.; Hejzlar, J. What Do Results of Common Sequential Fractionation and Single-Step Extractions Tell Us about P Binding with Fe and Al Compounds in Non-Calcareous Sediments? *Water Res.* **2013**, *47* (2), 547–557. https://doi.org/10.1016/j.watres.2012.10.053.

(146) Hatada, K.; Terawaki, Y.; Okuda, H. Quantitative Analysis by Nuclear Magnetic Resonance Using Precision Coaxial Tubing. *Organic Magnetic Resonance*. 1977, pp 518–522. https://doi.org/10.1002/mrc.1270090906.

(147) Evilia, R. Quantitative NMR Spectroscopy. *Anal. Lett.* **2001**, *34* (13), 2227–2236. https://doi.org/10.1081/AL-100107290.

(148) Malz, F.; Jancke, H. Validation of Quantitative NMR. *J. Pharm. Biomed. Anal.* **2005**, *38* (5), 813–823. https://doi.org/10.1016/j.jpba.2005.01.043.

(149) Jiang, H.; Chen, H.; Cai, N.; Zou, J.; Ju, X. Quantitative ^{31}P NMR Spectroscopy for the Determination of Fosfomycin and Impurity A in Pharmaceutical Products of Fosfomycin Sodium or Calcium. *Magn. Reson. Chem.* **2015**, *53* (6), 454–459. https://doi.org/10.1002/mrc.4224.

(150) Gard, D.; Burquin, J.; Gard, J. Quantitative Analysis of Short-Chain Phosphates by Phosphorus-31 Nuclear Magnetic Resonance and Interlaboratory Comparison with Infrared and Chromatographic Methods. *Anal. Chem.* **1992**, *64* (5), 557–561. https://doi.org/10.1021/ac00029a020.

(151) Cade-Menun, B.; Navaratnam, J.; Walbridge, M. Characterizing Dissolved and Particulate Phosphorus in Water with ^{31}P Nuclear Magnetic Resonance Spectroscopy. *Environ. Sci. Technol.* **2006**, *40* (24), 7874–7880. https://doi.org/10.1021/es061843e.

(152) Turner, B.; Newman, S.; Reddy, K. Overestimation of Organic Phosphorus in Wetland Soils by Alkaline Extraction and Molybdate Colorimetry. *Environ. Sci. Technol.* **2006**, *40* (10), 3349–3354. https://doi.org/10.1021/es052442m.

(153) Defforey, D.; Cade-Menun, B.; Paytan, A. A New Solution ^{31}P NMR Sample Preparation Scheme for Marine Sediments. *Limnol. Oceanogr. Methods* **2017**, *15* (4), 381–393. https://doi.org/10.1002/lom3.10166.

APPENDIX A: NMR Data for Chapter 2

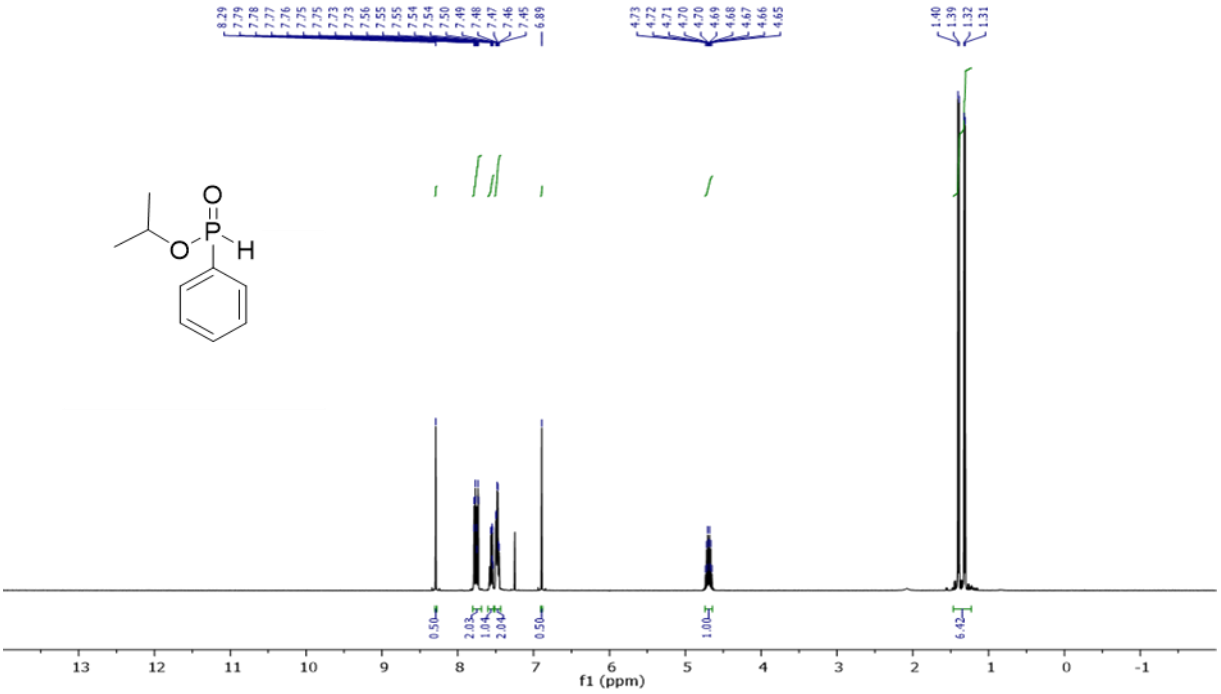

Figure A.1 ^{1}H NMR of compound **2-13**

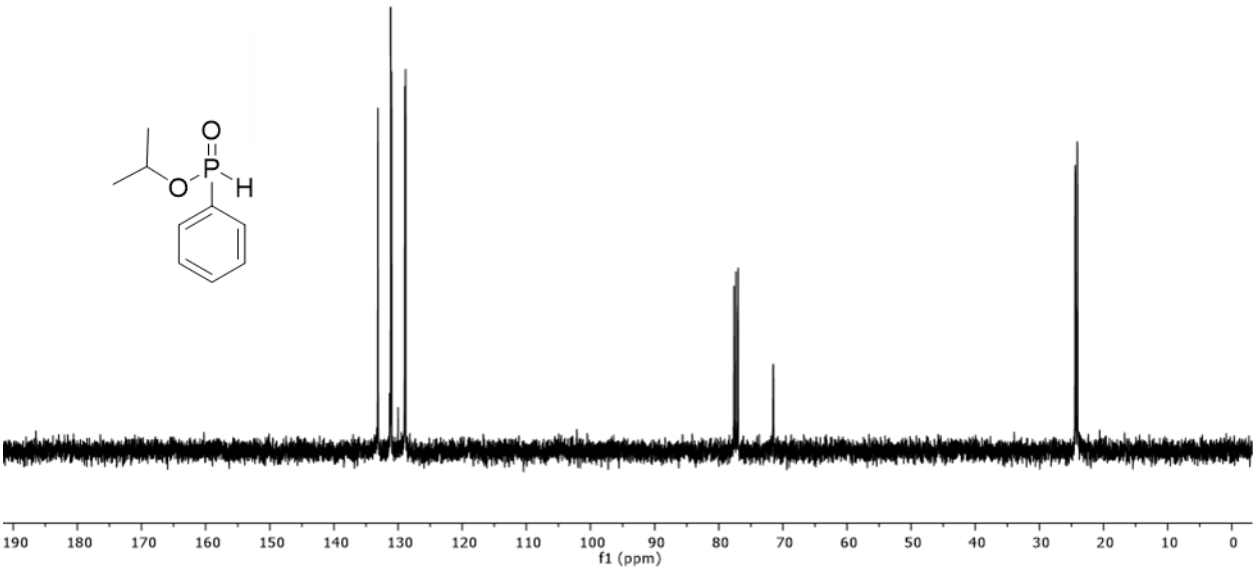

Figure A.2 ^{13}C NMR of compound **2-13**

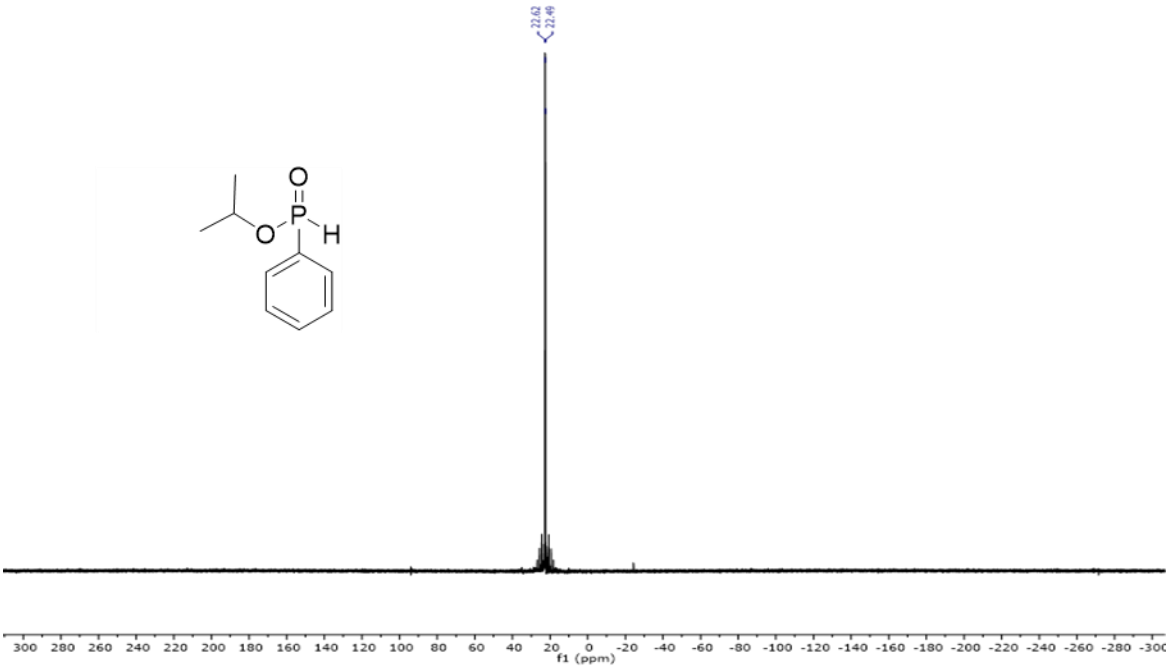

Figure A.3 ^{31}P NMR of compound **2-13**

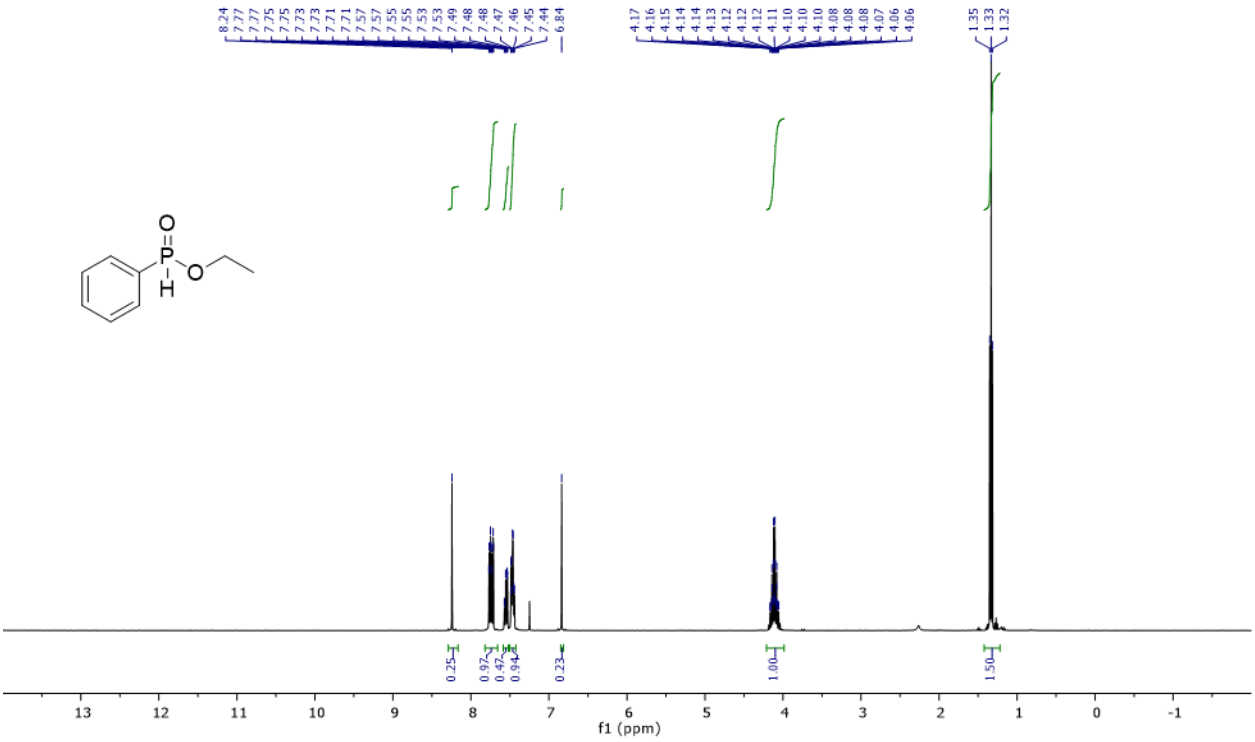

Figure A.4 ^{1}H NMR of compound **2-35**

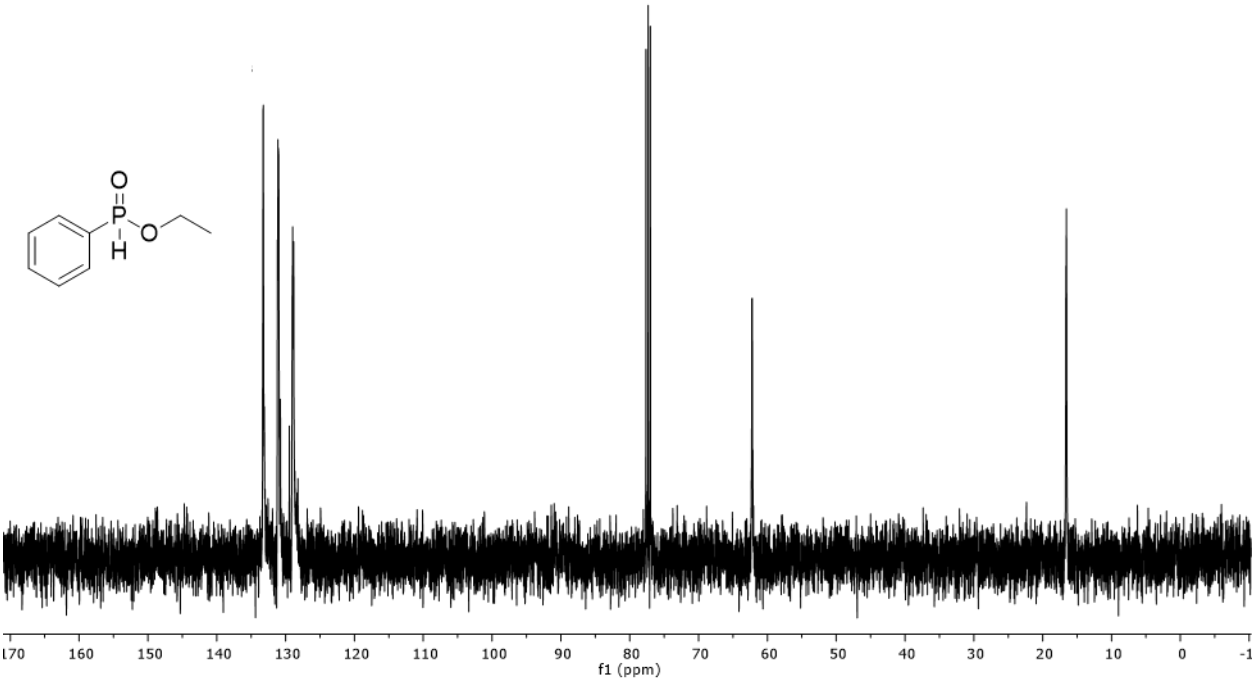

Figure A.5 ^{13}C NMR of compound **2-35**

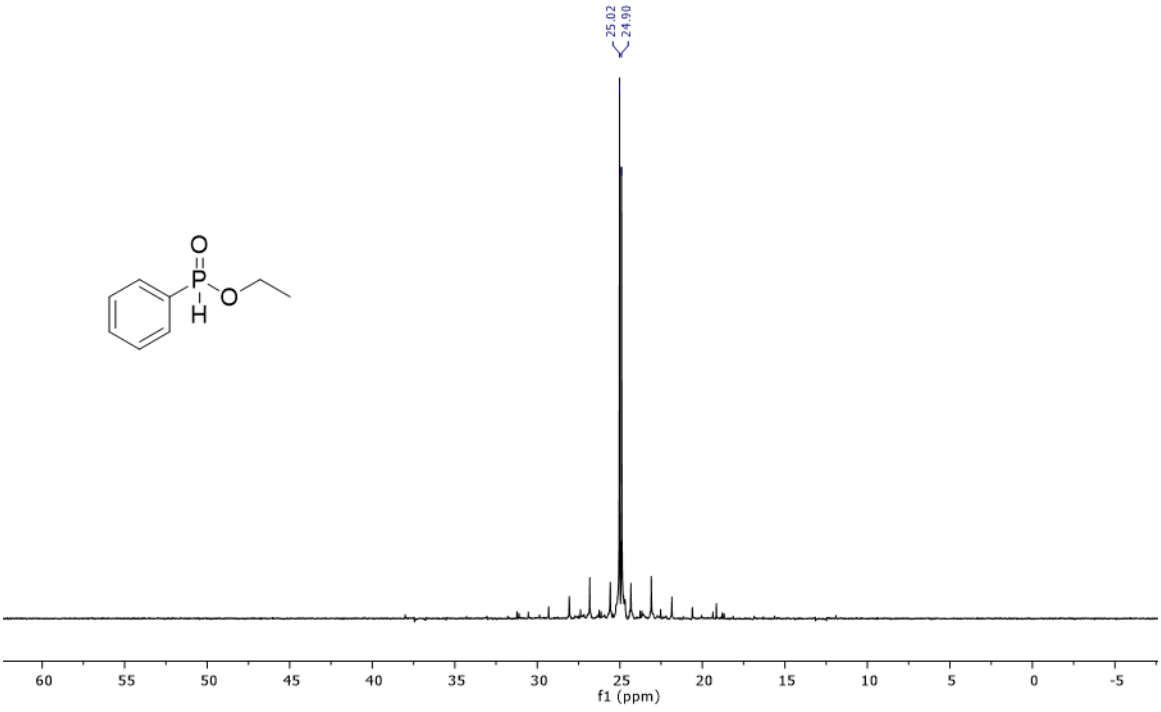

Figure A.6 ^{31}P NMR of compound **2-35**

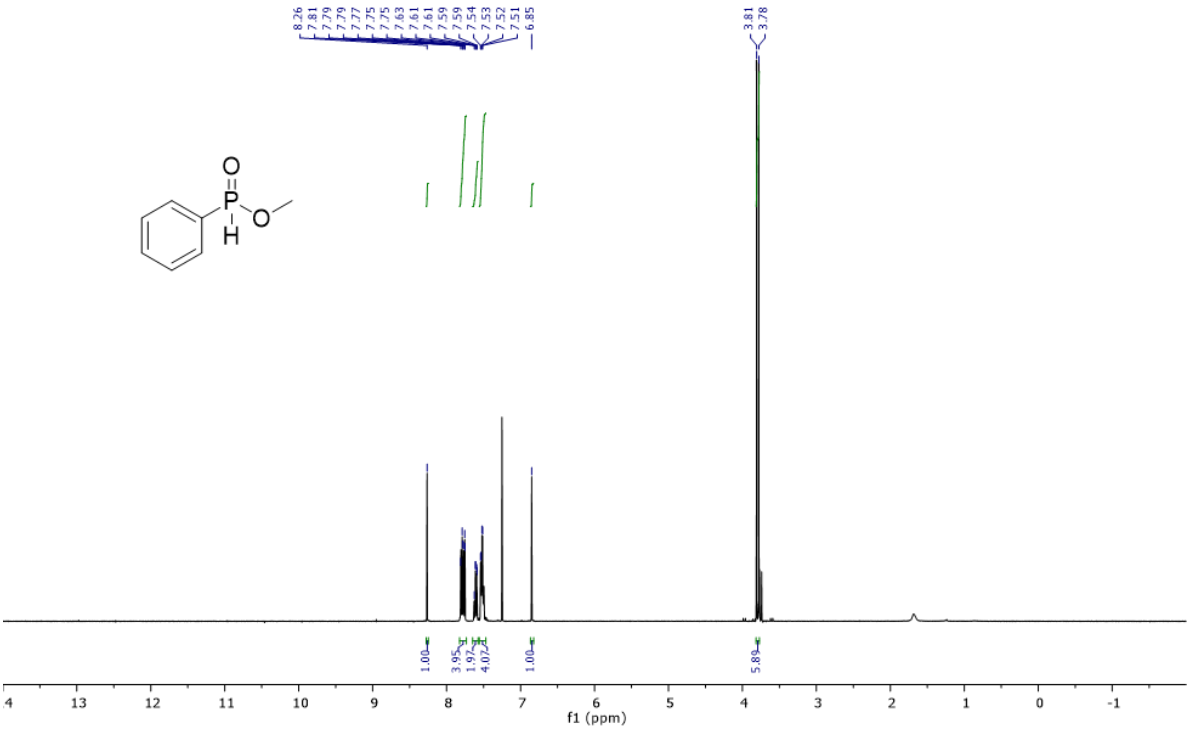

Figure A.7 ^{1}H NMR of compound **2-40**

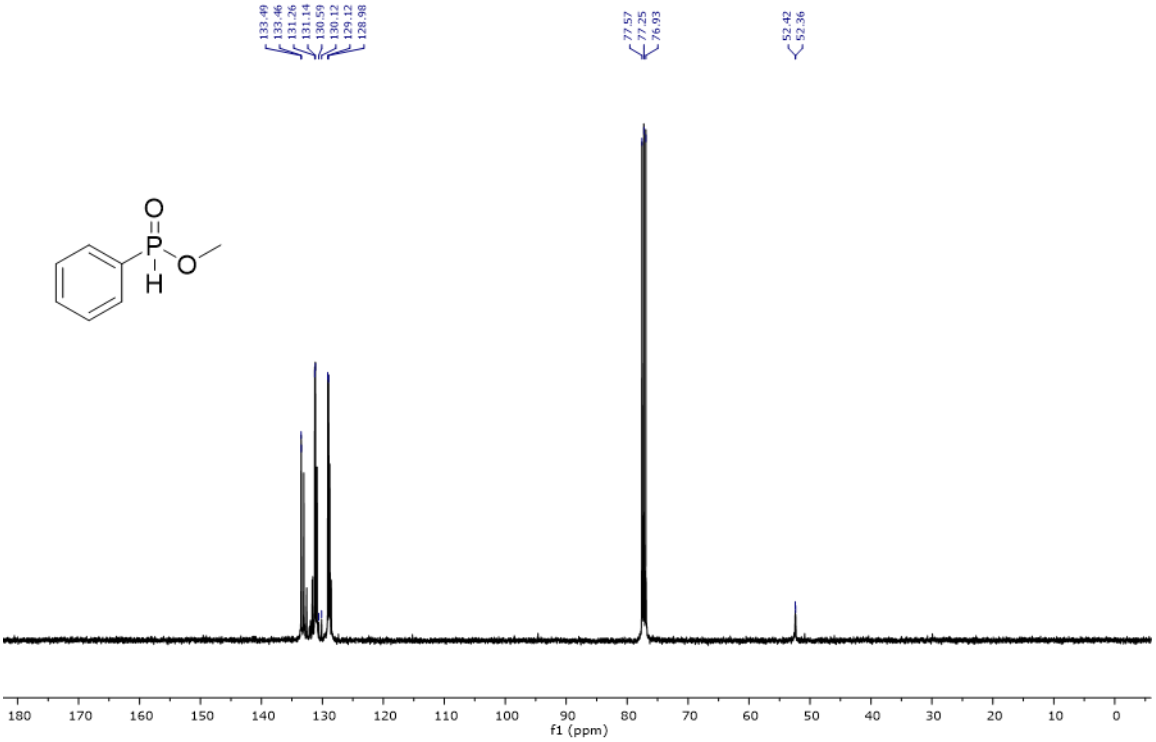

Figure A.8 ^{13}C NMR of compound **2-40**

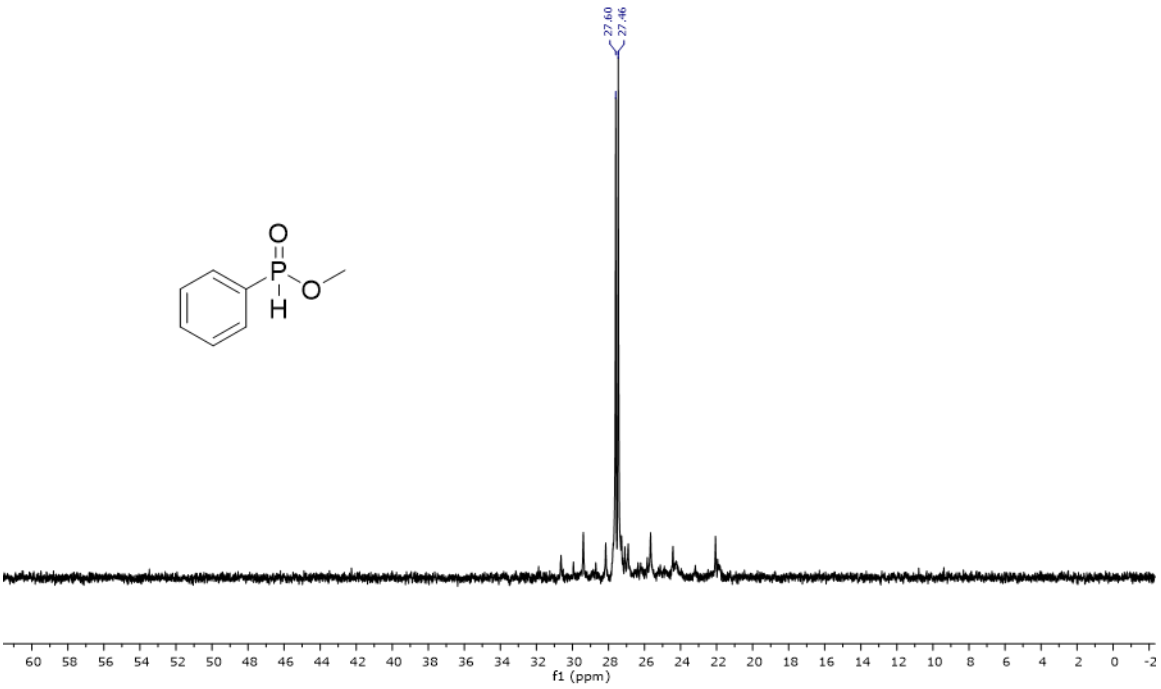

Figure A.9 ^{31}P NMR of compound **2-35**

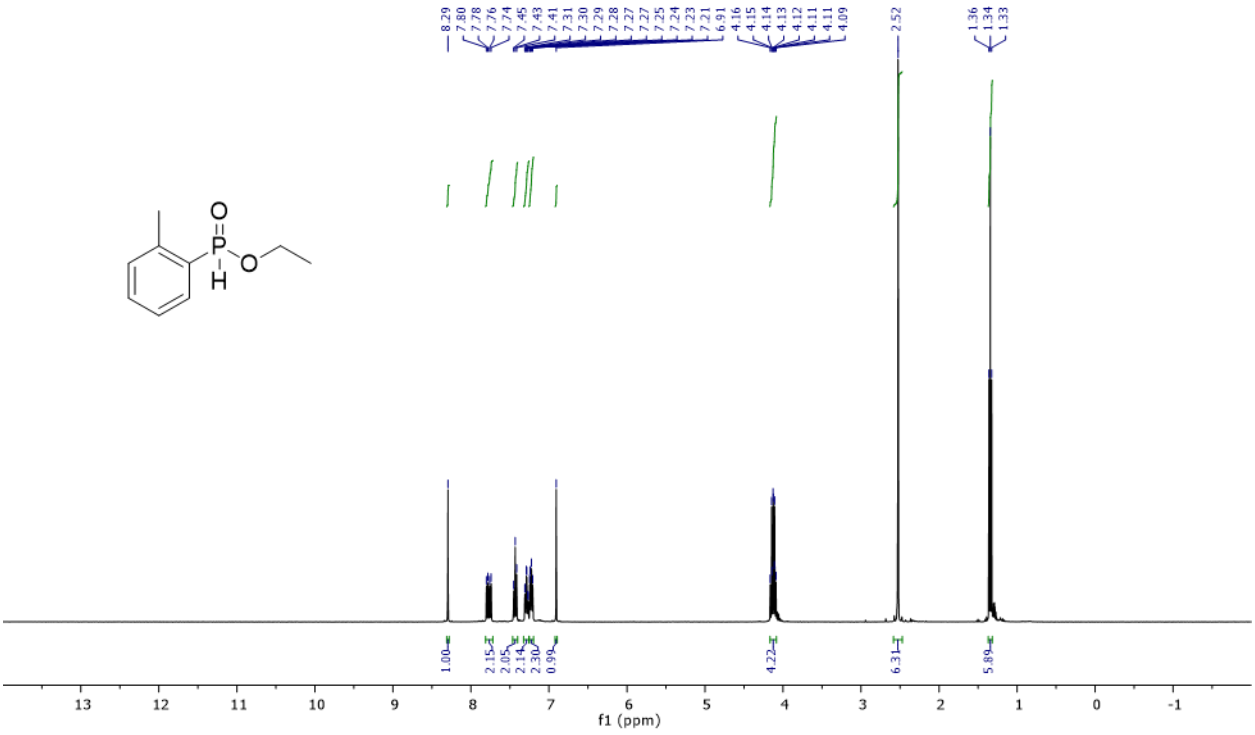

Figure A.10 ^{1}H NMR of compound **2-41**

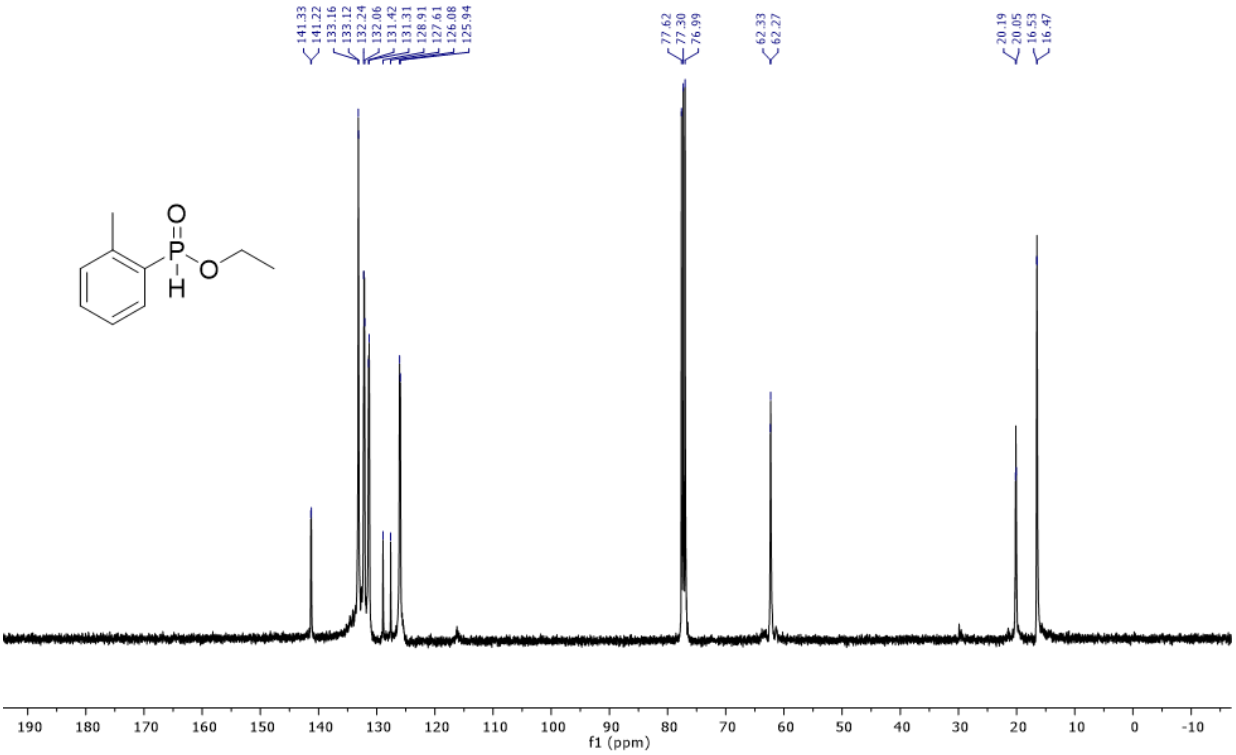

Figure A.11 ^{13}C NMR of compound **2-41**

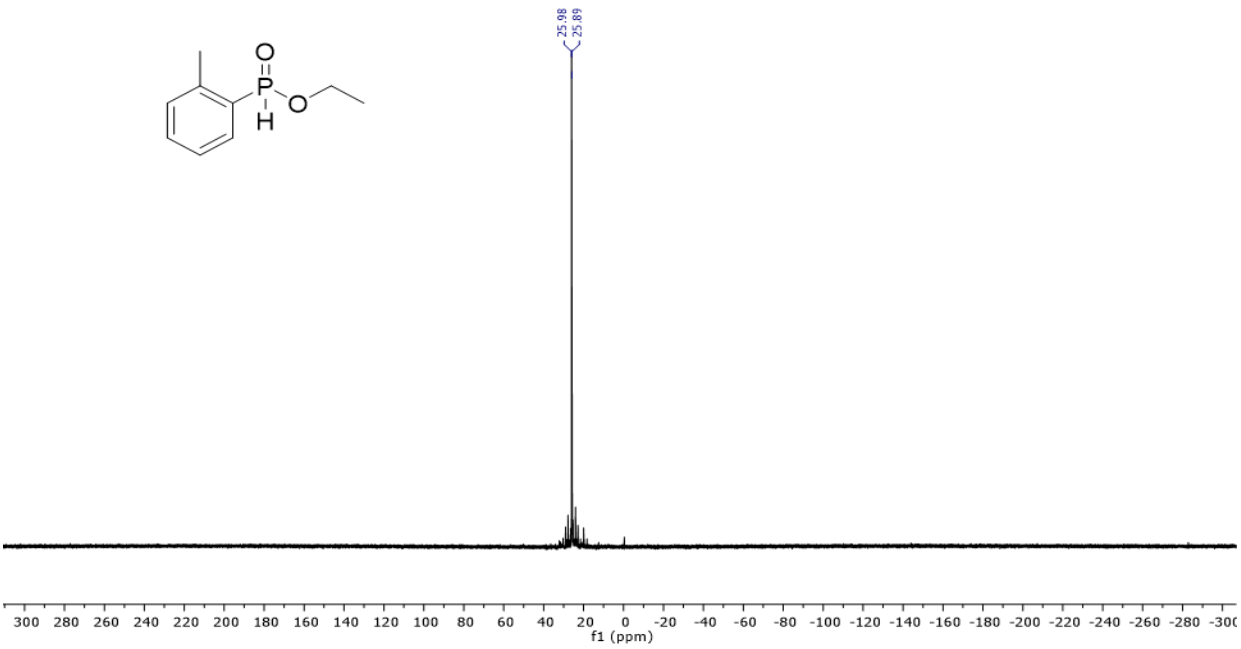

Figure A.12 ^{31}P NMR of compound **2-41**

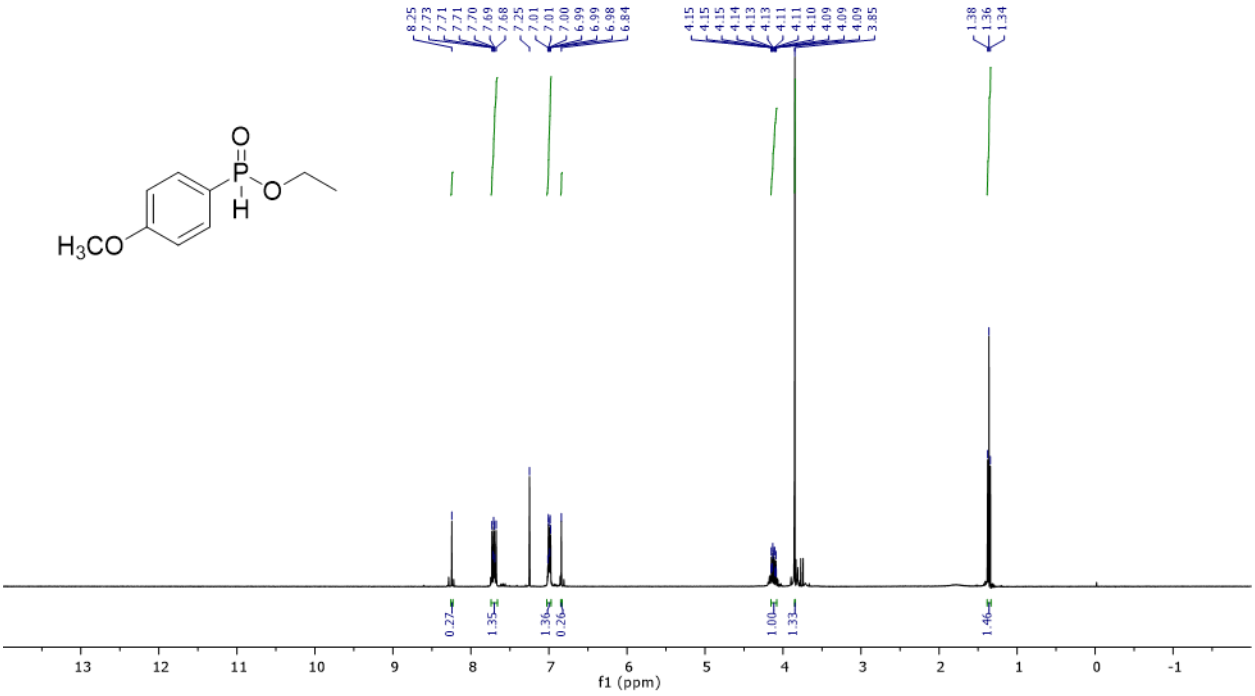

Figure A.13 ^{1}H NMR of compound **2-42**

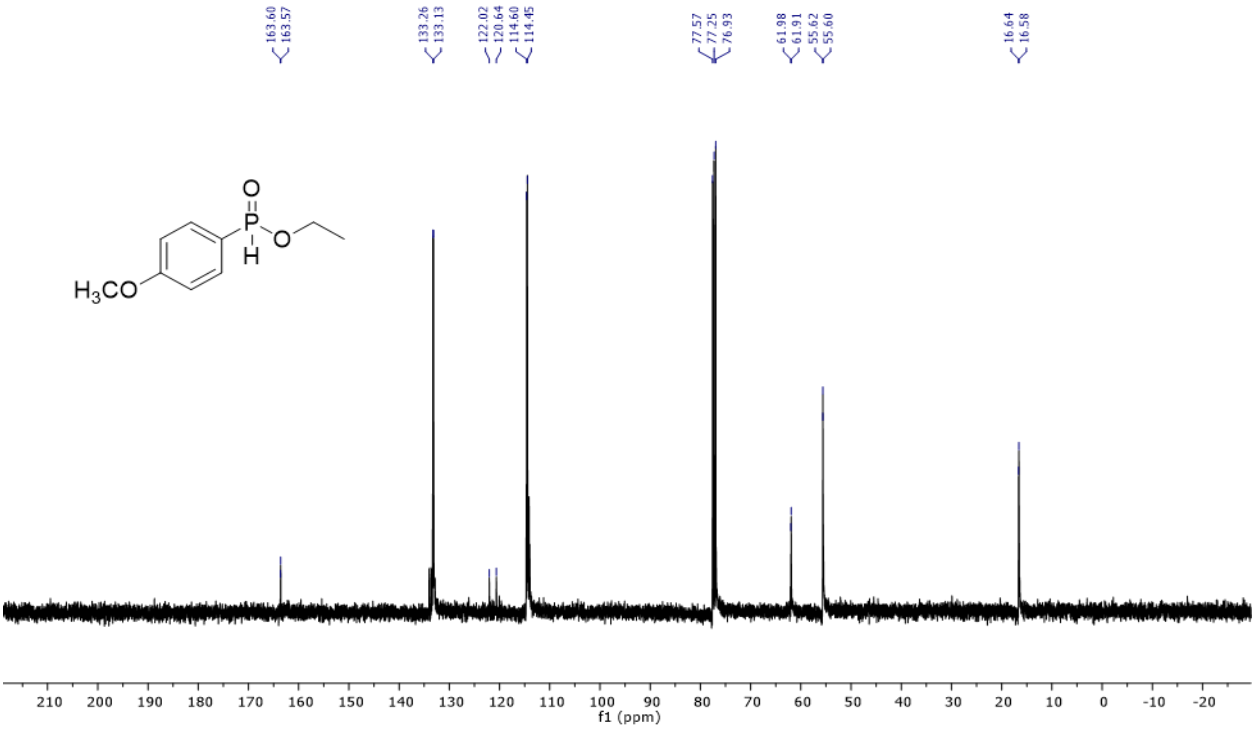

Figure A.14 ^{13}C NMR of compound **2-42**

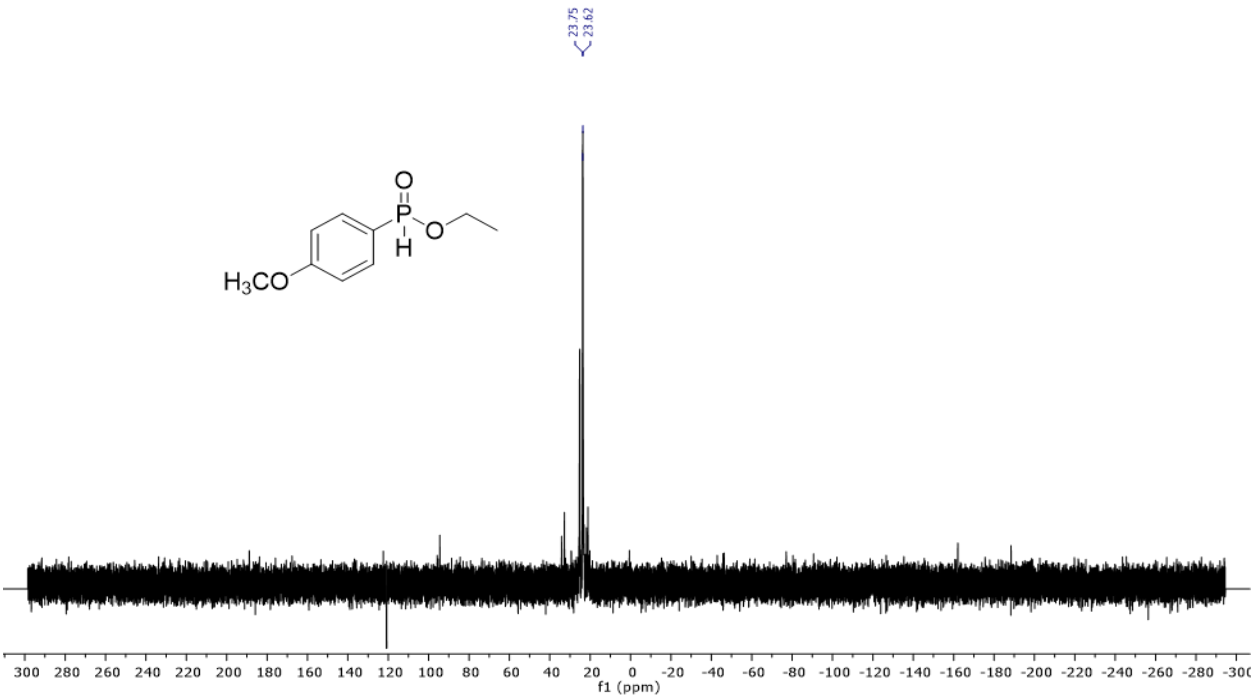

Figure A.15 ^{31}P NMR of compound **2-42**

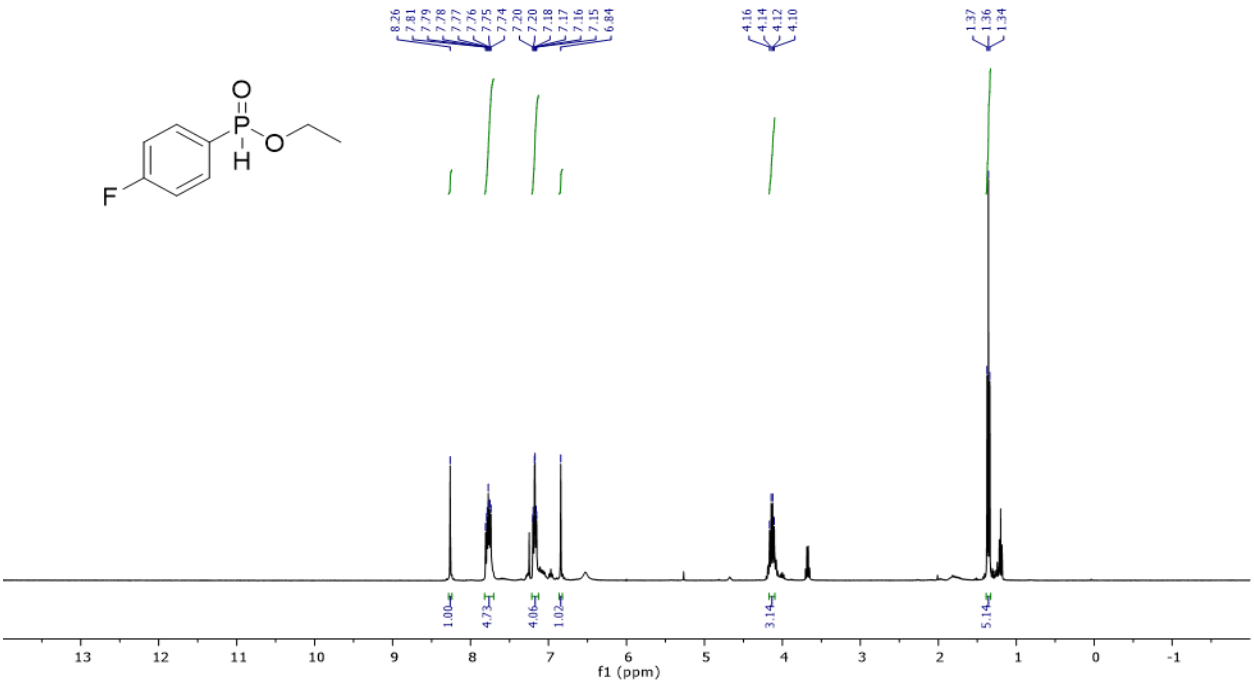

Figure A.16 ^{1}H NMR of compound **2-43**

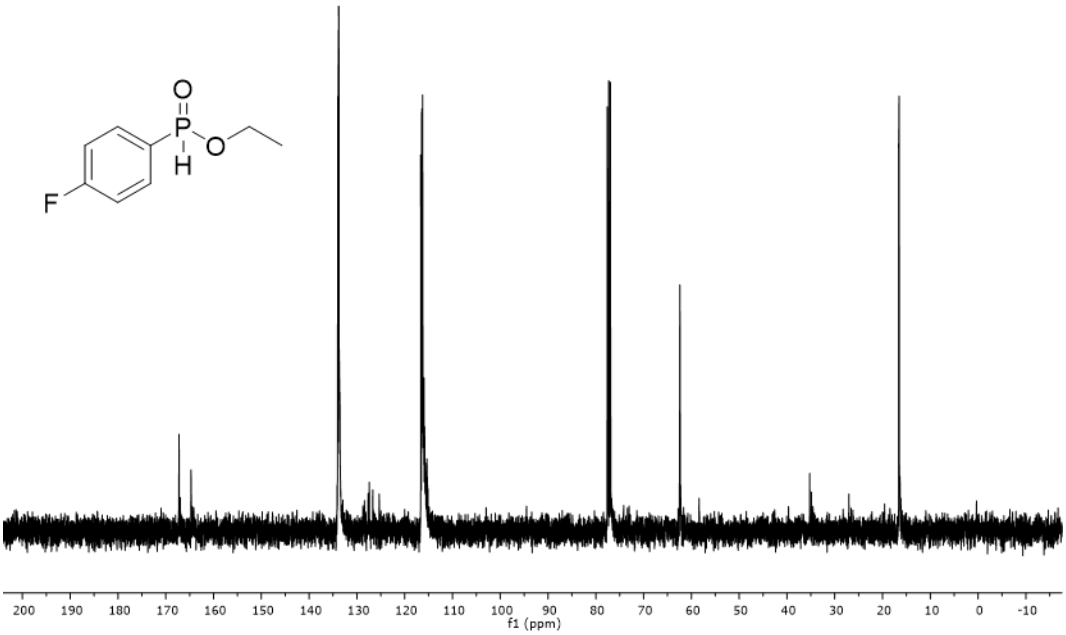

Figure A.17 ^{13}C NMR of compound **2-43**

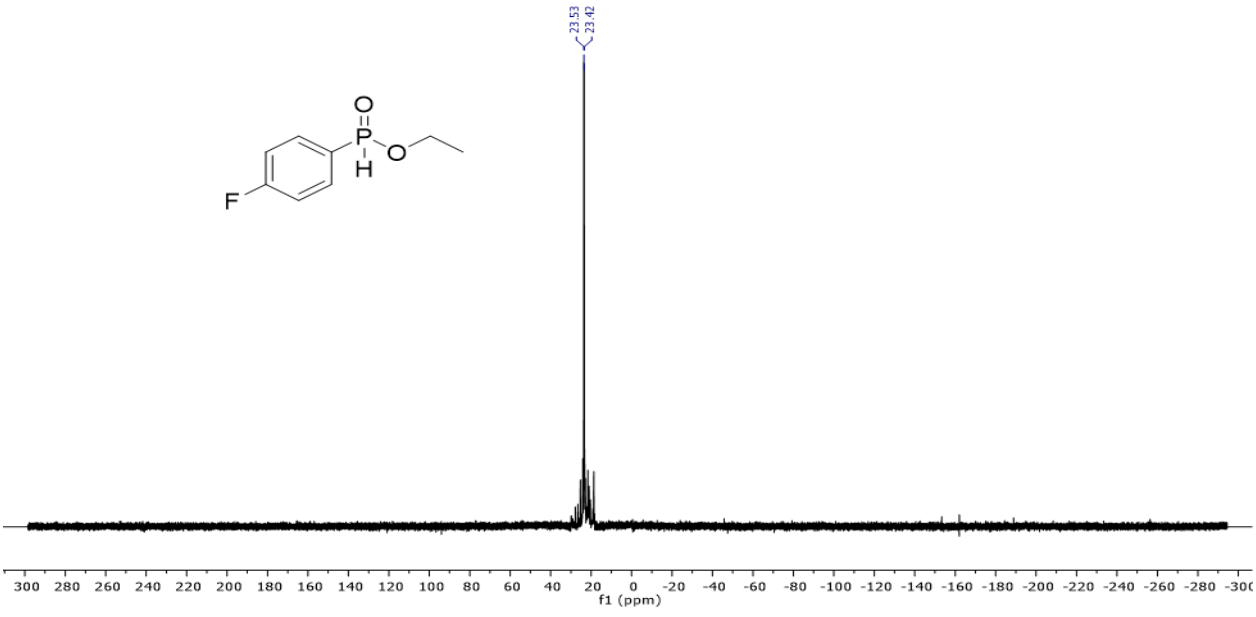

Figure A.18 ^{31}P NMR of compound **2-43**

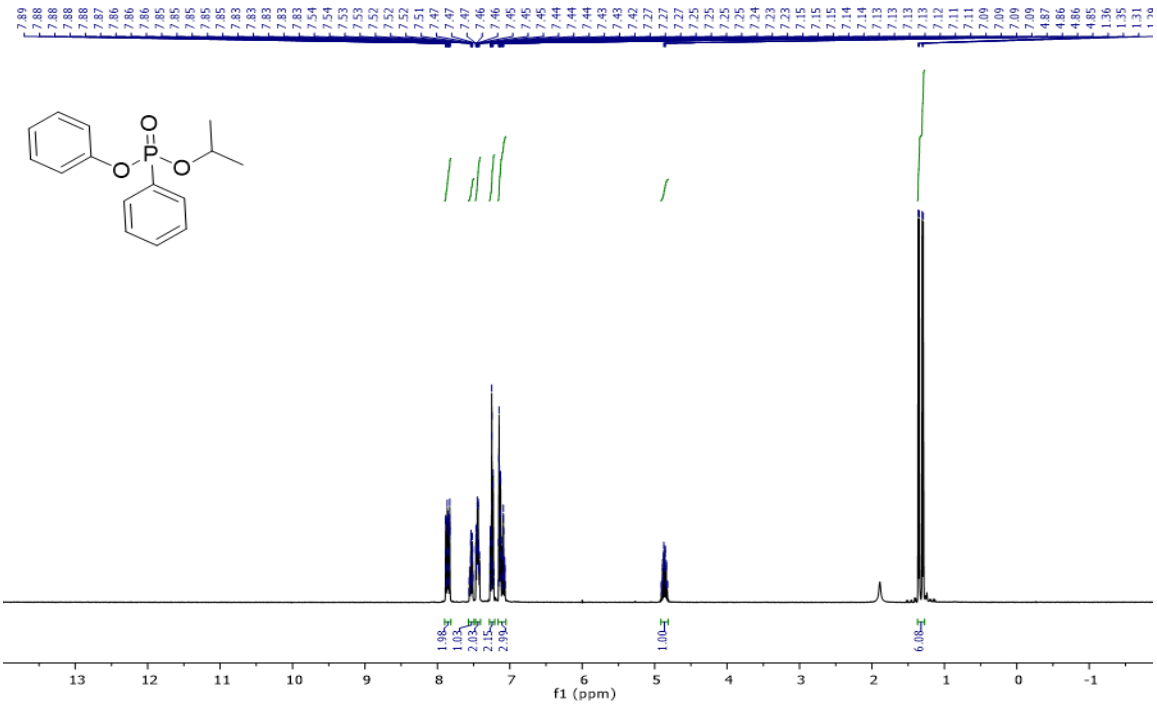

Figure A.19 ^{1}H NMR of compound **2-15**

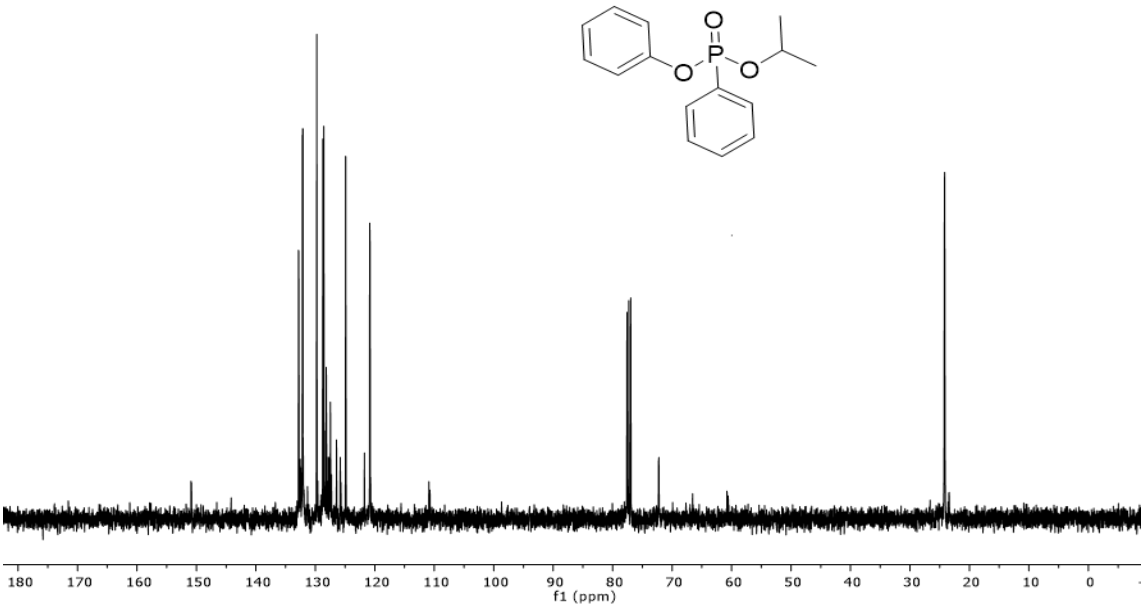

Figure A.20 ^{13}C NMR of compound **2-15**

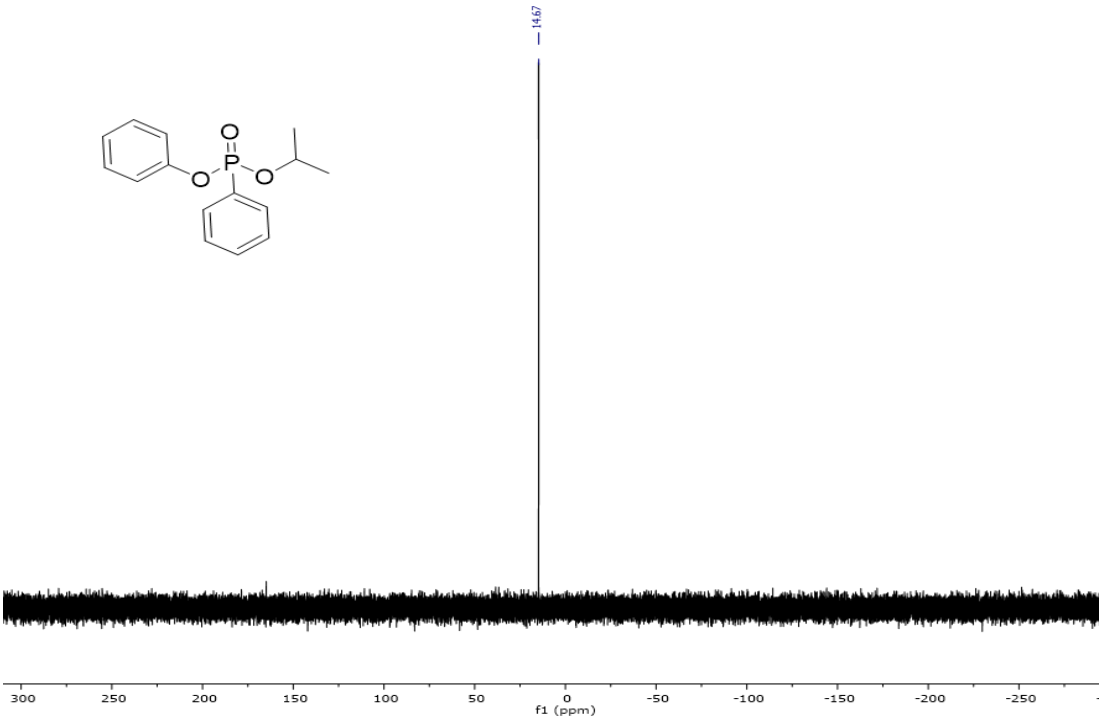

Figure A.21 ^{31}P NMR of compound **2-15**

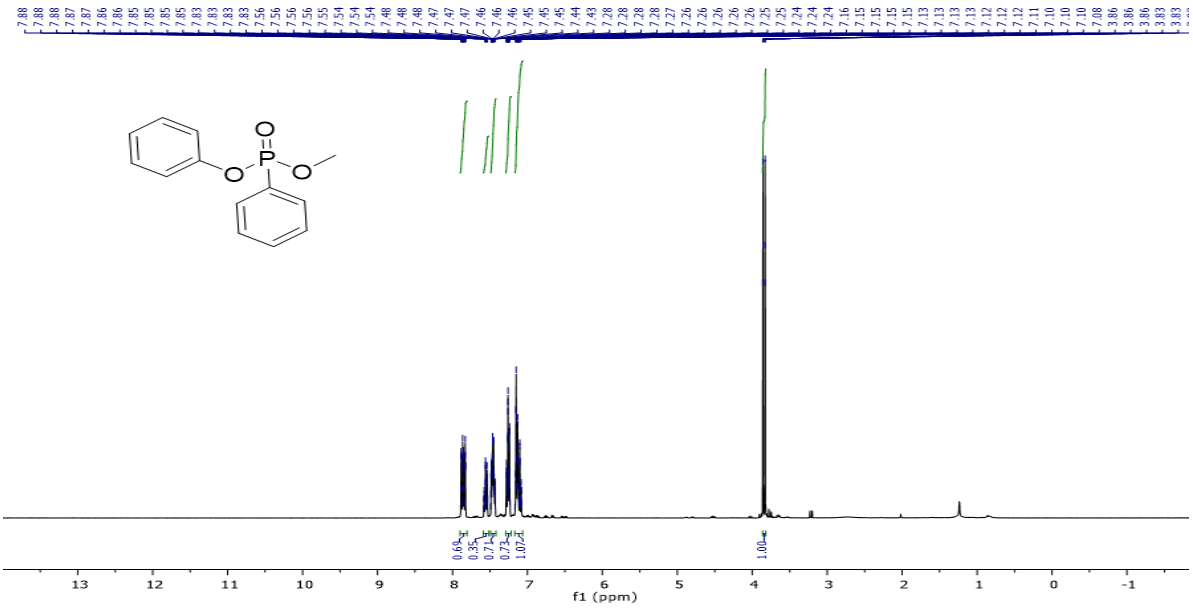

Figure A.22 ^{1}H NMR of compound **2-24**

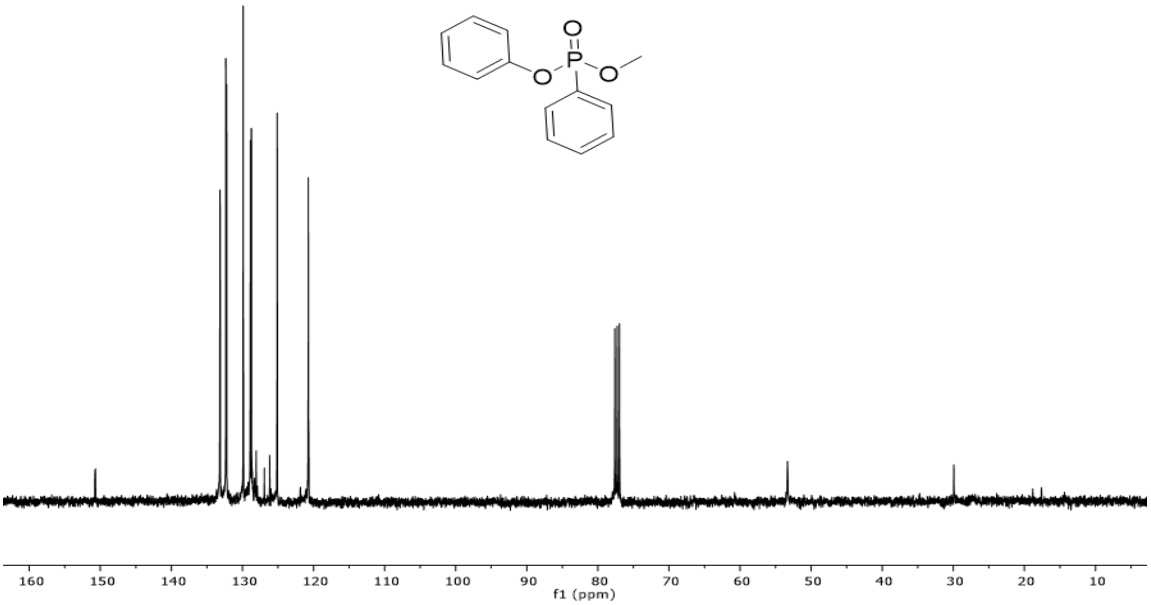

Figure A.23 ^{13}C NMR of compound **2-24**

Figure A.24 ^{31}P NMR of compound **2-24**

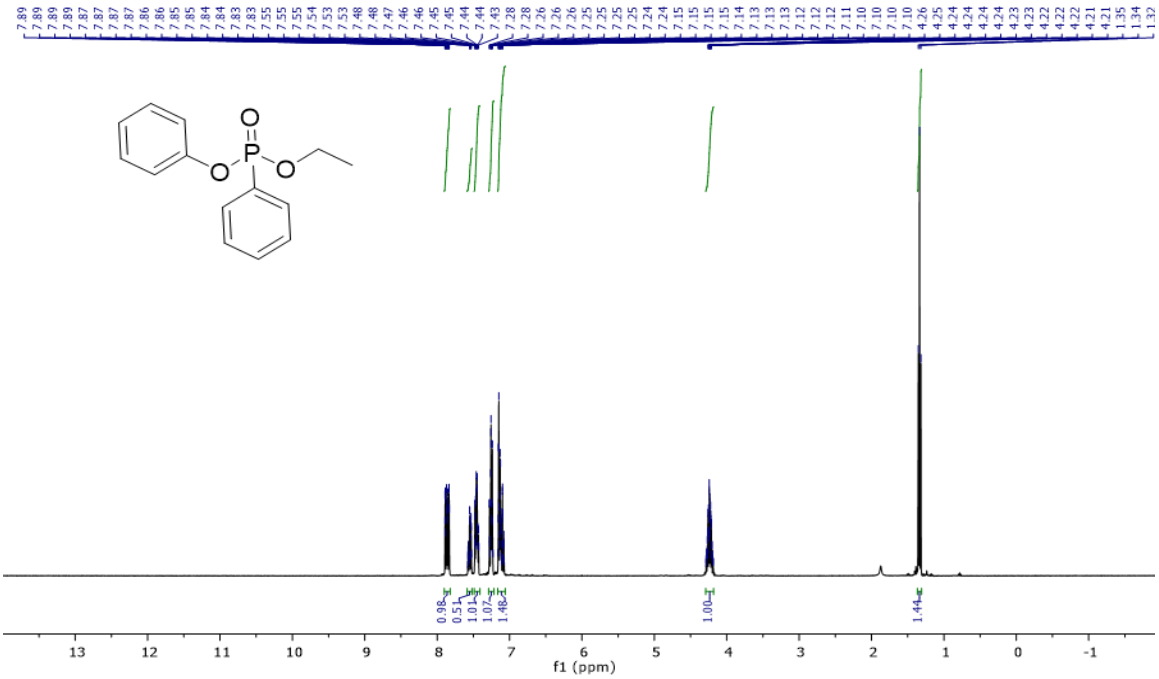

Figure A.25 ^{1}H NMR of compound **2-25**

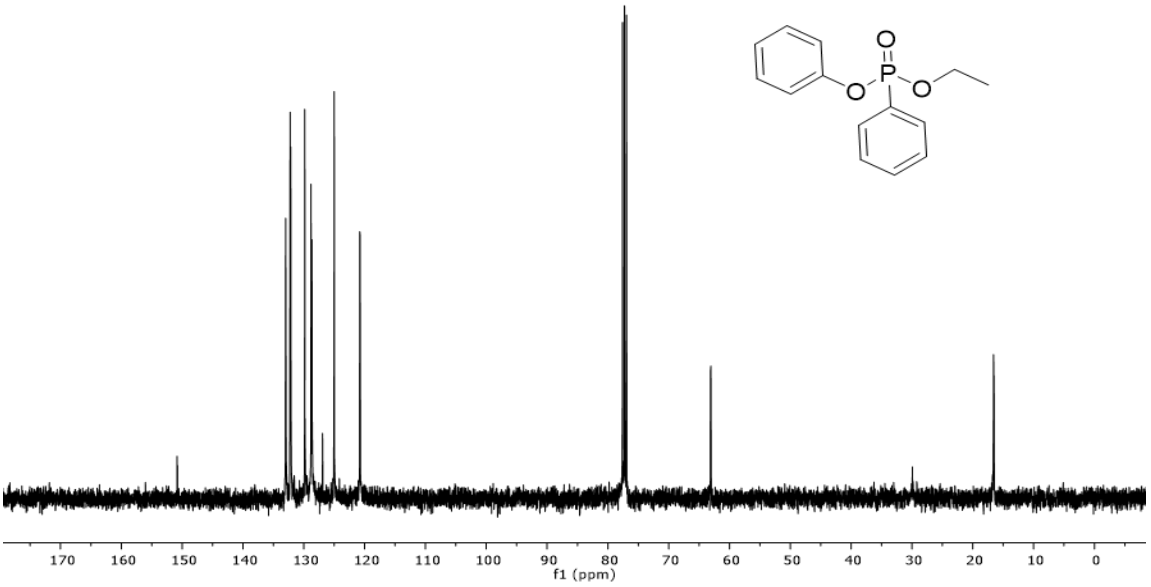

Figure A.26 ^{13}C NMR of compound **2-25**

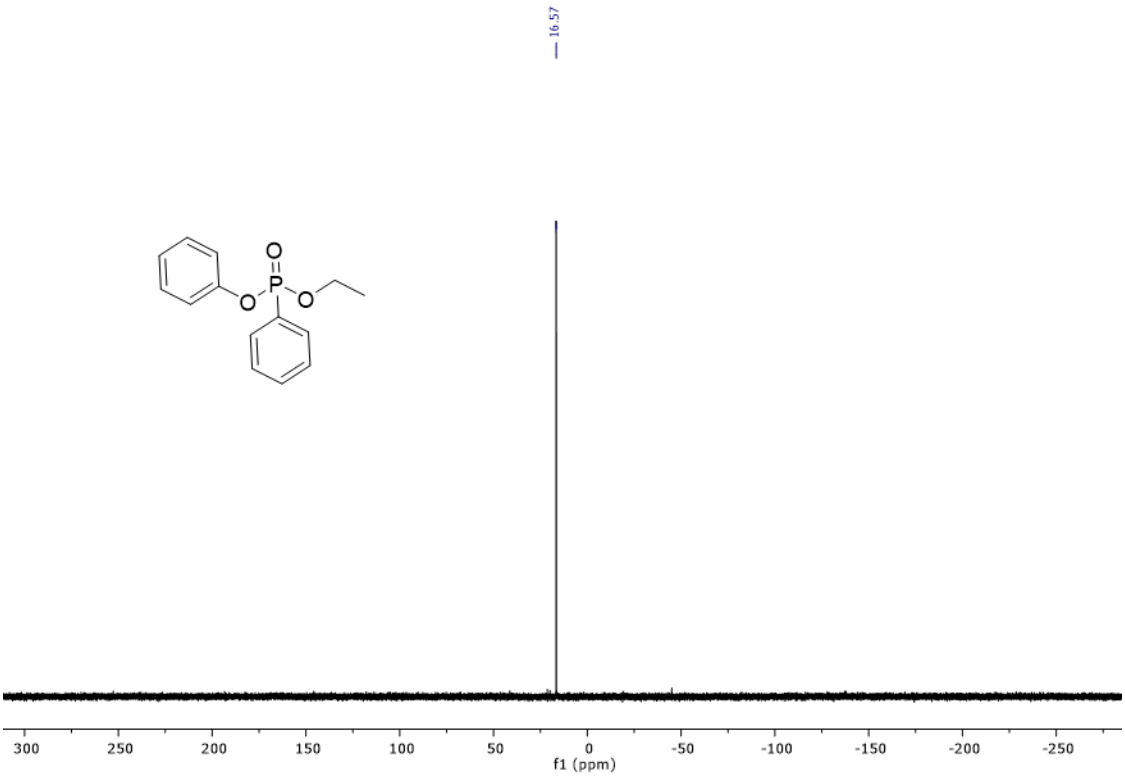

Figure A.27 ^{31}P NMR of compound **2-25**

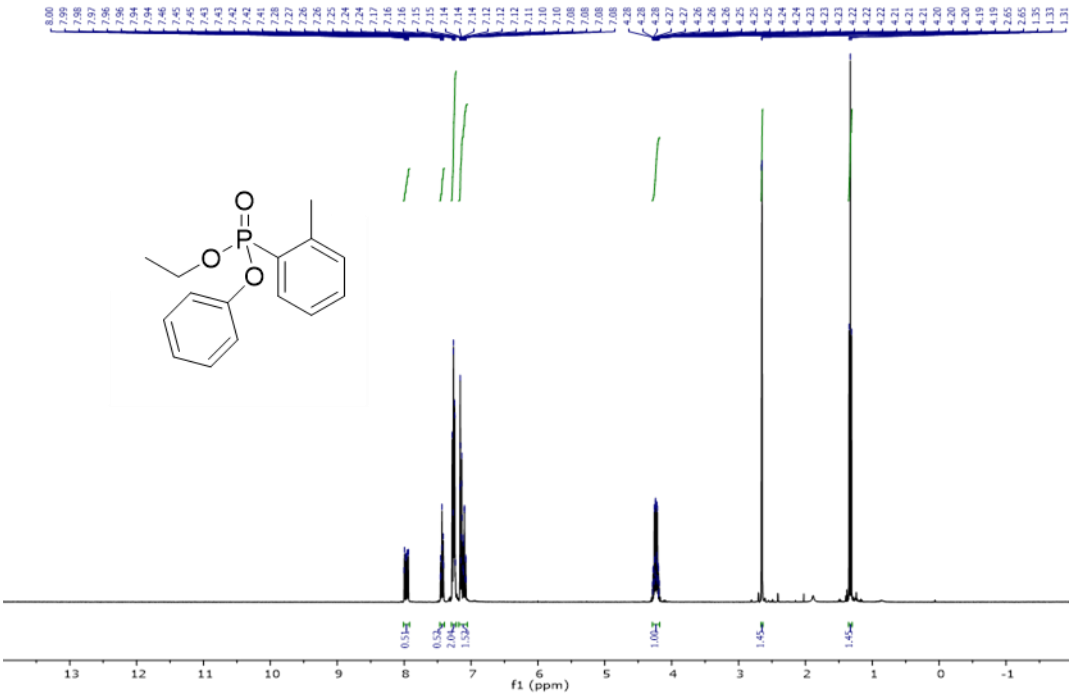

Figure A.28 ^{1}H NMR of compound **2-26**

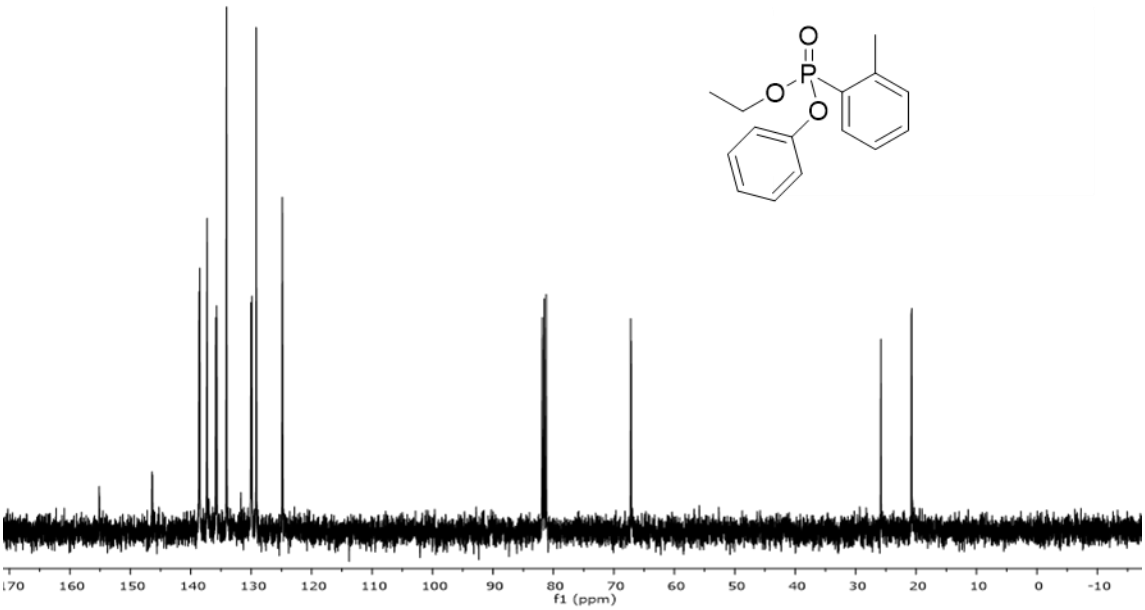

Figure A.29 ^{13}C NMR of compound **2-26**

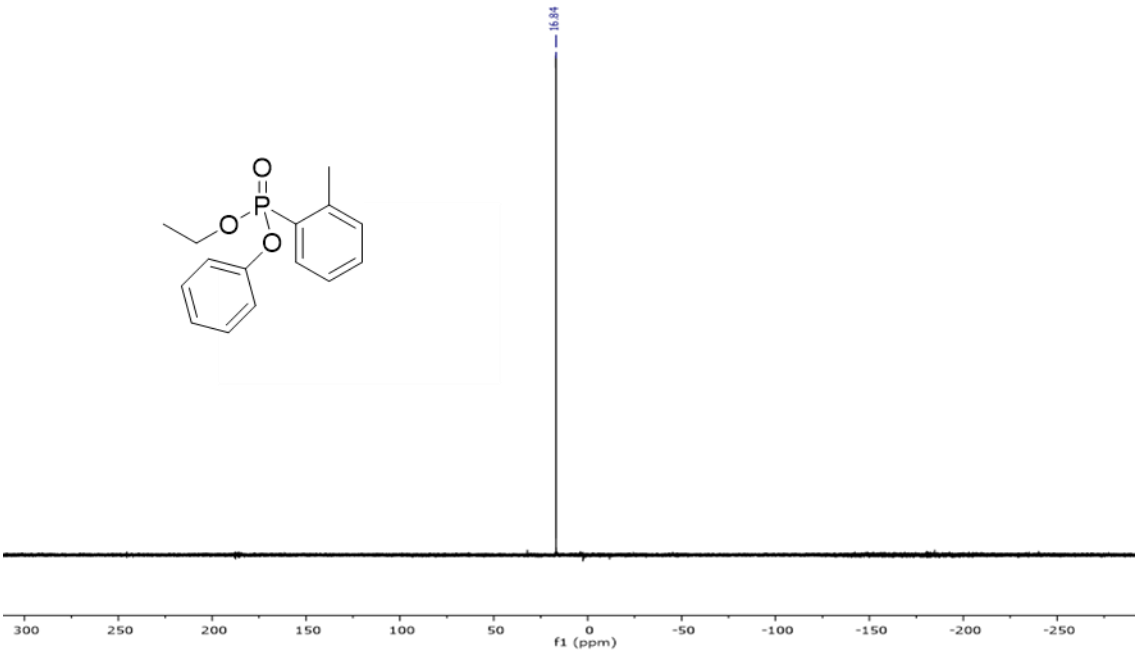

Figure A.30 ^{31}P NMR of compound **2-26**

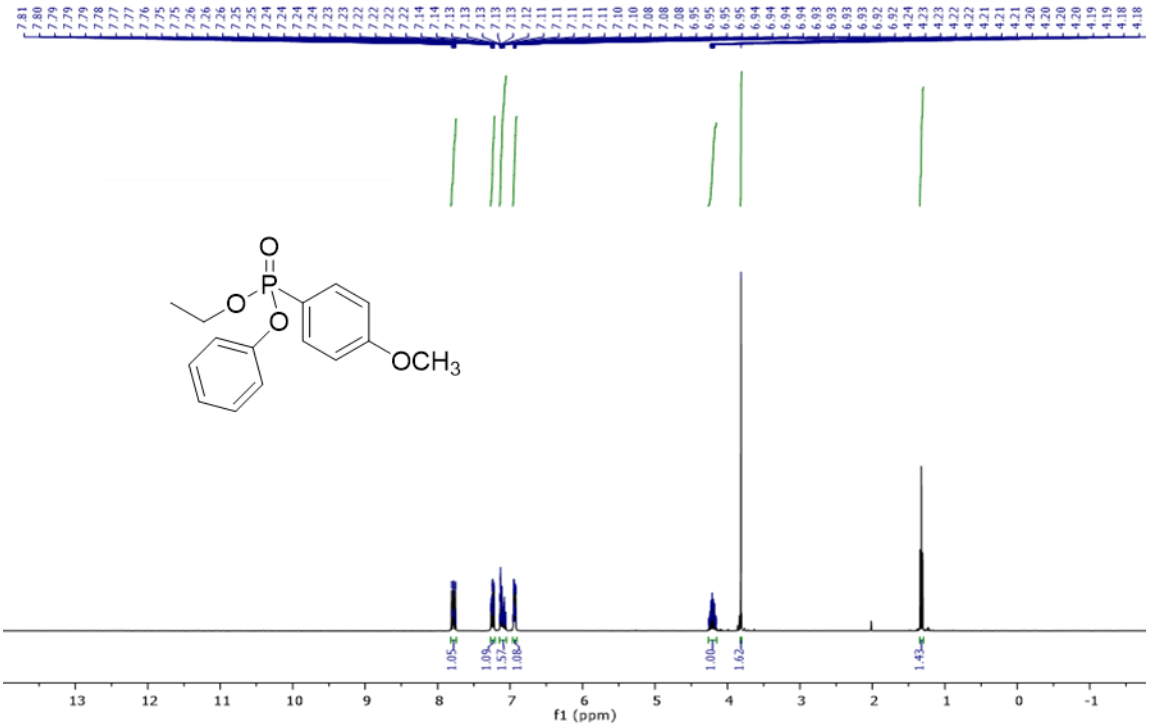

Figure A.31 ^{1}H NMR of compound **2-27**

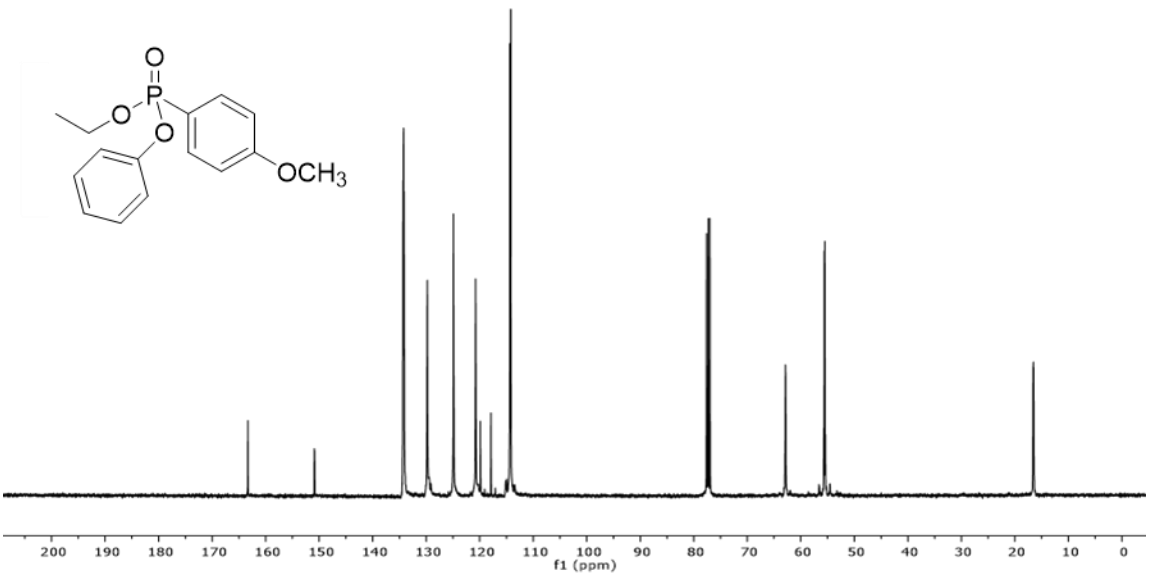

Figure A.32 ^{13}C NMR of compound **2-27**

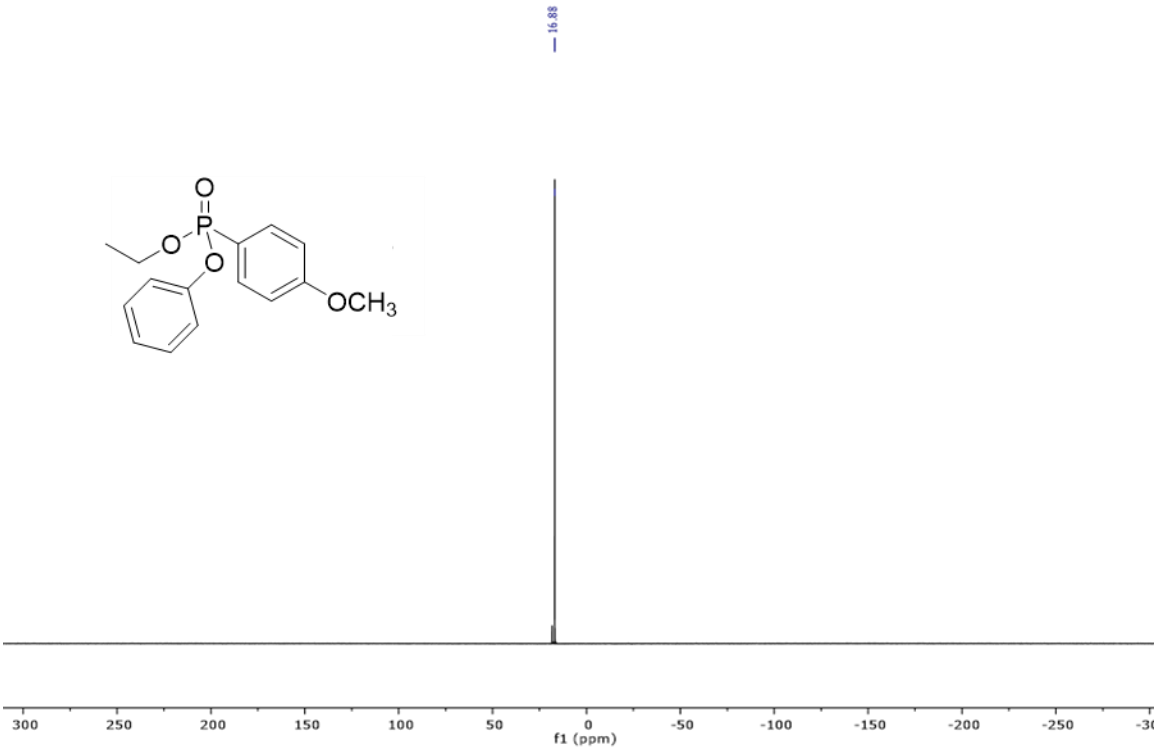

Figure A.33 ^{31}P NMR of compound **2-27**

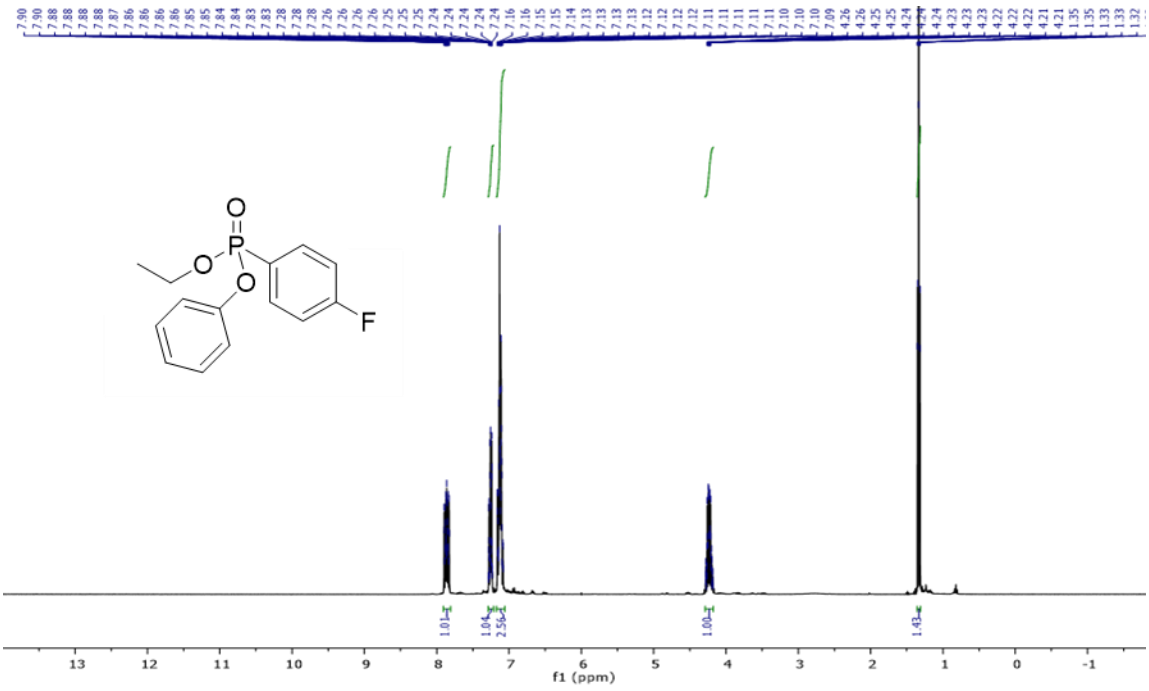

Figure A.34 ^{1}H NMR of compound **2-28**

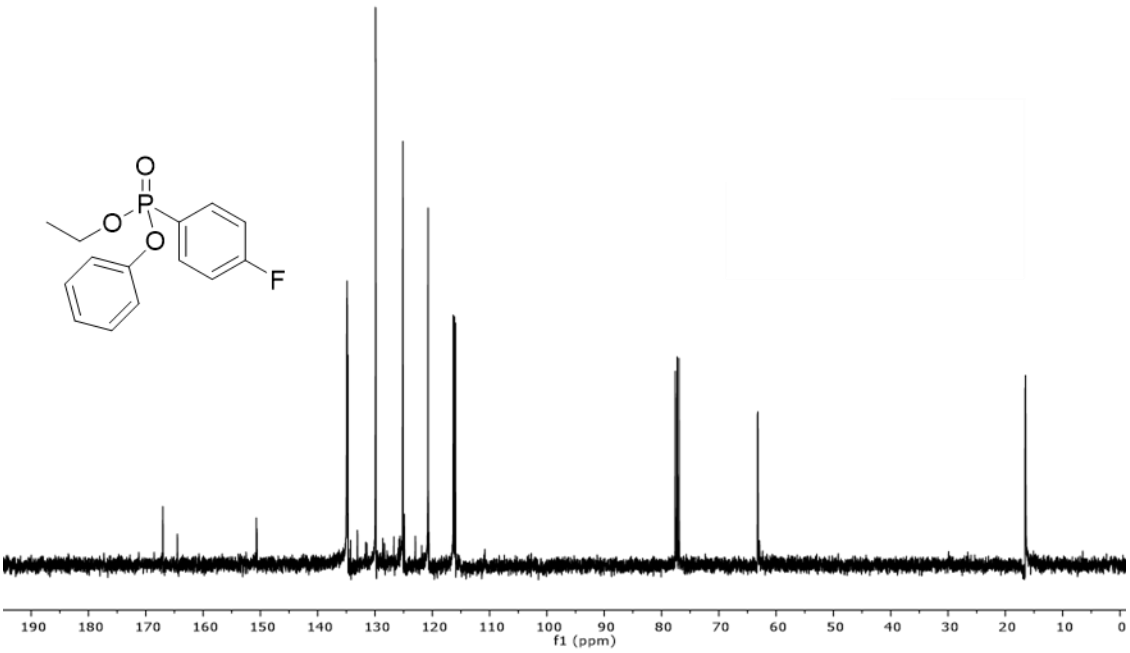

Figure A.35 ^{13}C NMR of compound **2-28**

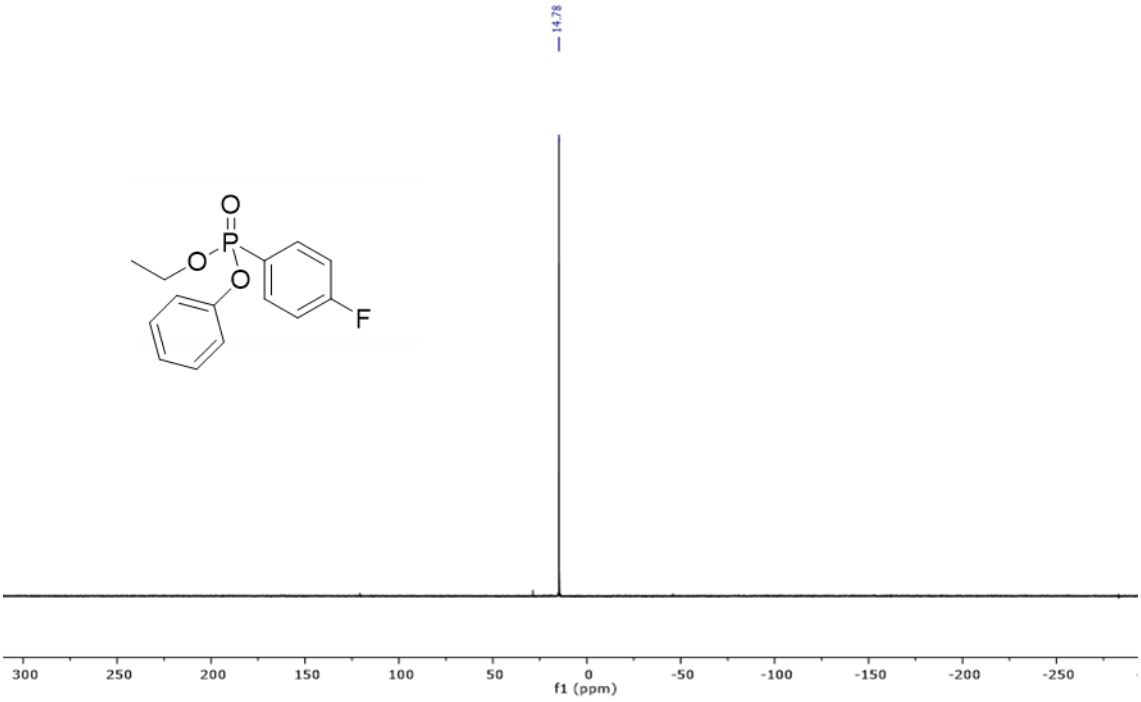

Figure A.36 ^{31}P NMR of compound **2-28**

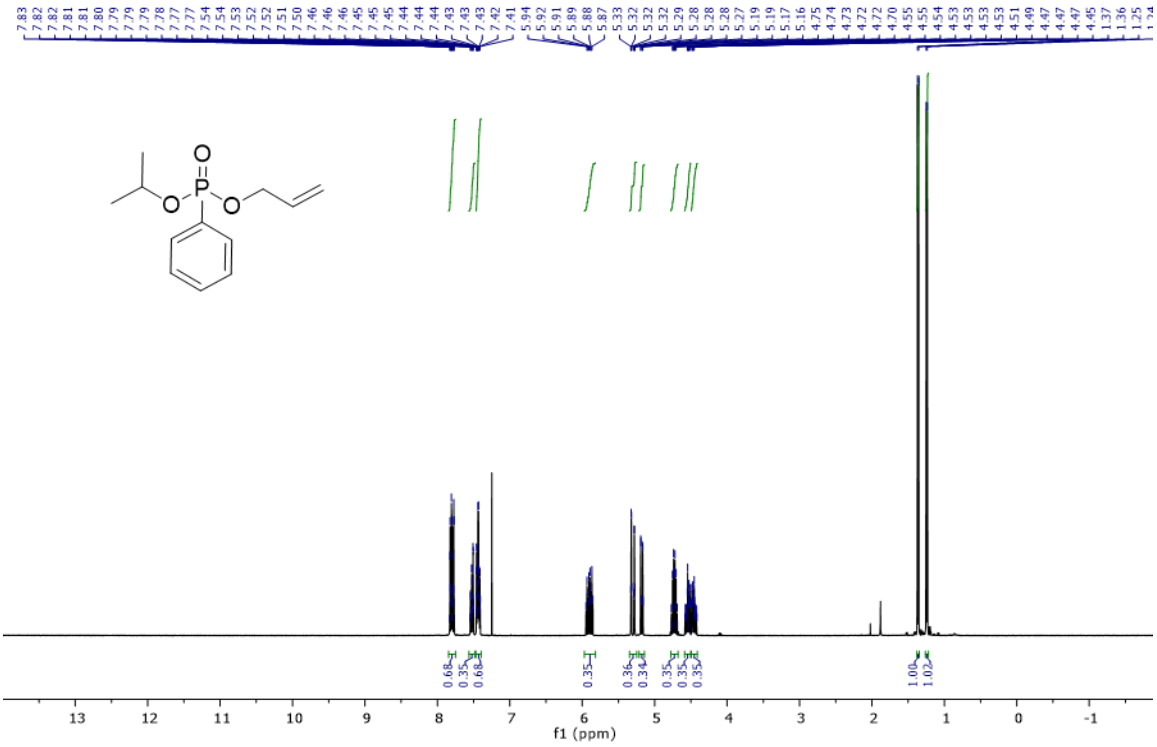

Figure A.37 ^{1}H NMR of compound **2-31**

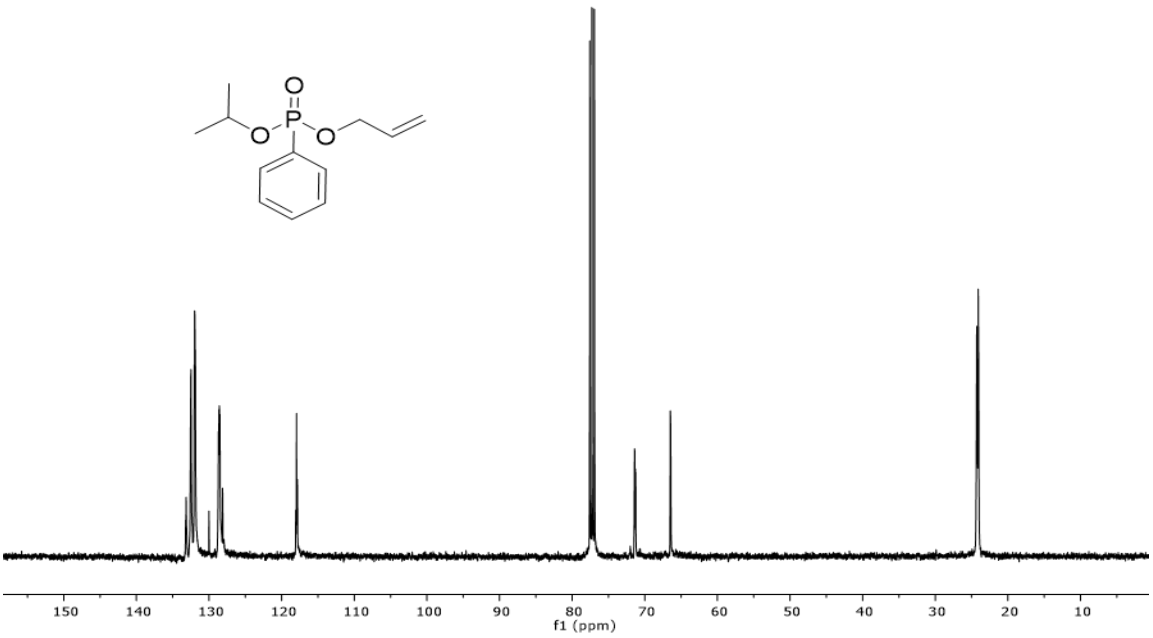

Figure A.38 ^{13}C NMR of compound **2-31**

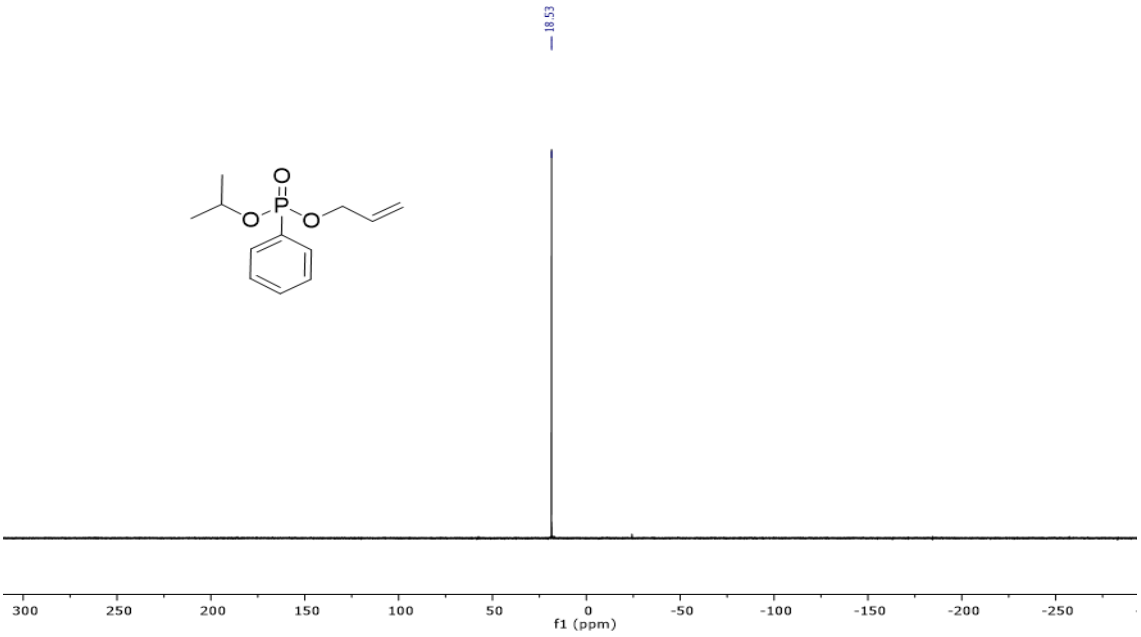

Figure A.39 ^{31}P NMR of compound **2-31**

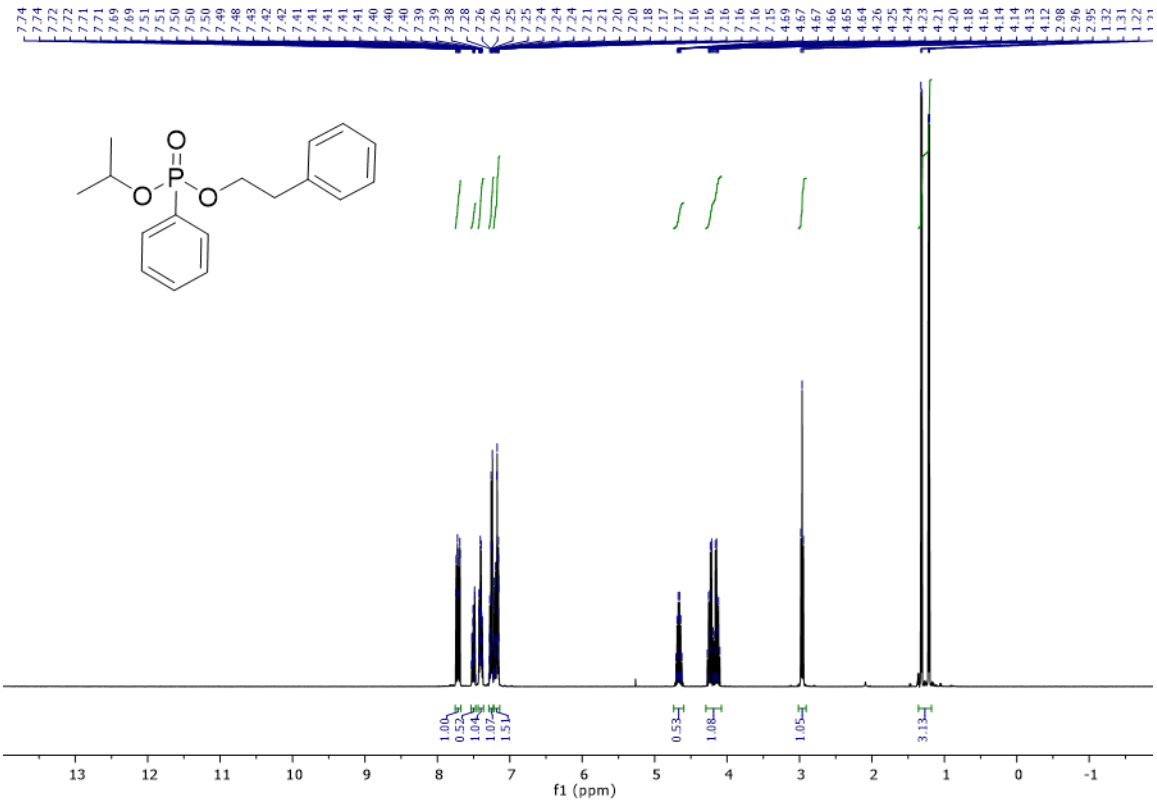

Figure A.40 ^{1}H NMR of compound **2-32**

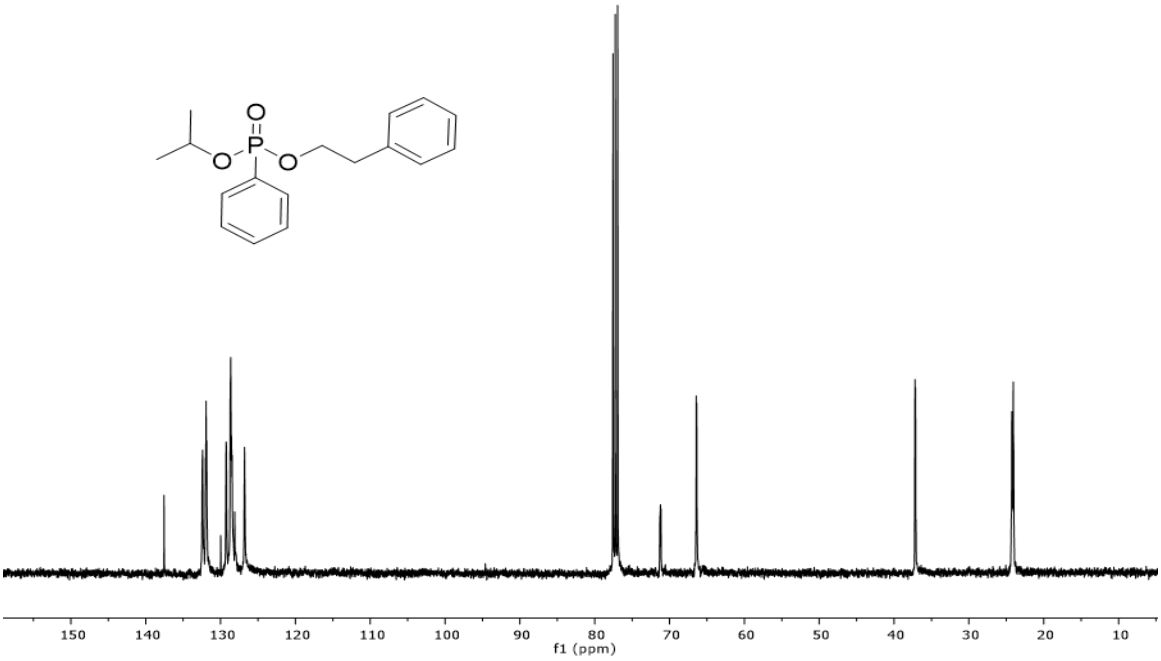

Figure A.41 ^{13}C NMR of compound **2-32**

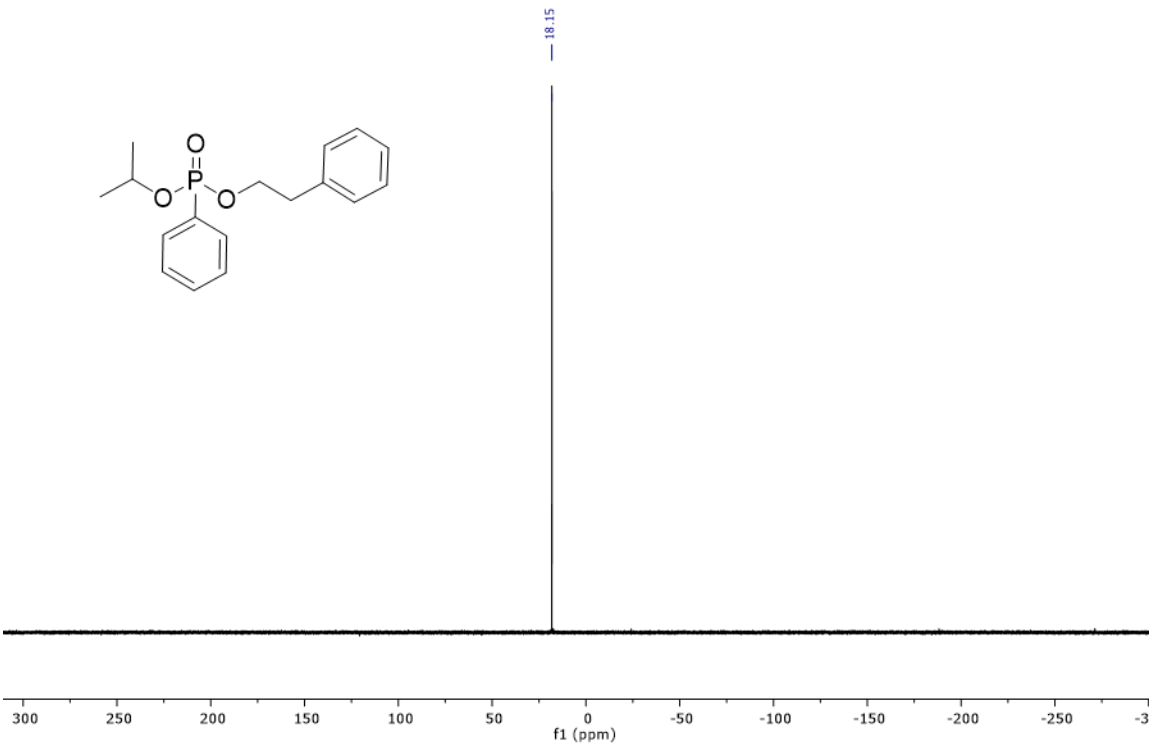

Figure A.42 ^{31}P NMR of compound **2-32**

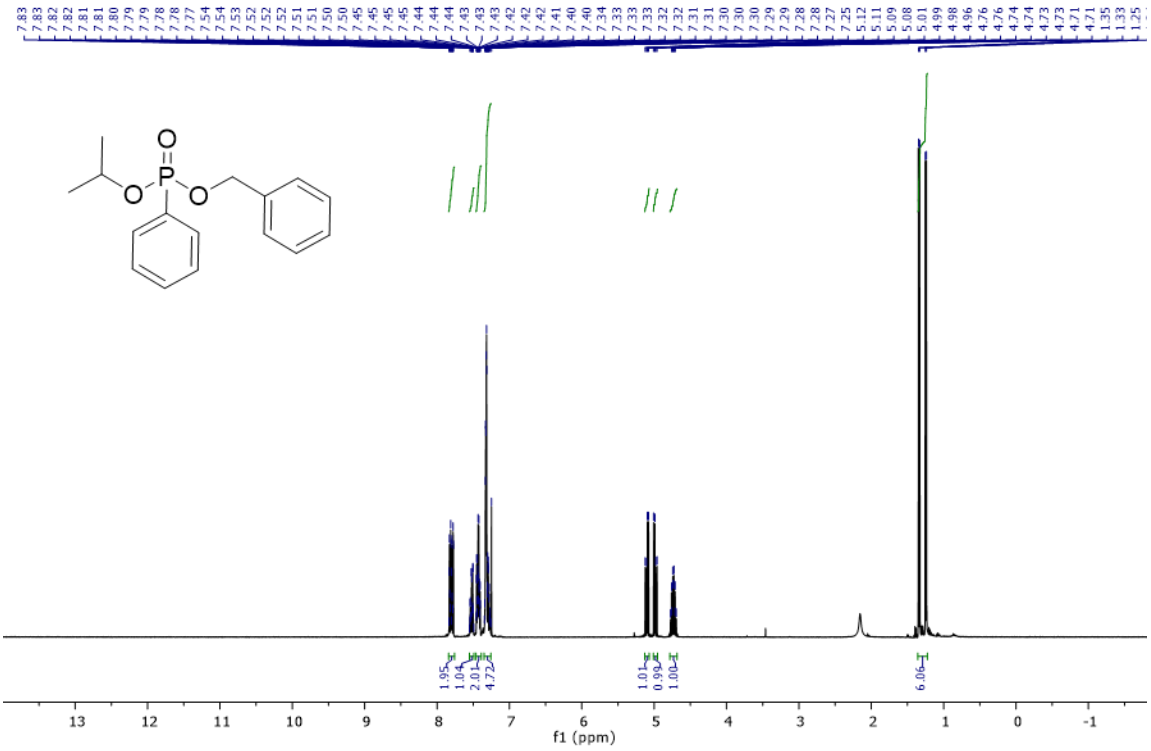

Figure A.43 ^{1}H NMR of compound **2-33**

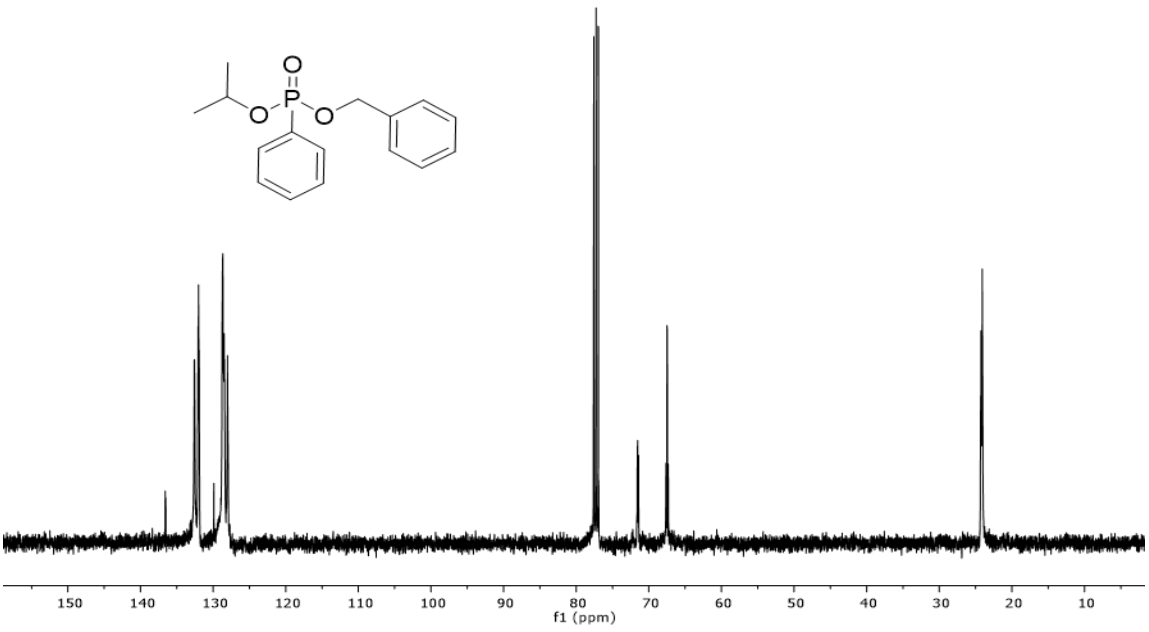

Figure A.44 ^{13}C NMR of compound **2-33**

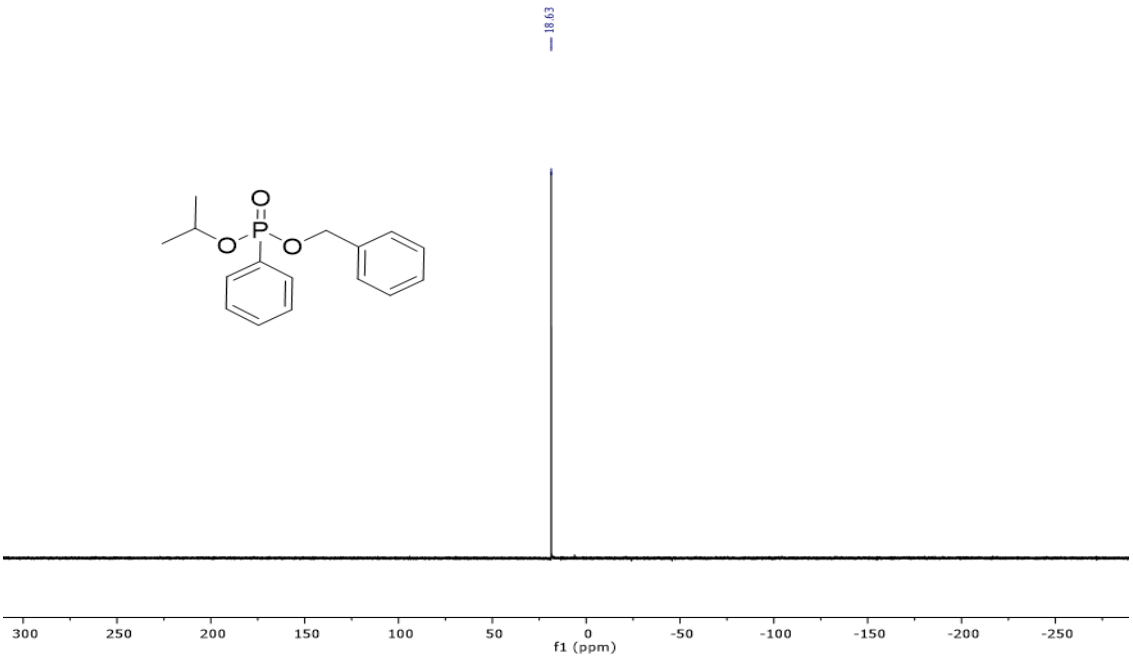

Figure A.45 ^{31}P NMR of compound **2-33**

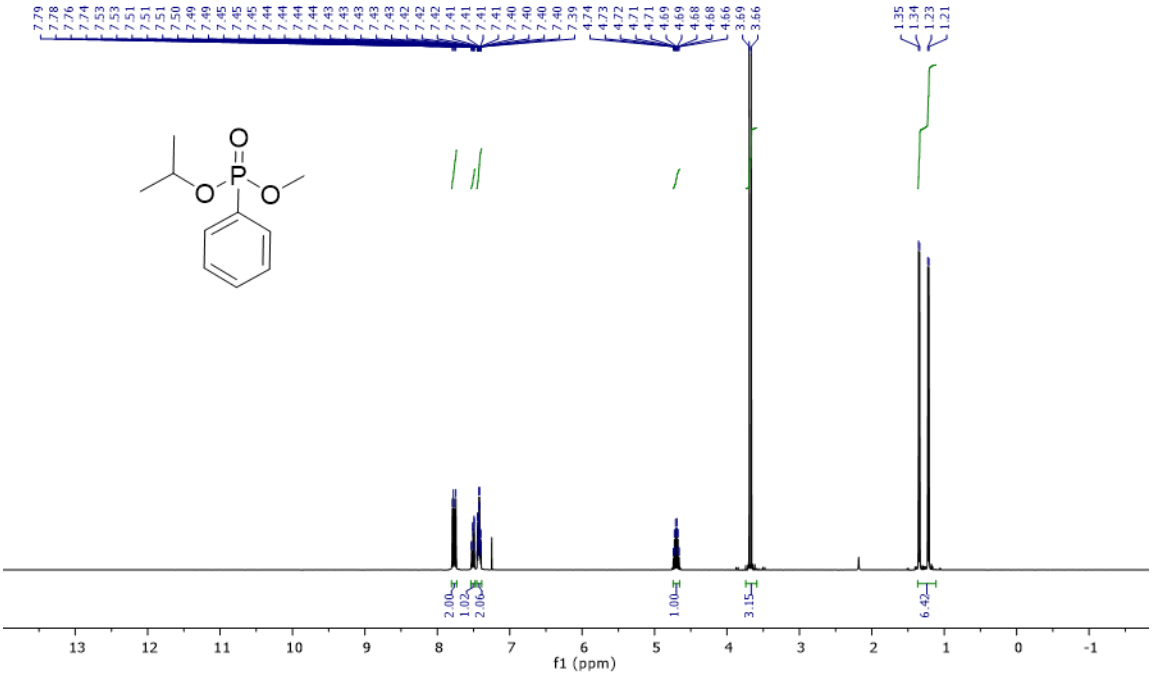

Figure A.46 ^{1}H NMR of compound **2-34**

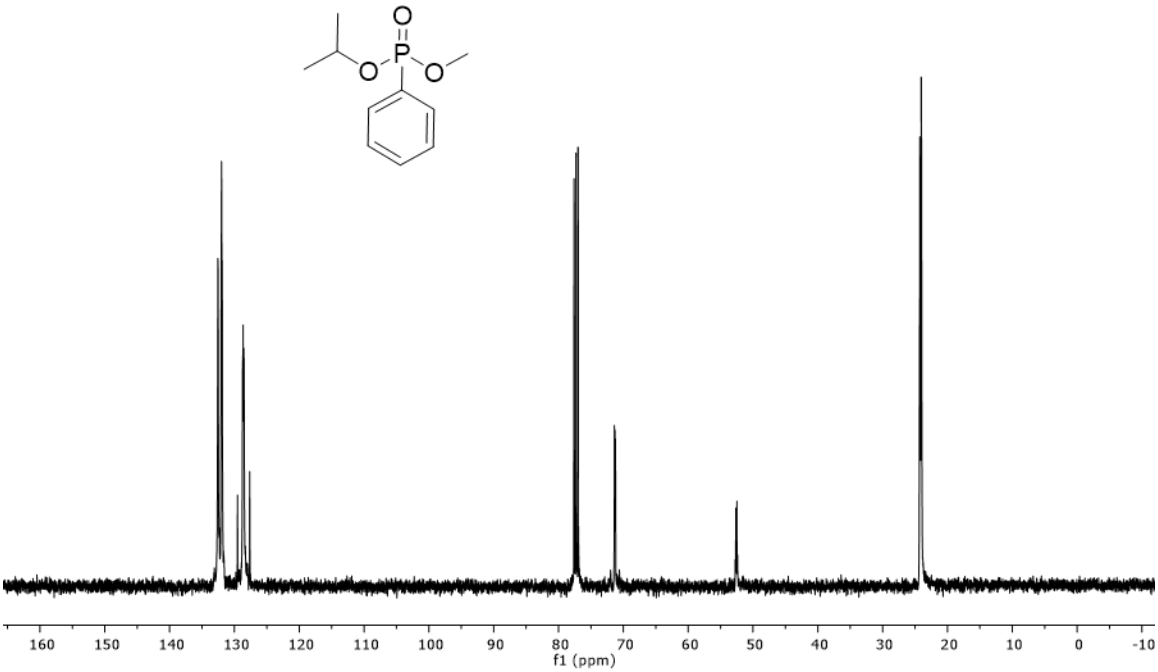

Figure A.47 ^{13}C NMR of compound **2-34**

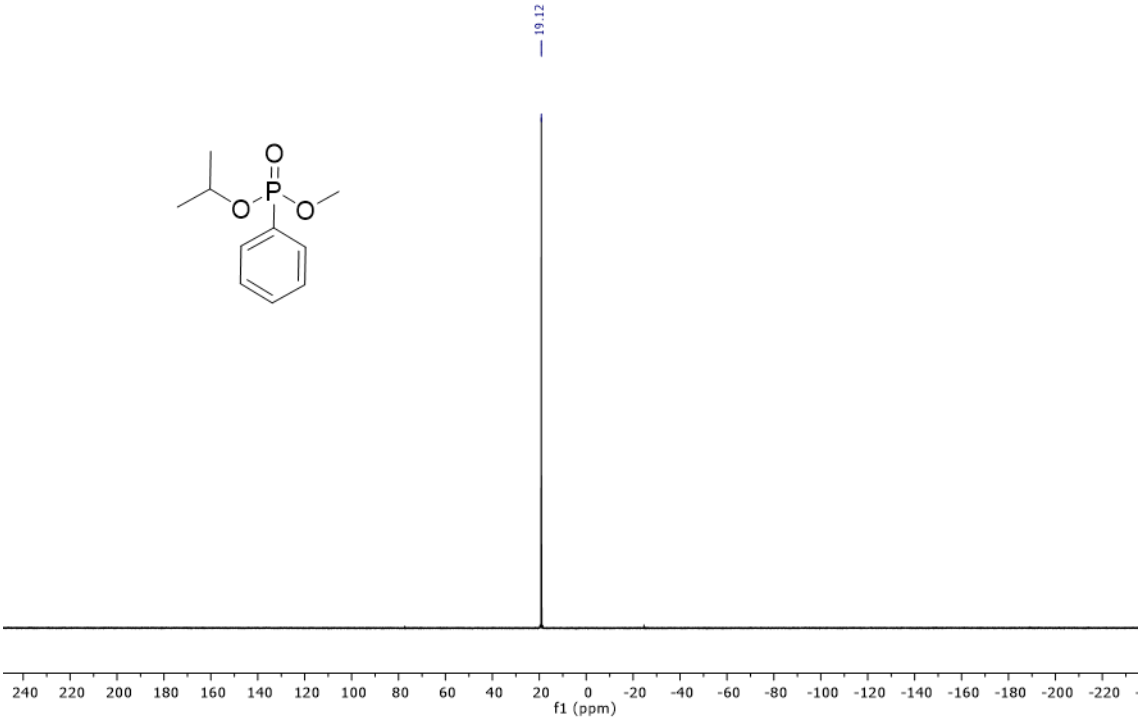

Figure A.48 ^{31}P NMR of compound **2-34**

APPENDIX B: Mass spectra for Chapter 2

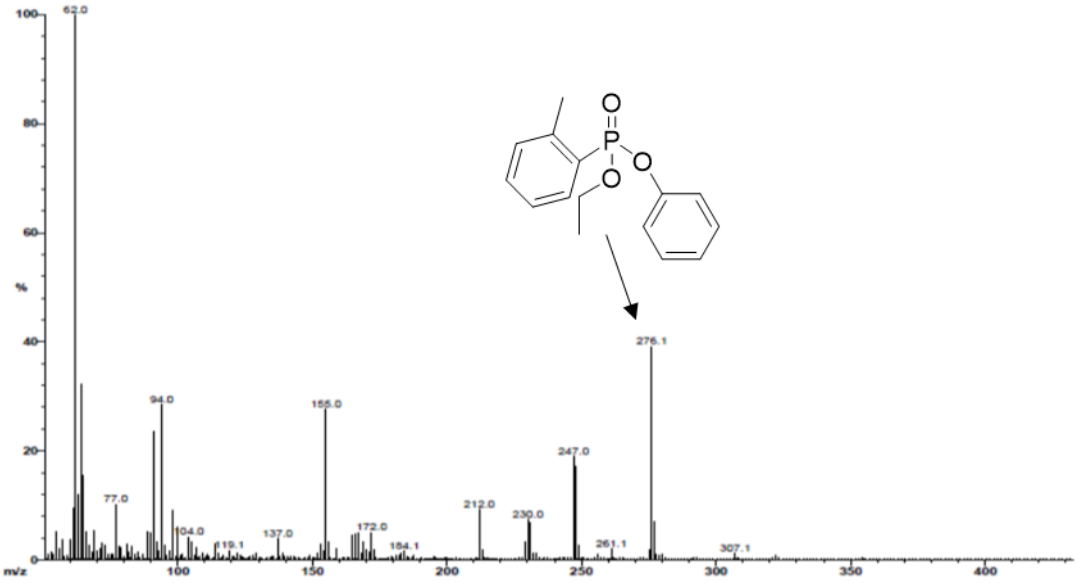

Figure B.1 Mass spectrum for compound **2-26**

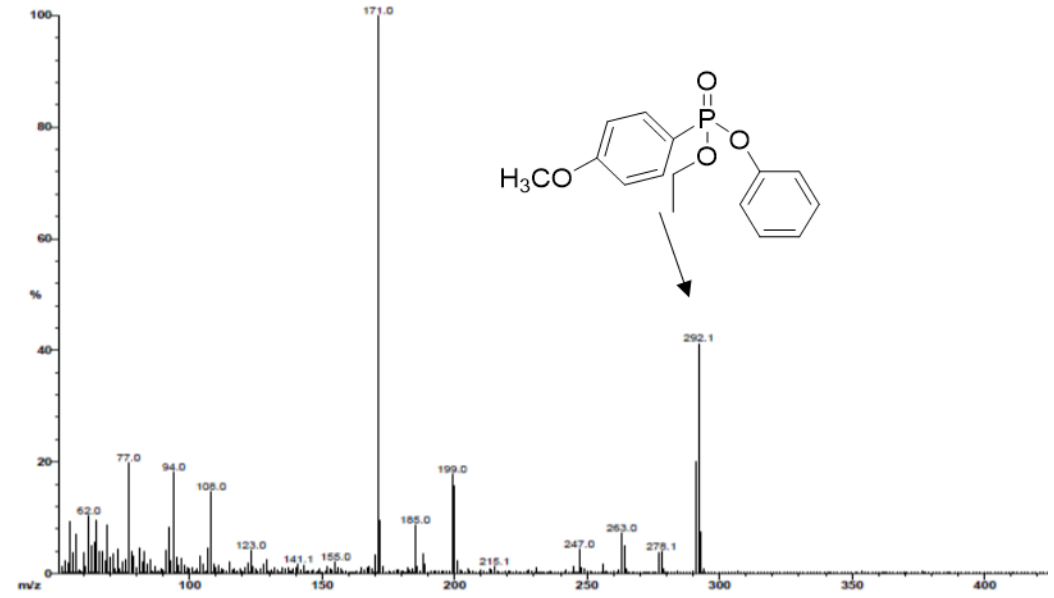

Figure B.2 Mass spectra for compound **2-27**

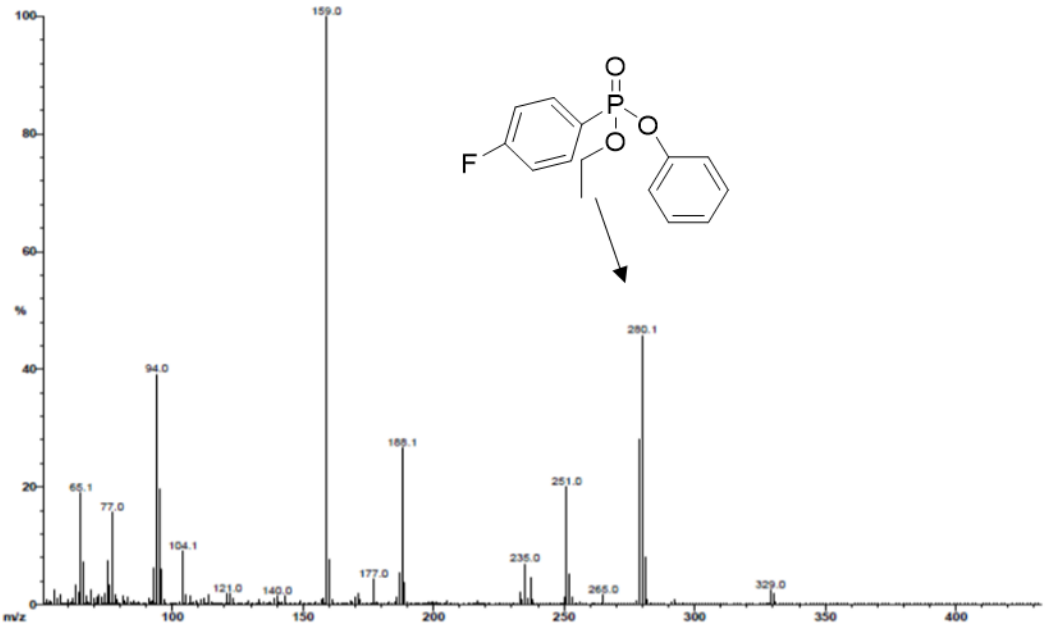

Figure B.3 Mass spectra for compound **2-28**

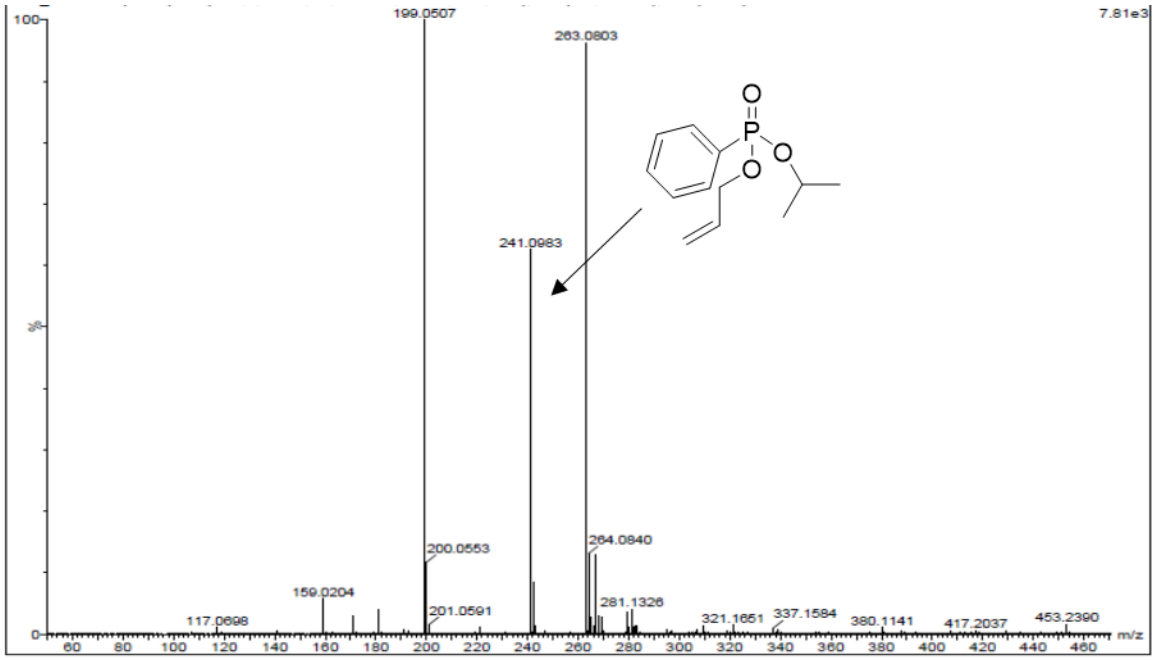

Figure B.4 Mass spectra for compound **2-31**

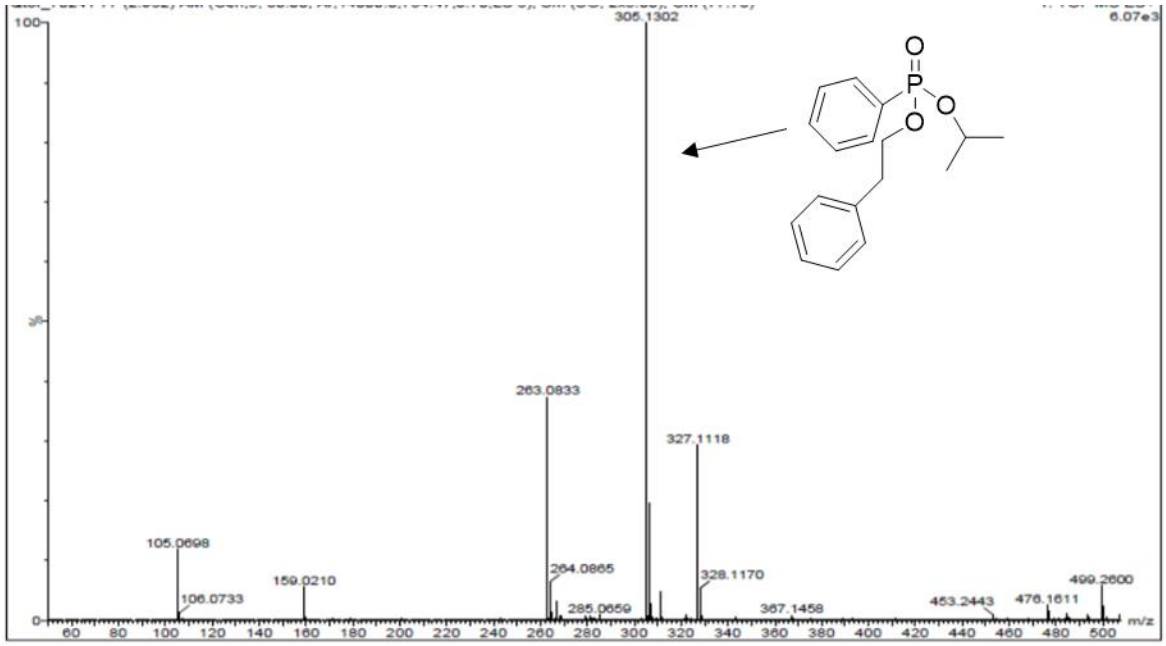

Figure B.5 Mass spectrum for compound **2-32**

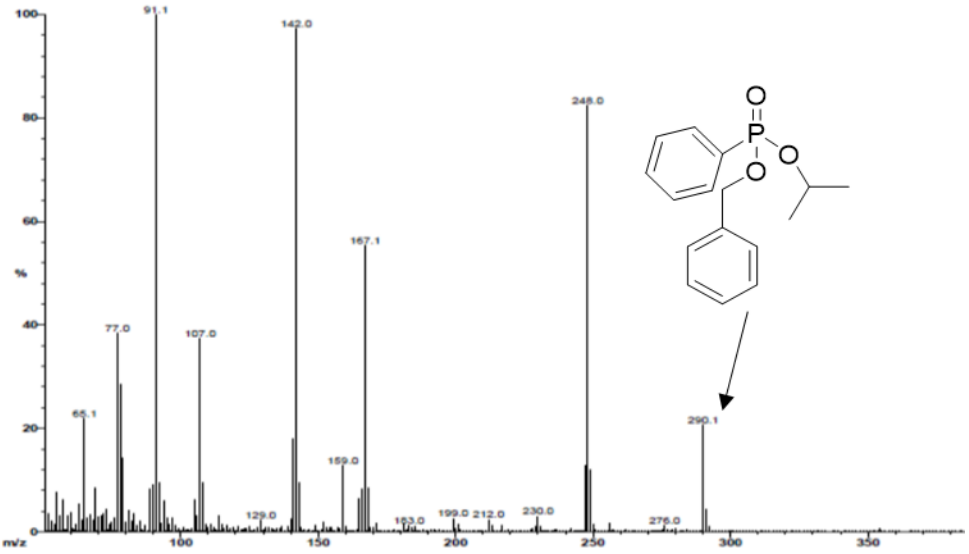

Figure B.6 Mass spectra for compound **2-33**

APPENDIX C: HPLC Chromatograms for Chapter 2

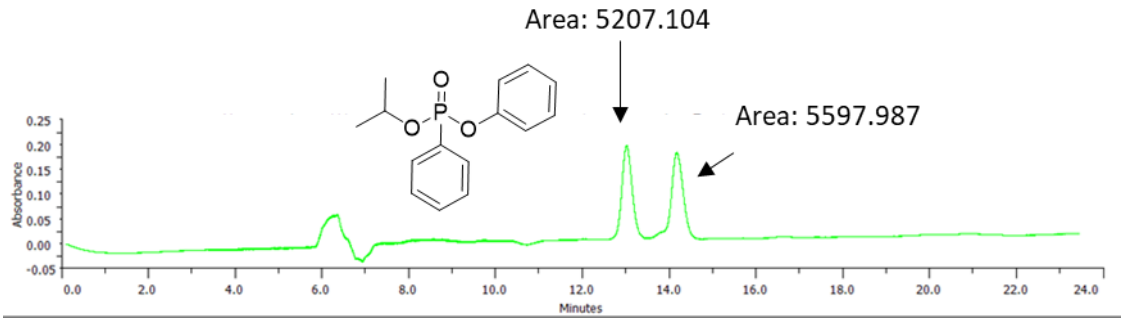

Figure C.1 HPLC chromatogram of racemic mixture **2-15** synthesized without using catalyst (Amylose 2)

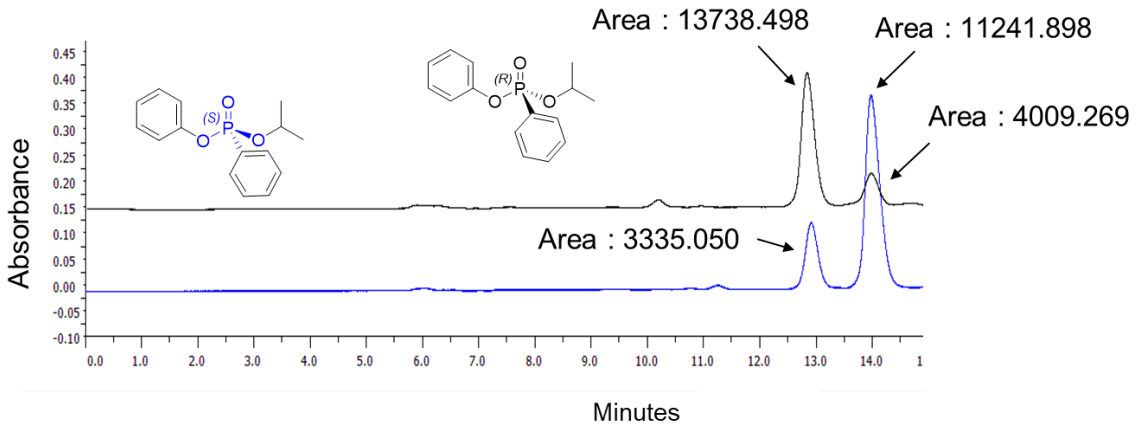

Figure C.2 HPLC chromatogram of compound **2-15** (Amylose 2)

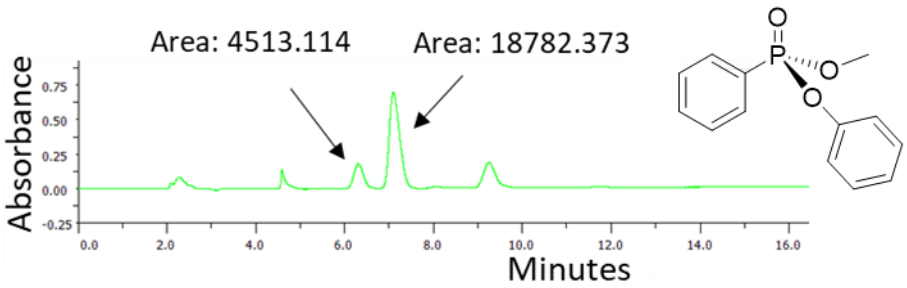

Figure C.3 HPLC chromatogram of **2-24** using 10 mol % of (*S*)-**2-16** (Amylose 2)

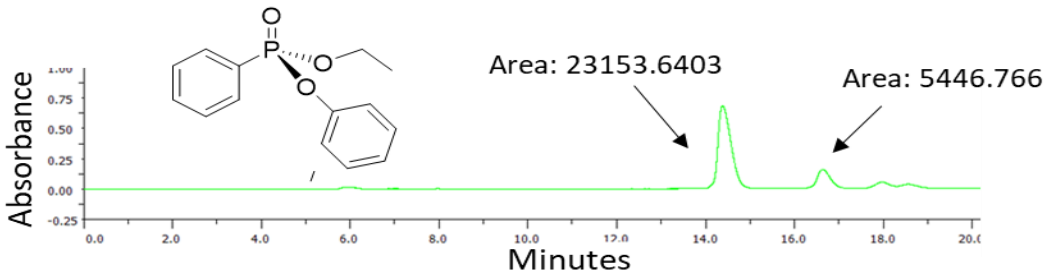

Figure C.4 HPLC chromatogram of **2-25** using (*S*)-**2-16** (Amylose 2)

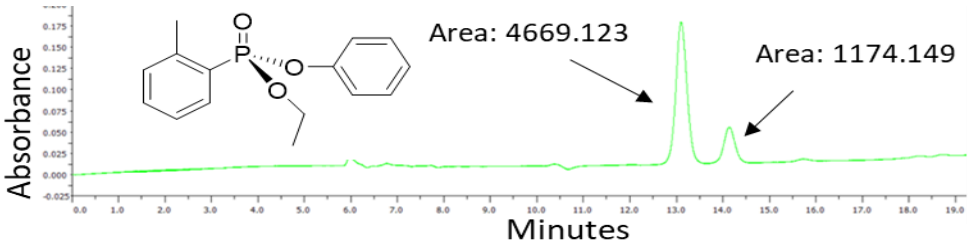

Figure C.5 HPLC chromatogram of **2-26** using 10 mol % of (*R*)-**2-16** (Amylose 2)

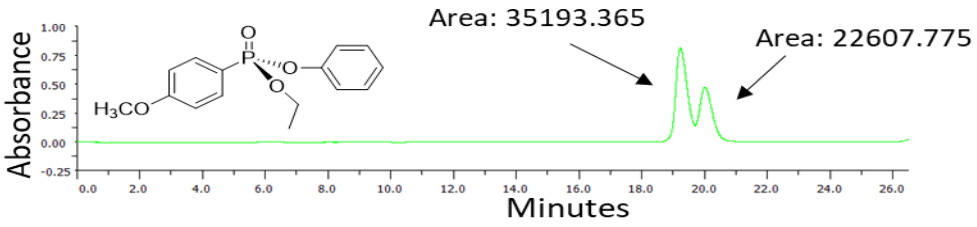

Figure C. HPLC chromatogram of **2-27** using 10 mol % of (*S*)-**2-16** (Amylose 2)

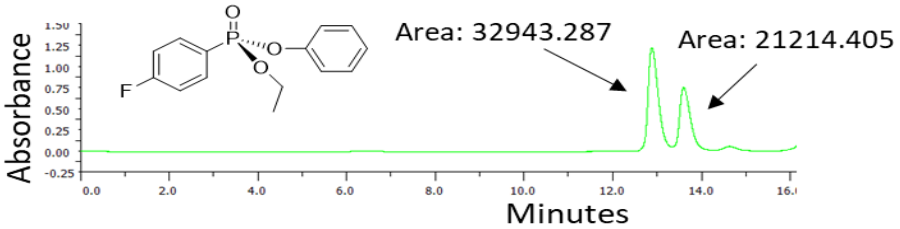

Figure C.7 HPLC chromatogram of **2-28** using 10 mol % of (*S*)-**2-16** (Amylose 2)

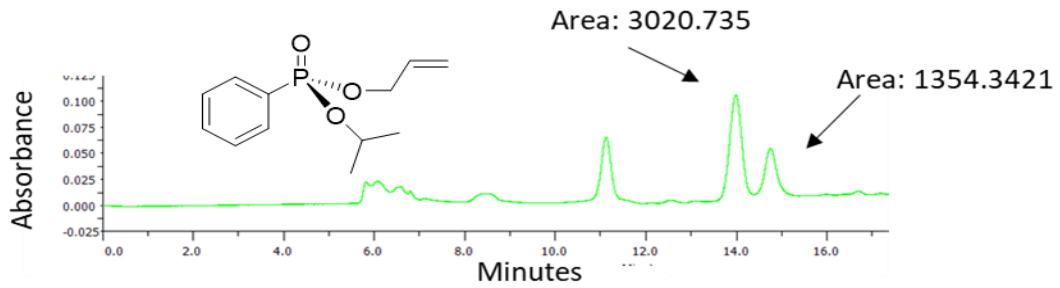

Figure C.8 HPLC chromatogram of **2-31** using 10 mol % of (*S*)-**2-16** (Amylose 2)

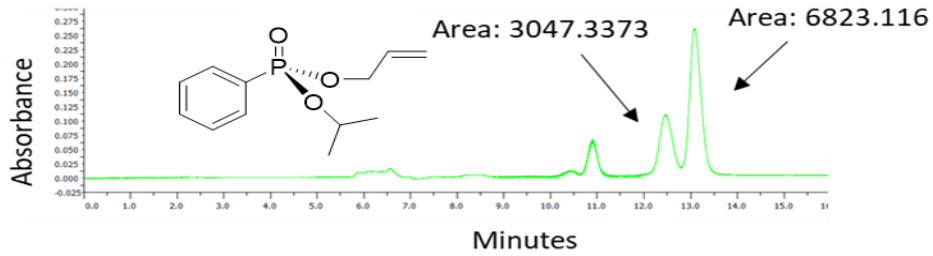

Figure C.9 HPLC chromatogram of **2-31** using 10 mol % of (*R*)-**2-16** (Amylose 2)

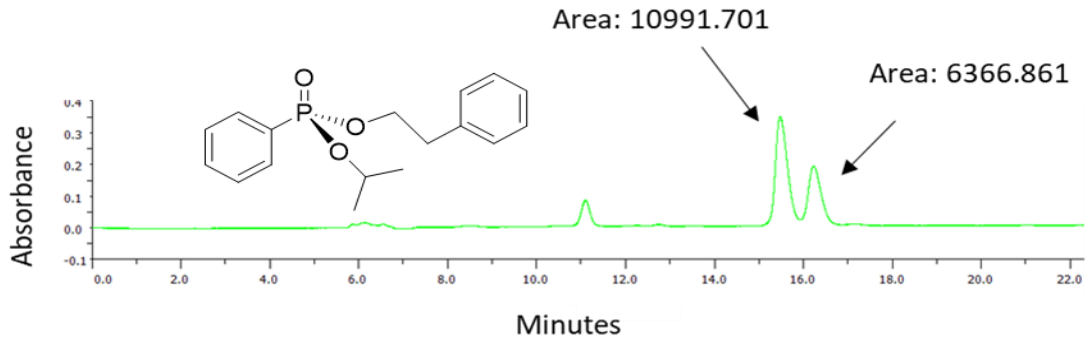

Figure C.10 HPLC chromatogram of **2-32** using 10 mol % of (*S*)-**2-16** (Amylose 2)

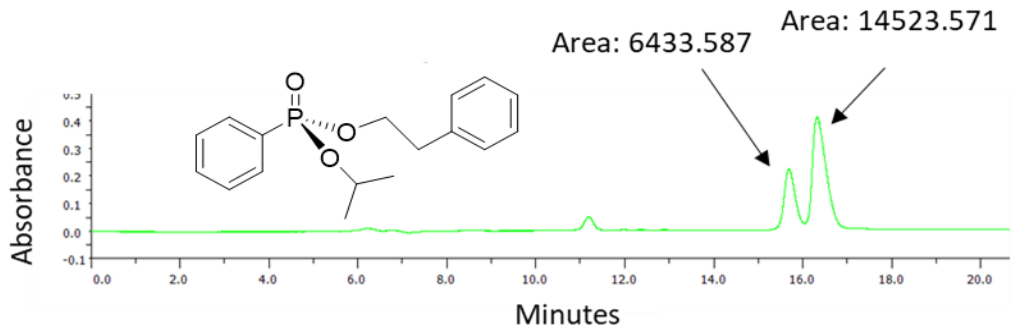

Figure C.11 HPLC chromatogram of **2-32** using 10 mol % of (*R*)-**2-16** (Amylose 2)

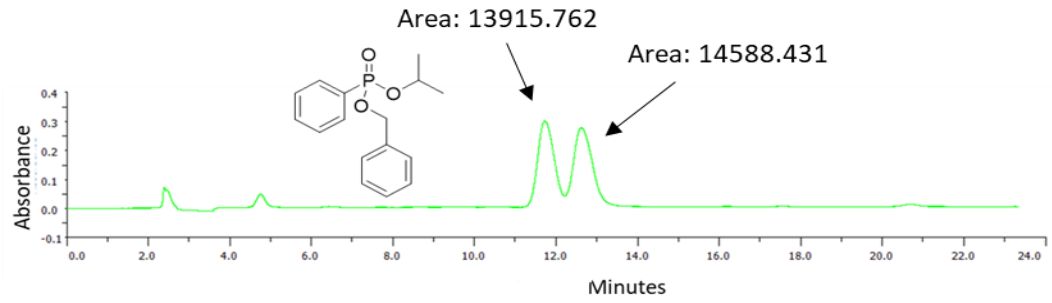

Figure C.12 HPLC chromatogram of racemic compound **2-33** without using (*S*)-**2-16** (Cellulose 2)

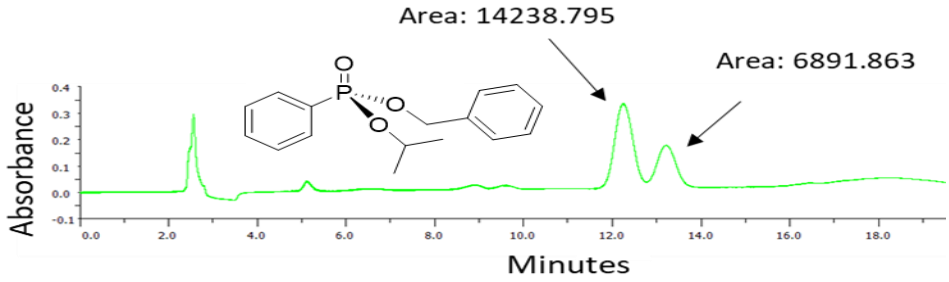

Figure C.13 HPLC chromatogram of **2-33** using 10 mol % of (*R*)-**2-16** (Cellulose 2)

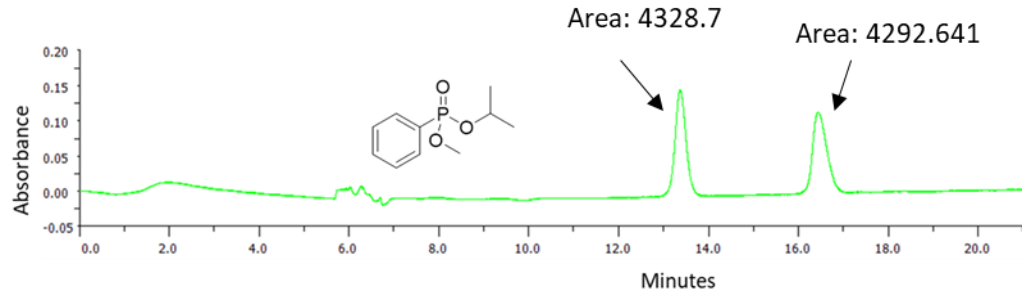

Figure C.14 HPLC chromatogram of racemic compound **2-34** without using (*S*)-**2-16** (Cellulose 2)

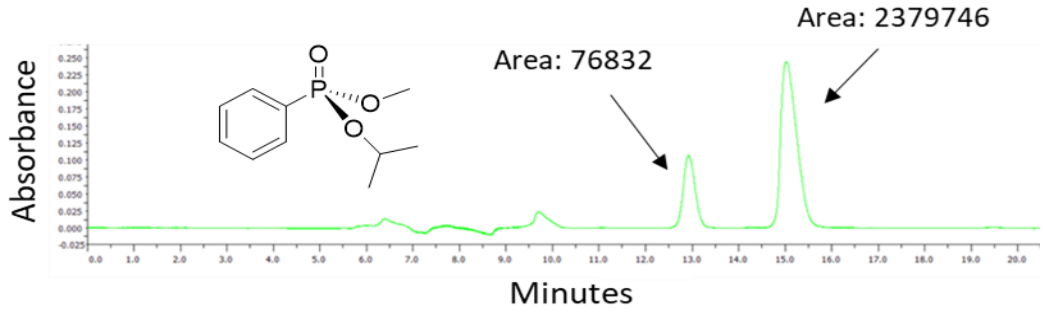

Figure C.15 HPLC chromatogram of **2-34** using 10 mol % of (*S*)-**2-16** (Cellulose 2)

APPENDIX D: NMR Data for Chapter 3

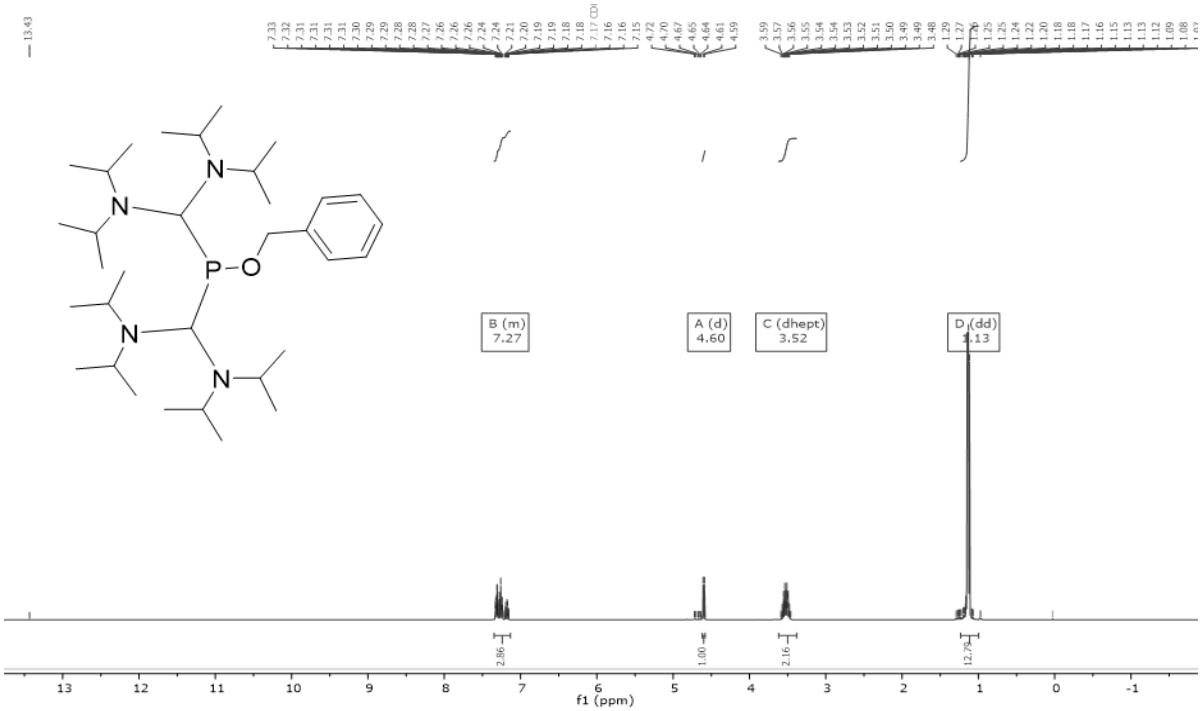

Figure D.1 ^{1}H NMR of compound **3-9**

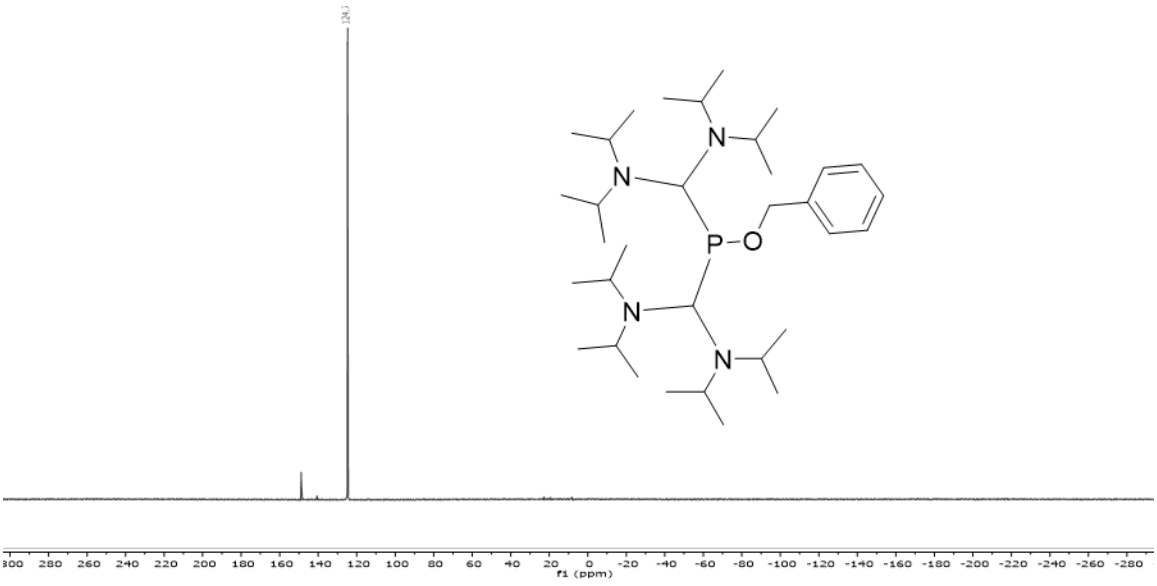

Figure D.2 ^{31}P NMR of compound **3-9**

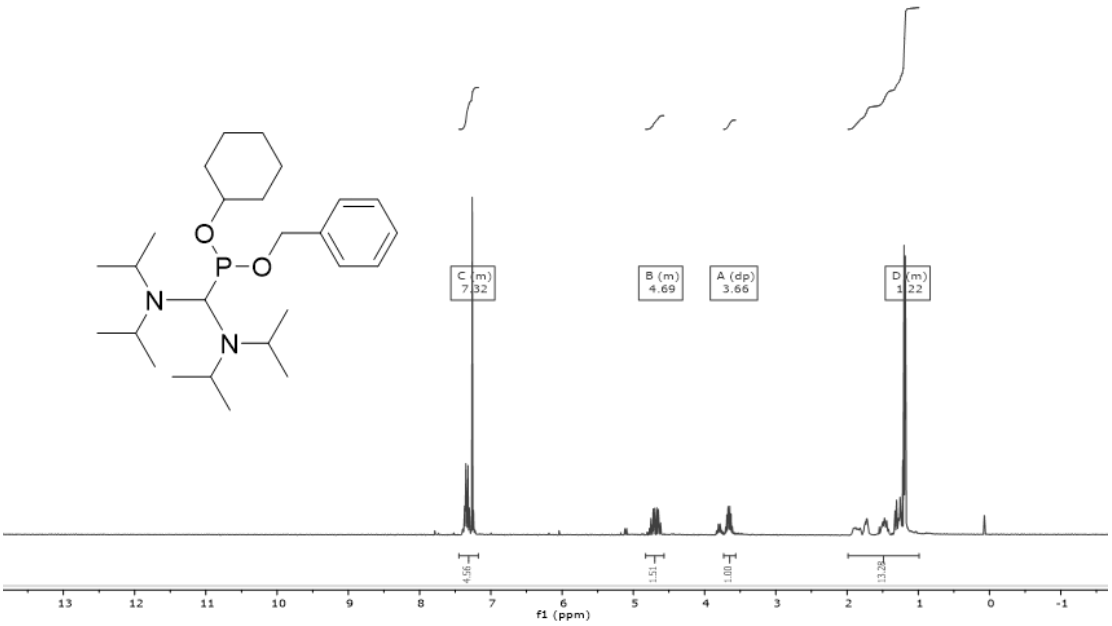

Figure D.3 ^{1}H NMR of compound **3-11**

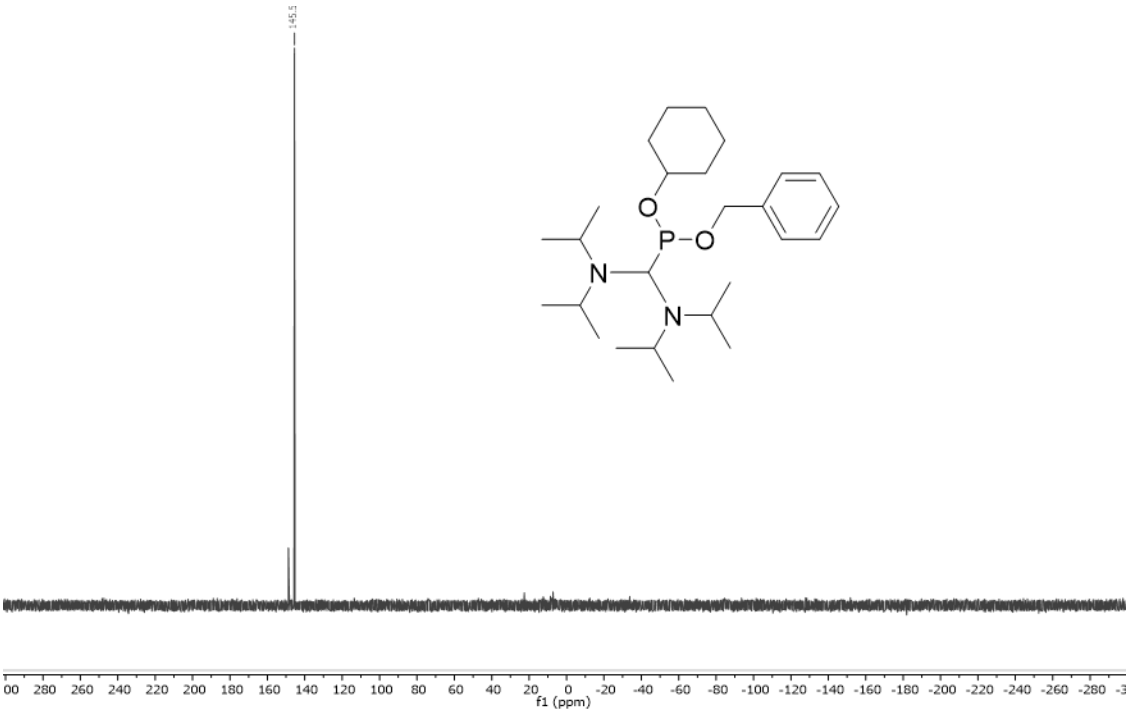

Figure D.4 ^{31}P NMR of compound **3-11**

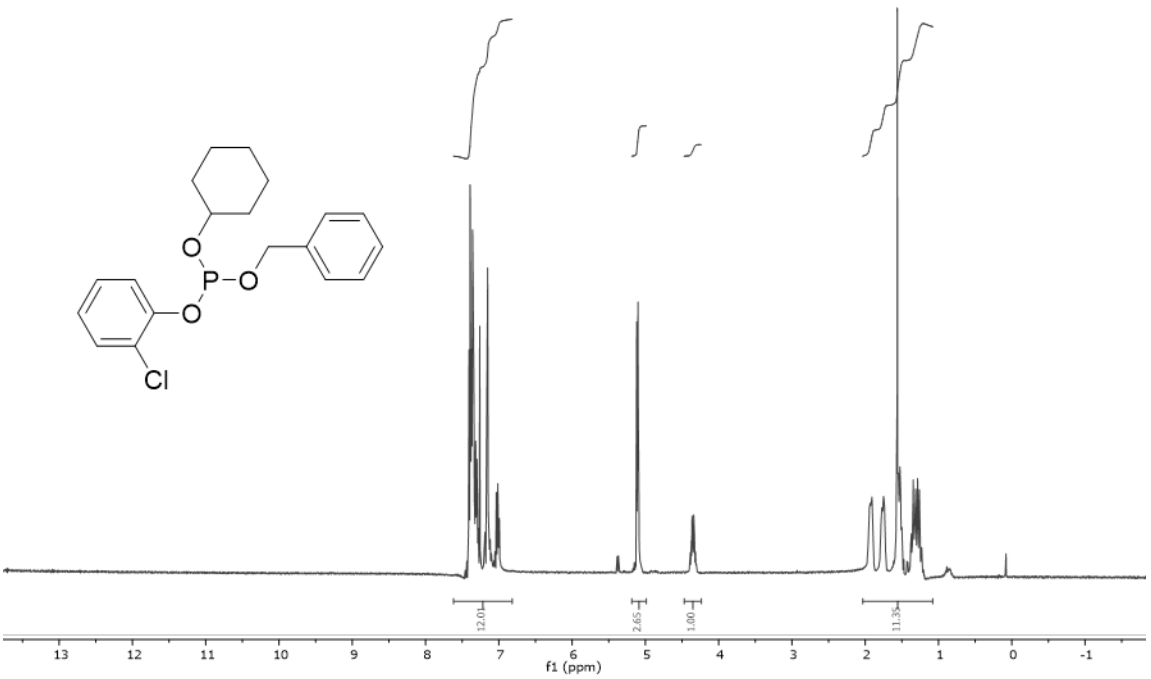

Figure D.5 ^{1}H NMR of compound **3-14**

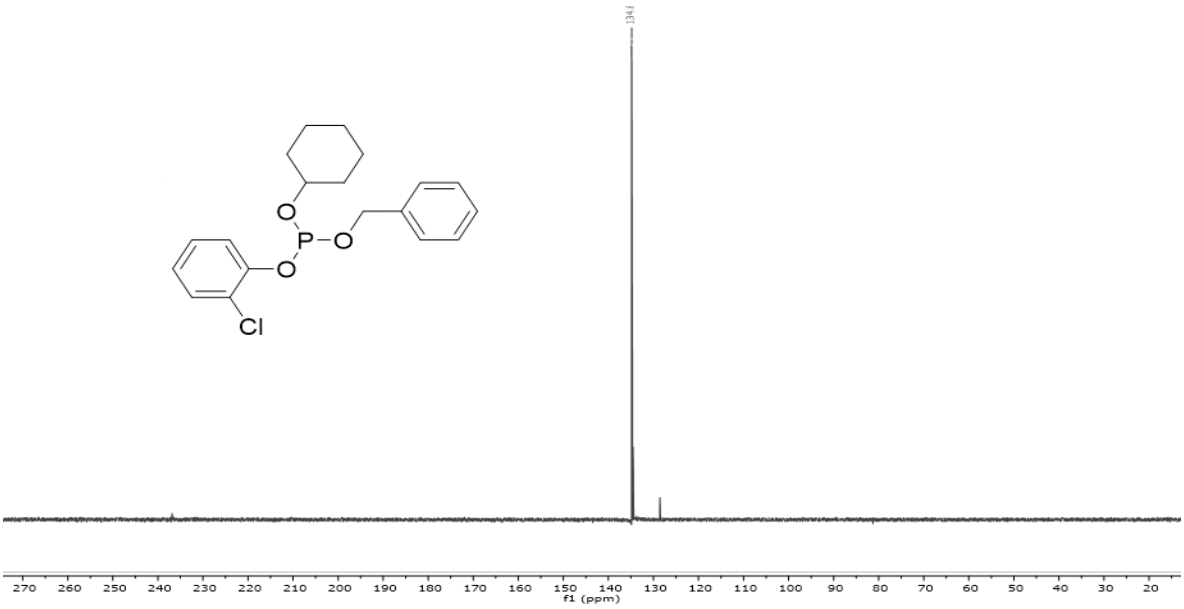

Figure D.6 ^{31}P- NMR of compound **3-14**

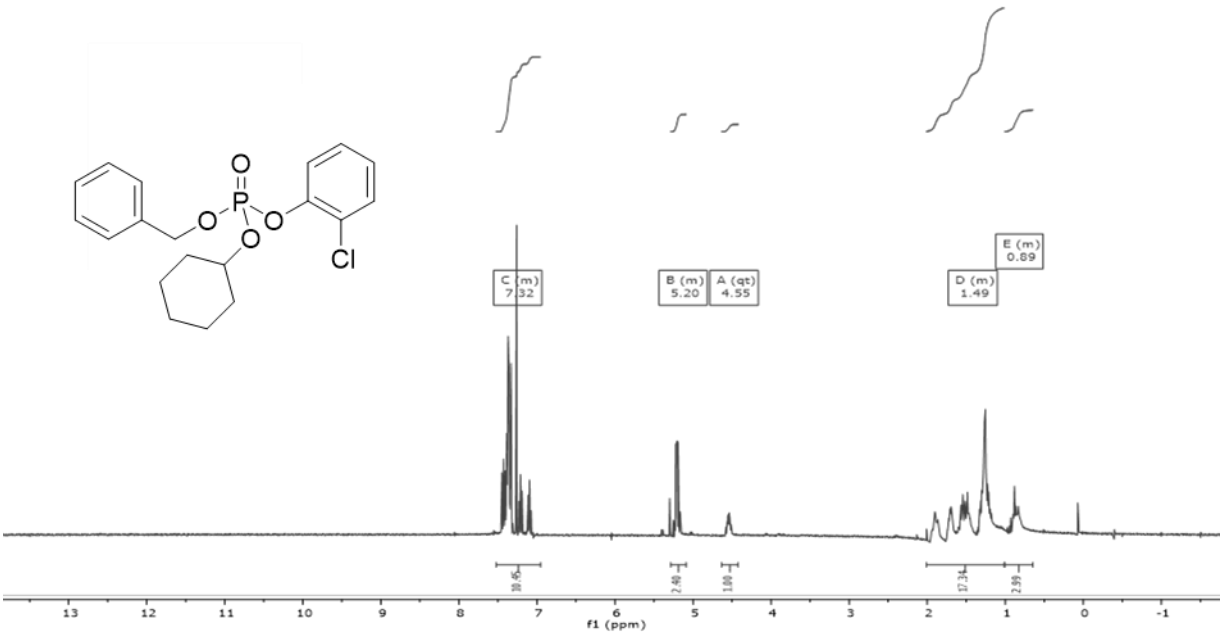

Figure D.7 ^{1}H NMR of compound **3-15**

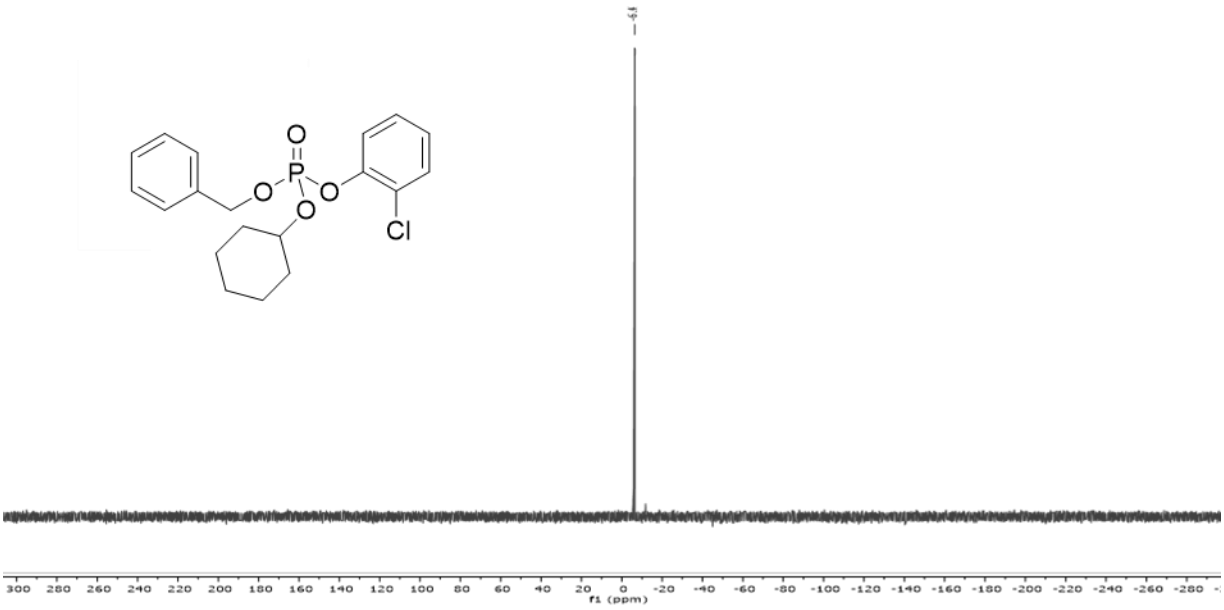

Figure D.8 ^{31}P- NMR of compound **3-15**

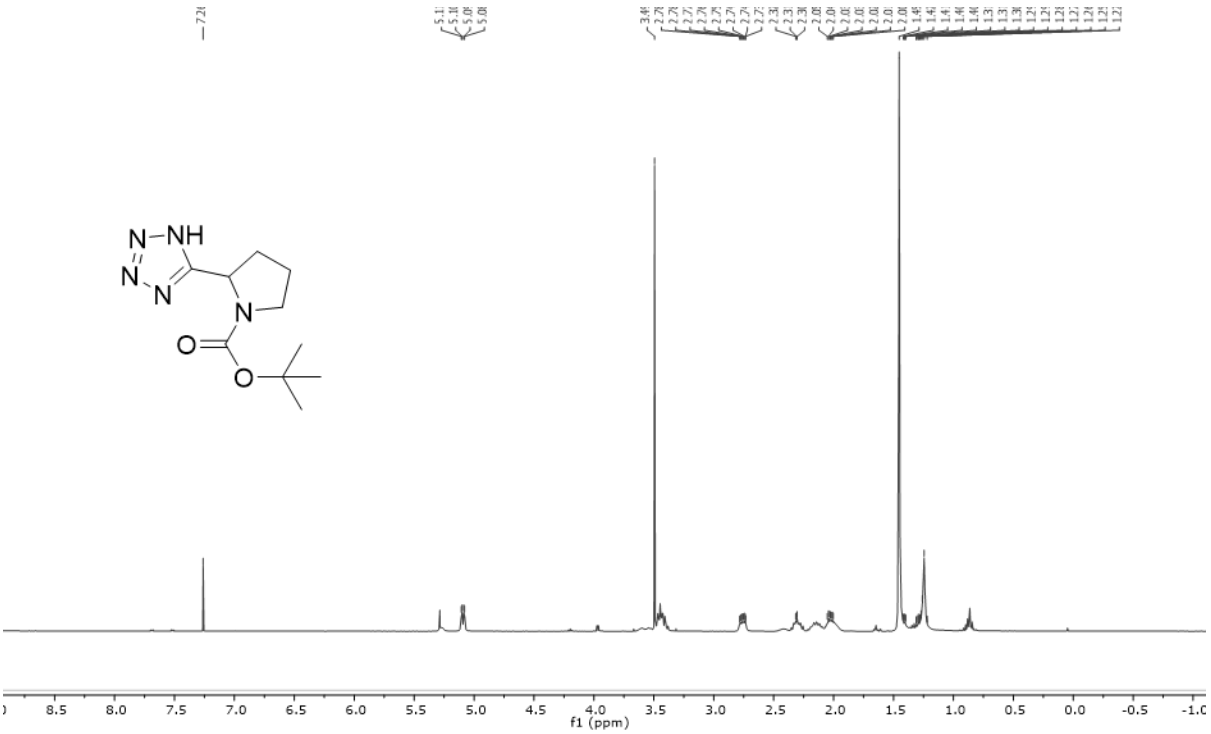

Figure D.9 ^{1}H NMR of compound **3-16**

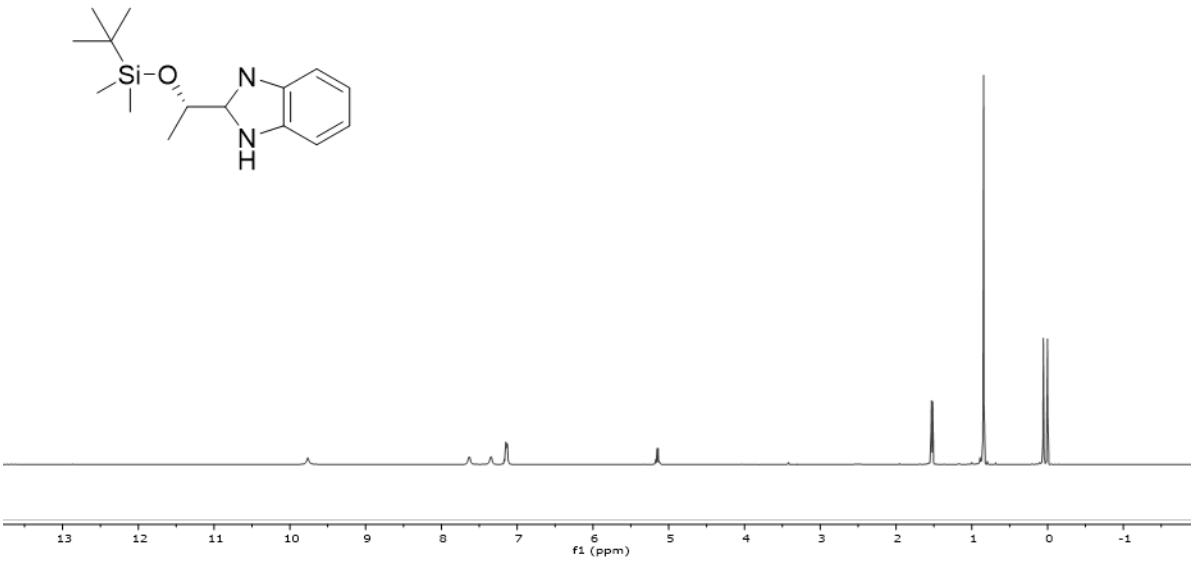

Figure D.10 ^{1}H NMR of compound **3-17**

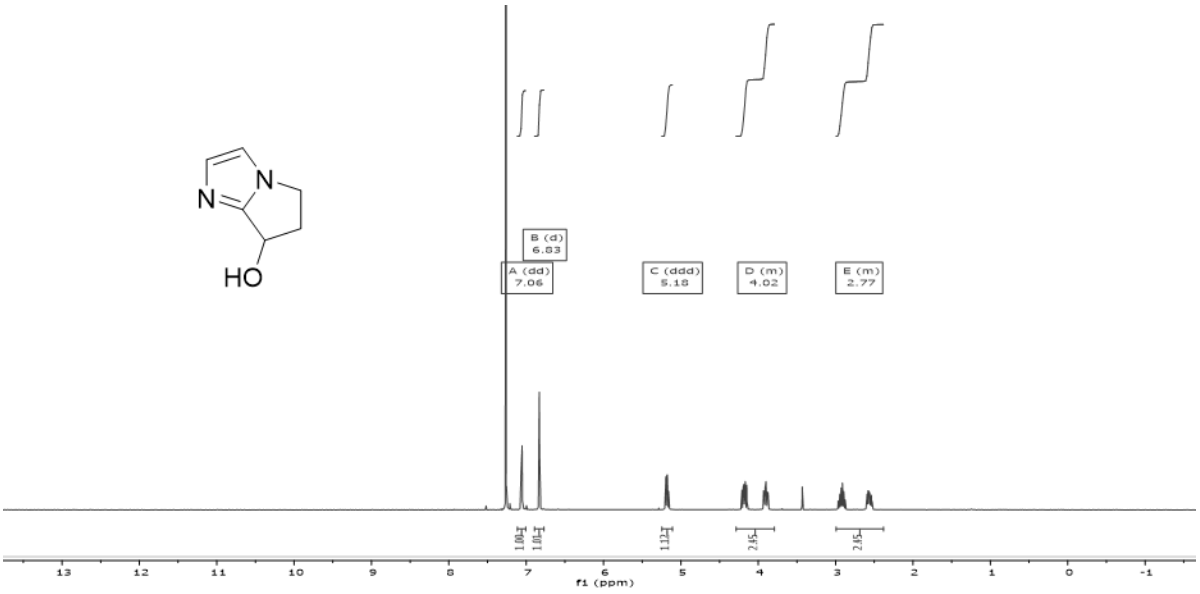

Figure D.11 ^{1}H NMR of compound **3-30**

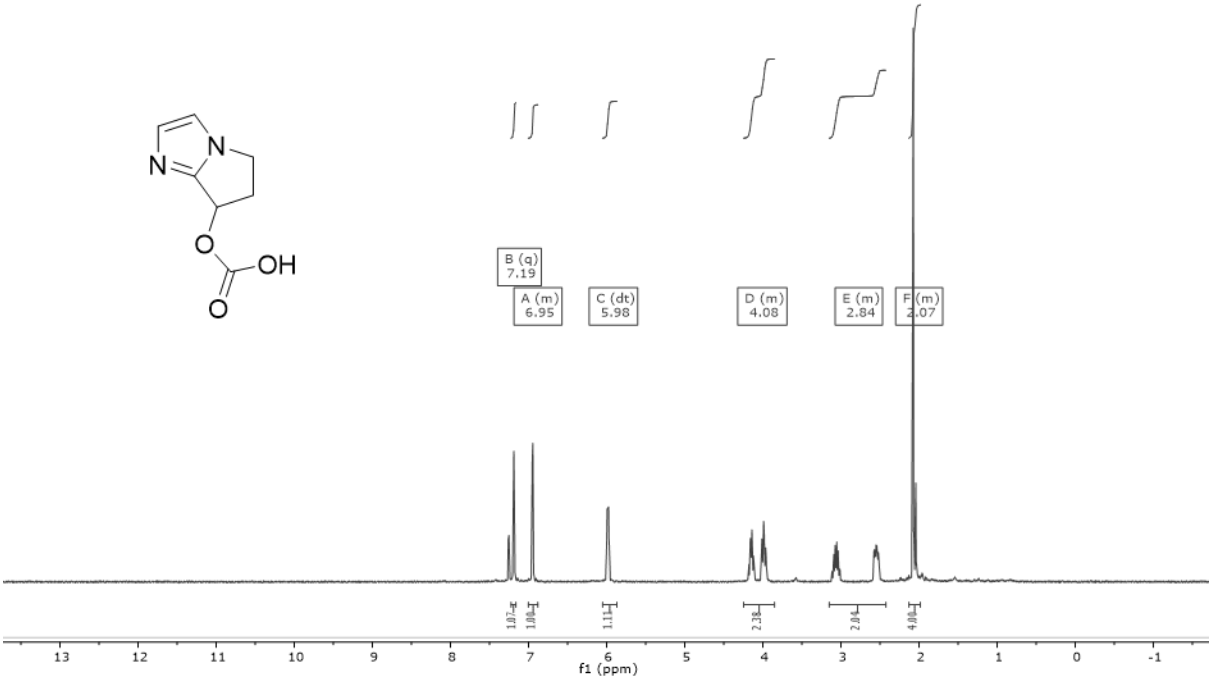

Figure D.12 ^{1}H NMR of compound **3-20**

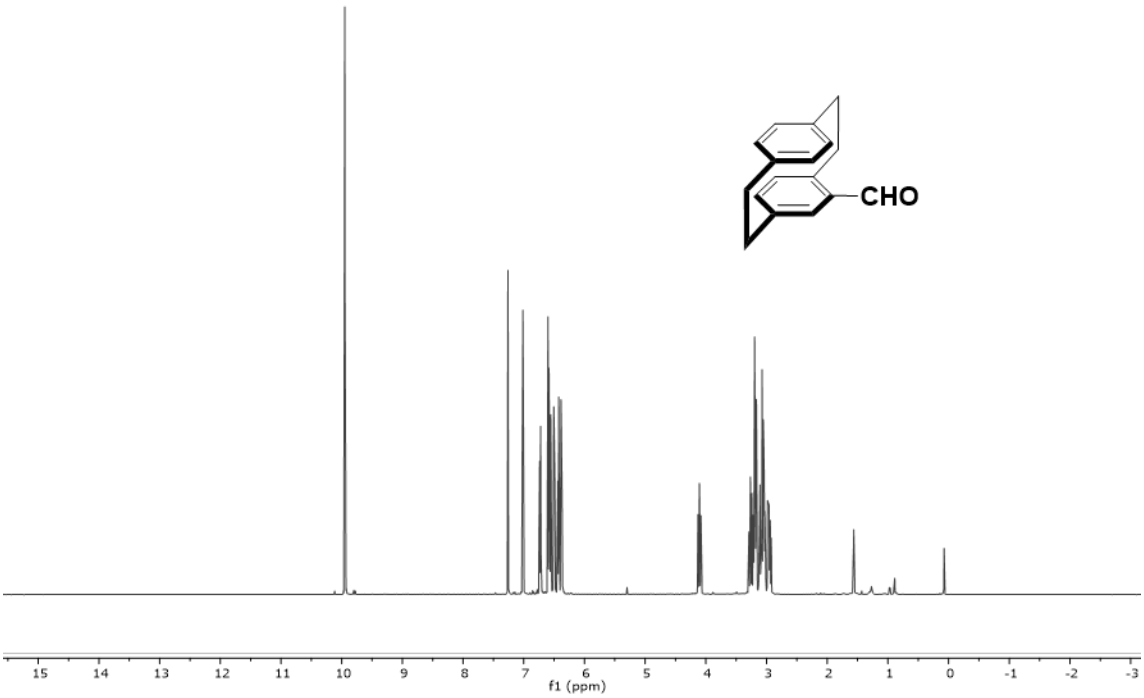

Figure D.13 ^{1}H NMR of compound **3-21**

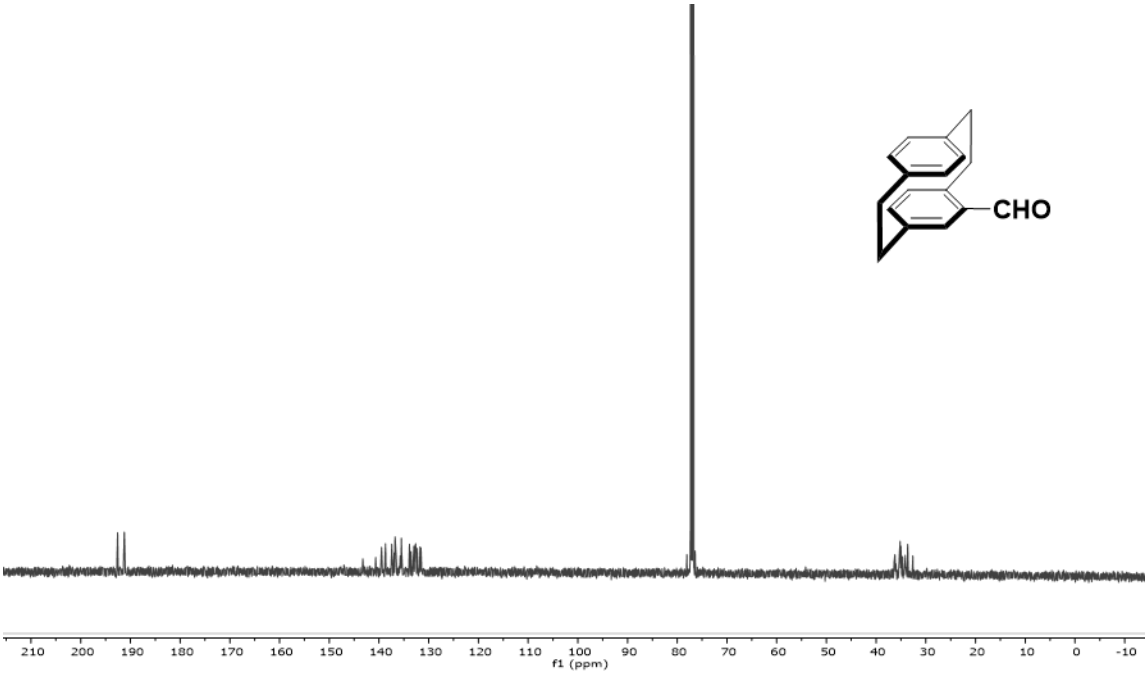

Figure D.14 ^{13}C-NMR of compound **3-21**

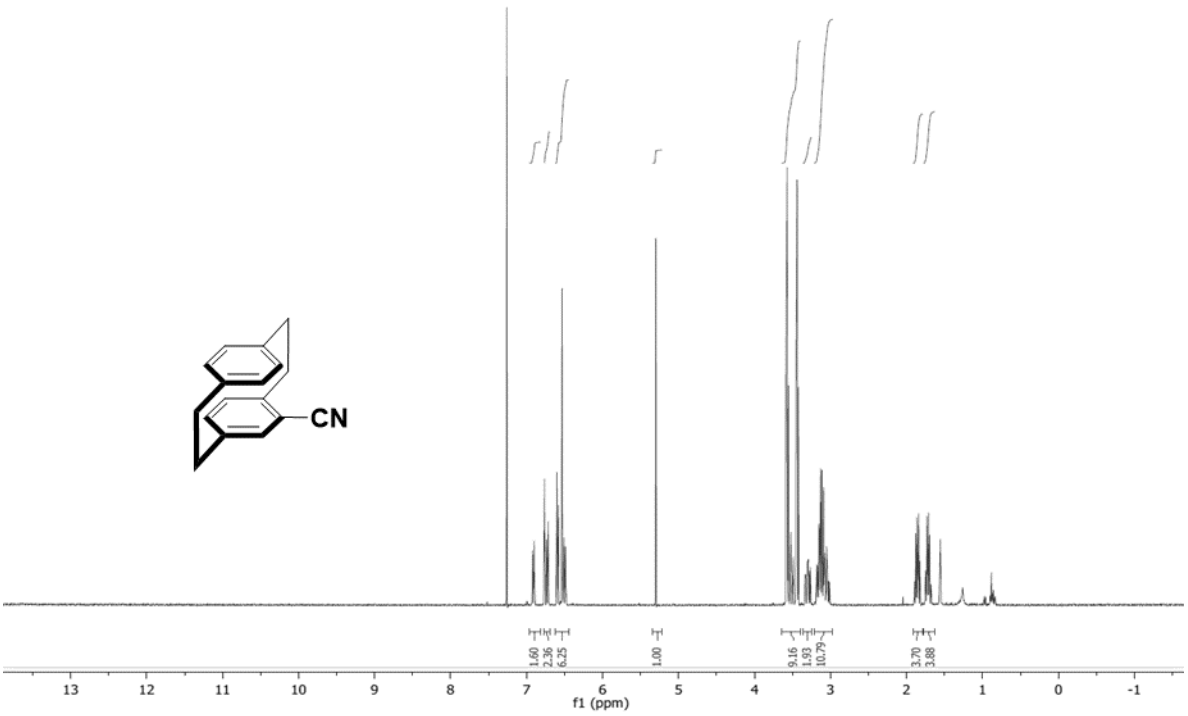

Figure D.15 ^{1}H NMR of compound **3-23**

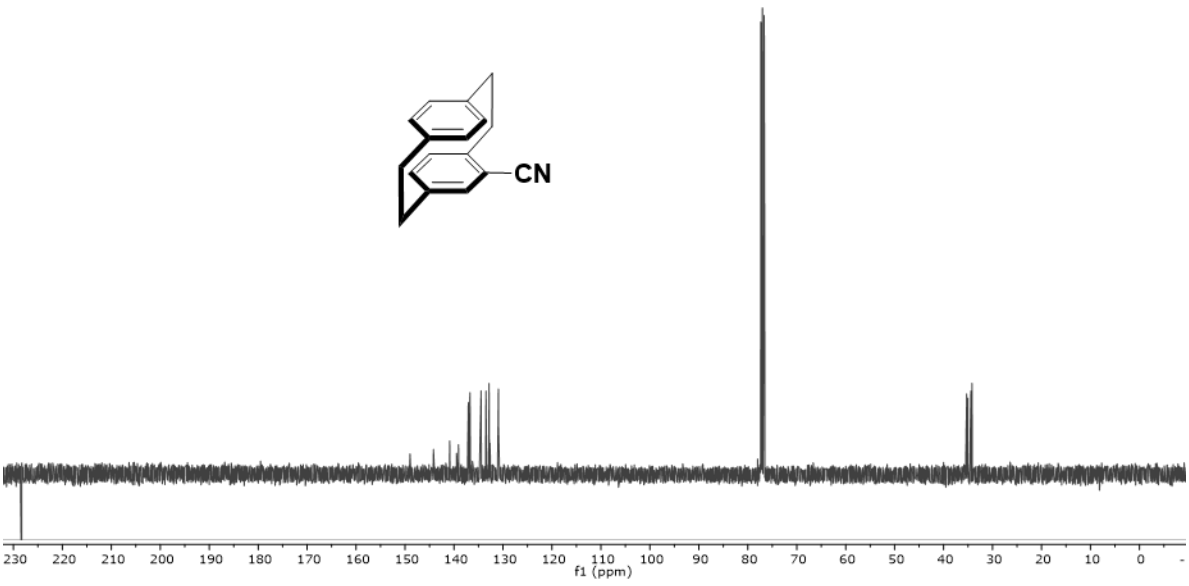

Figure D.16 ^{13}C-NMR of compound **3-23**

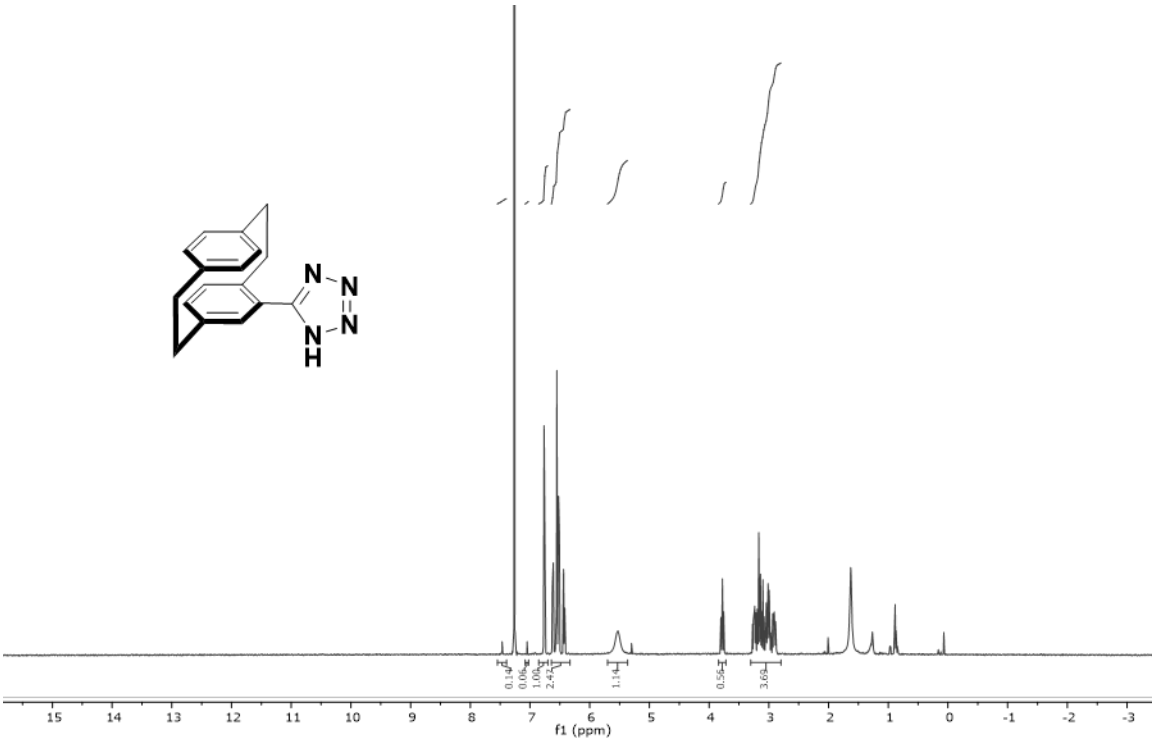

Figure D.17 ^{1}H NMR of compound **3-24**

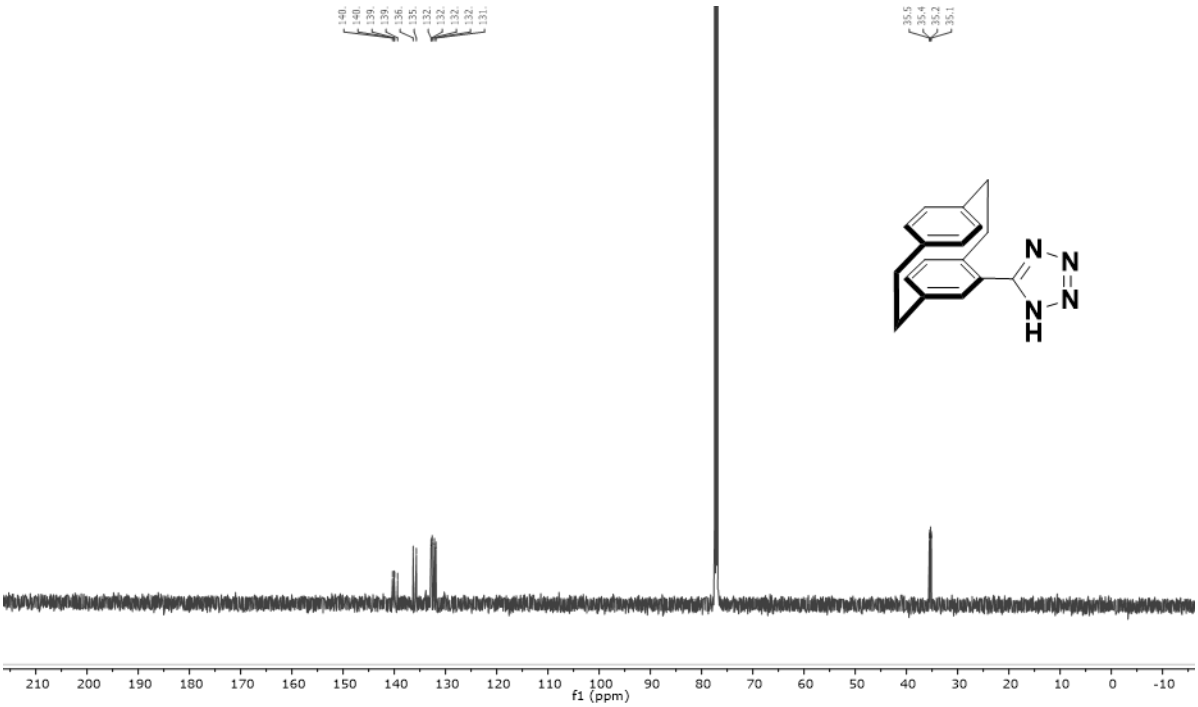

Figure D.18 ^{13}C-NMR of compound **3-24**

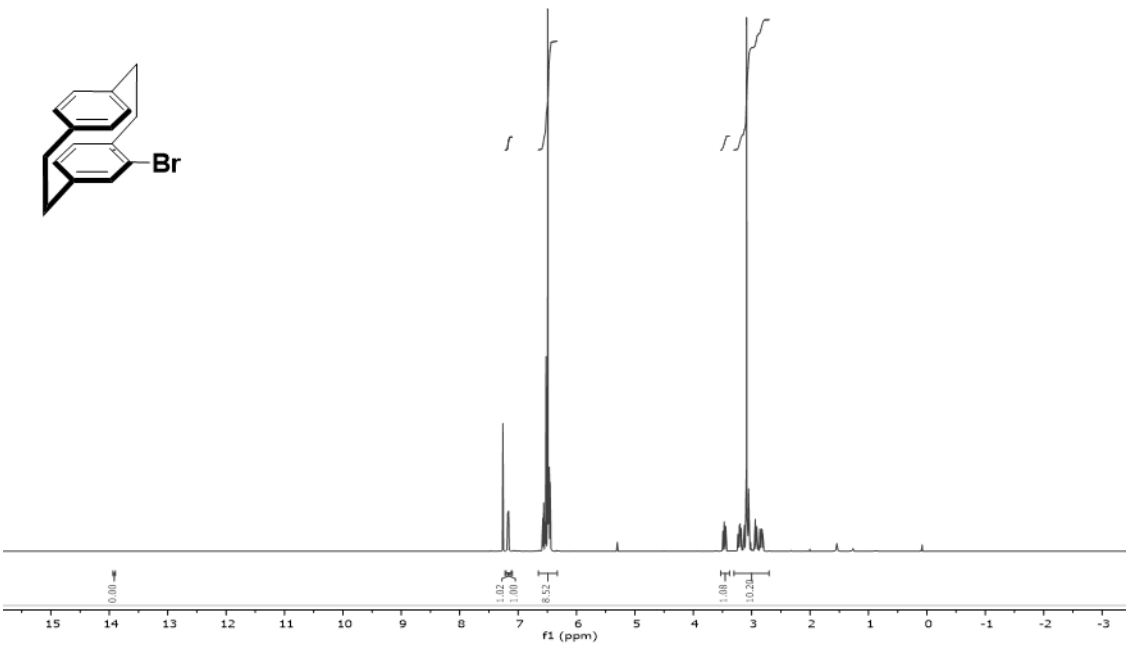

Figure D.19 ^{1}H NMR of compound **3-25**

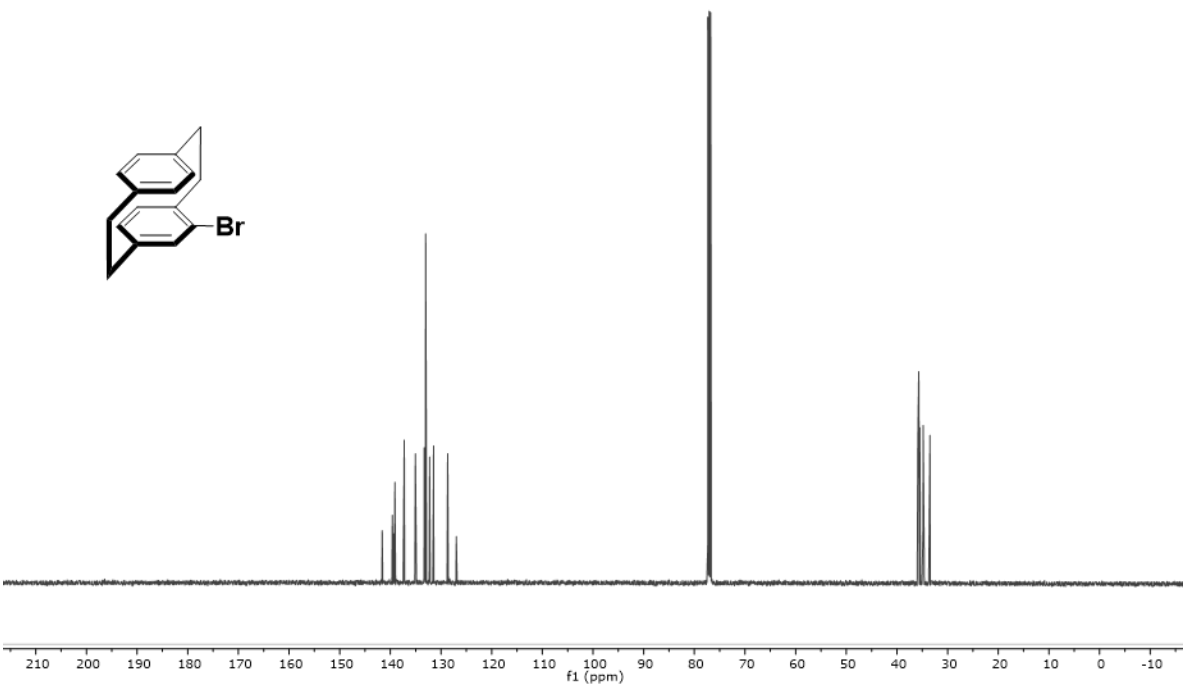

Figure D.20 ^{13}C-NMR of compound **3-25**

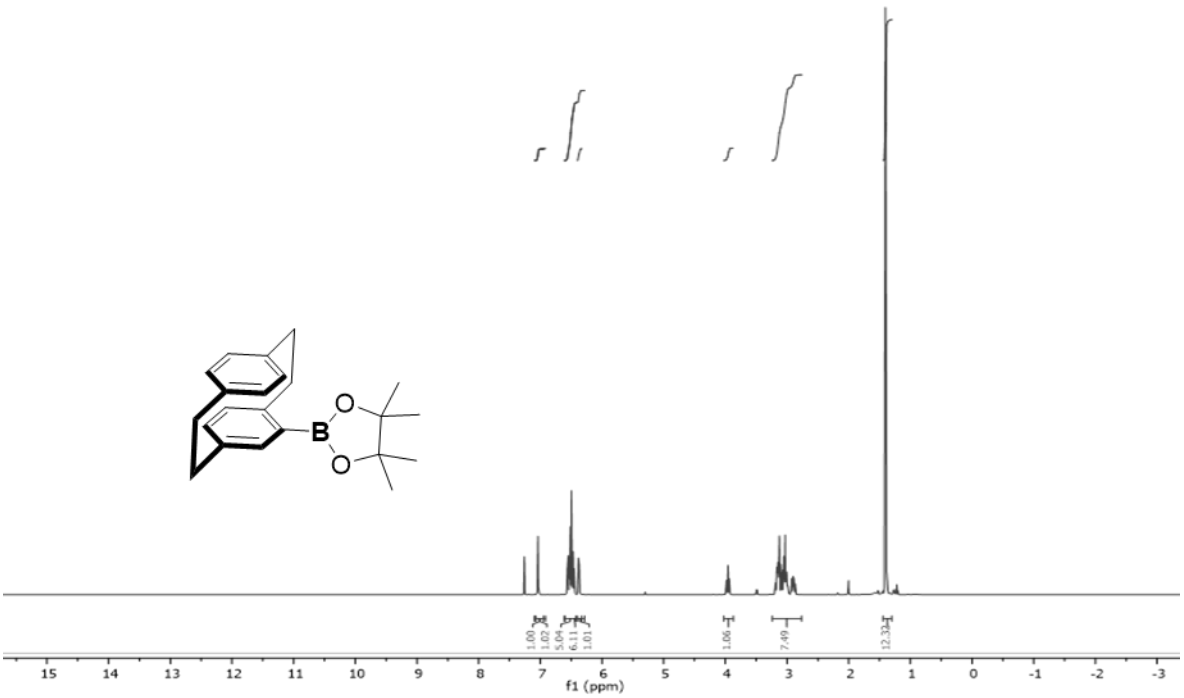

Figure D.21 ^{1}H NMR of compound **3-26**

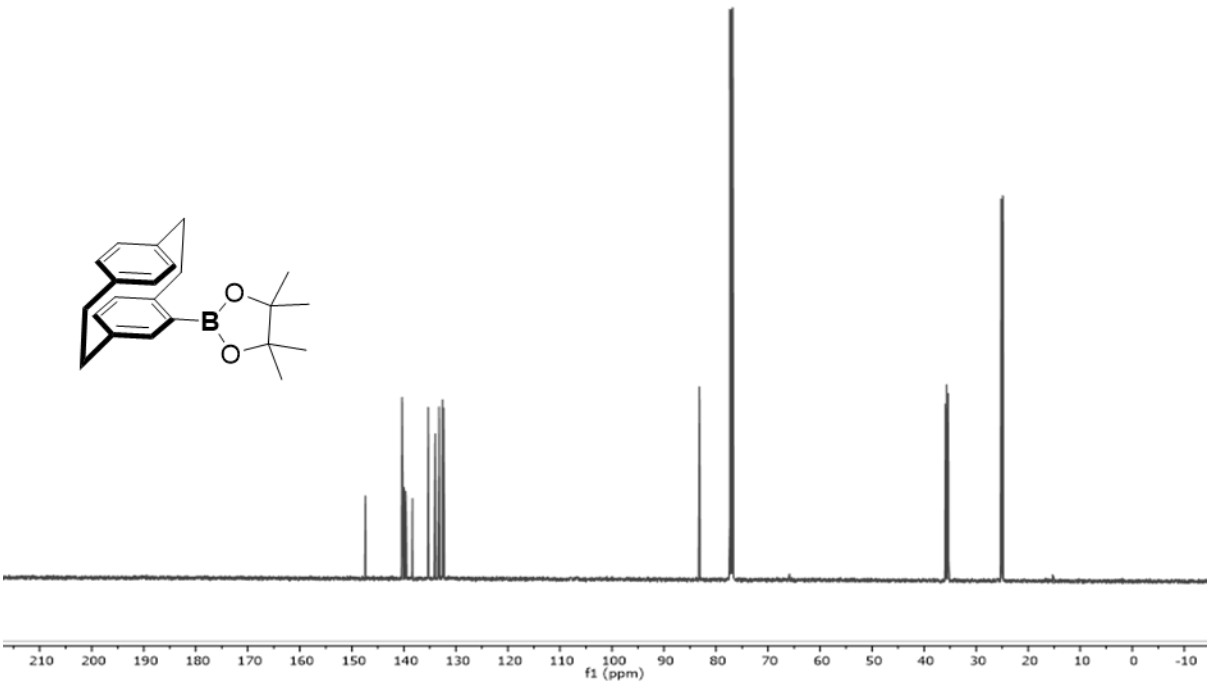

Figure D.22 ^{13}C-NMR of compound **3-26**

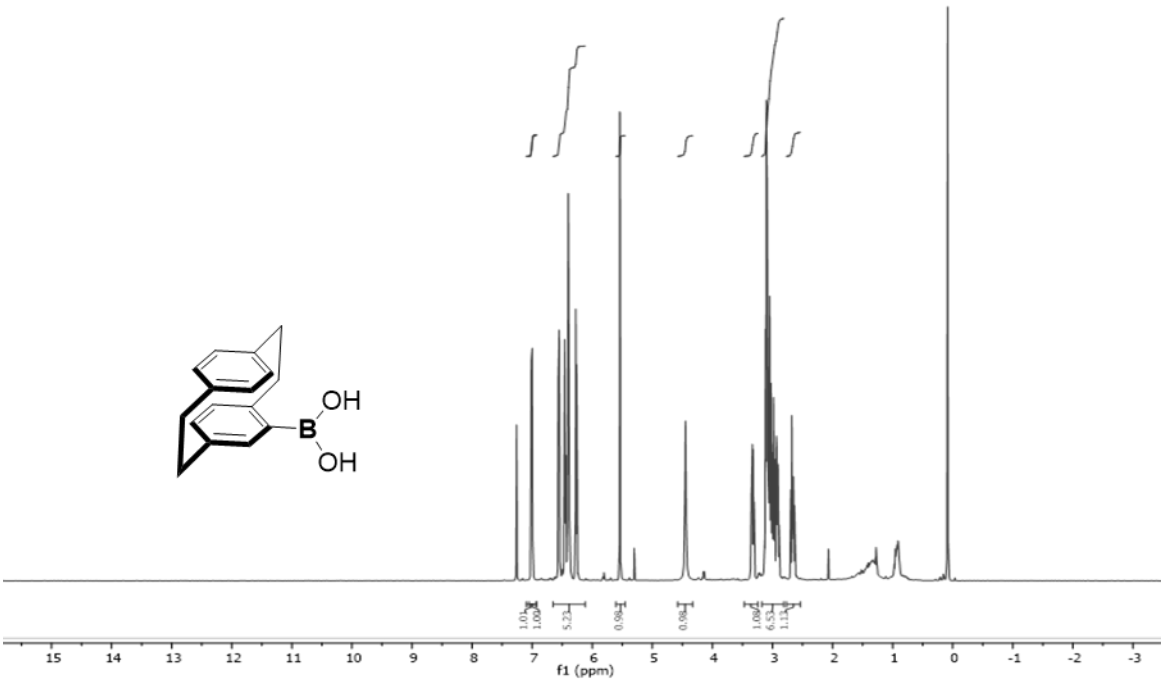

Figure D.23 ^{1}H NMR of compound **3-26**

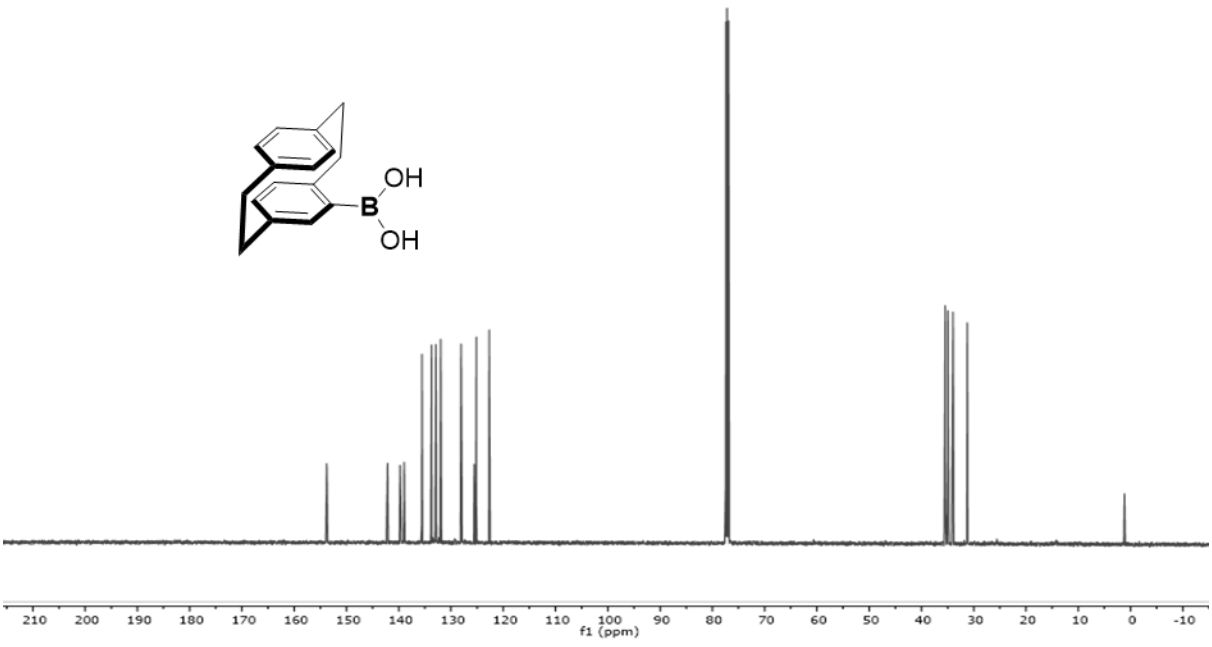

Figure D.24 ^{13}C-NMR of compound **3-27**

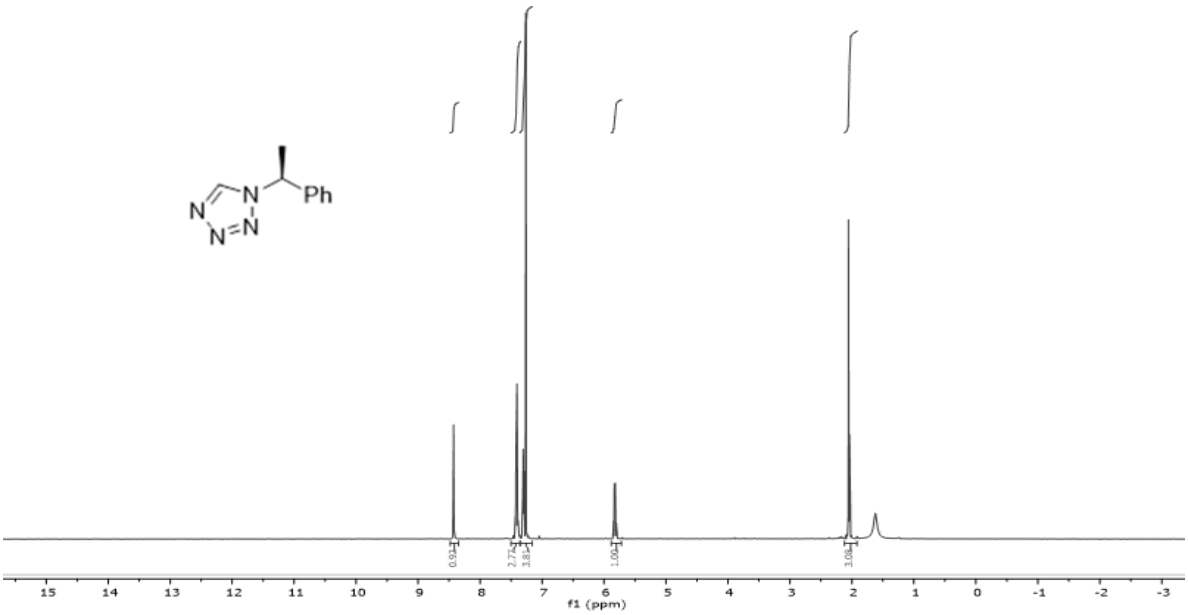

Figure D.25 ^{1}H NMR of compound **3-28**

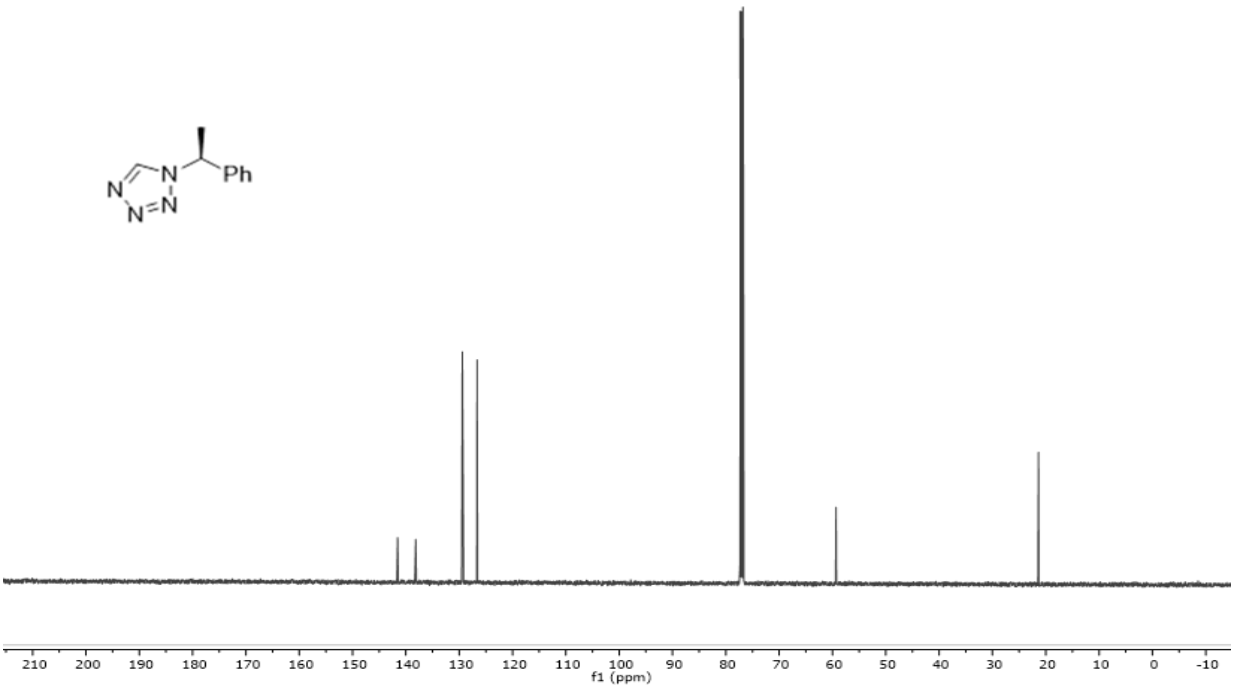

Figure D.26 ^{13}C-NMR of compound **3-28**

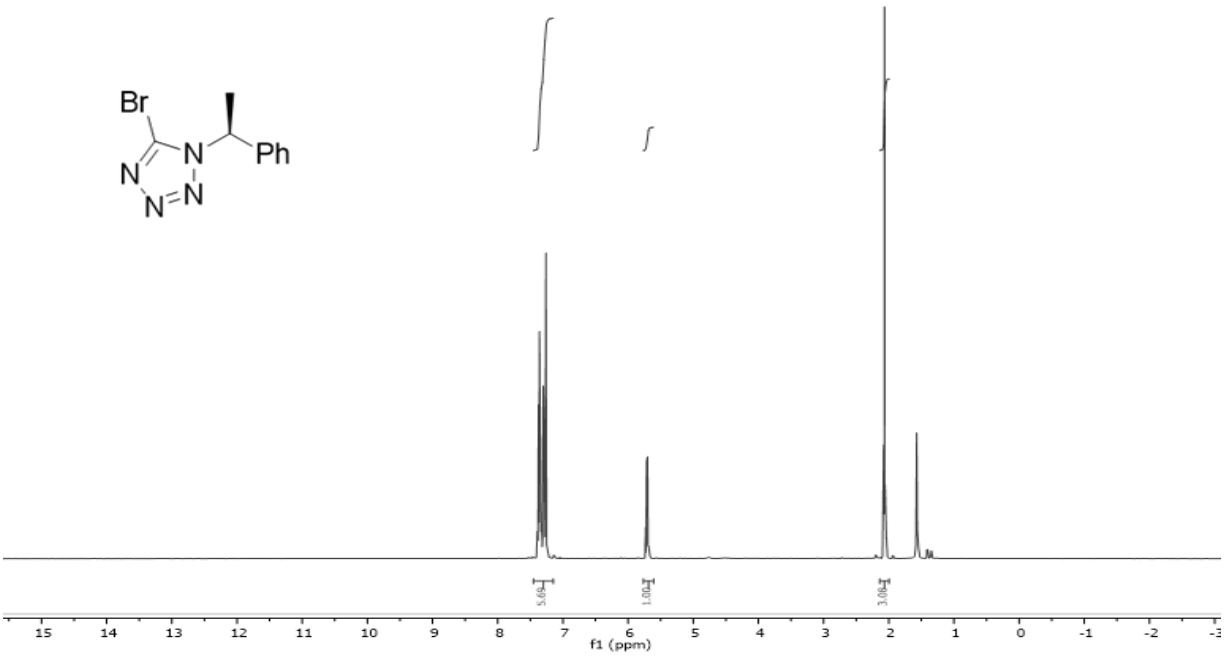

Figure D.27 ^{1}H NMR of compound **3-29**

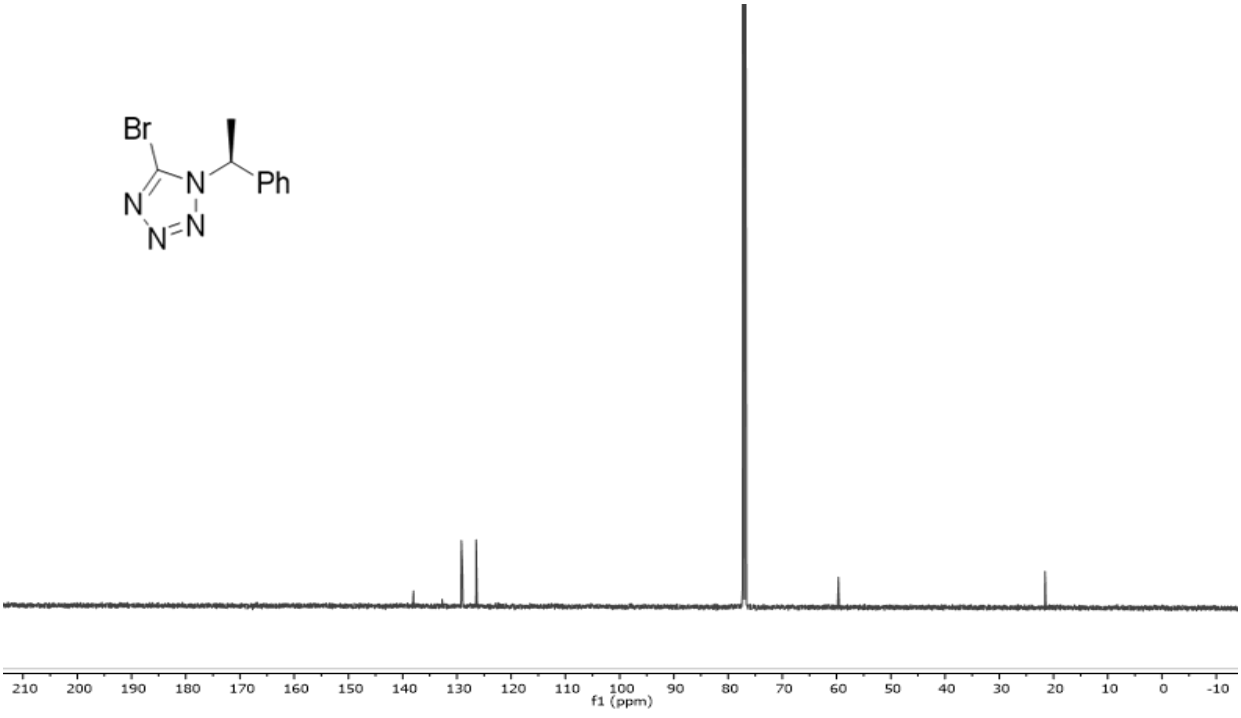

Figure D.28 ^{13}C-NMR of compound **3-29**

APPENDIX E: HPLC spectra for Chapter 3

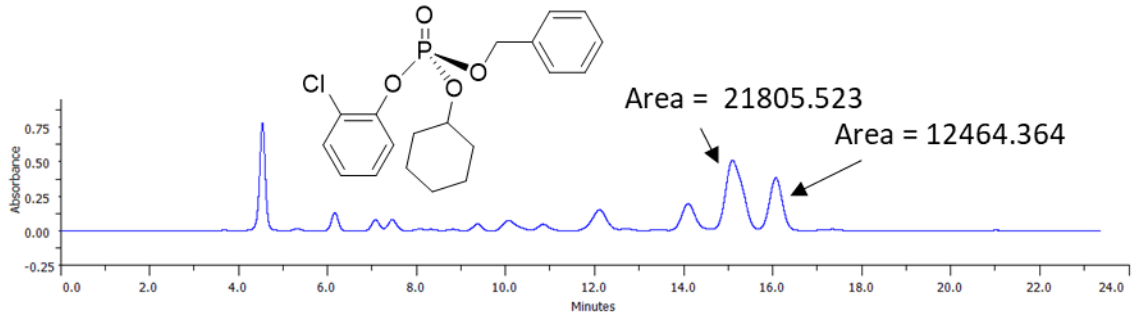

Figure E.1 Analytical HPLC chromatogram of **3-15** using 5 mol % of (*S*)-**3-16**

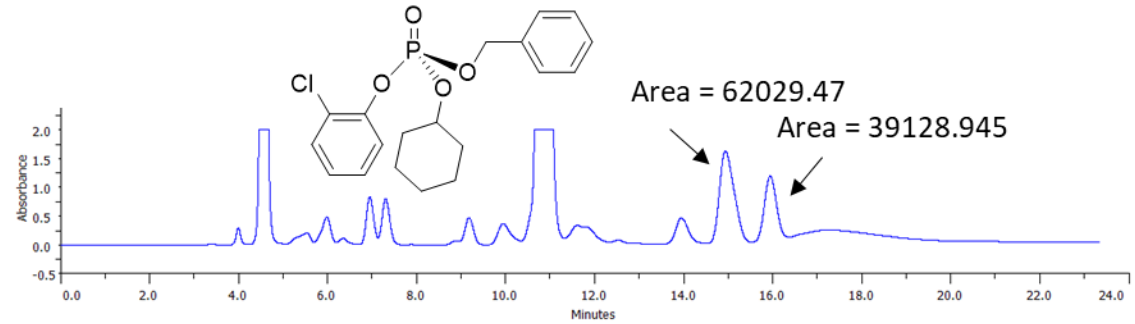

Figure E.2 Analytical HPLC chromatogram of **3-15** using 5 mol % of (*S*)-**3-18**

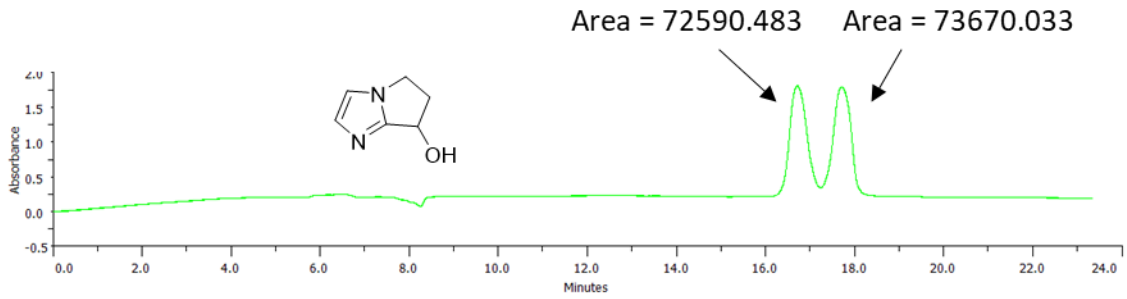

Figure E.3 HPLC chromatogram of racemic compound **3-30**

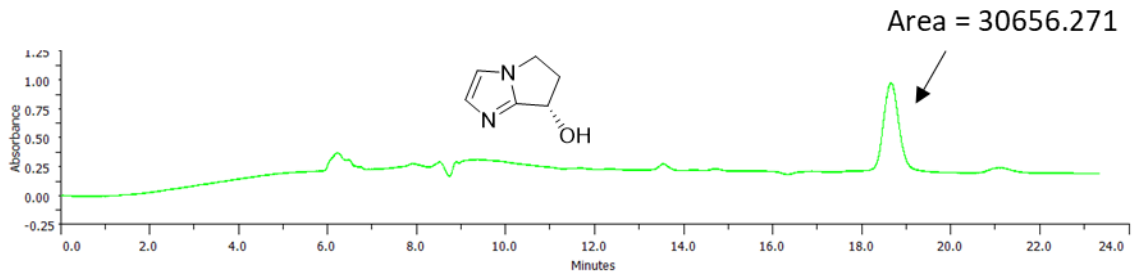

Figure E.4 HPLC chromatogram of enantioenriched compound **3-30** after enzymatic resolution

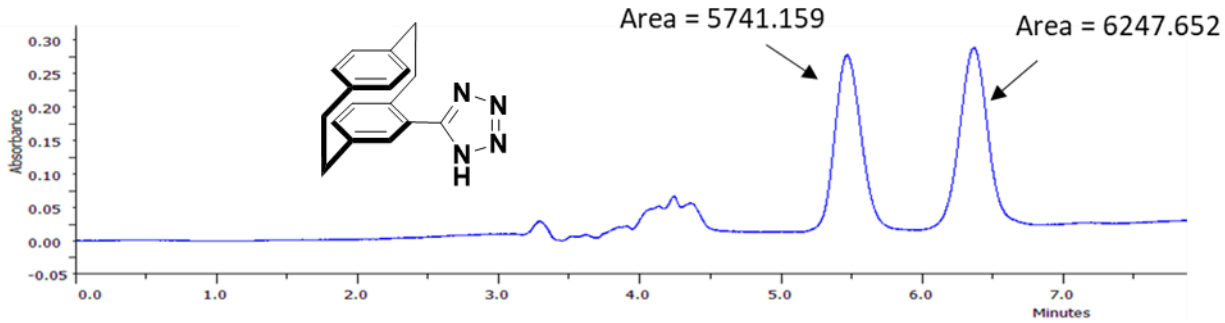

Figure E.5 HPLC chromatogram of compound **3-24**

APPENDIX F: NMR Data for Chapter 4

Table F.1 Calculated relative error % for replicate integration of ^{31}P NMR for samples.

Entry	Phosphonate	OrthoP	OrthoP Monoesters	Plipids	Pdiesters	PyroP
1-	11.024	1.308	0.004	15.712	5.8114	15.114
2-	37.796	1.373	3.181	0.191	0.525	1.878
3-	5.360	0.601	1.216	24.041	1.683	2.712
4-	42.183	4.465	17.816	33.038	3.18	24.713
5-	7.188	0.507	0.867	27.086	0.352	15.797
6-	19.61	0.074	0.328	7.163	0.651	25.932

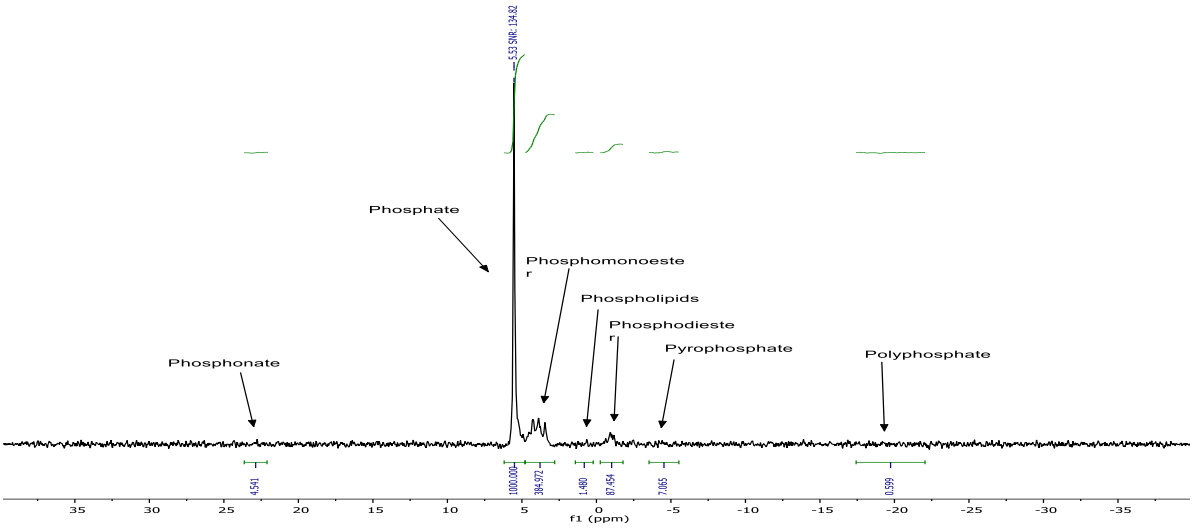

Figure F.1 Representative ^{31}P NMR spectra of the 0.25 M NaOH/0.05 M EDTA extracted surficial sediment in 25.1 cm depth of Highland Lake until the pH of the solution is pH 7.

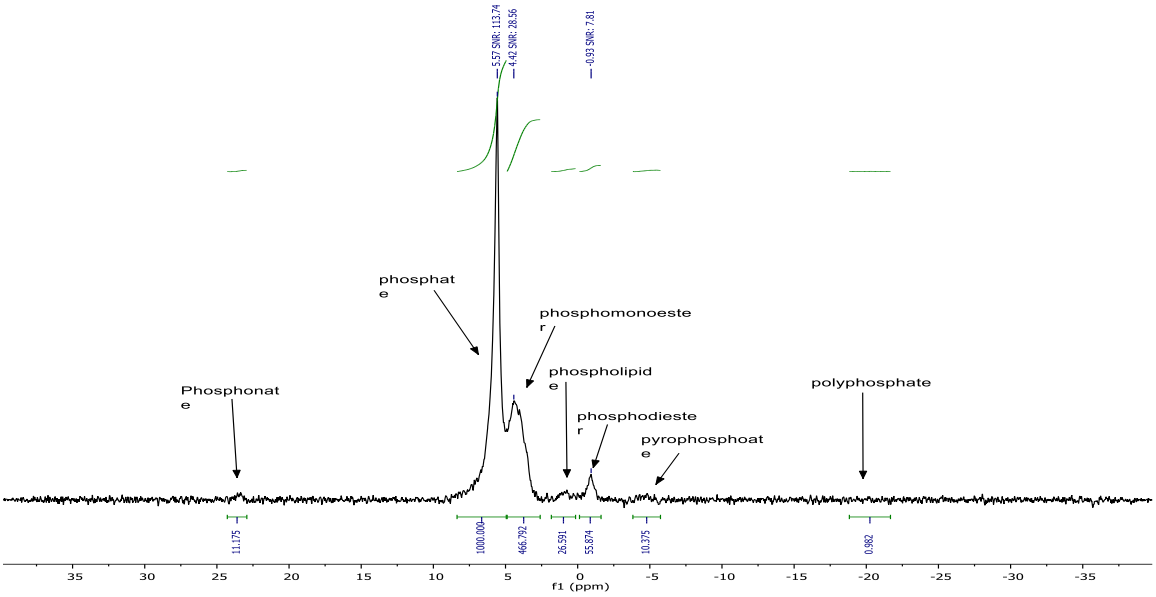

Figure F.2 Representative ^{31}P NMR spectrum of the 0.25 M NaOH/0.05 M EDTA extracted surficial sediment in 20.2 cm depth of Highland Lake until the pH of the solution is pH 7.

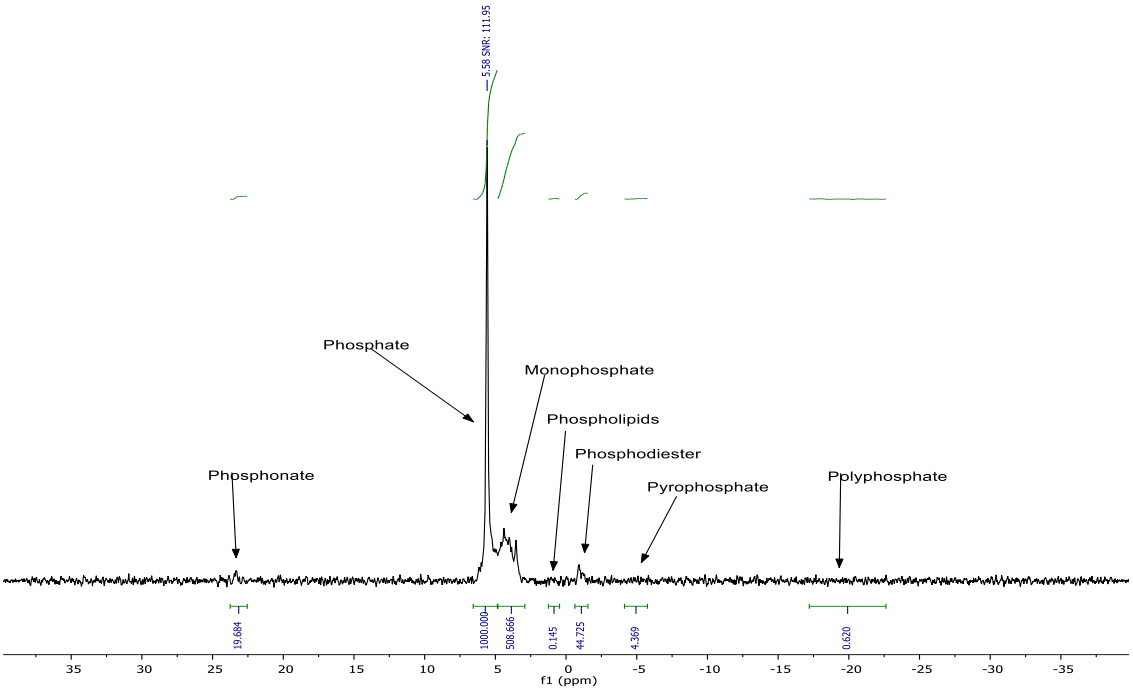

Figure F.3 Representative ^{31}P NMR spectrum of the 0.25 M NaOH/0.05 M EDTA extracted surficial sediment in 20.2 cm depth of Highland Lake until the pH of the solution is pH 13.

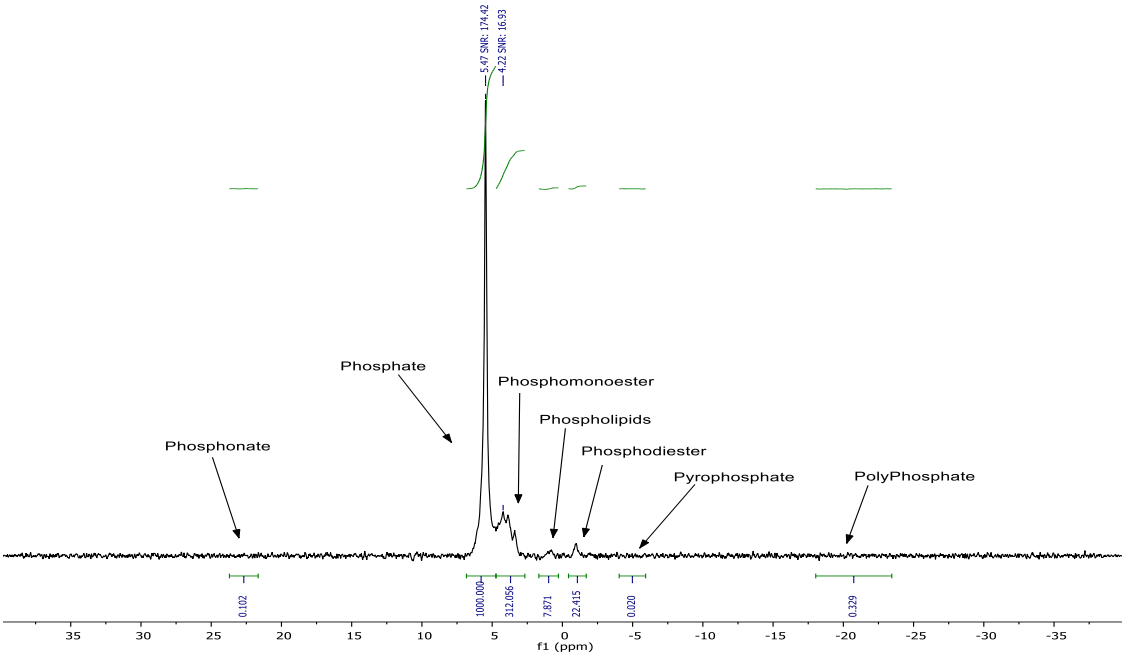

Figure F.4 Representative ^{31}P NMR spectrum of the 0.25 M NaOH/0.05 M EDTA extracted surficial sediment in 33.71 cm depth of Highland Lake until the pH of the solution is pH 7.

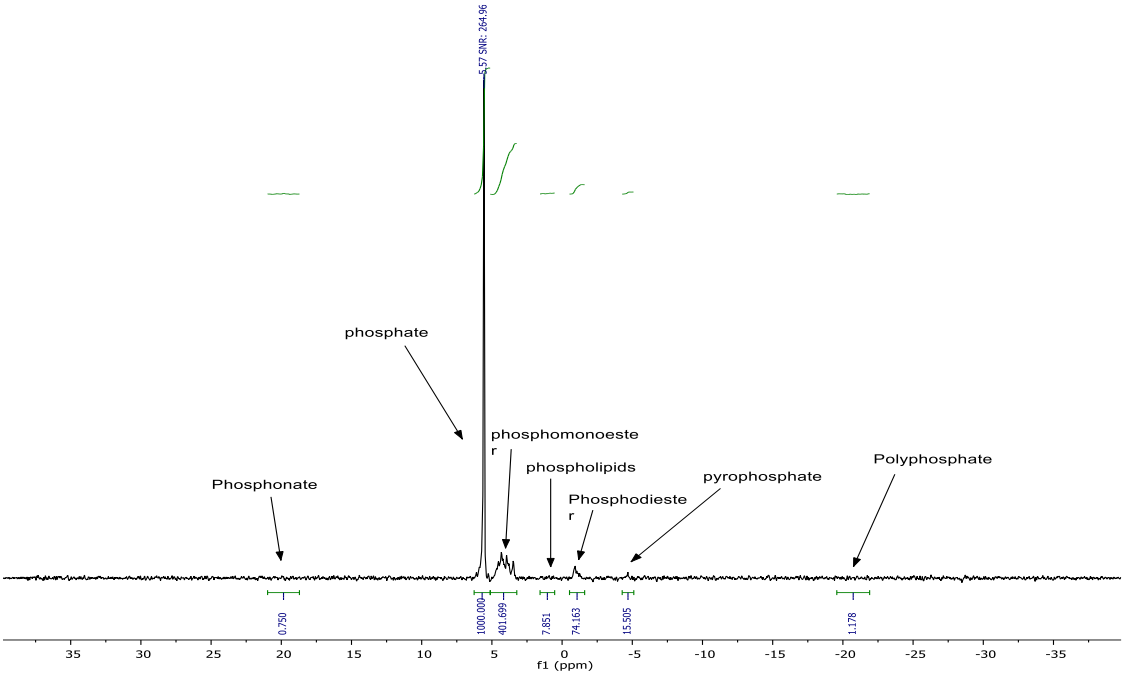

Figure F.5 Representative ^{31}P NMR spectrum of the 0.25 M NaOH/0.05 M EDTA extracted surficial sediment in 26.3 cm depth of Highland Lake until the pH of the solution is 7.

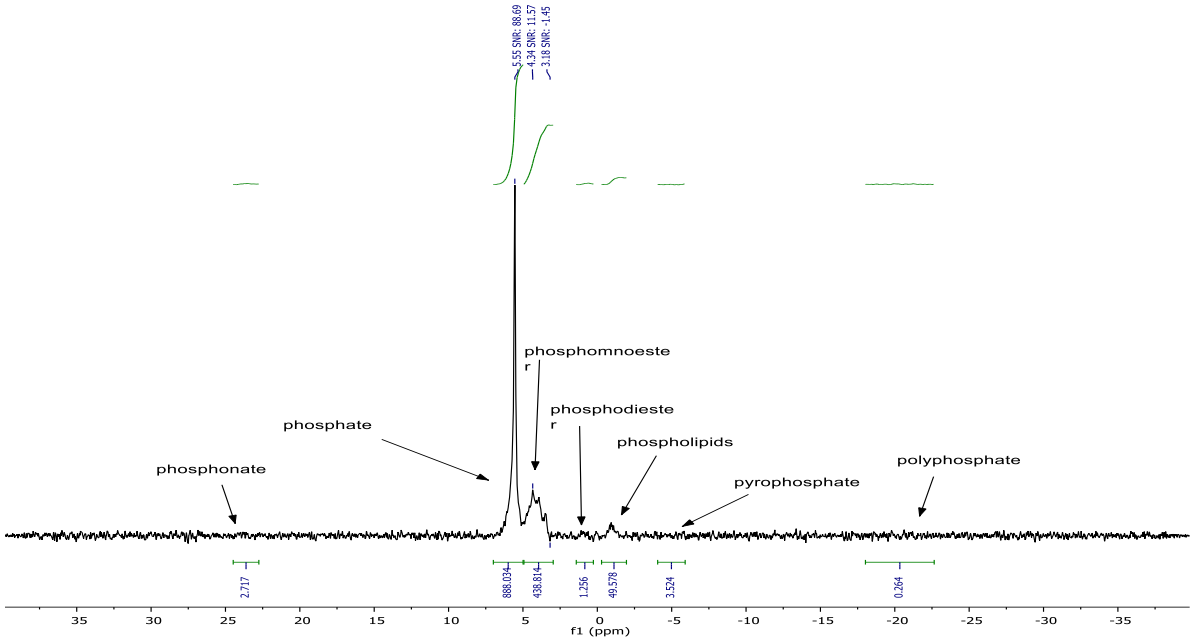

Figure F.6 Representative ^{31}P NMR spectrum of the 0.25 M NaOH/0.05 M EDTA extracted surficial sediment in 19 cm depth of Highland Lake until the pH of the solution is 7.

APPENDIX G: Copyright permission from authors and publishers

ELSEVIER LICENSE
TERMS AND CONDITIONS

May 06, 2020

This Agreement between University of Maine -- Ahmed Numan ("You") and Elsevier ("Elsevier") consists of your license details and the terms and conditions provided by Elsevier and Copyright Clearance Center.

License Number	4823161207832
License date	May 06, 2020
Licensed Content Publisher	Elsevier
Licensed Content Publication	Journal of Clinical Lipidology
Licensed Content Title	Novel therapies and new targets of treatment for familial hypercholesterolemia
Licensed Content Author	Anne Carol Goldberg
Licensed Content Date	September–October 2010
Licensed Content Volume	4
Licensed Content Issue	5
Licensed Content Pages	7
Start Page	350
End Page	356
Type of Use	reuse in a thesis/dissertation

Portion	figures/tables/illustrations
Number of figures/tables/illustrations	1
Format	electronic
Are you the author of this Elsevier article?	No
Will you be translating?	Yes, including English rights
Number of languages	1
Title	PhD candidate
Institution name	University of maine
Expected presentation date	Sep 2020
Order reference number	2
Portions	figure 1
Specific Languages	English
Requestor Location	University of Maine 19 lupin way, # 25F ORONO, ME 04473 United States Attn: University of Maine
Publisher Tax ID	98-0397604
Total	0.00 USD

ELSEVIER LICENSE
TERMS AND CONDITIONS

Apr 06, 2021

This Agreement between University of Maine -- Ahmed Numan ("You") and Elsevier ("Elsevier") consists of your license details and the terms and conditions provided by Elsevier and Copyright Clearance Center.

License Number	5043230202886
License date	Apr 06, 2021
Licensed Content Publisher	Elsevier
Licensed Content Publication	Talanta
Licensed Content Title	Characterizing phosphorus in environmental and agricultural samples by 31P nuclear magnetic resonance spectroscopy
Licensed Content Author	Barbara J. Cade-Menun
Licensed Content Date	Apr 15, 2005
Licensed Content Volume	66
Licensed Content Issue	2
Licensed Content Pages	13
Start Page	359
End Page	371

Type of Use	reuse in a thesis/dissertation
Portion	figures/tables/illustrations
Number of figures/tables/illustrations	1
Format	electronic
Are you the author of this Elsevier article?	No
Will you be translating?	No
Title	QUANTITATIVE ANALYSIS OF PHOSPHORUS IN ENIROMENTAL SAMPLES BY 31P NUCLEAR MAGNETIC RESONANCE SPECTROSCOPY
Institution name	University of Maine
Expected presentation date	May 2021
Portions	Fig 1.
Requestor Location	University of Maine 19 lupin way, # 25F ORONO, ME 04473 United States Attn: University of Maine
Publisher Tax ID	98-0397604
Total	0.00 USD
Terms and Conditions	

BIBLIOGRAPHY

Ahmed Numan was born in Baghdad, Iraq, on June 17th, 1985. He graduated from Al-Nahrain University with an undergrad degree in Chemistry in 2007. He then went on to obtain his Master's in Organic Chemistry, also from Al-Nahrain, in 2009. Before arriving in the United States, he worked in the oil industry. Ahmed joined the doctoral program at the University of Maine in 2015. Ahmed is a candidate for the Doctor of Philosophy degree in Chemistry from the University of Maine in August 2021.